Dibenzodiazepinone-type mAChR ligands: radio- and fluorescence labeling enable unveiling of dualsteric M_2R binding and conjugation to short peptides as an avenue to highly selective M_2R ligands

Dissertation

zur Erlangung des Doktorgrades der Naturwissenschaften (Dr. rer. nat.)

an der Fakultät für Chemie und Pharmazie

der Universität Regensburg

vorgelegt von

Andrea Pegoli

aus Senigallia (Italy)

2017

Die vorliegende Arbeit entstand in der Zeit von Oktober 2013 bis März 2017 unter der Leitung von Herrn Prof. Dr. A. Buschauer und Herrn Dr. M. Keller am Institut für Pharmazie der Naturwissenschaftlichen Fakultät IV – Chemie und Pharmazie- der Universität Regensburg.

Das Promotionsgesuch wurde eingereicht im März 2017

Tag der mündlichen Prüfung: 10.05.2017

Prüfungsausschuss:

Prof. Dr. B. Dick	(Vorsitzender)
Prof. Dr. A. Buschauer	(Erstgutachter)
Prof. Dr. G. Bernhardt	(Zweitgutachter)
Prof. Dr. S. Elz	(Drittprüfer)

a Laura

ACKNOWLEDGMENT

I would like to take this opportunity to thank all the people that have contributed to the realization of this work and have accompanied me during the period of my doctoral thesis. I would like to thank:

Dr. Max Keller, for the opportunity to work on this challenging and versatile project, for the inspiring and useful discussion, for the support during these years and for the constructive critic that made this work possible,

Prof. Dr. Armin Buschauer, for let me working in his research group, for the inspiring suggestions and for the scientific advice and support,

Prof. Dr. Günther Bernhardt, for his interest in the progress of the work, for his helpful advice and for the critical revision of the present thesis,

Dr. Nicholas Holliday, for his supervision during my staying at the University of Nottingham, for the stimulating conversations and for the constructive criticism,

Xueke She, for the synthesis of various dibenzodiazepinone-type MRs ligands described in Chapter 2-4 and for the valuable ideas,

Dr. David Wifling, for the molecular dynamics simulations of **19** and **33** at the M_2R described in Chapter 2, for the helpful discussions, and for the critical review of my manuscript,

Jessica Carpenter, for the help in carrying out confocal microscope experiments as well for her hospitality during me staying at the University of Nottingham,

Brigitte Wenzl and Susanne Bollwein for the cultivation of CHO-M_x cells and for their excellent support with radioligand binding assays,

Maria Beer-Krön and Dita Fritsch for the preparation of M_2-homogenates, for the cultivation of CHO-M_x cells and for the help with radioligand binding assays,

Elvira Schreiber, for the support with the investigation of fluorescent ligands at FACS,

Peter Richthammer for many tips and advices on the reparation of lab equipment as well as for the help with the preparation of the student Praktikum courses,

Karin Reindl for the friendly support with all the bureaucratic and organization matters,

Seema Rajani, for the support with the confocal microscope experiments at the University of Nottingham,

All employees of the analytical departments of the University of Regensburg for the NMR and mass spectra. Special thanks go to Fritz Kastner and Josef Kiermaier for the useful discussions and the excellent assistance,

Prof. Dr. Peter Gmeiner and Dr. Harald Hübner for performing IP1 functional assays at the M_2R reported in Chapter 2 and for the critical review of my manuscript,

The GRK 1910, for the financial support and for all the interesting events organized during the last years,

All the members of the GRK 1910, for the critical and helpful scientific discussions and for sharing their results during our retreatments,

Frauke Antoni, Nicole Plank, Timo Littmann, and Stefanie Dukorn with whom I have shared office/labs in the last years,

All my colleagues for the excellent working atmosphere and for the good time we had in and outside the University,

All the PhD students and Post-Docs in the Cell Signaling group at the University of Nottingham for the interesting conversations and the help in the lab,

Un ringraziamento speciale (ed in ordine sparso) va a Andrea, Matteo, Salvatore, Polyssena, Nadia e Valeria per tutte le serate passate insieme (e per i frequenti postumi del giorno dopo). Grazie per aver reso il tutto un po' più divertente,

Mio padre e mia madre, perchè nonostante la distanza mi sono sempre stati vicini,

Ed infine Laura, per ogni singolo momento passato insieme.

Contents

Chapter 1
General introduction

1.1 Muscarinic acetylcholine receptors: an overview

Muscarinic acetylcholine receptors (MRs) belong to the class A of G-protein coupled receptors (GPCRs) and comprise five distinct subtypes, denoted M_1, M_2, M_3, M_4, and M_5 receptors.[1-4] The M_1, M_3 and M_5 subtypes preferentially couple to the $G_{q/11}$ family of G proteins, resulting in phospholipase C activation, hydrolysis of inositol phosphates and the mobilization of intracellular Ca^{2+}. By contrast, the M_2 and M_4 subtypes preferentially couple to the pertussis toxin sensitive $G_{i/o}$ family of G proteins, resulting in the inhibition of adenylyl cyclase activity with a decrease in cAMP formation.[5] Endogenously, the neurotransmitter acetylcholine (ACh) exerts its physiological function, regulated by hormonal and neuronal mechanisms, *via* activation of all five muscarinic receptor subtypes. Early pharmacological studies suggested at least three MR subtypes[6], but it lasted until the early 1990s, when all five subtypes had been cloned, that the diversity in the muscarinic receptor family was fully accepted.[2] MRs are widely distributed in the human body: whereas all five MR subtypes are expressed in different parts of the central nervous system (CNS), the M_1R, M_2R, M_3R and M_5R are also located in the periphery (Table 1). Due to the broad distribution of MRs in the human organism and their involvement in numerous physiological processes, several diseases such as chronic obstructive pulmonary disease (COPD), overactive bladder, glaucoma and CNS related diseases like schizophrenia and Alzheimer's disease have been correlated to an impaired cholinergic signaling (Table 1).[7-14]

Table 1. Overview of MR subtypes, distribution, effector proteins and associated disease.

Subtype	Distribution	Effectors	Associated diseases
M_1R	○ CNS[15] ○ stomach[16]	G_q	○ Alzheimer's disease ○ peptic ulcers
M_2R	○ CNS[15] ○ PNS[17] ○ myocardium[15]	G_i (preferentially) G_s	○ Alzheimer's disease ○ cardiomyopathy ○ Chagas' disease
M_3R	○ CNS[15] ○ smooth muscles[18] ○ endocrine and exocrine glands[19] ○ urinary bladder[10]	G_q	○ overacting bladder (OAB) ○ chronic obstructive pulmonary disease (COPD) ○ glaucoma
M_4R	○ CNS[15]	G_i	○ Parkinson's disease
M_5R	○ CNS[15] ○ iris[20]	G_q	○ schizophrenia ○ dementia ○ drug addiction

All MR subtypes share a high degree of homology in the sequence constituting the acetylcholine (orthosteric) binding site. Therefore, the development of highly subtype selective, orthosterically binding MR ligands has been very challenging. The highly conserved Asp $103^{3.32}$ was suggested to be crucial for the activation of the receptors (as reported for many class A GPCRs) by agonist binding and for the binding of the majority of described antagonists, too.[21-23] In addition to the orthosteric binding site, MRs present various less conserved allosteric binding sites, which can be addressed by allosteric ligands modulating agonist or antagonist function.[24-29] The recently reported crystal structures of the M_1R (inactive state[23]), M_2R (inactive state[21], active state[29], and active state in complex with an allosteric modulator[29]), M_3R (inactive state[22]) and M_4R (inactive state[23]) provided insight into the binding of molecules to MRs, in particular for the understanding of the receptor subtype selectivity, ligand induced activation and binding of modulators to allosteric binding pockets.[30] Notably, the discovery of allosteric compounds, capable of selectively modulating one MR subtype, led to an increased application of the dualsteric ligand approach to MRs. Basically, the dualsteric ligand approach consists in connecting an orthosteric agonist or antagonist with an allosteric modulator in order to gain affinity by the interaction of the orthosteric pharmacophore with the endogenous ligand binding site, and selectivity through the interaction of the allosterically interacting moiety with an allosteric binding site.[24, 31-38]

1.2 Allosteric modulation of GPCRs and MRs

The development of the allosteric model was prompted by the observation that the activity of certain enzymes could be modified, in either a negative or a positive fashion, by the binding of ligands to sites that are topographically distinct from the substrate binding site.[39, 40] To describe this phenomenon the *cooperativity factor* (α) was introduced, which refers to the ability of an allosteric ligand to modulate the affinity of an orthosteric binder at the orthosteric binding site. The simplest allosteric GPCR model assumes that the binding of an allosteric ligand to its site modulates only the affinity of the orthosteric ligand and not the interaction between receptor and G-protein; this model is referred to as the allosteric ternary complex model (ATCM) (Figure 1A), first reported by Lefkowitz and coworkers.[41] In the ATCM, the crosstalk between the orthosteric and the allosteric ligand is governed by the ligand concentration, the equilibrium dissociation constants (K_A and K_B, respectively, *cf.* Figure 1A) and the cooperativity factor α (Figure 1A). Values of α between 0 and 1 indicate a negative cooperativity, whereas values higher that 1 indicate a positive cooperativity.[5] The allosteric two state model[42] (ATSM) (Figure 1B) is an extension of the classic ATCM in which additional parameters like the constitutive interconversion between an active and an inactive receptor state (R* and R, respectively) governed by the isomerization constant L (*cf.* Figure 1B), the ability of the orthosteric *and* the allosteric ligand to modulate the transition of the receptor between different states (governed by the parameters α and β, *cf.* Figure 1B), the ability of each ligand to allosterically modulate the affinity of other compounds (termed as “binding cooperativity”, γ, *cf.* Figure 1B) and the ability of either ligands to modulate the transition to an active receptor state when both ligands are bound, termed as “activation cooperativity” (δ, *cf.* Figure 1B), are taken into account.[5]

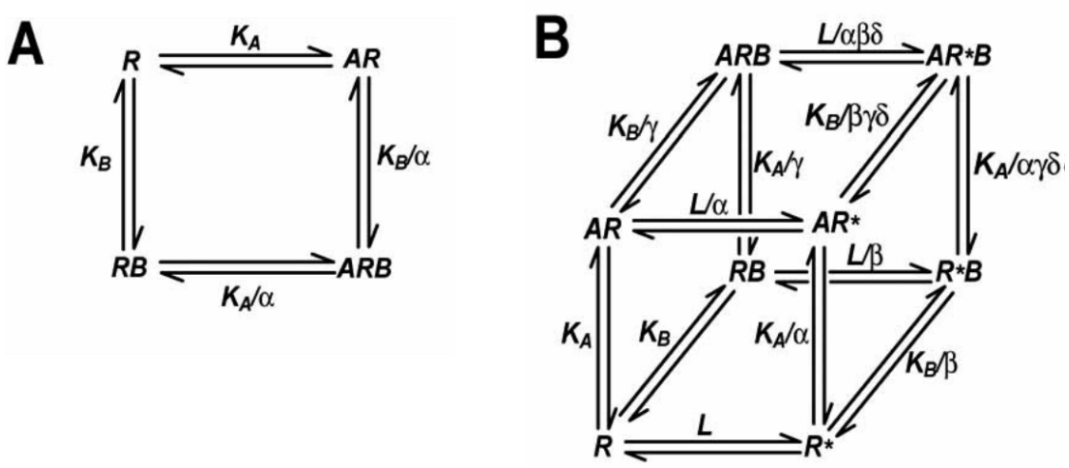

Figure 1. Allosteric GPCR models. A) The simple allosteric ternary complex model (ATCM), which describes the interaction between an orthosteric ligand, A, and allosteric modulator, B, in terms of their equilibrium dissociation constants (K_A, K_B) and the cooperativity factor, α, which describes the magnitude and direction of the allosteric effect on ligand binding affinity. B) The allosteric two state model (ATSM), which describes allosteric modulator effects on affinity, efficacy and the receptor equilibrium between active (R*) and inactive (R) states. L: isomerization constant; α and β: cooperativity factors; γ: "binding cooperativity"; δ: "activation cooperativity" (*cf.* section 1.2) (adapted from Gregory *et al.*[5]).

1.2.1 Methods to investigate allosteric interactions

1.2.1.1 Radioligand binding assays

Several approaches are described for studying allosteric mechanisms at GPCRs. One of the first evidences of a non-competitive interaction came from the observation that gallamine and hexamethonium-type compounds (i.e. W84, Figure 5) did not show a competitive interaction with the orthosteric antagonist [^{3}H]*N*-methylscopolamine ([^{3}H]NMS) at the muscarinic M_2 receptor.[43-45] Radioligand binding assays can directly provide represent data to deduce allosteric behavior.[46] For instance, [^{3}H]NMS saturation binding experiments performed at the M_2R in the presence of the negative allosteric modulator gallamine: the modulator is able to shift the radioligand binding curves to the right, and, most importantly, at progressively increasing concentrations of the allosteric modulator no further rightward shift of the saturation isotherm is observed.[47] Likewise, the negative allosteric modulator W84 is not able to fully "displace" [^{3}H]NMS (when used at a concentration resulting in a receptor occupancy $\rho > 0.80$) in equilibrium binding experiments at the M_2R (Figure 2, red curve). Moreover, allosteric modulators such as W84 cause a retardation of [^{3}H]NMS dissociation from the M_2R.[48, 49] By contrast, the positive allosteric modulator alcuronium is capable of enhancing [^{3}H]NMS binding at the M_2R (Figure 2, black curve). Notably, whereas a positive allosteric modulation can be easily identified by using radioligand binding assays due to the enhanced binding of the (orthosteric) radioligand to the receptor, the identification of a negative allosteric modulation based on radioligand

equilibrium studies is more difficult, as curves, comparable to those resulting from competitive interactions (especially if low radioligand concentrations ($\rho < 0.5$) are used), are obtained. One of the methods of choice to investigate competitive and non-competitive interaction at GPCRs is based on a "Schild-like" protocol relying radioligand saturation binding experiments in the presence of orthosteric or allosteric ligands. Whereas a competitive interaction will result in a parallel rightward shift of the saturation isotherms (with a slope not different from unity), a non-competitive interaction will lead to a partial and saturable curve shift (with a slope different from unity).[46, 50] Radioligand saturation binding studies in the presence of allosteric modulators were performed in order to prove allosteric binding of gallamine at the M_2R (radioligand: [^{3}H]NMS) and oleamide at the 5-HT_7 receptor (radioligand: [^{3}H]5-HT).[47, 51].

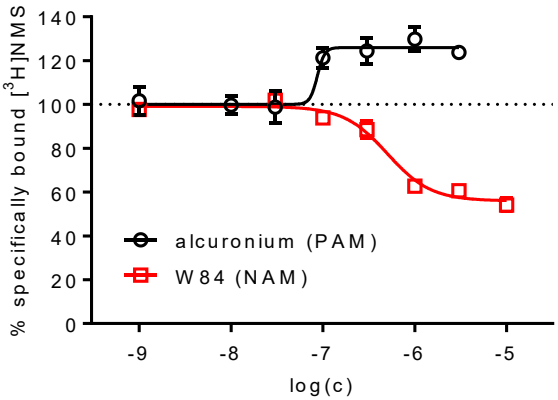

Figure 2. Concentration dependent effects of alcuronium (positive allosteric modulator, PAM) and W84 (negative allosteric modulator, NAM) on the equilibrium binding of [^{3}H]NMS (K_d = 0.09 nM) determined at live CHO-hM_2 cells. [^{3}H]NMS concentrations applied: 0.1 nM (ρ = 0.53, alcuronium) and 2.0 nM (ρ = 0.96 nM, W84). W84 concentration dependent curve was extrapolated from Chapter 2 (Figure 8C). Alcuronium binding experiments were performed according to the protocol for radioligand competition binding experiments described in Chapter 2 (experimental section).

1.2.1.2 Functional assays

Functional assays are often used to study allosterism at GPCRs. According to the simple ATCM (Figure 1), an allosteric modulator that effects the affinity of an orthosteric agonist, but not its efficacy, will cause a rightward (NAM) or leftward (PAM) saturable shift of the concentration-response curve of the agonist with no change in basal response, maximal response, curve shape and slope. In case of a positive cooperativity, the agonist curves would be shifted leftward relative to the agonist control curve. However, as in case of radioligand binding assays, negative allosteric modulation may be misinterpreted as competitive antagonism, particularly for modulators exhibiting a strong negative cooperativity.[46] A straightforward method to discriminate between competitive and non-competitive mechanisms is to perform a Schild analysis.[52] Regarding the M_2R, increasing concentrations of the allosteric modulator LY2119620 (Figure 5) caused a leftward shift of the concentration-response curves of a series of MR agonists (ACh, oxotremorine-M and iperoxo) (Figure 3) obtained from [^{35}S]GTPγS-binding assays.[53] Pitfalls related with functional studies of allosteric interactions include, for instance, non-equilibrium conditions and heterogeneous receptor populations.[54] Moreover, the occurrence of saturable agonist removal mechanisms (i.e. extraneuronal uptake or enzymatic breakdown), can lead to a misinterpretation of the experimental results.[46]

1.3 Muscarinic receptor ligands (MRs ligands)

1.3.1 MR agonists

The endogenous agonist for MRs and for nicotinic acetylcholine receptors (nAChRs) is acetylcholine (ACh) that binds to the five MRs with rather low affinity (K_i = 0.3-48 μM).[55, 56] Biochemically, acetylcholine is synthesized by various neurons that express the enzyme choline acetyltransferase by transferring an acetyl group from acetylCoA to choline. Due to the presence of a positively charged ammonium group, preventing the penetration of lipid membranes, and its susceptibility to hydrolytic and enzymatic cleavage, acetylcholine is not suited as a drug. Several MR agonists were described over the past decades with different MR subtype selectivity profiles. Methacholine (Figure 3), which is the β-methyl analog of ACh, is commercialized as a diagnostic bronchoconstrictor agent.[57] Notably, methacholine has little effect at nAChRs.[58] Pilocarpine and aceclidine (Figure 3) are M_3R agonists therapeutically used to treat glaucoma[59]; the M_1R and M_3R agonist cevimeline (Figure 3) is an FDA approved drug for the management of dry mouth associated with the Sjögren's syndrome.[60] Xanomeline (Figure 3) is a MR agonist with M_1R preference, which has been proposed as a promising therapeutic candidate for the treatment of Alzeheimer’s disease

and schizophrenia.[61, 62] Oxotremorine, oxotremorine-M and carbachol (CCh) (Figure 3) act as a non-selective MR agonists and they are common and useful pharmacological tools for experimental studies requiring M_1R-M_5R receptor activation. Iperoxo (Figure 3), structurally related with oxotemorine-M, exhibits an enhanced affinity compared to the parent compound. Moreover, at the M_2R, iperoxo behaves as a "superagonist" exceeding the maximal effect of both, the endogenous neurotransmitter ACh and oxotremorine, in activating G_i/G_s signaling, when investigated in cell dynamic mass redistribution and [^{35}S]GTPγS-binding assays.[63] Noteworthy, iperoxo was co-crystalized in complex with the hM_2R in the active state in the presence and in the absence of a positive allosteric modulator (LY2119620).[29] The thieno[2,3-*b*]pyridine derivative VU 10010 (Figure 3) was reported to be able to selectively enhance M_4R cholinergic signaling in animal models although an ago-allosteric mechanism (that refers to modulators able to activate the receptor on their own *and* to enhance the binding of orthosteric agonists)[64] rather than an orthosteric interaction seems to be involved.[65]

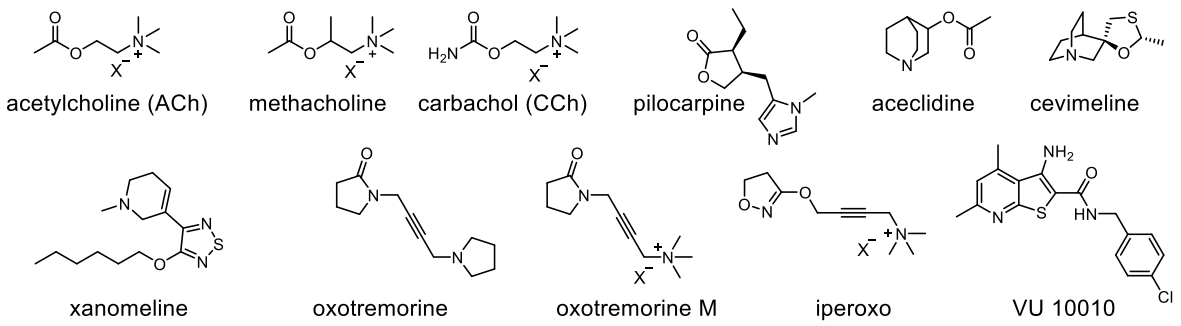

Figure 3. Structures of selected MR agonists reported in literature.

1.3.2 MR antagonists

For centuries, traditional and popular medicine has used the naturally occurring alkaloids atropine and scopolamine (Figure 4) to block the cholinergic transmission, although the lack of MR subtype selectivity is responsible for severe side effects associated with these alkaloids.[66] Muscarinic M_1 receptors are abundantly expressed in all major forebrain areas including the cerebral cortex, the hippocampus, and the striatum.[67] Several reports suggested that selective antagonism at M_1 receptors in the CNS promotes cognitive decline and memory impairment.[68] For instance, Prado-Alcalà and coworkers demonstrated that rats treated with the M_1R antagonists trihexyphenidyl and biperiden (Figure 4) showed a consistent loss of memory consolidation compared to the control, confirming the pivotal role of central M_1Rs for cognitive functions.[69] Notably, due to its inability to cross the blood-brain barrier (BBB), the M_1R antagonist pirenzepine (Figure 4) has been used for decades to treat peptic ulcers. Selective M_2R antagonism increases cholinergic neuronal transmission, in

both the brain and the periphery, by reducing autoreceptor function. In the last decades, several authors[70-74] suggested selective M_2 receptor antagonists or compounds acting as M_2R antagonists and M_1R agonists as a therapeutic approach to enhance cholinergic function in Alzheimer's disease, in particular at a stage where cholinergic tone is not completely lost.[15] Several attempts have been made in order to design selective M_2R antagonists. DIBA[75] and BIBN 99[76] (Figure 4) are tricyclic compounds with high affinity for the M_2R (pK_i = 9.52 and 7.52, respectively) and represent privileged scaffolds to develop selective M_2R antagonists. Interestingly, it was shown that BIBN 99 is mainly active in the CNS.[76] In addition, compounds structurally related to the alkaloid himbacine (Figure 4) were suggested as promising selective M_2R antagonists, although clinical data have not yet been reported.[77-80]. Muscarinic M_3 receptor blockade is one of the oldest treatments of asthma.[15] Moreover, M_3R antagonism is therapeutically relevant for the treatment of diseases like chronic obstructive pulmonary disease (COPD), overactive bladder (OAB) and hyperactive smooth muscle associated disorders. For instance tolterodine (Figure 4), which was reported to show a selective M_3 antagonism *in vivo*, and darifenacin (Figure 4) are approved drugs for the treatment of OAB. The bicyclic antagonist tiotropium (Figure 4), which was co-crystalized in complex with the hM_3R by Kobilka and coworkers[22], is still a blockbuster for the treatment of COPD. The M_4R is expressed in the corpus striatum, and it was suggested that M_4R activation exerts an inhibitory effect on dopamine D_1 receptor function.[81] Therefore, selective M_4R antagonists were developed for the treatment of Parkinson's disease (which is caused by impaired dopaminergic transmission). For instance, the benzoxazine derivative PD 0298029[82] (Figure 4) was described as a promising selective M_4R antagonist, although the poor bioavailability and the rapid metabolism in animal studies limited its use for *in vivo* research.[83] The M_5R is expressed by the dopamine-containing neurons of the pars compacta of the substantia nigra.[84] Thus, M_5R antagonism may be a useful approach to novel therapeutics for the treatment of both schizophrenia and compound addiction. However, only a few reports on selective M_5R antagonists can be found. For instance, the isoxazole derivative VU0488130 (Figure 4) was described as a lead for the development of new M_5R antagonists, showing more than 50-fold higher antagonism at the M_5R compared to the other MR subtypes (IC_{50}: M_5R = 0.45 µM; M_1-M_4R > 30 µM).[85]

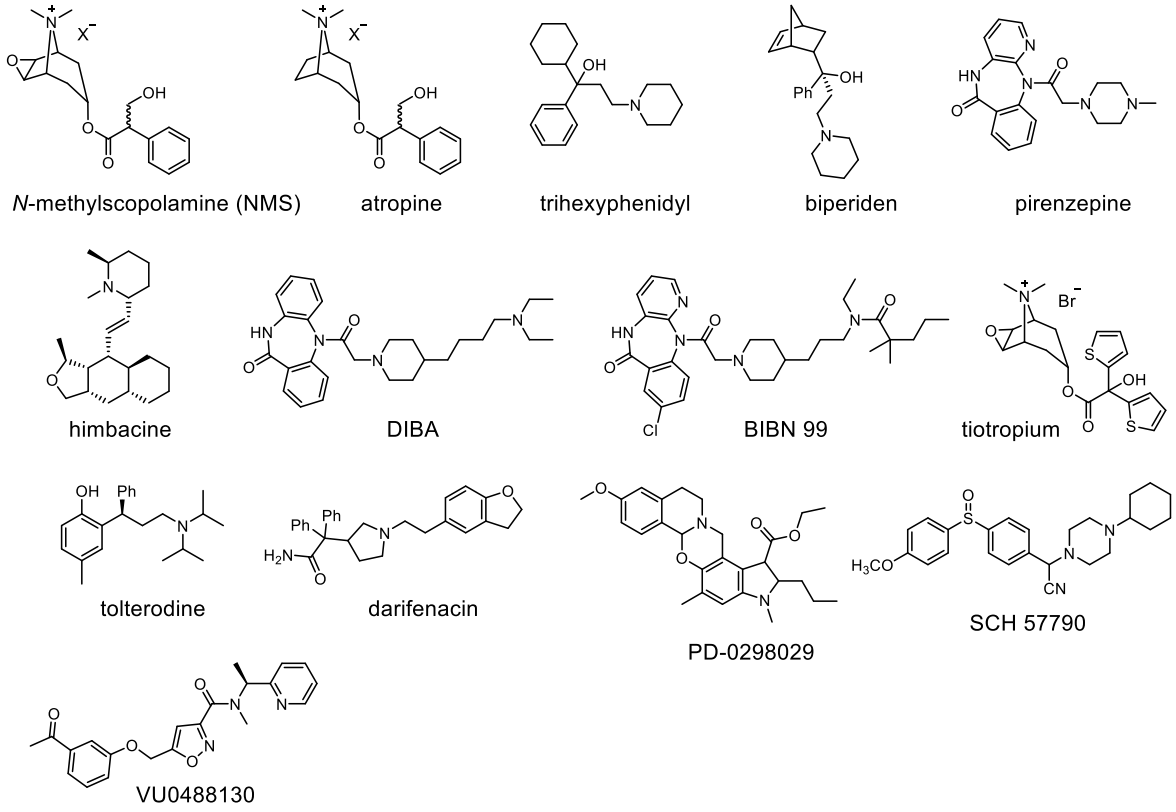

Figure 4. Structures of selected MR antagonists reported in the literature.

1.3.3 MR allosteric modulators

In the late 1960s, it was reported for the first time that a non-competitive interaction between the orthosteric mAchR agonist carbachol and neuromuscular blocking agents such as gallamine, or alkene-ammonium compounds such as W84 (Figure 5), had been observed.[43, 44] Later on, numerous negative (NAM) and positive (PAM) allosteric modulators were described for the five MR subtypes. BQCA (PAM) for the M_1R[86], W84 (NAM), LY2119620 (PAM) and alcuronium (PAM) for the M_2R[43, 49, 53, 87], brucine (PAM) for the M_2/M_3[55, 88], LY2033298 (PAM) for the M_4[89], and VU-0238429 (PAM) for the M_5R[90] (Figure 5) are only a few examples of numerous MR modulators reported in literature. In addition, several putative allosteric agonists, able to activate the receptor on their own by binding to an allosteric site, were identified.[91] The recently reported M_2R structure in the active state, co-crystalized in complex with the agonist iperoxo and the positive allosteric modulator LY2119620 (Figure 5), gave, for the first time, an insight into the receptor residues involved in the formation of the “common” allosteric binding vestibule.[29] Notably, it was suggested that various allosteric sites are present in MRs although their exact locations are still unknown.[31, 92, 93] Due to the improved selectivity profiles compared to orthosteric ligands, and to the ability to modulate, positively or negatively, the action of the endogenous neurotransmitter ACh, the design of allosteric modulators emerged as an attractive

approach to target and regulate MRs. However, no high-affinity (K_i < 0.1 µM) MR allosteric modulators are reported to date.[37]

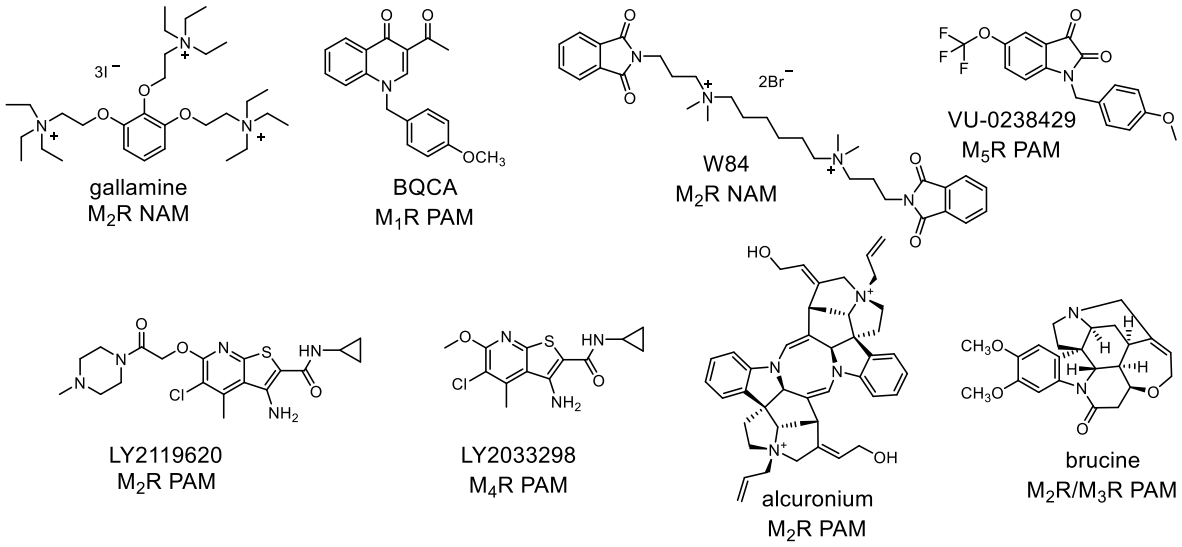

Figure 5. Representative MR allosteric modulators reported in literature.

1.3.4 Dualsteric/bitopic MR ligands

The dualsteric/bitopic ligand approach, i.e. the design of compounds, which interact simultaneously with the orthosteric and an allosteric receptor binding site, has emerged as a promising strategy to design high-affinity selective GPCR ligands.[31-33, 35-38] A straight forward method of developing dualsteric ligands is the connection of an orthosteric ligand to an allosteric modulator through a linker.[34, 94] However, also non-dimeric ligands such as the M_2R partial agonist McN-A-343 (Figure 6A), were recently suggested to interact with both the orthosteric and the "common" allosteric binding site of the M_2R.[95] To back this up, the binding of McN-A-343 was shown to be sensitive to the mutation of the key residue Asp $103^{3.32}$ of the orthosteric site, and to the mutation of Tyr 177^{ECL2}, which is part of the allosteric vestibule of the M_2 receptor.[96] Analogously, there is experimental evidence that the agonists AC-42 and 77-LH-28-1 (Figure 6A) interact dualsterically with the M_1R.[97-99] Regarding the M_2R, Holzgrabe and coworkers synthesized and pharmacologically characterized a series of dualsteric/bitopic binders constructed by linking an orthosteric agonist (iperoxo) or antagonist (NMS, atropine) with an allosterically interacting phthalimide moiety (derived from the allosteric modulator W84) through an aliphatic carbon chain (Figure 6B).[100] Steinfeld and coworkers reported the synthesis of a potent M_2R antagonist, THRX-160209 (Figure 6B), designed by connecting the orthosterically binding moiety 3-BHP with the allosteric scaffold 4-ABP (Figure 6B). Data from radioligand binding experiments suggested that THRX-160209 is able to interact with both the orthosteric and the allosteric site at the M_2R. Interestingly, the M_2R affinity of THRX-160209 was several orders of magnitudes

higher compared to the single entities 3-BHP and 4-ABP (M_2R pK_i: 9.51 (THRX-160209), 5.39 (3-BHP) and 5.70 (4-ABP)).[101]

In addition, to improved selectivity and receptor affinity, it was suggested that dualsteric ligands can be capable of inducing biased signaling at a pleiotropic receptor. To endorse this hypothesis, M_2R binding of iper-6-phth (Figure 6B) was shown to result in a selective activation of the G_i, but not the G_s signaling pathway, demonstrating functional selectivity of this compound.[102, 103] Moreover, recently, Bock and coworkers suggested that not only the choice of the allosteric and orthosteric pharmacophoric groups, but also the variation of the linker, which directs the orientation of these pharmacophores towards each other and the receptor, allow the design of biased M_2R ligands associated to different signaling phenotypes.[102] The benzimidazolinone derivative TBPB (Figure 6A) was described as a M_1R selective allosteric agonist[104], before its dualsteric binding mode was unveiled by the use of structurally truncated analogs of this ligand.[105]

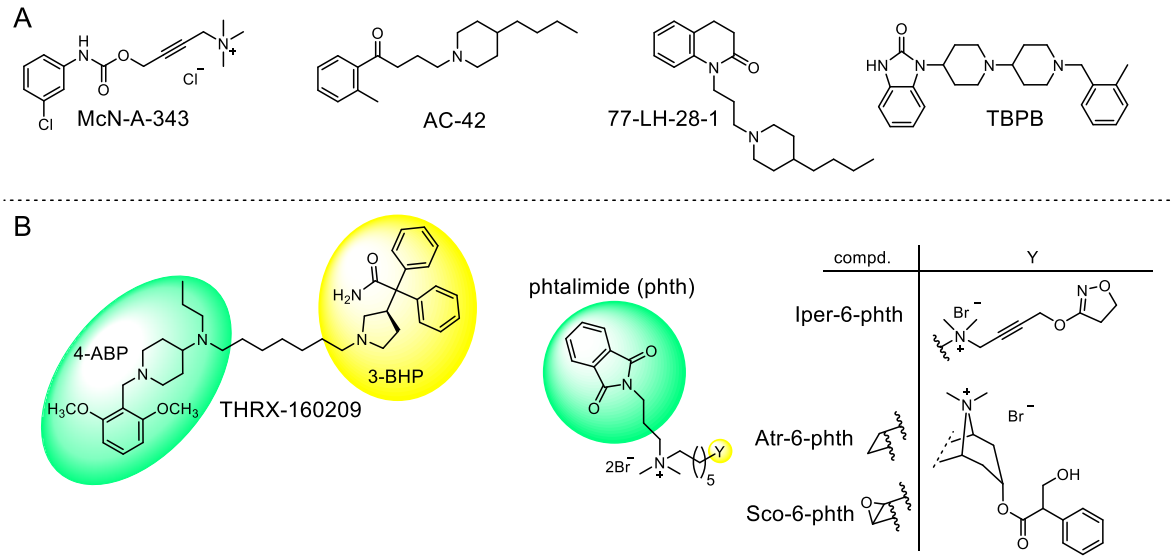

Figure 6. (A) MR ligands reported to interact in a dualsteric manner. (B) Examples of rationally designed dualsteric M_2R modulators obtained by connecting orthosterically (yellow) with allosterically binding ligands (green) through a linker.

1.3.5 Dimeric MR ligands

Numerous studies suggested that GPCRs can form dimers or higher ordered oligomers.[106] Regarding MRs, it was suggested that the M_1, M_2 and the M_3 receptor can homodimerize.[107-109] The formation of MR heterodimers (e.g. M_1/M_2, M_2/M_3, M_1/M_3) was suggested, too.[107] Although many factors have to be considered for the design of bivalent ligands that are able to "bridge" GPCR dimers (choice of the pharmacophore, point of attachment and structure of the linker), homo- and heterobivalent GPCR ligands are considered potential tools to investigate receptor dimerization.[106, 110-112] It should be mentioned that there is no sharp differentiation between a heterodimeric or heterobivalent and a dualsteric ligand (*cf*. section 1.3.4). The term "dualsteric ligand" is usually preferred for compounds, which are supposed to address different binding sites of a single receptor protomer, in particular in the MR field.

Homo and heterobivalent MR ligands derived from the agonist xanomeline (Figure 7) were reported to exhibit higher M_2R affinity compared to the monomeric ligand[113, 114], whereas the multimeric antagonist tripitramine (Figure 7) was suggested to interact with numerous binding sites at the MRs.[115] Moreover, two DIBA-derived (*cf*. Figure 4) dibenzodiazepinone-type homodimeric MR ligands (UNSW-MK250 and UNSW-MK262, Figure 7), exhibiting high M_2R affinity, were recently reported.[116]

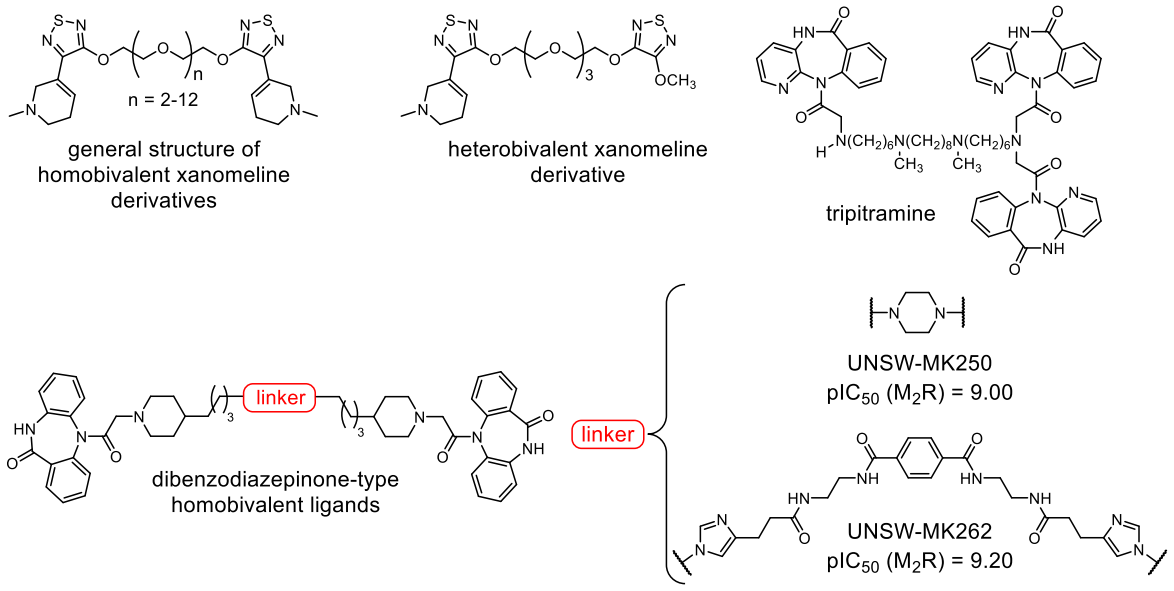

Figure 7. Examples of reported homo and heterobivalent M_2R ligands.

1.4 Radioligands for MRs

The first GPCR radioligand binding assay was described in 1970 by Lefkowitz and coworkers using a [^{125}I]-adrenocorticotropic hormone to determine its binding affinity at adrenocorticotropic receptors.[117] Since then, ^{3}H- or ^{125}I-labeled ligands have been widely used to determine the affinity of GPCR ligands.[118] Today, radioligand-based assays are still routinely used in many laboratories due to their robustness and reproducibility. Over the years, several tritium-labeled MR ligands were produced and characterized. Due to their high affinity at all five MR subtypes and their high stability, the radiolabeled antagonists [^{3}H]*N*-methylscopolamine ([^{3}H]NMS) and [^{3}H]quinuclidin-3-yl-benzilate ([^{3}H]QNB) (Table 2) have been predominantly used. Concerning MR agonists, the endogenous neurotransmitter ACh was recently tritium labeled to unveil the positive allosteric cooperativity between thiochrome and ACh at the M_4R.[119]. The tritium-labeled MR agonist [^{3}H]oxotremorine-M was used, e.g., for binding studies at solubilized MRs from rat myocardium.[120, 121] The MR antagonist [^{3}H]darifenacin was synthesized by Pfizer as the first M_3R selective radioligand (Table 2).[122] Several tricyclic MR antagonists were tritium labeled during the last decades. For instance, saturation binding studies with [^{3}H]pirenzepine (Table 2) were performed at different tissue preparations to show the ability of pirenzepine to discriminate between different MR subtypes by selective binding to the M_1R.[1] Telenzepine, a bioisosteric analog of pirenzepine, was reported to exhibit an increased M_1R affinity compared to pirenzepine (pK_i (M_1R): 9.4 *vs*. 7.9).[123, 124] Thus, a tritiated analog of telenzepine (Table 2) was synthesized as a M_1R selective radioligand with improved affinity. Using [^{3}H]telenzepine, the two atropisomeric forms (due to the slow rotation of the exocyclic amide bond, there exist two stable isomers of telenzepine) were shown to exhibit different M_1R affinities.[124, 125] The pyridobenzodiazepinone-type MR antagonist AF-DX 384 (Table 2) was radiolabeled in order to investigate its binding mode at the M_2R. Based on radioligand binding studies with [^{3}H]AF-DX 384, a bitopic/dualsteric binding mode of AF-DX 384 at the M_2R was suggested.[48] The synthesis of tritium-labeled analogs of allosteric MR modulators was reported as a useful approach to investigate allosterism at MRs. For instance, the tritiated versions of the allosteric modulators dimethyl-W84 and LY2119620 (Table 2) were synthesized in order to study allosteric modulation at the M_2R.[126, 127]

Table 2. Overview of reported tritium-labeled MR ligands.

Radioligand	Structure	agonist/ antagonist/ allosteric modulator
[^{3}H]acetylcholine	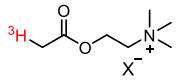	agonist
[^{3}H]oxotremorine-M	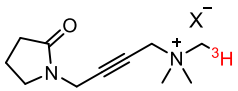	agonist
[^{3}H]NMS	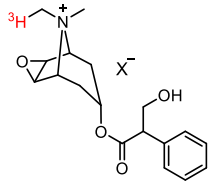	antagonist
[^{3}H]QNB	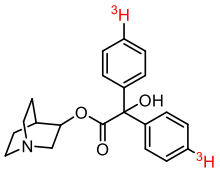	antagonist
[^{3}H]tiotropium	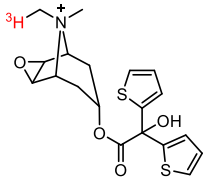	antagonist
[^{3}H]darifenacin	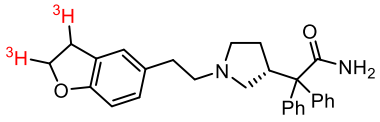	antagonist
[^{3}H]4-DAMP	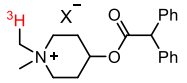	antagonist
[^{3}H]pirenzepine	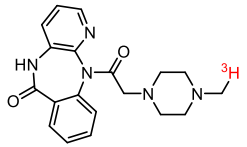	antagonist
[^{3}H]telenzepine*	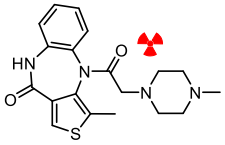	antagonist
[^{3}H]AF-DX 384	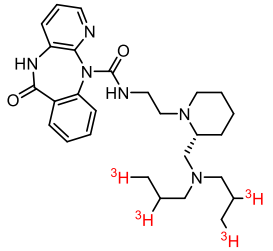	antagonist
[^{3}H]dimethyl W84	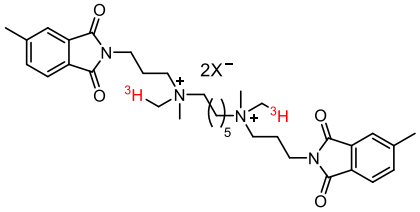	allosteric modulator
[^{3}H]LY2119620	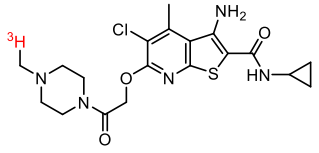	allosteric modulator

*The position of the tritium isotopes is not specified in the literature.

1.5 Scope and objectives

The family of muscarinic acetylcholine receptors (MRs) comprises five different subtypes, named M_1R-M_5R, that are widely distributed in the human body, being expressed in both the CNS and the periphery. Various diseases such as Alzheimer's disease, chronic obstructive pulmonary disease (COPD), overacting bladder (OAB) and glaucoma are associated with impaired cholinergic signaling. Due to the high conservation of the orthosteric (acetylcholine) binding pocket within the MR subtypes, the development of highly subtype-selective MR ligands has been extremely challenging. Thus, there is still a need for highly selective molecular tools and therapeutics acting at MRs. As MRs comprise several less conserved accessory (allosteric) binding sites, various allosteric MR ligands (modulators) were reported; however, allosteric modulators with high affinity are still lacking. The dualsteric ligand approach, that is, the design of ligands, which interact simultaneously with the orthosteric pocket and an allosteric site, was suggested as a promising strategy to develop high-affinity and selective ligands.[24, 31-38] A rational design of (dualsteric) MR ligands is supposed to benefit from the reported crystal structures of the M_1R-M_4R.[21-23, 29]

Recently, a series of M_2 subtype-preferring dibenzodiazepinone-type MR ligands derived from the M_2R antagonist DIBA, comprising two high-affinity homodimeric analogs, was synthesized and investigated in terms of MR binding.[116] This class of compounds represents interesting MR ligands, including leads for the development of highly selective M_2R antagonists. Therefore, this doctoral thesis was aiming at an elucidation of the M_2R binding mode of monomeric and dimeric dibenzodiazepinone-type ligands by means of preparing and studying radiolabeled and fluorescently labeled derivatives. Moreover, the development of dibenzodiazepinone-type MR ligands with improved M_2R selectivity was envisaged.

In order to get access to radiolabeld dimeric dibenzodiazepinone-type ligands, which can be conveniently prepared from commercially available labeling reagents such as succinimidyl [^{3}H]propionate, compounds containing a linker with a primary amino group in the center, had to be designed and prepared (Figure 8). Moreover, a monomeric and a dimeric [^{3}H]propionylated dibenzodiazepinone derivative had to be synthesized and investigated by saturation binding studies (including experiments in the presence of reported allosteric M_2R ligands), association and dissociation experiments, and equilibrium binding (competition binding) studies involving various orthosteric and allosteric MR ligands. Molecular dynamics simulations (up to 3 µs) of the M_2R bound to selected compounds (for instance the "cold" forms of the studied radiolabeled dibenzodiazepinone derivatives) had been considered to investigate the M_2R binding mode by computational methods.

In addition, a small series of fluorescently labeled dibenzodiazepinone-type MR ligands (including two homodimeric derivatives) had to be prepared using red-emitting cyanine dyes. The fluorescent ligands had to be characterized with respect to M_2R binding using flow cytometry, high-content imaging analysis and confocal microscopy.

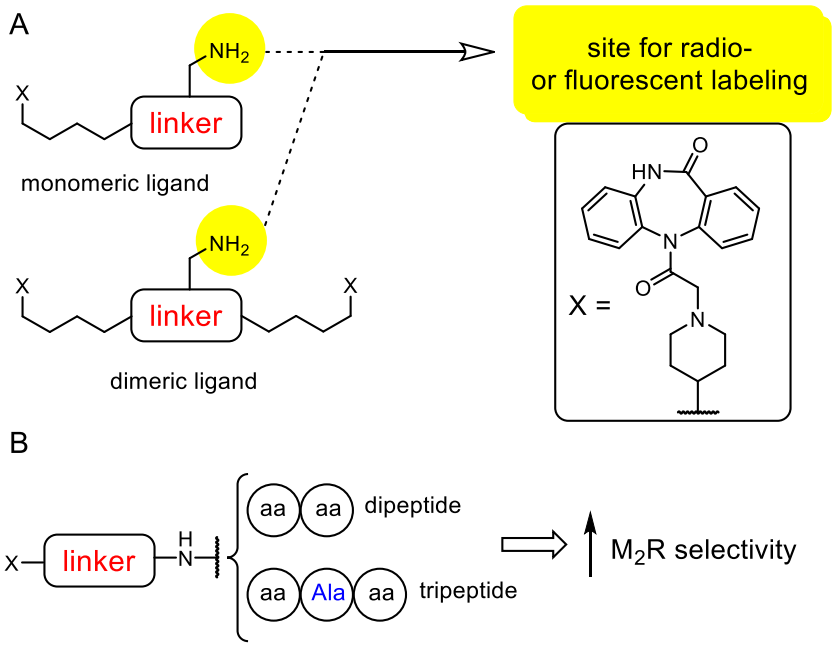

Figure 8. Schematic representation of the scope of the thesis. (A) Structure of amino-functionalized monomeric and homodimeric dibenzodiazepinone-type MR ligands to be used as precursors for radio- and fluorescence labeling. (B) General structure of dibenzodiazepinone-type MR ligands conjugated to short peptides.

Finally, the dibenzodiazepinone pharmacophore had to be conjugated to various di- and tripeptides *via* two different linkers as a new approach to improve the M_2R selectivity (Figure 8). The affinity and the selectivity profile of these compounds had to be assessed by radioligand competition binding studies at CHO-hM_xR cells (x = 1-5) using the antagonist [^{3}H]NMS as orthosteric radioliganand.

1.6 References

(1) Hammer, R.; Berrie, C. P.; Birdsall, N. J.; Burgen, A. S.; Hulme, E. C. Pirenzepine distinguishes between different subclasses of muscarinic receptors. *Nature* **1980,** *283*, 90-92.

(2) Bonner, T. I.; Buckley, N. J.; Young, A. C.; Brann, M. R. Identification of a family of muscarinic acetylcholine receptor genes. *Science* **1987,** *237*, 527-532.

(3) Caulfield, M. P. Muscarinic receptors--characterization, coupling and function. *Pharmacol. Ther.* **1993,** *58*, 319-379.

(4) Caulfield, M. P.; Birdsall, N. J. International Union of Pharmacology. XVII. Classification of muscarinic acetylcholine receptors. *Pharmacol. Rev.* **1998,** *50*, 279-290.

(5) Gregory, K. J.; Sexton, P. M.; Christopoulos, A. Allosteric modulation of muscarinic acetylcholine receptors. *Curr. Neuropharmacol.* **2007,** *5*, 157-167.

(6) Birdsall, N. J. M.; Hulme, E. C. Muscarinic receptor subclasses. *Trends Pharmacol. Sci.* **1983,** *4*, 459-463.

(7) Borda, E. S.; Sterin-Borda, L. Antiadrenergic and muscarinic receptor antibodies in Chagas' cardiomyopathy. *Int. J. Cardiol.* **1996,** *54*, 149-156.

(8) Dean, B.; Bymaster, F. P.; Scarr, E. Muscarinic receptors in schizophrenia. *Curr. Mol. Med.* **2003,** *3*, 419-426.

(9) Clader, J. W.; Wang, Y. Muscarinic receptor agonists and antagonists in the treatment of Alzheimer's disease. *Curr. Pharm. Des.* **2005,** *11*, 3353-3361.

(10) Abrams, P.; Andersson, K. E.; Buccafusco, J. J.; Chapple, C.; de Groat, W. C.; Fryer, A. D.; Kay, G.; Laties, A.; Nathanson, N. M.; Pasricha, P. J.; Wein, A. J. Muscarinic receptors: their distribution and function in body systems, and the implications for treating overactive bladder. *Br. J. Pharmacol.* **2006,** *148*, 565-578.

(11) Fowler, C. J.; Griffiths, D.; de Groat, W. C. The neural control of micturition. *Nat. Rev. Neurosci.* **2008,** *9*, 453-466.

(12) Peretto, I.; Petrillo, P.; Imbimbo, B. P. Medicinal chemistry and therapeutic potential of muscarinic M3 antagonists. *Med. Res. Rev.* **2009,** *29*, 867-902.

(13) Almasieh, M.; Zhou, Y.; Kelly, M. E.; Casanova, C.; Di Polo, A. Structural and functional neuroprotection in glaucoma: role of galantamine-mediated activation of muscarinic acetylcholine receptors. *Cell Death Dis.* **2010,** *1*, e27.

(14) Dean, B.; Scarr, E. Possible involvement of muscarinic receptors in psychiatric disorders: a focus on schizophrenia and mood disorders. *Curr. Mol. Med.* **2015,** *15*, 253-264.

(15) Eglen, R. M. Overview of muscarinic receptor subtypes. *Handb. Exp. Pharmacol.* **2012**, 3-28.

(16) Nelson, D. K.; Pieramico, O.; Dahmen, G.; Dominguez-Munoz, J. E.; Malfertheiner, P.; Alder, G. M1-muscarinic mechanisms regulate interdigestive cycling of motor and secretory activity in human upper gut. *Dig. Dis. Sci.* **1996,** *41*, 2006-2015.

(17) Calcutt, N. A.; Smith, D. R.; Frizzi, K.; Sabbir, M. G.; Chowdhury, S. K.; Mixcoatl-Zecuatl, T.; Saleh, A.; Muttalib, N.; Van der Ploeg, R.; Ochoa, J.; Gopaul, A.; Tessler, L.; Wess, J.; Jolivalt, C. G.; Fernyhough, P. Selective antagonism of muscarinic receptors is neuroprotective in peripheral neuropathy. *J. Clin. Invest.* **2017,** *127*, 608-622.

(18) Ehlert, F. J.; Ostrom, R. S.; Sawyer, G. W. Subtypes of the muscarinic receptor in smooth muscle. *Life Sci.* **1997,** *61*, 1729-1740.

(19) Beroukas, D.; Goodfellow, R.; Hiscock, J.; Jonsson, R.; Gordon, T. P.; Waterman, S. A. Up-regulation of M3-muscarinic receptors in labial salivary gland acini in primary Sjogren's syndrome. *Lab. Invest.* **2002,** *82*, 203-210.

(20) Gil, D. W.; Krauss, H. A.; Bogardus, A. M.; WoldeMussie, E. Muscarinic receptor subtypes in human iris-ciliary body measured by immunoprecipitation. *Invest. Ophthalmol. Vis. Sci.* **1997,** *38*, 1434-1442.

(21) Haga, K.; Kruse, A. C.; Asada, H.; Yurugi-Kobayashi, T.; Shiroishi, M.; Zhang, C.; Weis, W. I.; Okada, T.; Kobilka, B. K.; Haga, T.; Kobayashi, T. Structure of the human M2 muscarinic acetylcholine receptor bound to an antagonist. *Nature* **2012,** *482*, 547-551.

(22) Kruse, A. C.; Hu, J.; Pan, A. C.; Arlow, D. H.; Rosenbaum, D. M.; Rosemond, E.; Green, H. F.; Liu, T.; Chae, P. S.; Dror, R. O.; Shaw, D. E.; Weis, W. I.; Wess, J.; Kobilka, B. K. Structure and dynamics of the M3 muscarinic acetylcholine receptor. *Nature* **2012,** *482*, 552-556.

(23) Thal, D. M.; Sun, B.; Feng, D.; Nawaratne, V.; Leach, K.; Felder, C. C.; Bures, M. G.; Evans, D. A.; Weis, W. I.; Bachhawat, P.; Kobilka, T. S.; Sexton, P. M.; Kobilka, B. K.; Christopoulos, A. Crystal structures of the M1 and M4 muscarinic acetylcholine receptors. *Nature* **2016,** *531*, 335-340.

(24) Mohr, K.; Trankle, C.; Holzgrabe, U. Structure/activity relationships of M2 muscarinic allosteric modulators. *Recept. Channels* **2003,** *9*, 229-240.

(25) Voigtlander, U.; Johren, K.; Mohr, M.; Raasch, A.; Trankle, C.; Buller, S.; Ellis, J.; Holtje, H. D.; Mohr, K. Allosteric site on muscarinic acetylcholine receptors: identification of two amino acids in the muscarinic M2 receptor that account entirely for the M2/M5 subtype selectivities of some structurally diverse allosteric ligands in N-methylscopolamine-occupied receptors. *Mol. Pharmacol.* **2003,** *64*, 21-31.

(26) Wess, J. Allosteric binding sites on muscarinic acetylcholine receptors. *Mol. Pharmacol.* **2005,** *68*, 1506-1509.

(27) Presland, J. Identifying novel modulators of G protein-coupled receptors via interaction at allosteric sites. *Curr. Opin. Drug Discov. Dev.* **2005,** *8*, 567-576.

(28) Conn, P. J.; Christopoulos, A.; Lindsley, C. W. Allosteric modulators of GPCRs: a novel approach for the treatment of CNS disorders. *Nat. Rev. Drug Discov.* **2009,** *8*, 41-54.
(29) Kruse, A. C.; Ring, A. M.; Manglik, A.; Hu, J.; Hu, K.; Eitel, K.; Hubner, H.; Pardon, E.; Valant, C.; Sexton, P. M.; Christopoulos, A.; Felder, C. C.; Gmeiner, P.; Steyaert, J.; Weis, W. I.; Garcia, K. C.; Wess, J.; Kobilka, B. K. Activation and allosteric modulation of a muscarinic acetylcholine receptor. *Nature* **2013,** *504*, 101-106.
(30) Shonberg, J.; Kling, R. C.; Gmeiner, P.; Lober, S. GPCR crystal structures: Medicinal chemistry in the pocket. *Biorg. Med. Chem.* **2015,** *23*, 3880-3906.
(31) Birdsall, N. J. M.; Lazareno, S. Allosterism at muscarinic receptors: ligands and mechanisms. *Mini-Rev. Med. Chem.* **2005,** *5*, 523-543.
(32) Antony, J.; Kellershohn, K.; Mohr-Andra, M.; Kebig, A.; Prilla, S.; Muth, M.; Heller, E.; Disingrini, T.; Dallanoce, C.; Bertoni, S.; Schrobang, J.; Trankle, C.; Kostenis, E.; Christopoulos, A.; Holtje, H. D.; Barocelli, E.; De Amici, M.; Holzgrabe, U.; Mohr, K. Dualsteric GPCR targeting: a novel route to binding and signaling pathway selectivity. *FASEB J.* **2009,** *23*, 442-450.
(33) De Amici, M.; Dallanoce, C.; Holzgrabe, U.; Trankle, C.; Mohr, K. Allosteric ligands for G protein-coupled receptors: a novel strategy with attractive therapeutic opportunities. *Med. Res. Rev.* **2010,** *30*, 463-549.
(34) Mohr, K.; Trankle, C.; Kostenis, E.; Barocelli, E.; De Amici, M.; Holzgrabe, U. Rational design of dualsteric GPCR ligands: quests and promise. *Br. J. Pharmacol.* **2010,** *159*, 997-1008.
(35) Valant, C.; Robert Lane, J.; Sexton, P. M.; Christopoulos, A. The best of both worlds? Bitopic orthosteric/allosteric ligands of g protein-coupled receptors. *Annu. Rev. Pharmacool. Toxicol.* **2012,** *52*, 153-178.
(36) Lane, J. R.; Sexton, P. M.; Christopoulos, A. Bridging the gap: bitopic ligands of G-protein-coupled receptors. *Trends Pharmacol. Sci.* **2013,** *34*, 59-66.
(37) Kruse, A. C.; Kobilka, B. K.; Gautam, D.; Sexton, P. M.; Christopoulos, A.; Wess, J. Muscarinic acetylcholine receptors: novel opportunities for drug development. *Nat. Rev. Drug Discov.* **2014,** *13*, 549-560.
(38) Christopoulos, A. Advances in G protein-coupled receptor allostery: from function to structure. *Mol. Pharmacol.* **2014,** *86*, 463-478.
(39) Monod, J.; Jacob, F. Teleonomic mechanisms in cellular metabolism, growth, and differentiation. *Cold Spring Harb. Symp. Quant. Biol.* **1961,** *26*, 389-401.
(40) Monod, J.; Changeux, J. P.; Jacob, F. Allosteric proteins and cellular control systems. *J. Mol. Biol.* **1963,** *6*, 306-329.

(41) De Lean, A.; Stadel, J. M.; Lefkowitz, R. J. A ternary complex model explains the agonist-specific binding properties of the adenylate cyclase-coupled beta-adrenergic receptor. *J. Biol. Chem.* **1980,** *255*, 7108-7117.

(42) Hall, D. A. Modeling the functional effects of allosteric modulators at pharmacological receptors: an extension of the two-state model of receptor activation. *Mol. Pharmacol.* **2000,** *58*, 1412-1423.

(43) Lullmann, H.; Ohnesorge, F. K.; Schauwecker, G. C.; Wassermann, O. Inhibition of the actions of carbachol and DFP on guinea pig isolated atria by alkane-bis-ammonium compounds. *Eur. J. Pharmacol.* **1969,** *6*, 241-247.

(44) Clark, A. L.; Mitchelson, F. The inhibitory effect of gallamine on muscarinic receptors. *Br. J. Pharmacol.* **1976,** *58*, 323-331.

(45) Stockton, J. M.; Birdsall, N. J.; Burgen, A. S.; Hulme, E. C. Modification of the binding properties of muscarinic receptors by gallamine. *Mol. Pharmacol.* **1983,** *23*, 551-557.

(46) Christopoulos, A.; Kenakin, T. G protein-coupled receptor allosterism and complexing. *Pharmacol. Rev.* **2002,** *54*, 323-374.

(47) Gregory, K. J.; Sexton, P. M.; Christopoulos, A. Overview of receptor allosterism. *Curr. Protoc. Pharmacol.* **2010,** *Chapter 1*, Unit 1 21.

(48) Trankle, C.; Andresen, I.; Lambrecht, G.; Mohr, K. M2 receptor binding of the selective antagonist AF-DX 384: possible involvement of the common allosteric site. *Mol. Pharmacol.* **1998,** *53*, 304-312.

(49) Trankle, C.; Mies-Klomfass, E.; Cid, M. H.; Holzgrabe, U.; Mohr, K. Identification of a [3H]Ligand for the common allosteric site of muscarinic acetylcholine M2 receptors. *Mol. Pharmacol.* **1998,** *54*, 139-145.

(50) Hulme, E. C.; Trevethick, M. A. Ligand binding assays at equilibrium: validation and interpretation. *Br. J. Pharmacol.* **2010,** *161*, 1219-1237.

(51) Hedlund, P. B.; Carson, M. J.; Sutcliffe, J. G.; Thomas, E. A. Allosteric regulation by oleamide of the binding properties of 5-hydroxytryptamine7 receptors. *Biochem. Pharmacol.* **1999,** *58*, 1807-1813.

(52) Arunlakshana, O.; Schild, H. O. Some quantitative uses of drug antagonists. *Br. J. Pharmacol. Chemother.* **1959,** *14*, 48-58.

(53) Croy, C. H.; Schober, D. A.; Xiao, H.; Quets, A.; Christopoulos, A.; Felder, C. C. Characterization of the novel positive allosteric modulator, LY2119620, at the muscarinic M(2) and M(4) receptors. *Mol. Pharmacol.* **2014,** *86*, 106-115.

(54) Kenakin, T. *Pharmacologic Analysis of Drug-Receptor Interaction, 3rd edition*. Lippincott Williams & Wilkins: **1997**.

(55) Jakubik, J.; Bacakova, L.; El-Fakahany, E. E.; Tucek, S. Positive cooperativity of acetylcholine and other agonists with allosteric ligands on muscarinic acetylcholine receptors. *Mol. Pharmacol.* **1997,** *52*, 172-179.

(56) Cheng, K.; Khurana, S.; Chen, Y.; Kennedy, R. H.; Zimniak, P.; Raufman, J. P. Lithocholylcholine, a bile acid/acetylcholine hybrid, is a muscarinic receptor antagonist. *J. Pharmacol. Exp. Ther.* **2002,** *303*, 29-35.

(57) Opazo Saez, A.; Du, T.; Wang, N. S.; Martin, J. G. Methacholine-induced bronchoconstriction and airway smooth muscle in the guinea pig. *J. Appl. Physiol.* **1996,** *80*, 437-444.

(58) Craig, C. R.; Stitzel, R. E. *Modern pharmacology with clinical application*. Lippincott Williams & Wilkins **2004**.

(59) Keren, G.; Treister, G. Effect of aceclidine(+) isomer and pilocarpine on the intraocular pressure decrease and the miosis in glaucomatous eyes. Effect on accommodation in normal eyes of young subjects. *Ophthalmologica* **1980,** *180*, 181-187.

(60) Fox, R. I.; Konttinen, Y.; Fisher, A. Use of muscarinic agonists in the treatment of Sjogren's syndrome. *Clin. Immunol.* **2001,** *101*, 249-263.

(61) Bodick, N. C.; Offen, W. W.; Levey, A. I.; Cutler, N. R.; Gauthier, S. G.; Satlin, A.; Shannon, H. E.; Tollefson, G. D.; Rasmussen, K.; Bymaster, F. P.; Hurley, D. J.; Potter, W. Z.; Paul, S. M. Effects of xanomeline, a selective muscarinic receptor agonist, on cognitive function and behavioral symptoms in Alzheimer disease. *Arch. Neurol.* **1997,** *54*, 465-473.

(62) Shekhar, A.; Potter, W. Z.; Lightfoot, J.; Lienemann, J.; Dube, S.; Mallinckrodt, C.; Bymaster, F. P.; McKinzie, D. L.; Felder, C. C. Selective muscarinic receptor agonist xanomeline as a novel treatment approach for schizophrenia. *Am. J. Psychiatry* **2008,** *165*, 1033-1039.

(63) Schrage, R.; Seemann, W. K.; Klockner, J.; Dallanoce, C.; Racke, K.; Kostenis, E.; De Amici, M.; Holzgrabe, U.; Mohr, K. Agonists with supraphysiological efficacy at the muscarinic M2 ACh receptor. *Br. J. Pharmacol.* **2013,** *169*, 357-370.

(64) Schwartz, T. W.; Holst, B. Ago-allosteric modulation and other types of allostery in dimeric 7TM receptors. *J. Recept. Signal Transduct. Res.* **2006,** *26*, 107-128.

(65) Nawaratne, V.; Leach, K.; Felder, C. C.; Sexton, P. M.; Christopoulos, A. Structural determinants of allosteric agonism and modulation at the M4 muscarinic acetylcholine receptor: identification of ligand-specific and global activation mechanisms. *J. Biol. Chem.* **2010,** *285*, 19012-19021.

(66) Moulton, B. C.; Fryer, A. D. Muscarinic receptor antagonists, from folklore to pharmacology; finding drugs that actually work in asthma and COPD. *Br. J. Pharmacol.* **2011,** *163*, 44-52.

(67) Levey, A. I. Immunological localization of m1-m5 muscarinic acetylcholine receptors in peripheral tissues and brain. *Life Sci.* **1993,** *52*, 441-448.

(68) Bartus, R. T.; Dean, R. L., 3rd; Beer, B.; Lippa, A. S. The cholinergic hypothesis of geriatric memory dysfunction. *Science* **1982,** *217*, 408-414.

(69) Roldan, G.; Bolanos-Badillo, E.; Gonzalez-Sanchez, H.; Quirarte, G. L.; Prado-Alcala, R. A. Selective M1 muscarinic receptor antagonists disrupt memory consolidation of inhibitory avoidance in rats. *Neurosci. Lett.* **1997,** *230*, 93-96.

(70) Packard, M. G.; Regenold, W.; Quirion, R.; White, N. M. Post-training injection of the acetylcholine M2 receptor antagonist AF-DX 116 improves memory. *Brain Res.* **1990,** *524*, 72-76.

(71) Hock, C.; Maddalena, A.; Heuser, I.; Naber, D.; Oertel, W.; von der Kammer, H.; Wienrich, M.; Raschig, A.; Deng, M.; Growdon, J. H.; Nitsch, R. M. Treatment with the selective muscarinic agonist talsaclidine decreases cerebrospinal fluid levels of total amyloid beta-peptide in patients with Alzheimer's disease. *Ann. N.Y. Acad. Sci.* **2000,** *920*, 285-291.

(72) Greenlee, W.; Clader, J.; Asberom, T.; McCombie, S.; Ford, J.; Guzik, H.; Kozlowski, J.; Li, S.; Liu, C.; Lowe, D.; Vice, S.; Zhao, H.; Zhou, G.; Billard, W.; Binch, H.; Crosby, R.; Duffy, R.; Lachowicz, J.; Coffin, V.; Watkins, R.; Ruperto, V.; Strader, C.; Taylor, L.; Cox, K. Muscarinic agonists and antagonists in the treatment of Alzheimer's disease. *Farmaco* **2001,** *56*, 247-250.

(73) Beach, T. G.; Walker, D. G.; Potter, P. E.; Sue, L. I.; Fisher, A. Reduction of cerebrospinal fluid amyloid beta after systemic administration of M1 muscarinic agonists. *Brain Res.* **2001,** *905*, 220-223.

(74) Sheardown, M. J. Muscarinic M1receptor agonists and M2 receptor antagonists as therapeutic targets in Alzheimer’s disease. *Expert Opin. Ther. Pat.* **2002,** *12*, 863-870.

(75) Gitler, M. S.; Reba, R. C.; Cohen, V. I.; Rzeszotarski, W. J.; Jin, B.; Baumgold, J. A novel m2-selective muscarinic antagonist: binding characteristics and autoradiographic distribution in rat brain. *Brain Res.* **1992,** *582*, 253-260.

(76) Doods, H.; Entzeroth, M.; Ziegler, H.; Schiavi, G.; Engel, W.; Mihm, G.; Rudolf, K.; Eberlein, W. Characterization of BIBN 99: a lipophilic and selective muscarinic M2 receptor antagonist. *Eur. J. Pharmacol.* **1993,** *242*, 23-30.

(77) Boyle, C. D.; Lachowicz, J. E. Orally active and selective benzylidene ketal M2 muscarinic receptor antagonists for the treatment of Alzheimer's disease. *Drug Dev. Res.* **2002,** *56*, 310-320.

(78) Bohme, T. M.; Keim, C.; Kreutzmann, K.; Linder, M.; Dingermann, T.; Dannhardt, G.; Mutschler, E.; Lambrecht, G. Structure-activity relationships of dimethindene derivatives as new M2-selective muscarinic receptor antagonists. *J. Med. Chem.* **2003,** *46*, 856-867.

(79) Takadoi, M.; Terashima, S. Preparation of decahydronaphtho[2,3-c]furan derivatives as M2 muscarinic receptor antagonists. JP13344 2003055871, CAN 139:101314, **2003**.

(80) Eglen, R. M. Muscarinic receptor subtype pharmacology and physiology. *Prog. Med. Chem.* **2005,** *43*, 105-136.

(81) Gomeza, J.; Zhang, L.; Kostenis, E.; Felder, C.; Bymaster, F.; Brodkin, J.; Shannon, H.; Xia, B.; Deng, C.; Wess, J. Enhancement of D1 dopamine receptor-mediated locomotor stimulation in M(4) muscarinic acetylcholine receptor knockout mice. *Proc. Natl. Acad. Sci. U. S. A.* **1999,** *96*, 10483-10488.

(82) Bohme, T. M.; Augelli-Szafran, C. E.; Hallak, H.; Pugsley, T.; Serpa, K.; Schwarz, R. D. Synthesis and pharmacology of benzoxazines as highly selective antagonists at M(4) muscarinic receptors. *J. Med. Chem.* **2002,** *45*, 3094-3102.

(83) King, F. D.; Lawton, G. *Progress in Medicinal Chemistry, Volume 43*. Elsevier Science: **2005**.

(84) Felder, C. C.; Bymaster, F. P.; Ward, J.; DeLapp, N. Therapeutic opportunities for muscarinic receptors in the central nervous system. *J. Med. Chem.* **2000,** *43*, 4333-4353.

(85) Gentry, P. R.; Kokubo, M.; Bridges, T. M.; Cho, H. P.; Smith, E.; Chase, P.; Hodder, P. S.; Utley, T. J.; Rajapakse, A.; Byers, F.; Niswender, C. M.; Morrison, R. D.; Daniels, J. S.; Wood, M. R.; Conn, P. J.; Lindsley, C. W. Discovery, synthesis and characterization of a highly muscarinic acetylcholine receptor (mAChR)-selective M5-orthosteric antagonist, VU0488130 (ML381): a novel molecular probe. *ChemMedChem* **2014,** *9*, 1677-1682.

(86) Shirey, J. K.; Brady, A. E.; Jones, P. J.; Davis, A. A.; Bridges, T. M.; Kennedy, J. P.; Jadhav, S. B.; Menon, U. N.; Xiang, Z.; Watson, M. L.; Christian, E. P.; Doherty, J. J.; Quirk, M. C.; Snyder, D. H.; Lah, J. J.; Levey, A. I.; Nicolle, M. M.; Lindsley, C. W.; Conn, P. J. A selective allosteric potentiator of the M1 muscarinic acetylcholine receptor increases activity of medial prefrontal cortical neurons and restores impairments in reversal learning. *J. Neurosci.* **2009,** *29*, 14271-14286.

(87) Jakubik, J.; Bacakova, L.; el-Fakahany, E. E.; Tucek, S. Subtype selectivity of the positive allosteric action of alcuronium at cloned M1-M5 muscarinic acetylcholine receptors. *J. Pharmacol. Exp. Ther.* **1995,** *274*, 1077-1083.

(88) Gharagozloo, P.; Lazareno, S.; Popham, A.; Birdsall, N. J. Allosteric interactions of quaternary strychnine and brucine derivatives with muscarinic acetylcholine receptors. *J. Med. Chem.* **1999,** *42*, 438-445.

(89) Gannon, R. L.; Millan, M. J. LY2033298, a positive allosteric modulator at muscarinic M(4) receptors, enhances inhibition by oxotremorine of light-induced phase shifts in hamster circadian activity rhythms. *Psychopharmacology* **2012,** *224*, 231-240.

(90) Foster, D. J.; Gentry, P. R.; Lizardi-Ortiz, J. E.; Bridges, T. M.; Wood, M. R.; Niswender, C. M.; Sulzer, D.; Lindsley, C. W.; Xiang, Z.; Conn, P. J. M5 receptor activation produces opposing physiological outcomes in dopamine neurons depending on the receptor's location. *J. Neurosci.* **2014,** *34*, 3253-3262.

(91) Lane, J. R.; Abdul-Ridha, A.; Canals, M. Regulation of G protein-coupled receptors by allosteric ligands. *ACS Chem. Neurosci.* **2013,** *4*, 527-534.

(92) Espinoza-Fonseca, L. M.; Trujillo-Ferrara, J. G. Identification of multiple allosteric sites on the M1 muscarinic acetylcholine receptor. *FEBS Lett.* **2005,** *579*, 6726-6732.

(93) Espinoza-Fonseca, L. M.; Trujillo-Ferrara, J. G. The existence of a second allosteric site on the M1 muscarinic acetylcholine receptor and its implications for drug design. *Bioorg. Med. Chem. Lett.* **2006,** *16*, 1217-1220.

(94) Mohr, K.; Schmitz, J.; Schrage, R.; Trankle, C.; Holzgrabe, U. Molecular alliance-from orthosteric and allosteric ligands to dualsteric/bitopic agonists at G protein coupled receptors. *Angew. Chem. Int. Ed.* **2013,** *52*, 508-516.

(95) Mitchelson, F. J. The pharmacology of McN-A-343. *Pharmacol. Ther.* **2012,** *135*, 216-245.

(96) Valant, C.; Gregory, K. J.; Hall, N. E.; Scammells, P. J.; Lew, M. J.; Sexton, P. M.; Christopoulos, A. A novel mechanism of G protein-coupled receptor functional selectivity. Muscarinic partial agonist McN-A-343 as a bitopic orthosteric/allosteric ligand. *J. Biol. Chem.* **2008,** *283*, 29312-29321.

(97) Spalding, T. A.; Trotter, C.; Skjaerbaek, N.; Messier, T. L.; Currier, E. A.; Burstein, E. S.; Li, D.; Hacksell, U.; Brann, M. R. Discovery of an ectopic activation site on the M(1) muscarinic receptor. *Mol. Pharmacol.* **2002,** *61*, 1297-1302.

(98) Spalding, T. A.; Ma, J. N.; Ott, T. R.; Friberg, M.; Bajpai, A.; Bradley, S. R.; Davis, R. E.; Brann, M. R.; Burstein, E. S. Structural requirements of transmembrane domain 3 for activation by the M1 muscarinic receptor agonists AC-42, AC-260584, clozapine, and N-desmethylclozapine: evidence for three distinct modes of receptor activation. *Mol. Pharmacol.* **2006,** *70*, 1974-1983.

(99) Lebon, G.; Langmead, C. J.; Tehan, B. G.; Hulme, E. C. Mutagenic mapping suggests a novel binding mode for selective agonists of M1 muscarinic acetylcholine receptors. *Mol. Pharmacol.* **2009,** *75*, 331-341.

(100) Schmitz, J.; van der Mey, D.; Bermudez, M.; Klockner, J.; Schrage, R.; Kostenis, E.; Trankle, C.; Wolber, G.; Mohr, K.; Holzgrabe, U. Dualsteric muscarinic antagonists--orthosteric binding pose controls allosteric subtype selectivity. *J. Med. Chem.* **2014,** *57*, 6739-6750.

(101) Steinfeld, T.; Mammen, M.; Smith, J. A.; Wilson, R. D.; Jasper, J. R. A novel multivalent ligand that bridges the allosteric and orthosteric binding sites of the M2 muscarinic receptor. *Mol. Pharmacol.* **2007,** *72*, 291-302.

(102) Bock, A.; Merten, N.; Schrage, R.; Dallanoce, C.; Batz, J.; Klockner, J.; Schmitz, J.; Matera, C.; Simon, K.; Kebig, A.; Peters, L.; Muller, A.; Schrobang-Ley, J.; Trankle, C.; Hoffmann, C.; De Amici, M.; Holzgrabe, U.; Kostenis, E.; Mohr, K. The allosteric vestibule of a seven transmembrane helical receptor controls G-protein coupling. *Nat. Commun.* **2012,** *3*, 1044.

(103) Bock, A.; Mohr, K. Dualsteric GPCR targeting and functional selectivity: the paradigmatic M(2) muscarinic acetylcholine receptor. *Drug Discovery Today: Technol.* **2013,** *10*, e245-252.

(104) Jones, C. K.; Brady, A. E.; Davis, A. A.; Xiang, Z.; Bubser, M.; Tantawy, M. N.; Kane, A. S.; Bridges, T. M.; Kennedy, J. P.; Bradley, S. R.; Peterson, T. E.; Ansari, M. S.; Baldwin, R. M.; Kessler, R. M.; Deutch, A. Y.; Lah, J. J.; Levey, A. I.; Lindsley, C. W.; Conn, P. J. Novel selective allosteric activator of the M1 muscarinic acetylcholine receptor regulates amyloid processing and produces antipsychotic-like activity in rats. *J. Neurosci.* **2008,** *28*, 10422-10433.

(105) Keov, P.; Valant, C.; Devine, S. M.; Lane, J. R.; Scammells, P. J.; Sexton, P. M.; Christopoulos, A. Reverse engineering of the selective agonist TBPB unveils both orthosteric and allosteric modes of action at the M(1) muscarinic acetylcholine receptor. *Mol. Pharmacol.* **2013,** *84*, 425-437.

(106) Hiller, C.; Kuhhorn, J.; Gmeiner, P. Class A G-protein-coupled receptor (GPCR) dimers and bivalent ligands. *J. Med. Chem.* **2013,** *56*, 6542-6559.

(107) Goin, J. C.; Nathanson, N. M. Quantitative analysis of muscarinic acetylcholine receptor homo- and heterodimerization in live cells: regulation of receptor down-regulation by heterodimerization. *J. Biol. Chem.* **2006,** *281*, 5416-5425.

(108) Hern, J. A.; Baig, A. H.; Mashanov, G. I.; Birdsall, B.; Corrie, J. E.; Lazareno, S.; Molloy, J. E.; Birdsall, N. J. Formation and dissociation of M1 muscarinic receptor dimers seen by total internal reflection fluorescence imaging of single molecules. *Proc. Natl. Acad. Sci. U. S. A.* **2010,** *107*, 2693-2698.

(109) Hu, J.; Thor, D.; Zhou, Y.; Liu, T.; Wang, Y.; McMillin, S. M.; Mistry, R.; Challiss, R. A.; Costanzi, S.; Wess, J. Structural aspects of M(3) muscarinic acetylcholine receptor dimer formation and activation. *FASEB J.* **2012,** *26*, 604-616.

(110) Bhushan, R. G.; Sharma, S. K.; Xie, Z.; Daniels, D. J.; Portoghese, P. S. A bivalent ligand (KDN-21) reveals spinal delta and kappa opioid receptors are organized as heterodimers that give rise to delta(1) and kappa(2) phenotypes. Selective targeting of delta-kappa heterodimers. *J. Med. Chem.* **2004,** *47*, 2969-2972.

(111) Berque-Bestel, I.; Lezoualc'h, F.; Jockers, R. Bivalent ligands as specific pharmacological tools for G protein-coupled receptor dimers. **2008,** *Curr. Drug Discovery Technol.*, 312-318.

(112) Arnatt, C. K.; Zhang, Y. Bivalent ligands targeting chemokine receptor dimerization: molecular design and functional studies. *Curr. Top. Med. Chem.* **2014,** *14*, 1606-1618.

(113) Rajeswaran, W. G.; Cao, Y.; Huang, X.-P.; Wroblewski, M. E.; Colclough, T.; Lee, S.; Liu, F.; Nagy, P. I.; Ellis, J.; Levine, B. A.; Nocka, K. H.; Messer, W. S., Jr. Design, Synthesis, and Biological Characterization of Bivalent 1-Methyl-1,2,5,6-tetrahydropyridyl-1,2,5-thiadiazole Derivatives as Selective Muscarinic Agonists. *J. Med. Chem.* **2001,** *44*, 4563-4576.

(114) Cao, Y.; Zhang, M.; Wu, C.; Lee, S.; Wroblewski, M. E.; Whipple, T.; Nagy, P. I.; Takacs-Novak, K.; Balazs, A.; Toroes, S.; Messer, W. S., Jr. Synthesis and Biological Characterization of 1-Methyl-1,2,5,6-tetrahydropyridyl-1,2,5-thiadiazole Derivatives as Muscarinic Agonists for the Treatment of Neurological Disorders. *J. Med. Chem.* **2003,** *46*, 4273-4286.

(115) Chiarini, A.; Budriesi, R.; Bolognesi, M. L.; Minarini, A.; Melchiorre, C. In vitro characterization of tripitramine, a polymethylene tetraamine displaying high selectivity and affinity for muscarinic M2 receptors. *Br. J. Pharmacol.* **1995,** *114*, 1507-1517.

(116) Keller, M.; Trankle, C.; She, X.; Pegoli, A.; Bernhardt, G.; Buschauer, A.; Read, R. W. M2 Subtype preferring dibenzodiazepinone-type muscarinic receptor ligands: Effect of chemical homo-dimerization on orthosteric (and allosteric?) binding. *Biorg. Med. Chem.* **2015,** *23*, 3970-3990.

(117) Lefkowitz, R. J.; Roth, J.; Pastan, I. Radioreceptor assay of adrenocorticotropic hormone: new approach to assay of polypeptide hormones in plasma. *Science* **1970,** *170*, 633-635.

(118) Zhang, R.; Xie, X. Tools for GPCR drug discovery. *Acta Pharmacol. Sin.* **2012,** *33*, 372-384.

(119) Lazareno, S.; Dolezal, V.; Popham, A.; Birdsall, N. J. Thiochrome enhances acetylcholine affinity at muscarinic M4 receptors: receptor subtype selectivity via cooperativity rather than affinity. *Mol. Pharmacol.* **2004,** *65*, 257-266.

(120) Berrie, C. P.; Birdsall, N. J.; Haga, K.; Haga, T.; Hulme, E. C. Hydrodynamic properties of muscarinic acetylcholine receptors solubilized from rat forebrain. *Br. J. Pharmacol.* **1984,** *82*, 839-851.

(121) Berrie, C. P.; Birdsall, N. J.; Hulme, E. C.; Keen, M.; Stockton, J. M. Solubilization and characterization of guanine nucleotide-sensitive muscarinic agonist binding sites from rat myocardium. *Br. J. Pharmacol.* **1984,** *82*, 853-861.

(122) Smith, C. M.; Wallis, R. M. Characterisation of [3H]-darifenacin as a novel radioligand for the study of muscarinic M3 receptors. *J. Recept. Signal Transduct. Res.* **1997,** *17*, 177-184.

(123) Watson, M.; Roeske, W. R.; Johnson, P. C.; Yamamura, H. I. [3H]Pirenzepine identifies putative M1 muscarinic receptors in human stellate ganglia. *Brain Res.* **1984,** *290*, 179-182.

(124) Eveleigh, P.; Hulme, E. C.; Schudt, C.; Birdsall, N. J. The existence of stable enantiomers of telenzepine and their stereoselective interaction with muscarinic receptor subtypes. *Mol. Pharmacol.* **1989,** *35*, 477-483.

(125) Clayden, J.; Moran, W. J.; Edwards, P. J.; LaPlante, S. R. The challenge of atropisomerism in drug discovery. *Angew. Chem. Int. Ed.* **2009,** *48*, 6398-6401.

(126) Trankle, C.; Weyand, O.; Voigtlander, U.; Mynett, A.; Lazareno, S.; Birdsall, N. J.; Mohr, K. Interactions of orthosteric and allosteric ligands with [3H]dimethyl-W84 at the common allosteric site of muscarinic M2 receptors. *Mol. Pharmacol.* **2003,** *64*, 180-190.

(127) Schober, D. A.; Croy, C. H.; Xiao, H.; Christopoulos, A.; Felder, C. C. Development of a radioligand, [(3)H]LY2119620, to probe the human M(2) and M(4) muscarinic receptor allosteric binding sites. *Mol. Pharmacol.* **2014,** *86*, 116-123.

Chapter 2

Radiolabeled dibenzodiazepinone-type muscarinic receptor ligands enable unveiling of dualsteric binding at the M_2R

Note: prior to the submission of this thesis, parts of this Chapter have already been submitted for publication in cooperation with partners. For detailed information on the nature of this collaboration see Acknowledgements and declaration of collaborations. "*Reprinted (adapted) with permission from Pegoli, A., She, X., Wifling, D., Huebner, H., Bernhardt, G., Gmeiner, P., Keller, M., Radiolabeled Dibenzodiazepinone-Type Antagonists Give Evidence of Dualsteric Binding at the M_2 Muscarinic Acetylcholine Receptor, J. Med. Chem., 2017, 60, 3314-3334. Copyright 2017 American Chemical Society".*

2.1. Introduction

In humans, the family of muscarinic acetylcholine receptors (M receptors, MRs) comprises five subtypes (M_1R-M_5R), which belong to the GPCR superfamily class A and mediate the action of the neurotransmitter acetylcholine in the CNS as well as in the periphery. For instance, the M_2R is expressed in the myocardium mediating a negative chronotropic and inotropic effect and it acts as a presynaptic autoreceptor in both the brain and the periphery.[1] Accordingly, selective M_2R antagonism in the CNS, resulting in enhanced cholinergic transmission, was suggested as an approach to increase cholinergic function in Alzheimer's disease.[2-5] In general, MRs represent important drug targets, however, there is still a need for highly subtype selective pharmaceuticals acting at MRs, because the development of selective ligands has been highly challenging due the high conservation of the acetylcholine (orthosteric) binding site. As MRs exhibit several distinct allosteric binding sites, which are less conserved than the orthosteric site[6, 7] these 7-TM receptors emerged as a prototypic receptor class to study allosterism at GPCRs.[8, 9] Numerous allosteric MR modulators were reported (for instance compounds **7**,[10] **8** (W84)[11] and **9** (LY2119620),[12, 13] Figure 1A), but allosteric ligands with high affinity are lacking.[14] The linkage of an orthosteric MR ligand to an allosteric modulator, called the dualsteric (or bitopic[15]) ligand approach, was suggested as a promising strategy to develop subtype selective MR ligands.[8, 14, 16-20] The rational design of dualsteric MR ligands is supposed to benefit from the recently reported crystal structures of the M_1, M_2, M_3, and M_4 receptor.[7, 21-23] In case of the M_2R, linking of non-selective MR ligands with allosteric modulators was reported to result in dualsteric ligands with peculiar pharmacological profiles with respect to subtype binding, the nature of allosteric cooperativity and functional selectivity (for instance **12**-**16**, Figure 1B).[24-28]

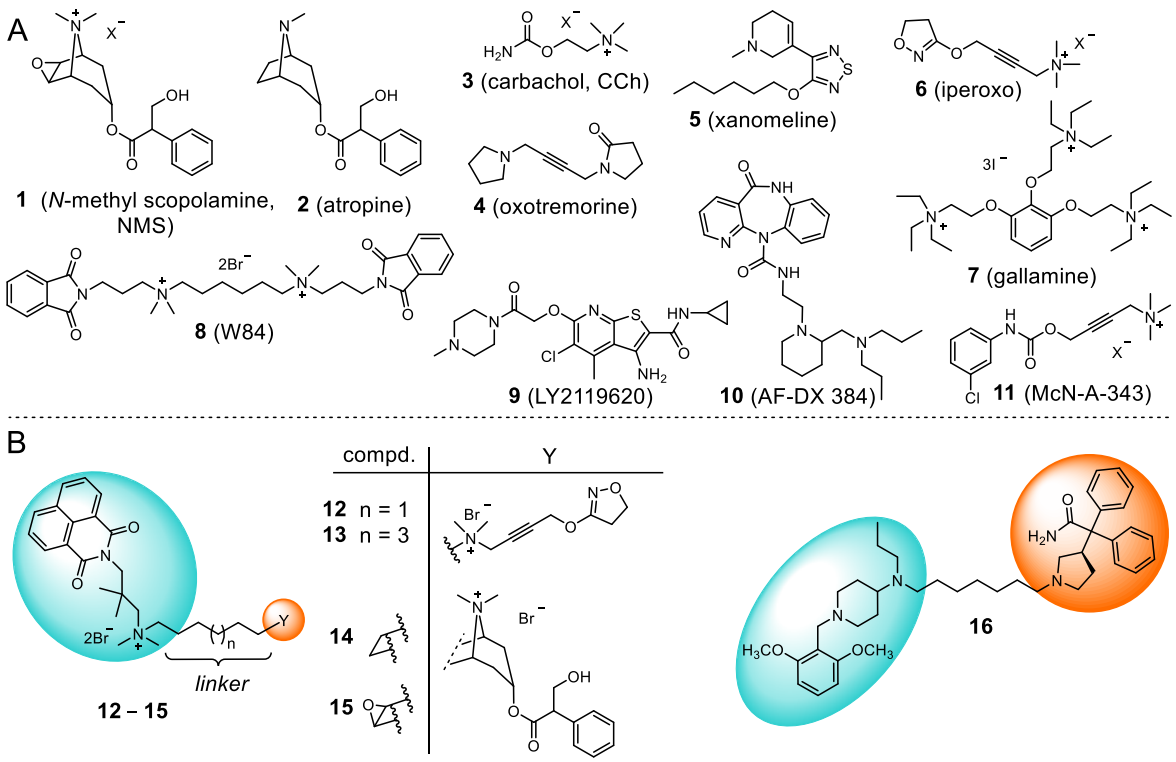

Figure 1. (A) Structures of reported M_2R antagonists (**1**, **2**, **10**), agonists (**3-6, 11**) and allosteric modulators (**7-9**). Compounds **10** and **11** were also reported to bind to the allosteric vestibule of the M_2R.[29, 30] (B) Examples of rationally designed dualsteric M_2R modulators obtained by connecting orthosterically (orange) with allosterically binding ligands (cyan) through a linker.[26, 28]

Recently, a series of dibenzodiazepinone-type M_2R subtype-preferring antagonists, derived from **17** (Figure 2A), including two homodimeric compounds (**20** and **21**, Figure 2A), were reported.[31] Compounds **20** and **21** showed the highest M_2R affinity (for K_i values see Table 1) and their retarding effect on the dissociation of [^{3}H]NMS from the M_2R was more pronounced compared with monomeric derivatives (**18**, **19**, Figure 2A) indicating an involvement of allosteric binding sites in the interaction of these compounds with the M_2R.[31] These findings are supported by previous reports on the M_2R binding profile of **10** (AF-DX 384)[32] (Figure 1A), which is structurally closely related to **17** (Figure 2A), and was suggested to interact with the orthosteric as well as with the allosteric binding site. It is noteworthy that the use of the tritiated form of **10** proved to be a valuable approach to investigate the binding mode.[29]

The present study aims at the elucidation of the binding mode of complex ligands such as the dibenzodiazepinone derivatives **20** and **21** at the M_2R. For this purpose we designed congeners of **20** and **21**, which can be conveniently prepared as tritium-labeled ligands, by introducing a branched ring structure in the center of the molecule intended to bear the radiolabel (Figure 2B). For comparison, the tritium-labeled form of **19**, representing the monomeric counterpart of the dimeric ligand **20** (Figure 2A), was synthesized and also

studied in saturation binding assays including experiments in the presence of allosteric modulators (Schild-like analysis). Moreover, kinetic investigations, equilibrium competition binding studies and molecular dynamics simulations were performed.

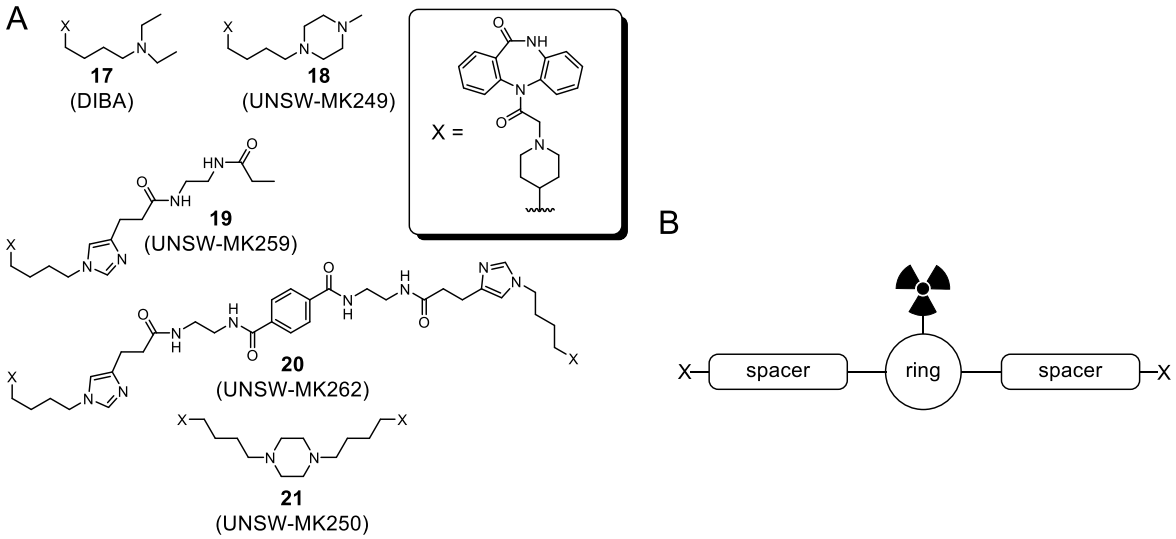

Figure 2. (A) Structures of recently reported DIBA-derived MR antagonists, including the homodimeric compounds **20** and **21**. (B) Schematic presentation of radiolabeled homodimeric DIBA derivatives, used as tools to investigate the binding mode at the M_2R.

2.2. Results and Discussion

2.2.1 Chemistry

The preparation of the homodimeric dibenzodiazepinone derivative **33**, containing an isophthalic acid moiety in the center, is outlined in Scheme 1. The crucial building block **29**, namely *N*-Boc protected aminomethylated isophthalic acid, was synthesized from **22** via azide **27**, following reported procedures with minor modifications (Scheme 1).[33, 34] Amidation of **29** with amine **30**,[31] using HBTU/HOBt as coupling reagent, and subsequent removal of the Boc group gave amine **31**, which represents a precursor for the preparation of differently functionalized dimeric MR ligands (e.g. radiolabeled and fluorescence labeled compounds). Propionylation of **31**, using succinimidyl propionate (**32**) afforded **33**, which represents the 'cold' form of a tritium-labeled dimeric MR ligand.

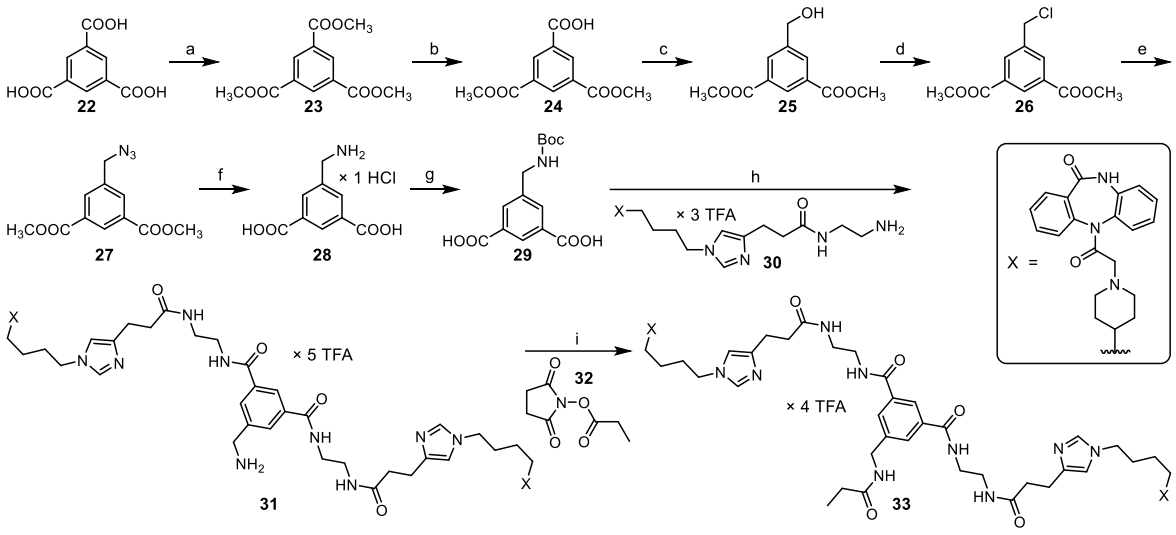

Scheme 1. Synthesis of the homodimeric MR ligand **33**. Reagent and conditions: (a) H_2SO_4, MeOH, reflux, 24 h, 99%; (b) $NaOH_{aq}$ 1 M, MeOH, rt, 18 h, 75%; (c) $(CH_3)_2S{\cdot}BH_3$, THF, rt, 24 h, 87%; (d) $SOCl_2$, reflux, 90 min, 98%; (e) NaN_3, acetone, reflux, 16 h, 96%; (f) (1) triphenylphosphine, H_2O/THF 5:1 (v/v), rt, 10 h, (2) $NaOH_{aq}$ 1 M, rt, 8 h, 71%; (g) di-*tert*-butyldicarbonate, triethylamine, H_2O/dioxane 1:1 (v/v), rt, 12 h, 61%; (h) (1) HOBt, TBTU, DIPEA, DMF, 60°C, 3 h (2) triethylamine/ CH_2Cl_2/H_2O 1:1:0.1 (v/v/v), rt, 3 h, 32%; (i) DIPEA, DMF, rt, 1 h, 90%.

The key intermediates for the synthesis of the homodimeric MR ligand **47**, containing a basic homopiperazine moiety in the center of the molecule, were bromide **38** and homopiperazine derivative **45c** (Scheme 2). Compound **38** was obtained by reduction of the carboxylated piperazine derivative **34** to the corresponding alcohol **35**, followed by *N*-alkylation of **35** with chloride **36** yielding alcohol **37**. The latter was converted to bromide **38** using perbromomethane and triphenylphosphine (Scheme 2). The synthesis of homopiperazine **45c** started with a nitro-Mannich reaction of dibenzylated ethylenediamine (**39**) and nitroethanol (**40**) yielding derivative **41**, which was converted into homopiperazine **42** by a retro-Henry reaction. Reduction of the nitro group in **42** using Raney-Nickel and hydrogen led to primary amine **43**, which was Boc-protected to obtain intermediate **44** (Scheme 2). Several attempts to debenzylate **44** by hydrogenolysis using 10% Pd/C and methanol or ethanol as solvent, failed due to solvent oxidation to formaldehyde and acetaldehyde, respectively, and formation of the cyclic aminal **45a** and the *N*-alkylated derivative **45b** (identified by NMR spectroscopy and mass spectrometry, data not shown). The use of 2,2,2-trifluoroethanol as solvent, preventing the Pd-catalyzed oxidation of the alcoholic solvent to the corresponding aldehyde,[35] enabled a successful debenzylation of **44**, affording homopiperazine **45c** without by-products. The alkylation of **45c** using bromide **38**, followed by Boc-deprotection led to the amino-functionalized dimeric dibenzodiazepinone derivative **46**, which was propionylated to give compound **47**, representing the ‘cold’ form of a tritium-labeled dimeric ligand as well. Imidazolyl propionic

acid derivative **50**, representing the terminal moiety of the side chain in **19** (*cf*. Figure 2), was prepared from urocanic acid derivative **48** (Scheme 2),[31] which was converted to **49** by hydrogenolytic reduction of the 'acrolein' double bond under acidic conditions resulting in a simultaneous cleavage of the Boc group (Scheme 2). Propanoylation of **49** using **32** yielded compound **50**. The homodimeric dibenzodiazepinone derivative **52** was prepared by alkylation of piperazine with chloride **36** (Scheme 2).

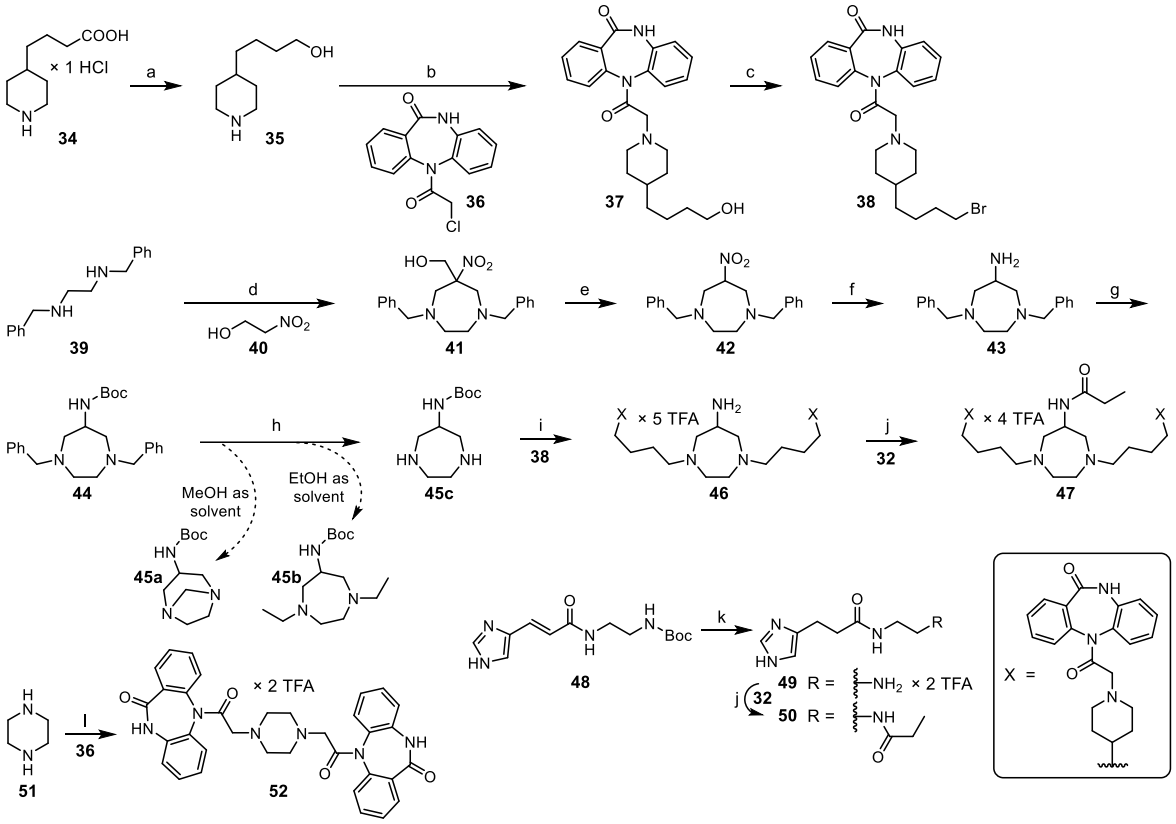

Scheme 2. Synthesis of the homodimeric MR ligands **47** and **52** and the imidazolyl propionic acid derivative **50**. Reagent and conditions: (a) $LiAlH_4$, THF, 0°C/reflux, 12 h, 89%; (b) K_2CO_3, acetonitrile, reflux, 5 h, 43%; (c) CBr_4, triphenylphosphine, CH_2Cl_2, -5°C/5°C, 5 h, 79%; (d) paraformaldehyde, EtOH/toluene 1:1 (v/v), reflux, 6 h, 87%; (e) potassium *tert*-butanolate, anhydrous THF, rt, 30 min, 95%; (f) H_2, Raney-Nickel, EtOH, rt, 12 h, 44%; (g) di-*tert*-butyldicarbonate, CH_3Cl, 0°C/rt, 5 h, 81%; (h) Pd/C (10%), H_2, 2,2,2-trifluoroethanol, 1 atm, rt, 12 h, 85%; (i) (1) K_2CO_3, DMF, 120 °C (microwave), 1.5 h (2) CH_2Cl_2/TFA/H_2O 1:1:0.1 (v/v/v), rt, 3 h, 37%; (j) DIPEA, DMF, rt, 1-1.5 h, 72% (47), 43% (50); (k) Pd/C (10%), H_2, MeOH/TFA 1:1 (v/v), 7.9 atm, rt, 12 h, 90%; (l) K_2CO_3, acetonitrile, 130°C (microwave), 30 min, 21%.

The chemical stability of compounds **19**, **33** and **47** was investigated in PBS (pH 7.4) at 23 °C over a period of 48 h. These dibenzodiazepinone derivatives showed excellent stabilities (Figure 3).

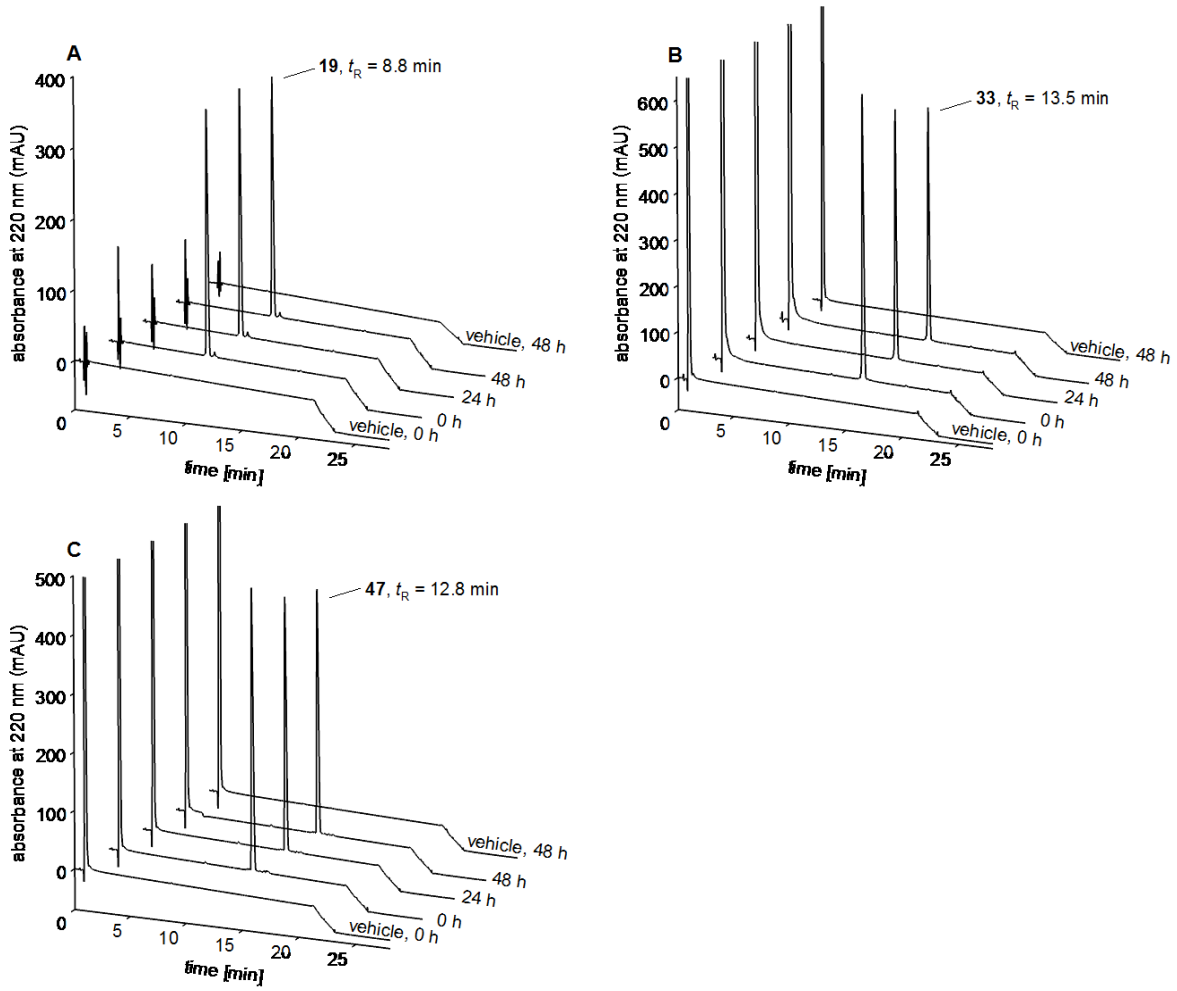

Figure 3. HPLC analysis of **19** (A), 33 (B) and **47** (C) after incubation in PBS (pH 7.4) at 23 °C for up to 48 h. **19**, **33** and **47** showed no decomposition. For HPLC conditions see experimental section.

2.2.2 Synthesis of radiolabeled dibenzodiazepinone derivatives

The tritium-labeled dibenzodiazepinone derivatives [^{3}H]**19**, [^{3}H]**33** and [^{3}H]**47** were obtained by treatment of an excess of the amine precursors **30**, **31** and **46**, respectively, with commercially available succinimidyl [^{3}H]propionate ([^{3}H]**32**) in the presence of DIPEA (Figure 4A). In order to facilitate the purification of [^{3}H]**47**, the excess of amine precursor **46** was 'quenched' by the addition of succinimidyl 4-fluorobenzoate (**53**), resulting in the formation of **54**, which could be conveniently separated from [^{3}H]**47** (Figure 4B). Purification by RP-HPLC afforded all radioligands in high radiochemical purity (99%, Figure 4C-E). [^{3}H]**19**, [^{3}H]**33** and [^{3}H]**47** proved to be stable upon storage in EtOH/H_2O (1:1 v/v) at −20 °C (Figure 5)

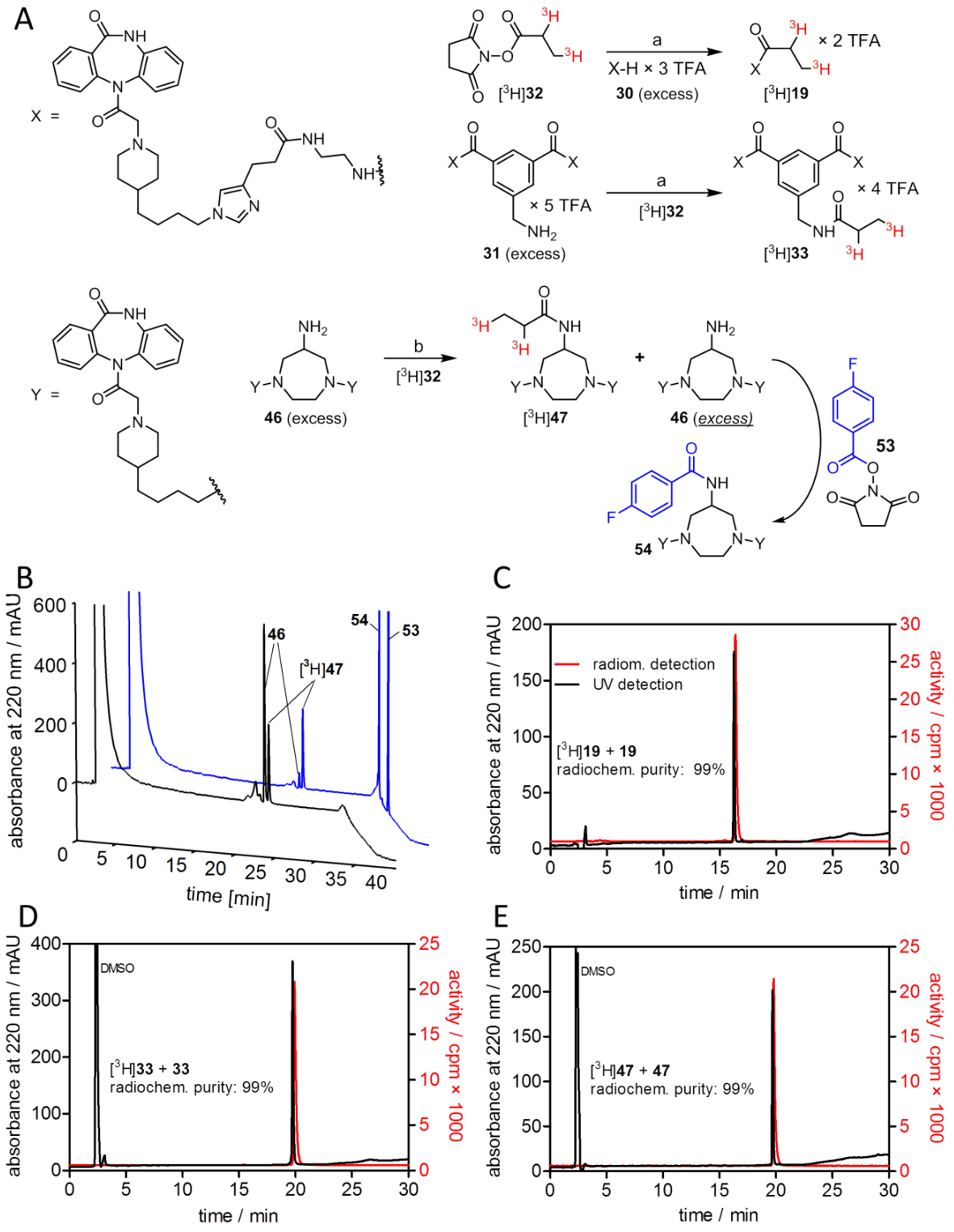

Figure 4. (A) Synthesis of the MR radioligands [^{3}H]**19**, [^{3}H]**33** and [^{3}H]**47** by [^{3}H]propionylation of the amine precursor **30**, **31** and **46**, respectively, using succinimidyl [^{3}H]propionate ([^{3}H]**32**). Reagents and conditions: (a) DIPEA, DMF, rt, 60 min, 39% ([^{3}H]**19**), 32% ([^{3}H]**33**); (b) (1) DIPEA, DMF, rt, 45 min, (2) **53**, rt, 60 min, 38%. The excess of **46** was 'quenched' by 4-fluorobenzoylation to facilitate the purification of [^{3}H]**47** (*cf.* B). (B) RP-HPLC monitoring of the synthesis of [^{3}H]**47** before (black line) and after (blue line) addition of the active ester **53**. (C-D) RP-HPLC analysis (conditions see experimental section) of [^{3}H]**19** (0.23 µM) (C), [^{3}H]**33** (0.20 µM) (D) and [^{3}H]**47** (0.20 µM) (E), each spiked with the 'cold' analog (**19** and **33**: 5 µM; **47**: 3 µM) analyzed 2 days after synthesis.

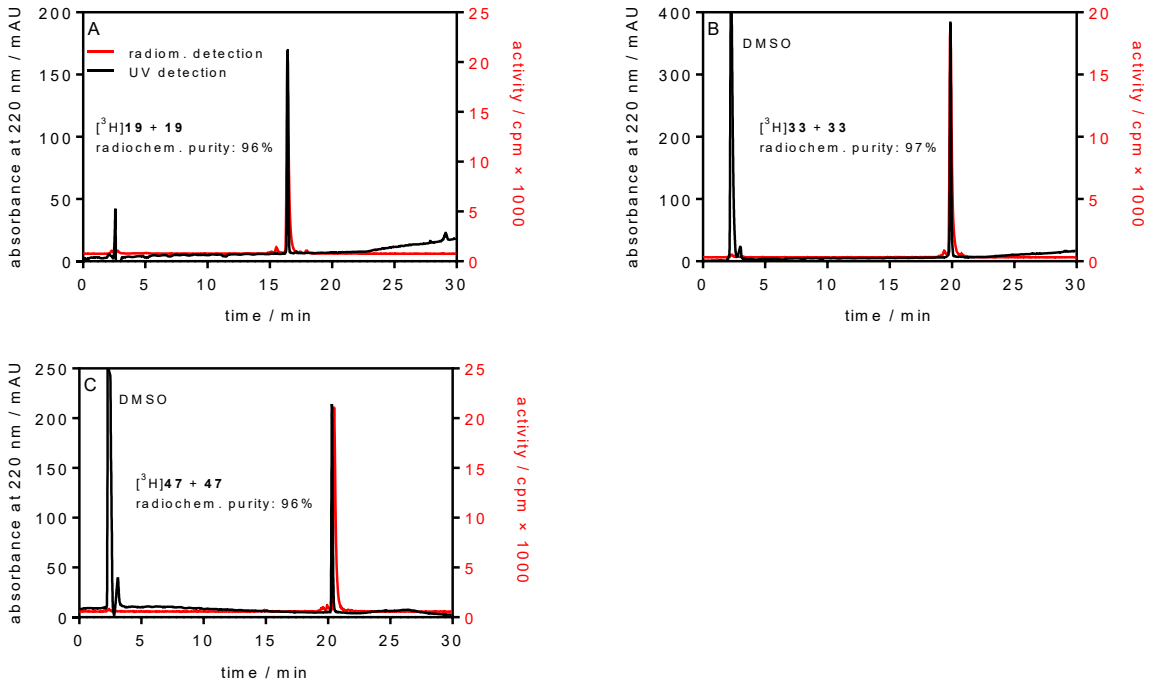

Figure 5. Long-term stability of the radioligands [^{3}H]**19**, [^{3}H]**33** and [^{3}H]**47**. (A) HPLC analysis of [^{3}H]**19** (0.18 µM) spiked with "cold" **19** (5 µM), analyzed 12 months after storage at −20 °C. (B) HPLC analysis of [^{3}H]**33** (0.17 µM) spiked with "cold" **33** (5 µM) analyzed 12 months after storage at −20 °C. (C) HPLC analysis of [^{3}H]**47** (0.2 µM) spiked with "cold" **47** (3 µM) analyzed 9 months after storage at −20 °C. For all the radioligands the radiochemical purity was >95%. HPLC conditions are provided in the experimental section.

2.2.3 Equilibrium competition binding studies with [^{3}H]NMS

M_1-M_5 receptor affinities of the dimeric dibenzodiazepinone derivatives **33** and **47** were investigated in equilibrium competition binding experiments using [^{3}H]NMS (structure of the 'cold' analog see Figure 1A) as orthosterically binding radioligand. The MR binding constants (pK_i values) are presented in Table 1 in comparison with previously reported M_1R-M_5R affinities of **18-21**. The transformation of the structures of **20** and **21** to **33** and **47**, respectively, by the introduction of a branched central linker moiety (Figure 2, Scheme 1 and Scheme 2) resulted only in a marginally decrease in M_2R affinity (Figure 6), and in a MR subtype selectivity profile comparable to that of the parent compounds **20** and **21** (Table 1). Steep curve slopes were observed for **33** at the M_1R (slope = −1.8) and M_2R (slope = −2.2) indicating a complex mechanism of binding (e.g. the involvement of more than one binding site). Moreover, equilibrium binding of [^{3}H]NMS at the M_2R in the presence of dibenzodiazepinone derivative **52** (*cf.* Scheme 2) and the reported M_2R allosteric modulator **9** was investigated. Compared to the homodimeric dibenzodiazepinone derivatives **33** and **47**, in which the pharmacophores are separated by complex linker moieties, the decrease in [^{3}H]NMS binding caused by compound **52** was considerably less pronounced by more than four orders of magnitude (Figure 7A). Similarly, the allosteric modulator **9** exhibited a

weak inhibitory effect on [^{3}H]NMS equilibrium binding (Figure 7B) being in agreement with a previously reported negative cooperativity between **9** and NMS.[22]

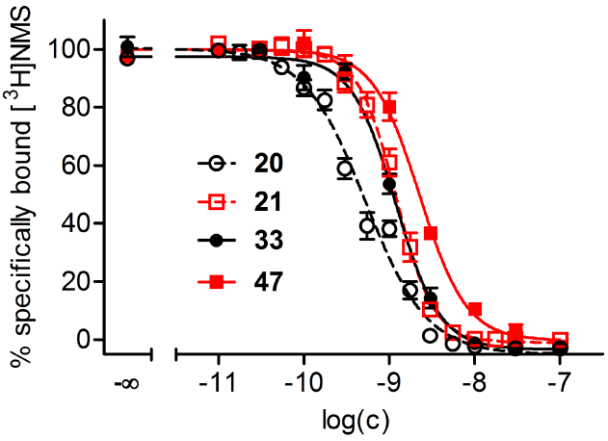

Figure 6. Effect of the homodimeric ligands **20**, **21**, **33** and **47** on M_2R equilibrium binding of [^{3}H]NMS (c = 0.2 nM, K_d = 0.09 nM) determined at CHO-hM_2 cells. Corresponding pK_i values: **20**: 9.7 ± 0.05, **33**: 9.39 ± 0.05, **21**: 9.51 ± 0.19, **47**: 9.15 ± 0.01. Data represent mean values ± SEM from at least three independent experiments (each performed in triplicate).

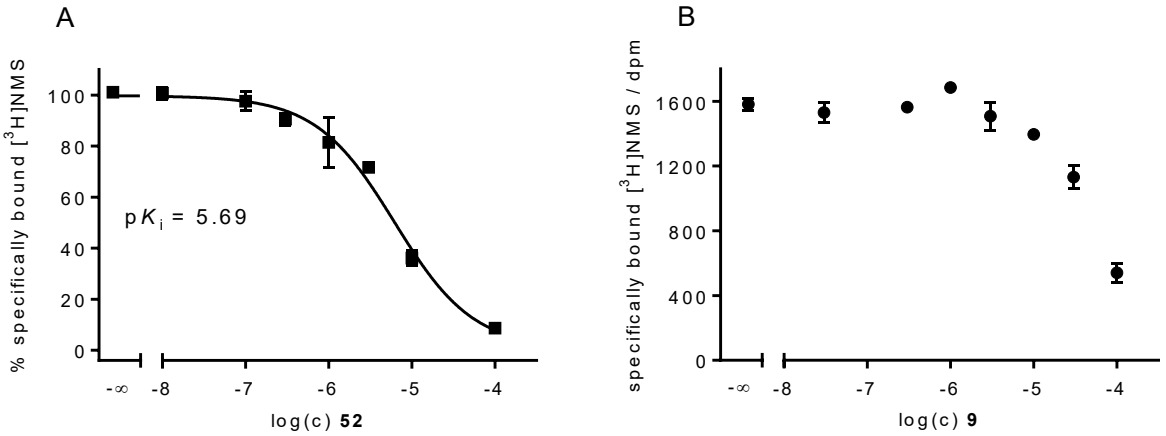

Figure 7. Effect of the homodimeric dibenzodiazepinone derivative **52** (A) and the allosteric M_2R modulator **9** (B) on M_2R equilibrium binding of [^{3}H]NMS (c = 0.2 nM, K_d = 0.09 nM) determined at intact CHO-hM_2 cells. (A) Mean values ± SEM from three independent experiments (each performed in triplicate). (B) Representative experiment performed in triplicate (at least two independent experiments were performed and gave comparable results).

Table 1. M_1-M_5 receptor affinities (pK_i values) of the DIBA derivatives **18-21**, **33** and **47**, obtained from equilibrium competition binding studies with [^{3}H]NMS at live CHO-hM_xR cells (x = 1-5)

compd.	M_1R		M_2R		M_3R		M_4R		M_5R	
	pK_i	slope[a]	pK_i	slope[a]	pK_i	slope[a]	pK_i	slope[a]	pK_i	slope[a]
18	8.01 ± 0.08	1.13 ± 0.10	9.17 ± 0.06	-1.25 ± 0.08	7.11 ± 0.08	-0.92 ± 0.09	8.49 ± 0.11	-0.99 ± 0.09	6.36 ± 0.09	-0.97 ± 0.14
19	8.07 ± 0.06	-1.11 ± 0.11	9.12 ± 0.05	-1.19 ± 0.06	7.22 ± 0.08	-1.09 ± 0.08	8.63 ± 0.02	-0.86 ± 0.03	6.75 ± 0.08	-0.68 ± 0.11
20	8.91 ± 0.05	-1.56 ± 0.08	9.71 ± 0.05	-1.27 ± 0.12	7.88 ± 0.03	-1.30 ± 0.09	9.19 ± 0.08	-1.17 ± 0.14	7.44 ± 0.10	-1.46 ± 0.18
21	9.00 ± 0.04	-1.32 ± 0.09	9.51 ± 0.19	-2.01 ± 0.07	8.17 ± 0.03	-1.05 ± 0.14	8.97 ± 0.08	-1.32 ± 0.17	7.64 ± 0.08	-1.09 ± 0.09
33	8.82 ± 0.10	-1.81 ± 0.16	9.39 ± 0.05	-2.17 ± 0.19	7.81 ± 0.01	-1.19 ± 0.11	9.33 ± 0.11	-1.17 ± 0.06	7.64 ± 0.04	-0.95 ± 0.13
47	8.15 ± 0.06	-1.29 ± 0.12	9.15 ± 0.01	-1.40 ± 0.06	6.70 ± 0.06	-1.15 ± 0.06	8.44 ± 0.09	-0.87 ± 0.08	7.11 ± 0.18	-1.06 ± 0.13

[a]Curve slope of the four-parameter logistic fit. Presented are mean values ± SEM from 3-9 independent experiments (each performed in triplicate). K_d values[31] / applied concentrations of [^{3}H]NMS: M_1: 0.12 / 0.2 nM; M_2: 0.090 / 0.2 nM; M_3: 0.089 / 0.2 nM; M_4: 0.040 / 0.1 nM; M_5: 0.24 / 0.3 nM. Data of **18-21** were previously reported as pIC_{50} values by Keller *et al*.[31] and were re-analyzed to obtain pK_i values.

2.2.4 Functional studies

The monomeric dibenzodiazepinone derivative **19** and the homodimeric congener **33** were investigated in an IP1 accumulation assay using HEK-293 cells transiently transfected with the human M_2R and the hybrid G-protein $G\alpha_{qi5\text{-}HA}$. **19** and **33** did not elicit IP1 accumulation when studied in agonist mode (Figure 8A), that is, they were incapable of stabilizing a G-protein activating conformation of the M_2R. In antagonist mode, **19** and **33** completely inhibited IP1 accumulation elicited by **3** (0.3 µM, ≈ EC_{80}), proving these compounds to be M_2R antagonists as previously reported for **10** (Figure 8B).[29] Furthermore, **19** and **33** were able to fully suppress the IP1 accumulation signal elicited by increasing concentration of CCh suggesting a competitive interaction between the orthosteric agonist CCh and the dibenzodiazepione-type MR ligands **19** and **33** (Figure 8C and 8D).

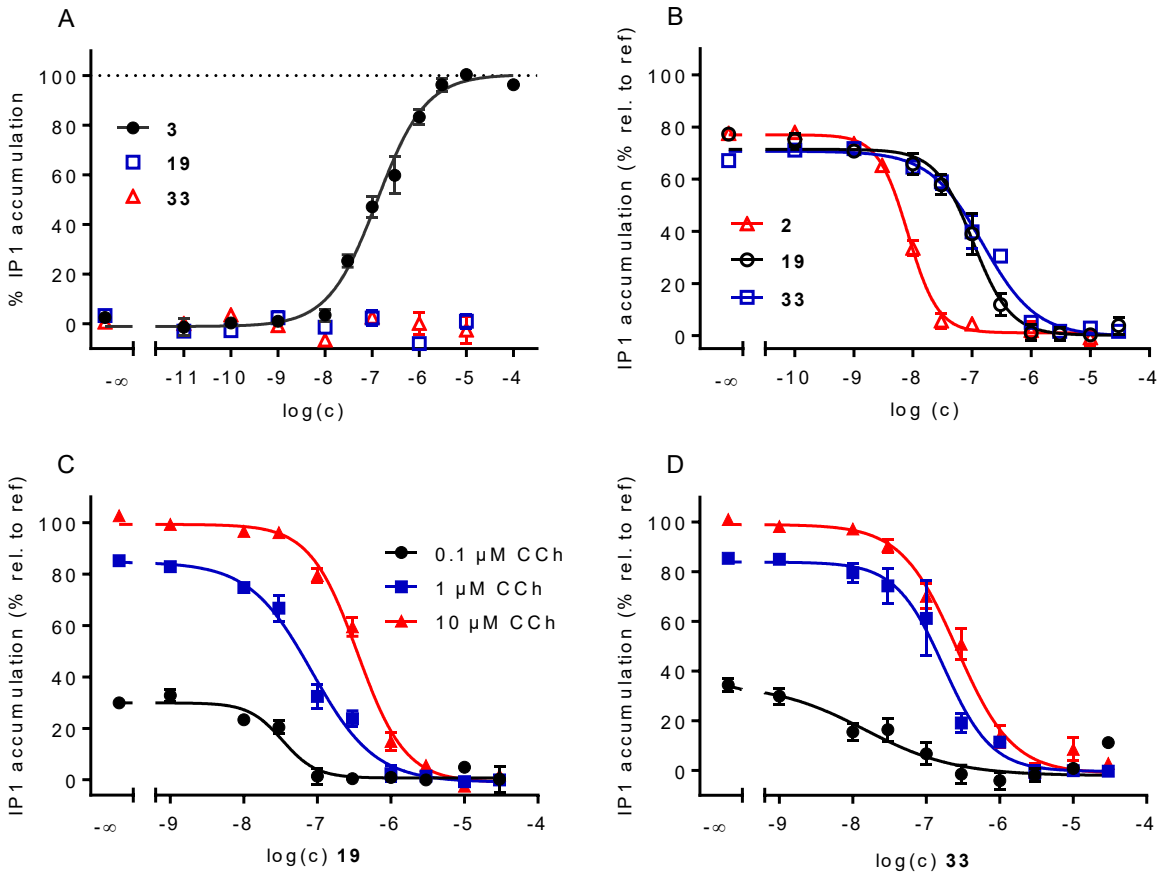

Figure 8. Investigation of M_2R agonism and antagonism of compounds **19** and **33** in an IP1 accumulation assay using HEK-hM_2-G_{qi} cells. (A) Concentration-dependent effect of **3**, **19** and **33** on the accumulation of IP1. **19** and **33** elicited no response. pEC_{50} of **3**: 6.93 ± 0.09 (mean ± SEM from 8 independent experiments performed in triplicate). (B) Concentration-dependent inhibition of the IP1 accumulation (induced by **3**, 0.3 µM) by **2**, **19** and **33**. Corresponding pK_b values: **2**: 8.63, **19**: 7.53, **33**: 7.36. Concentration-dependent inhibition of **19** (C) and **33** (D) on IP1 accumulation elicited by increasing concentration of CCh (0.1, 1 and 10 µM). Data represent the means ± SEM from at least five independent experiments (each performed in triplicate).

2.2.5 Characterization of [^{3}H]19, [^{3}H]33 and [^{3}H]47

Saturation binding experiments with the radiolabeled dibenzodiazepinone derivatives [^{3}H]**19**, [^{3}H]**33** and [^{3}H]**47** were performed at intact adherent CHO-hM_2 cells in white-transparent 96-wells plates revealing K_d values of 0.87, 1.1 and 8.6 nM, respectively (mean values from at least three independent experiments performed in triplicate) (Figure 9A, Figure 9B and Figure 9E). Whereas unspecific binding was very low in case of the monomeric ligand [^{3}H]**19** (<5% at the K_d) (Figure 9A), drastically increased unspecific binding (>60%) was a characteristic of the dimeric ligands [^{3}H]**33** and [^{3}H]**47** (Figure 9B and Figure 9E). Saturation binding studies with [^{3}H]**33** and [^{3}H]**47** performed with intact CHO-hM_2 cells in suspension ([^{3}H]**33**, Figure 9C) or with CHO-hM_2 cell homogenates ([^{3}H]**33** and [^{3}H]**47**, Figure 9D and Figure 9F), precluding unspecific binding of the radioligand to the

microplate, resulted in considerably lower unspecific binding (<15% at K_d), indicating that the dimeric ligands **33** and **47** strongly adsorb to polystyrene tissue-culture treated microplates (for experimental protocols see experimental section). The K_d values amounted to 0.31 nM ([^{3}H]**33**, suspended cells), 0.24 nM ([^{3}H]**33**, homogenates) and 6.0 nM ([^{3}H]**47**, homogenates) (mean values from at least three independent experiments performed in triplicate). Worth mentioning, the maximum number of M_2R binding sites per well (calculated from B_{max} values and the specific activities of the radioligands) obtained from experiments performed with the monomeric radioligand [^{3}H]**19** and the dimeric radioligand [^{3}H]**33** (same day and same seed of cells) were not different (data not shown), indicating that one molecule of dimeric radioligand did not bind simultaneously to the orthosteric pockets of putative M_2R dimers. In other words, these results suggested a ligand-receptor stoichiometry of 1:1 for both, the monomeric and the dimeric radioligand. In addition, saturation binding experiments were performed with [^{3}H]**33** at live CHO-hM_4 cells resulting in a K_d value of 0.67 nM (mean value from four independent experiments performed in triplicate) (Figure 10).

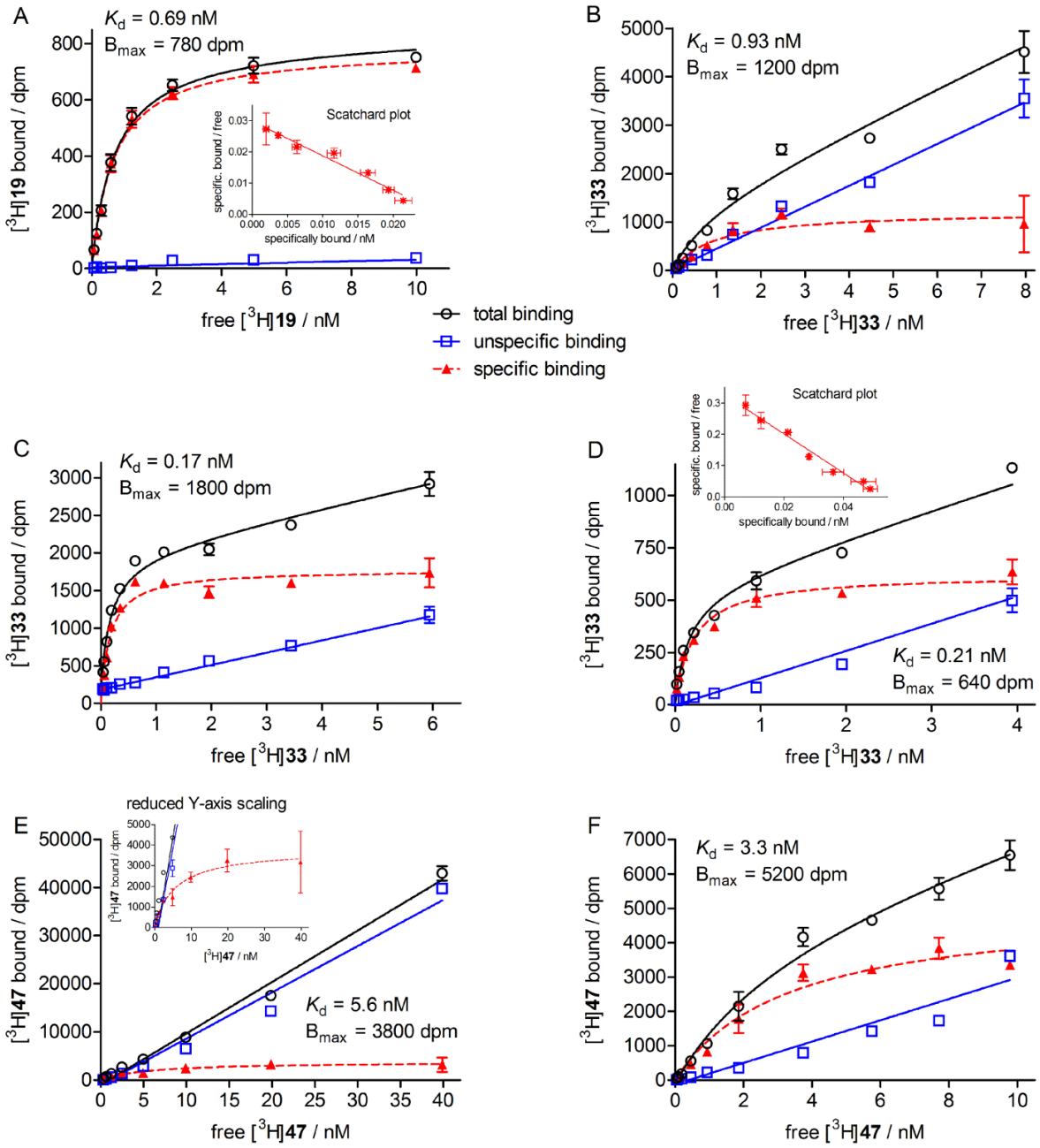

Figure 9. Representative saturation isotherms (in red) of specific M_2R binding of [^{3}H]**19** (A), [^{3}H]**33** (B-D) and [^{3}H]**47** (E, F) obtained from experiments either performed with live adherent CHO-hM_2 cells (A, B, E), live CHO-hM_2 cells in suspension (C) or CHO-hM_2 cell homogenates (D, F). Unspecific binding was determined in the presence of the orthosterically binding MR antagonist atropine (500-fold excess). Scatchard transformations are depicted for the optimized binding assay conditions (A, D). Experiments were performed in triplicate. Specific binding data were analyzed by an equation describing a one-site binding. Error bars of specific binding and error bars in the Scatchard plots represent propagated errors calculated according to the Gaussian law of errors. Error bars of total and unspecific binding represent the SEM.

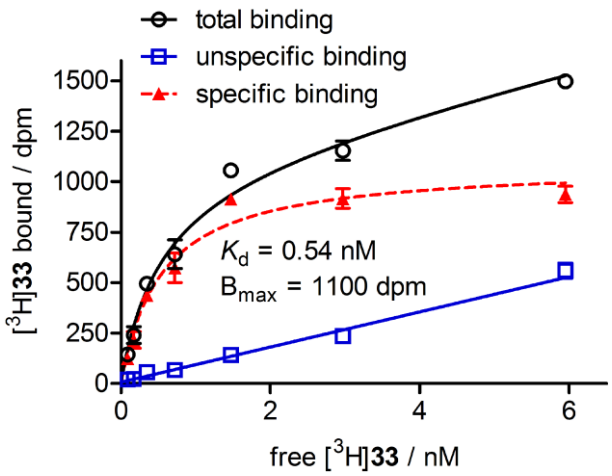

Figure 10. Saturation isotherm of specific M_4R binding of [^{3}H]**33** from a representative experiment performed with live CHO-hM_4 cells. Unspecific binding was determined in the presence of the orthosterically binding MR antagonist atropine (500-fold excess). Error bars of specific binding represent propagated errors calculated according to the Gaussian law of errors. Error bars of total and unspecific binding represent the SEM.

Notably, as the orthosteric antagonist **2**, used to determine unspecific binding, was able to completely prevent one-site (monophasic) specific binding of [^{3}H]**19**, [^{3}H]**33** and [^{3}H]**47** to the M_2R, these data strongly suggest that the dibenzodiazepinone derivatives **19**, **33** and **47** address the orthosteric binding site of the M_2R. Due to the lower affinity and inappropriate physicochemical properties (high unspecific binding) of [^{3}H]**47**, this radioligand was not considered with respect to further characterization, contrary to the monomeric radioligand [^{3}H]**19** and its dimerized analog [^{3}H]**33**. The association of both, [^{3}H]**19** and [^{3}H]**33**, to the M_2R could be described by a monophasic fit resulting in comparable k_{on} rates (Figure 11A, Figure 11C and Table 2). By contrast, the dissociation from the M_2R was different: whereas the monomeric ligand [^{3}H]**19** completely dissociated with a half-life of 71 min (monophasic decline), the dissociation of the dimeric dibenzodiazepinone derivative [^{3}H]**33** was incomplete, reaching a plateau at 67% of initially bound radioligand (Figure 11B and Figure 11D, respectively). This result suggests in part a (pseudo)irreversible (long lasting) binding of [^{3}H]**33**, which might be attributed to conformational adjustments of the receptor upon ligand binding,[36] or to an enhanced rebinding capability of the dimeric ligand by a simultaneous interaction with two or more binding sites.[37] However, the equilibrium dissociation constant of [^{3}H]**33**, calculated from k_{off} and k_{on} (K_d(kin) = k_{off}/k_{on} = 0.20 nM, (Table 2) was in good agreement with the K_d value derived from saturation binding experiments (K_d = 0.31 nM) indicating that [^{3}H]**33** follows (in part) the law of mass action.[38] An overview of the M_2R binding characteristics of [^{3}H]**19** and [^{3}H]**33** is provided in Table 2.

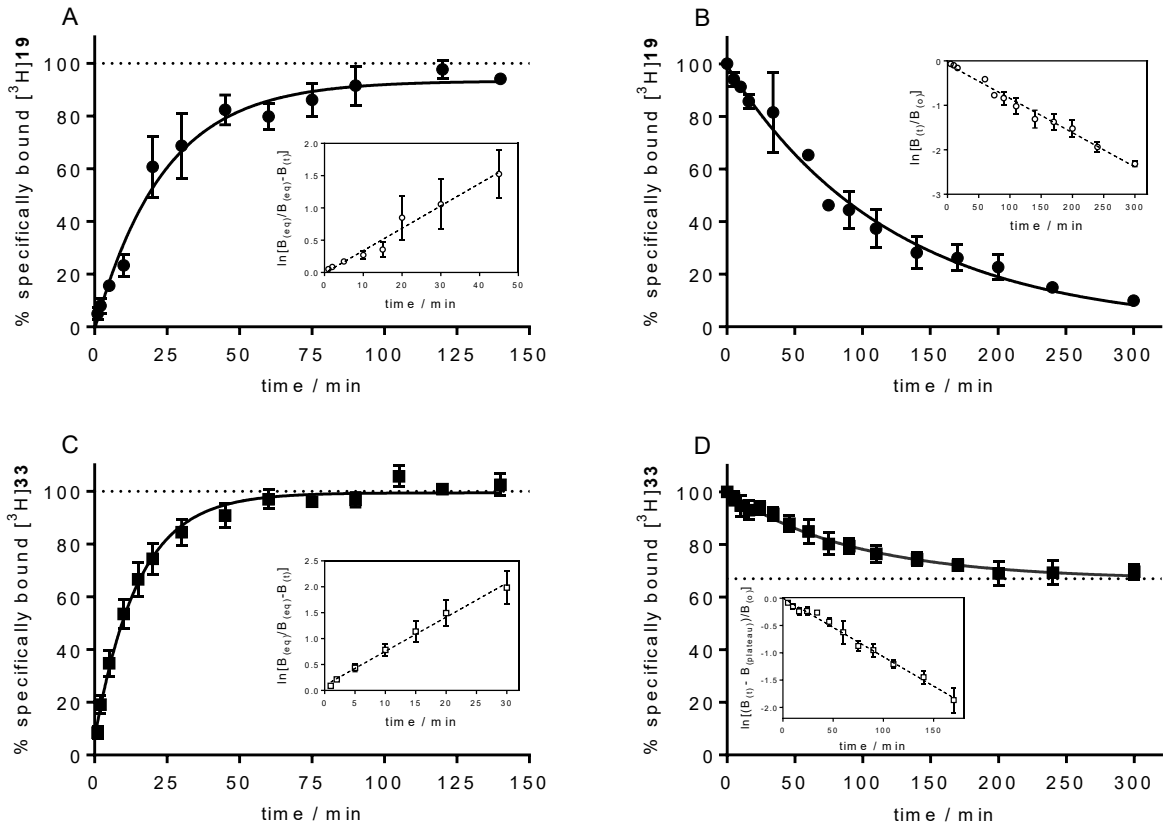

Figure 11. Association and dissociation kinetics of [^{3}H]**19** (A, B) and [^{3}H]**33** (C, D) determined at intact CHO-hM_2 cells at 23 °C. (A) Radioligand (c = 2 nM) association to the M_2R as a function of time (non-linear regression: k_{obs} = 0.042 min^{-1}); inset: ln[$B_{(eq)}$/($B_{(eq)}$-$B_{(t)}$)] versus time, k_{obs} = slope = 0.035 min^{-1}. (B) Radioligand (preincubation: 2 nM, 105 min) dissociation from the M_2R as a function of time, showing complete monophasic exponential decline (non-linear regression (black circles): k_{off} = 0.0091 min^{-1}, $t_{1/2}$ = 71 min); inset: ln[$B_{(t)}$/$B_{(0)}$] versus time, slope·(−1) = k_{off} = 0.0078 min^{-1}, $t_{1/2}$ = 89 min. (C) Radioligand (c = 1 nM) association to the M_2R as a function of time (non-linear regression: k_{obs} = 0.067 min^{-1}); inset: ln[$B_{(eq)}$/($B_{(eq)}$-$B_{(t)}$)] versus time, k_{obs} = slope = 0.066 min^{-1}. (D) Radioligand (preincubation: 1 nM, 90 min) dissociation from the M_2R as a function of time, showing incomplete monophasic exponential decline (non-linear regression (black squares): k_{off} = 0.011 min^{-1}, $t_{1/2}$ = 66 min, plateau = 67%); inset: ln[($B_{(t)}$-$B_{(plateau)}$)/$B_{(0)}$] versus time, slope·(−1) = k_{off} = 0.011 min^{-1}, $t_{1/2}$ = 66 min. Data represent means ± SEM from three (B, C, D) or four (A) independent experiments (each performed in triplicate).

Table 2. M_2R binding data of [^{3}H]**19**, [^{3}H]**33** and [^{3}H]**47** (at 23 ± 1 °C).

radioligand	K_i ('cold' analog) [nM][a]	K_d(sat) [nM][b]	K_d(kin) [nM][c]	k_{on} [$min^{-1} \cdot nM^{-1}$][d]	k_{off} [min^{-1}][e] $t_{1/2}$ [min][e]
[^{3}H]**19**	0.76 ± 0.05	0.87 ± 0.01	0.70 ± 0.10	0.013 ± 0.003	0.0091 ± 0.0016 71 ± 7
[^{3}H]**33**	0.41 ± 0.05	0.31 ± 0.08	0.20 ± 0.04	0.056 ± 0.010	0.011 ± 0.001 66 ± 9
[^{3}H]**47**	0.71 ± 0.01	6.0 ± 1.4	n.d	n.d	n.d

[a]Dissociation constant determined by equilibrium competition binding with [^{3}H]NMS at intact CHO-hM_2 cells; mean ± SEM from at least three independent experiments (performed in triplicate). [b]Equilibrium dissociation constant determined by saturation binding at intact CHO-hM_2 cells ([^{3}H]**19** and [^{3}H]**33**) and at CHO-hM_2 cell homogenates ([^{3}H]**47**); mean ± SEM from at least three independent experiments (performed in triplicate). [c]Kinetically derived dissociation constant ± propagated error (K_d(kin) = k_{off}/k_{on}). [d]Association rate constant ± propagated error, calculated from k_{obs}, k_{off} and the applied radioligand concentration (*cf*. Figure 6 and experimental section). [e]Dissociation rate constant and derived half-life; mean ± SEM from three independent experiments (performed in triplicate).

Binding of the monomeric dibenzodiazepinone derivative **19** to the orthosteric site was further supported by investigating the saturation binding of the orthosteric radioligand [^{3}H]NMS in the presence of **19** (Schild-like analysis). This experiment revealed a parallel rightward shift of the saturation isotherms of [^{3}H]NMS and a slope not different from unity of the corresponding 'Schild' regression, being indicative of a competitive interaction between **19** and the orthosteric radioligand [^{3}H]NMS (Figure 12).

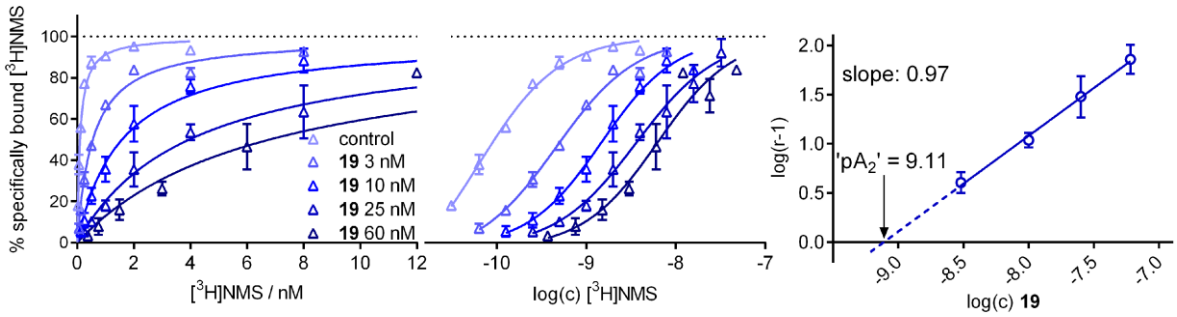

Figure 12. Saturation binding of [^{3}H]NMS at intact CHO-hM_2 cells in the presence of increasing concentrations of **19**. Presented are saturation isotherms of specific radioligand binding to the M_2R plotted in linear scale (left) and semi-logarithmic scale (middle), and the "Schild" regression (right) resulting from the rightward shift (ΔpK_d) of the saturation isotherm (log(r−1) plotted vs. log(concentration of **19**), where r = $10^{\Delta pKd}$). The presence of the dibenzodiazepinone derivative **19** led to a parallel rightward shift of the saturation curves of [^{3}H]NMS. The slope of the linear "Schild" regression was nearly equal to unity indicating a competitive interaction between [^{3}H]NMS and **19**. Data represent mean values ± SEM from at least three independent experiments (each performed in triplicate).

2.2.6 M_2R equilibrium competition binding with [^{3}H]19 and [^{3}H]33

Selected standard MR agonists (**4**, **5**) antagonists (**1**, **2**, **10**) and allosteric modulators (**7**, **8**) as well as the 'cold' forms of the radioligands (**19**, **33**) were investigated by equilibrium competition binding with [^{3}H]**19** or [^{3}H]**33**. The concentration-dependent effects of the investigated compounds on equilibrium binding of [^{3}H]**19** and [^{3}H]**33**, analyzed by four-parameter logistic fits, are depicted in Figure 13. The lower curve plateaus were throughout not significantly different from 0 (P >0.2), which either suggests a competitive mechanism or a strongly negative cooperativity between the studied compounds and the radiolabeled dibenzodiazepinone derivatives.[39] Generally, the pK_i values derived from this study were in good agreement with reported data (Table 3), although MR ligand affinities determined with the dimeric radioligand [^{3}H]**33** were consistently lower compared to M_2R affinities obtained from equilibrium competition binding experiments with [^{3}H]**19**. It is a matter of speculation whether the need for higher competitor concentrations for the displacement of the dimeric radioligand [^{3}H]**33** is caused by a multivalent binding mode of [^{3}H]**33** or not. Concerning this issue, experiments were repeated with **4** and **10**, applying a preincubation period of 90 min with the M_2R prior to the addition of [^{3}H]**33**, but did not result in an increase in the apparent pK_i of **4** and **10** (data not shown). In addition, the effect of the allosteric M_2R ligand **9** on the equilibrium binding of [^{3}H]**19** and [^{3}H]**33** was studied (Figure 13A and Figure 13B). The apparent pK_i values of 5.73 nM ([^{3}H]**19**) and 5.24 ([^{3}H]**33**) (Table 3) were in good agreement with the reported pK_B of **9** (pK_B = 5.77).[22]

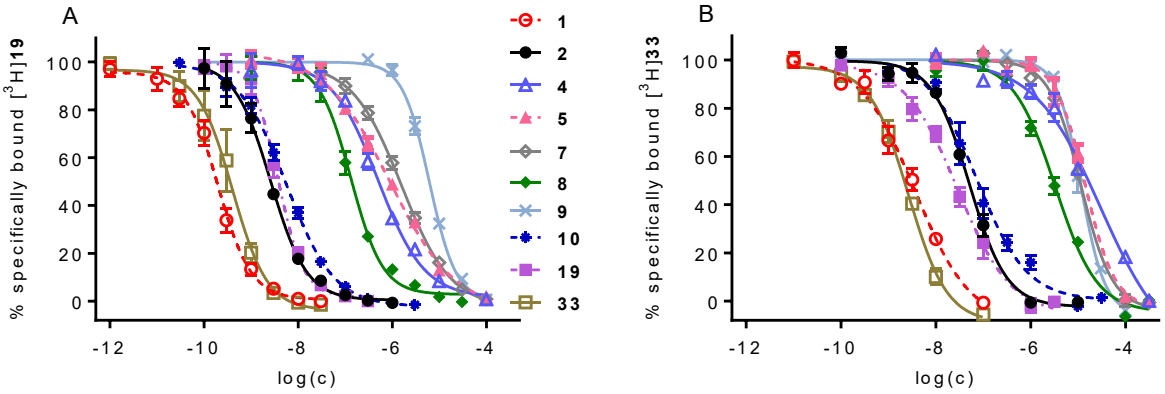

Figure 13. Concentration-dependent effects of various reported orthosteric (**1-5**), allosteric (**7**, **8**) and dualsteric (**10**, **19**, **33**) MR ligands on M_2R equilibrium binding of [^{3}H]**19** (c = 2 nM, K_d = 0.87 nM) (A) and [^{3}H]**33** (c = 0.5 nM, K_d = 0.24 nM except for competition binding experiments with compound **9** (c = 0.25 nM)) (B) determined at live CHO-hM_2 cells and at CHO-hM_2 cell homogenates, respectively. Data were analyzed by four-parameter logistic fits. Mean values ± SEM from at least three independent experiments (performed in triplicate).

Table 3. M_2R binding data (pK_i or pIC_{50}) of various orthosteric (**1**-**5**), allosteric (**7**-**9**) and dualsteric (**10**, **19** and **33**) MR ligands determined with [^{3}H]**19**, [^{3}H]**33** or [^{3}H]NMS.

Ligand	[^{3}H]**19** pK_i ± SEM[a]	[^{3}H]**33** pK_i ± SEM[b]	[^{3}H]NMS pK_i^* or pIC_{50}^{**} (± SEM)
1	10.2 ± 0.10	8.92 ± 0.03	9.7*[c]
2	9.09 ± 0.04	7.77 ± 0.04	7.8-9.2*[d]
4	6.83 ± 0.05	5.00 ± 0.12	5.0-6.6*[d]
5	6.57 ± 0.05	5.35 ± 0.03	6.5-7.4*[e]
7	6.33 ± 0.04	5.43 ± 0.01	6.11 ± 0.09**[f]
8	7.40 ± 0.03	5.97 ± 0.05	6.32 ± 0.18**[f]
9	5.73 ± 0.03	5.24 ± 0.05	<4.5**[g]
10	8.76 ± 0.07	7.63 ± 0.13	8.2*[d]
19	8.96 ± 0.06	7.99 ± 0.10	9.12 ± 0.05*[h]
33	9.97 ± 0.20	8.98 ± 0.05	9.39 ± 0.05*[h]

[a]Determined by equilibrium (competition) binding with [^{3}H]**19** (c = 2 nM) at intact CHO-hM_2 cells; mean values ± SEM from at least 3 independent experiments (performed in triplicate). [b]Determined by equilibrium (competition) binding with [^{3}H]**33** (c = 0.5 nM) at CHO-hM_2 cell homogenates; mean values ± SEM from at least three independent experiments (performed in triplicate). [c]Dei *et al.*[40] [d]pK_i values from equilibrium (competition) binding experiments reported in the literature (data taken from the IUPHAR/BPS database (guidetopharmacology.org, (Nov. 2016)). [e]Jakubik *et al.*[41] [f]pIC_{50} values obtained from nonlinear four-parameter logistic curve analyses of data characterizing the inhibition of [^{3}H]NMS (c = 0.2 nM) equilibrium binding at live CHO-hM_2 cells; mean ± SEM from at least 3 independent experiments (performed in triplicate). [g]Inhibitory effect on M_2R equilibrium binding of [^{3}H]NMS (c = 0.2 nM) at intact CHO-hM_2 cells (*cf.* Figure 7B). [h]pK_i values taken from Table 1.

In order to verify a putative competitive mechanism of the allosteric modulator **8** with [^{3}H]**19** and [^{3}H]**33** at the M_2R, equilibrium competition binding studies were performed applying increasing fixed concentrations/receptor occupancies of the radioligands (Figure 14A and Figure 14B). In the same manner, a reference experiment was performed with **8** and the orthosteric radioligand [^{3}H]NMS (Figure 14C). The control experiment with [^{3}H]NMS revealed an elevation of the lower plateau of the curves and the pIC_{50} of **8** was unaffected, indicating a non-competitive mechanism as reported previously.[29] By contrast, the lower plateau of the curves did not increase in case of [^{3}H]**19** and [^{3}H]**33**, and a rightward shift of the pIC_{50} of **8** was observed (Figure 14). These data support a competitive mechanism[39] between the allosteric M_2R ligand **8** and the dibenzodiazepinone-type ligands **19** and **33** and, consequently, a dualsteric binding mode of **19** and **33** at the M_2R.

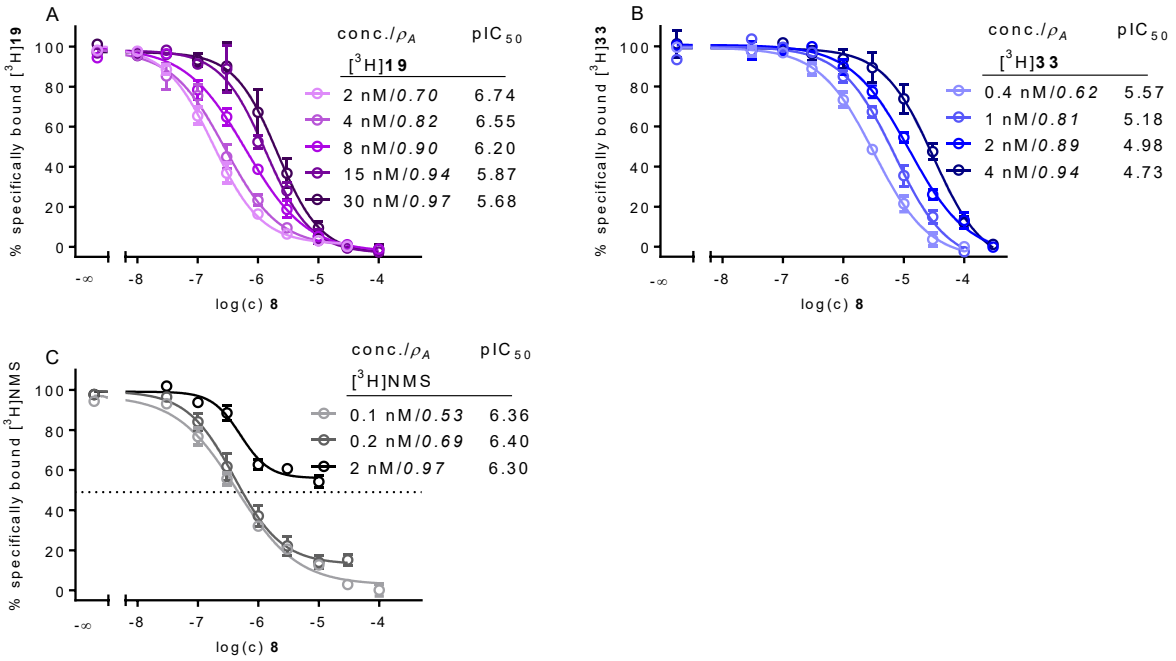

Figure 14. Effect of the allosteric MR modulator **8** on M_2R equilibrium binding of [^{3}H]**19** (K_d = 0.87 nM) (A), [^{3}H]**33** (K_d = 0.24 nM) (B) and [^{3}H]NMS (K_d = 0.09 nM) (C) using various radioligand concentrations. Experiments were performed at intact CHO-hM_2 cells (A, C) or at CHO-hM_2 cell homogenates (B). Unspecific binding was determined in the presence of atropine (500-fold excess to [^{3}H]**19**, [^{3}H]**33** or [^{3}H]NMS). Data were analyzed by four-parameter logistic fits. In case of [^{3}H]**19** and [^{3}H]**33** increasing radioligand concentrations resulted in a parallel rightward shift of the curves, which reached 0% specific radioligand binding throughout, indicating a competitive mechanism (A, B). In contrast, curves of [^{3}H]NMS equilibrium binding obtained in the presence of increasing concentrations of **8** were not rightward-shifted, instead, the lower plateau of the curve appeared to be elevated at increased radioligand concentrations, indicating negative allosteric cooperativity between **8** and [^{3}H]NMS (C). Data represent mean values ± SEM from at least three independent experiments (performed in triplicate). ρ_A = fractional receptor occupancy.

2.2.7 Schild-like analysis with 8 and 9 at the M_2R using [^{3}H]19 and [^{3}H]33

In order to substantiate the studies on the binding mode of [^{3}H]**19** and [^{3}H]**33** at the M_2R, saturation binding of [^{3}H]**19** and [^{3}H]**33** in the presence of the allosteric modulators **8** and **9** were performed (Figure 15). This kind of experiment is equivalent to the Schild analysis used to investigate the inhibiting effect of a receptor antagonist on the response elicited by an agonist and is considered the experiment of choice to unveil non-competitive mechanisms.[39, 42, 43] Increasing concentrations of **8** led to a parallel rightward shift of the saturation isotherms of both, the monomeric ligand [^{3}H]**19** and the homodimeric ligand [^{3}H]**33**, resulting in linear 'Schild' regressions with a slope not different from unity (Figure 15A and Figure 15C, Table 4), indicating a competitive mechanism between the allosteric M_2R ligand **8** and the dibenzodiazepinone-type ligands **19** and **33**. Likewise, the allosteric modulator **9**, which was co-crystallized with the M_2R bound to **6**,[22] elicited a parallel

rightward shift of [^{3}H]**19** saturation isotherms, again yielding a linear 'Schild' regression with a slope not different from unity (Figure 15B, Table 4). The 'pA_2' values derived from these 'Schild' regressions were in a good accordance with the pK_i values from equilibrium competition binding studies with [^{3}H]**19** and [^{3}H]**33** as well as with reported affinities (pK_A or pK_B) of **8** and **9** (Table 4). With regard to the fact that the dibenzodiazepinone derivatives **19** and **33** address the M_2R orthosteric binding site (see above) the results of the Schild-like analyses strongly suggested a dualsteric binding mode of **19** and **33** at the M_2R, that is, a simultaneous binding to the orthosteric site and the allosteric vestibule.

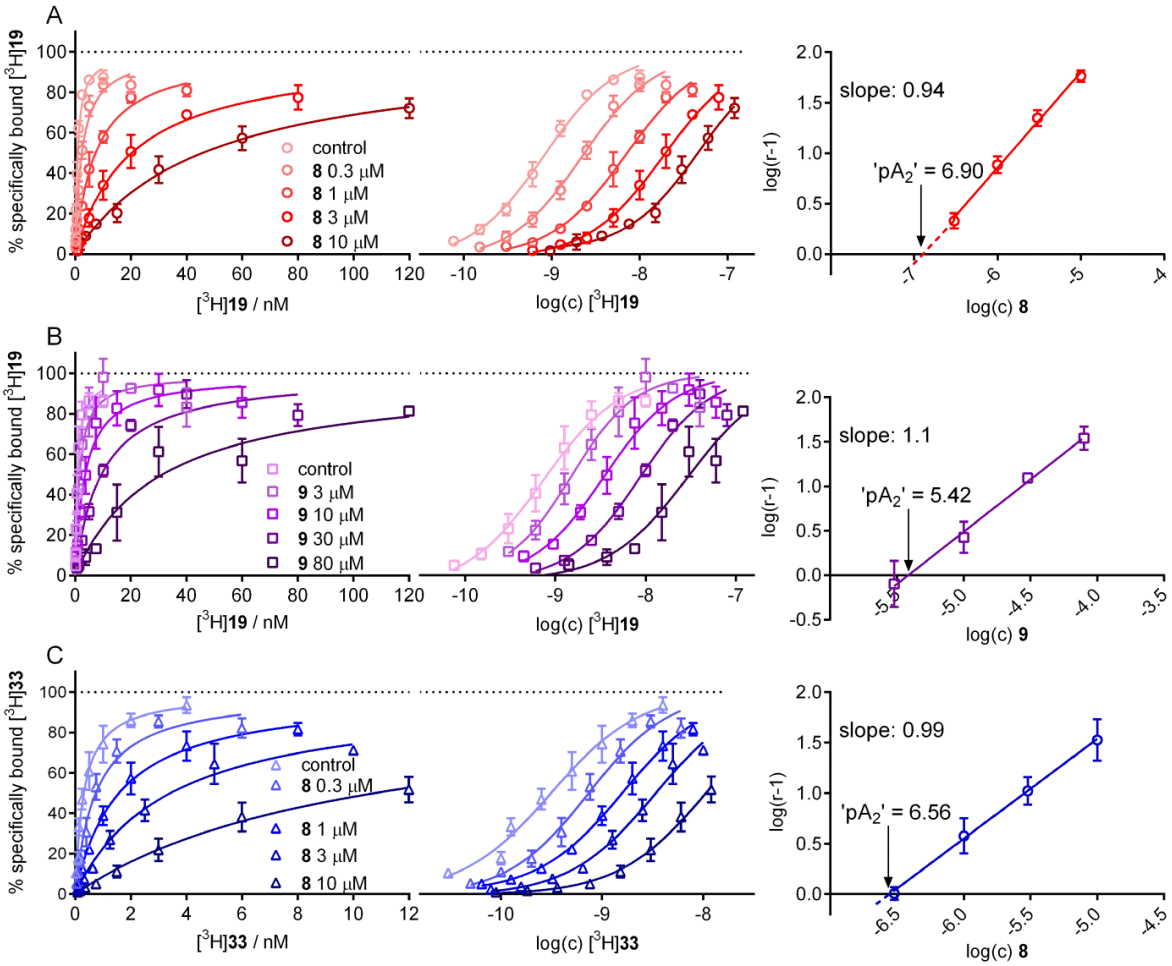

Figure 15. Saturation binding of [^{3}H]**19** in the presence of increasing concentrations of **8** (A) or **9** (B), and of [^{3}H]**33** in the presence of increasing concentrations of **8** (C). Presented are saturation isotherms of specific radioligand binding to the M_2R in linear scale (left) and semi-logarithmic scale (middle), and 'Schild' regressions (right) resulting from the rightward shifts (ΔpK_d) of the saturation isotherms (log(r−1) plotted vs. log(concentration allosteric modulator), where $r = 10^{\Delta pKd}$). The presence of the allosteric modulator (**8**, **9**) led to a parallel rightward shift of the saturation isotherms of both, the monomeric ([^{3}H]**19**) and the homodimeric ([^{3}H]**33**) radiolabeled dibenzodiazepinone derivative. In all cases the slope of the linear 'Schild' regression was nearly equal to unity indicating a competitive interaction between the radioligands and the investigated allosteric ligands. Experiments were performed at intact CHO-hM_2 cells (A, B) or at CHO-hM_2 cell homogenates (C). Data represent mean values ± SEM from at least three independent experiments (each performed in triplicate).

Table 4. Summary of M_2R binding data of the allosteric M_2R modulators **8** and **9** determined by the use of the radiolabeled dibenzodiazepinone derivatives [^{3}H]**19** and [^{3}H]**33.**

allosteric ligand	used radioligand	slope[a]	'pA_2'[b]	pK_i[c]	pK_A^* or pK_B^{**}
8	[^{3}H]**19**	0.94 ± 0.04	6.81 ± 0.02	7.39 ± 0.03	6.00/6.53*[d]
9	[^{3}H]**19**	1.1 ± 0.1	5.45 ± 0.09	5.73 ± 0.03	5.77**[e]
8	[^{3}H]**33**	0.98 ± 0.06	6.58 ± 0.01	5.91 ± 0.06	6.00/6.53*[d]

[a]Slope of the 'Schild' regression constructed based on radioligand binding data from saturation binding experiments in the presence of increasing fixed concentrations of the allosteric ligands **8** or **9**; mean values ± SEM from at least three sets of independent saturation binding experiments (performed in triplicate). The slope of the linear 'Schild' regression was not statistically different from unity (P >0.2). [b]The 'pA_2' value corresponds to the X-axis intercept of the linear 'Schild' regression (*cf.* Figure 15) and reflects the affinity of the investigated allosteric ligands. [c]pK_i values taken from Table 3. [d]Mohr *et al*.[44] [e]Kruse *et al*.[22]

2.2.8 Molecular dynamics simulations

Aiming at a verification of the conclusions drawn from the experimental data by computational methods, MD simulation of the human M_2R bound to the dibenzodiazepinone derivative **19** or **33** (2 and 3 µs, respectively) were performed. Simulations were prepared by induced fit docking of **19** and **33** to the M_2R in the inactive state (Figure 16).

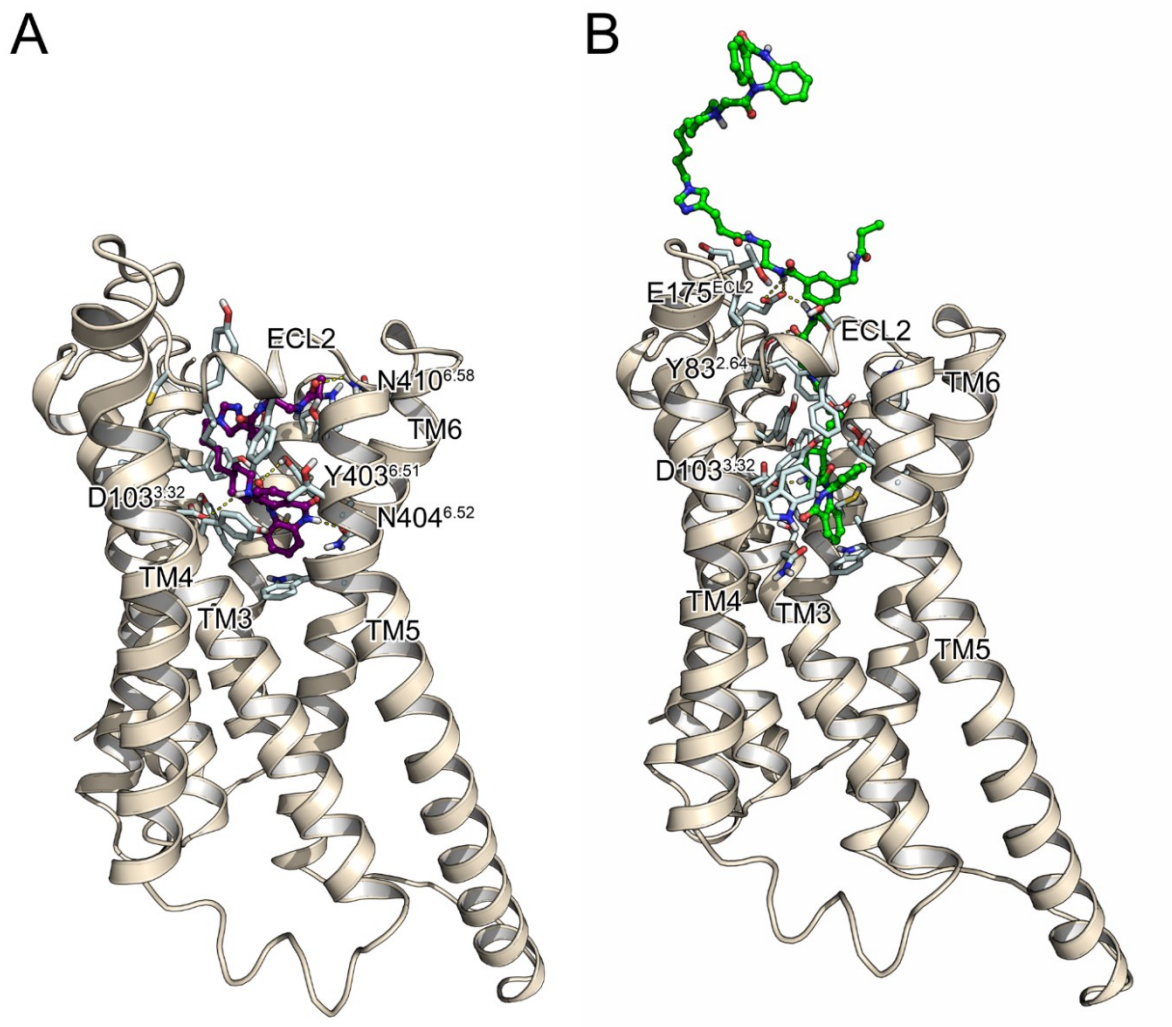

Figure 16. Induced fit docking-derived binding poses of the dibenzodiazepinone derivatives **19** (A) and **33** (B) at the human M_2R (inactive state, PDB ID 3UON), which were used as initial coordinates for the MD simulations (*cf*. experimental section).

The docking-derived orientation of **19** showed interactions of **19** with the lower part of the allosteric vestibule (Figure 16A), which was, regardless of minor conformational changes, persistent during the 2-µs simulation (Figure 17A and Figure 18). Amino acid residues reported to be involved in binding of the allosteric M_2R ligand **9**[22] appeared to be in close proximity to the monomeric ligand **19** and amino acid residues interacting with **19** (Figure 17A). These data suggested a (partial) overlap of the binding sites of **9** and **19**, which is consistent with the results of the experiments presented in Figure 15B (Schild-like analysis). Notably, the backbone contact between the propionamide moiety in **19** and $I178^{ECL2}$ suggested that **19** reaches the extracellular surface of the M_2R.

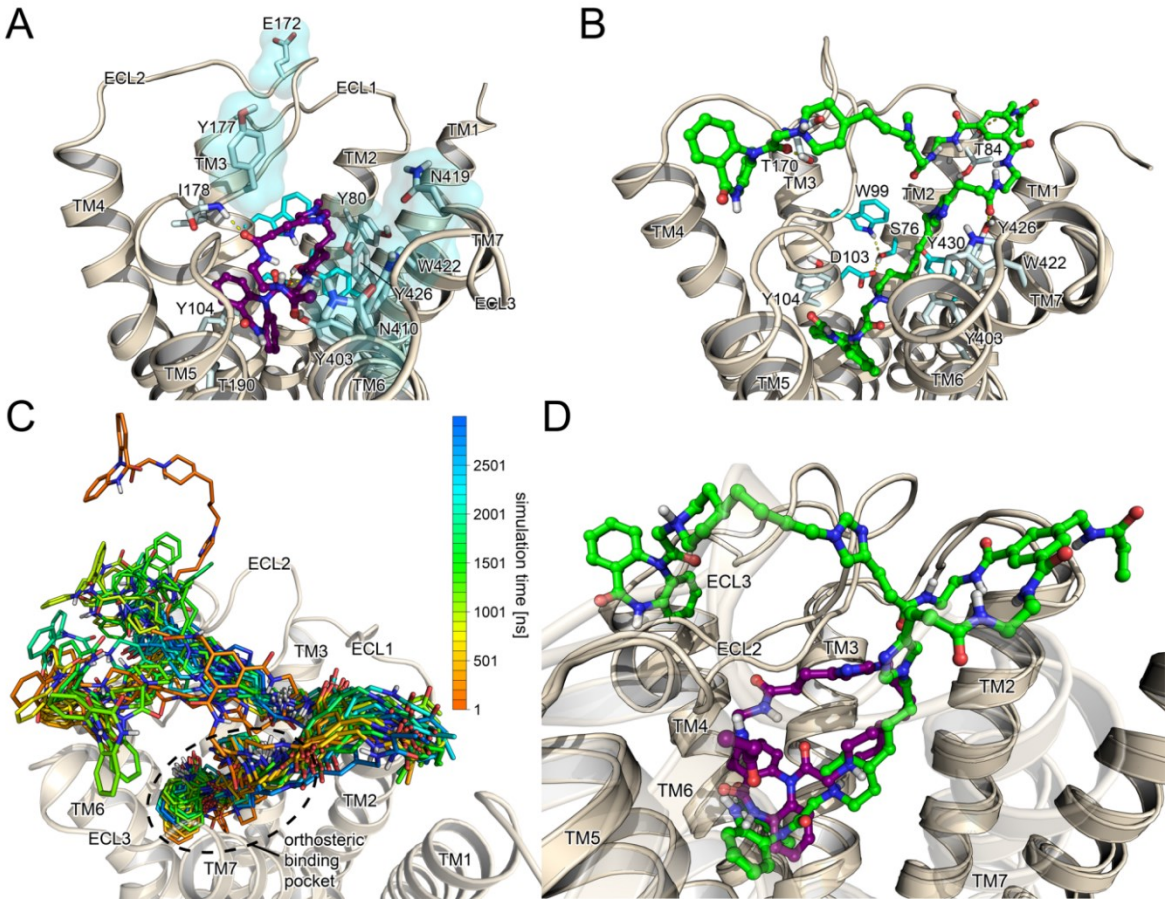

Figure 17. Molecular dynamics simulation of the human M_2R (inactive state, PDB ID 3UON) bound to the dibenzodiazepinone derivatives **19** and **33** (2 and 3 µs, respectively). (A) Cluster 1 binding pose of **19** (shown in purple). (B) Cluster 1 binding pose of **33** (shown in green). In A and B carbon atoms of amino acids constituting the $D103^{3.32}$-$W99^{3.28}$-$S76^{2.57}$-$Y430^{7.43}$ cluster are highlighted in cyan (only assigned in B). Key amino acids suggested to interact with **19** were $Y104^{3.33}$ (π-π), $I178^{ECL2}$ (HB), $T190^{5.42}$ (HB) and $Y403^{6.51}$ (HB) (A). Key amino acids suggested to interact with **33** were $T84^{2.65}$ (HB), $D103^{3.32}$ (HB), $Y104^{3.33}$ (π-π), $T170^{ECL2}$ (HB), $Y403^{6.51}$ (HB), $W422^{7.35}$ (HB) and $Y426^{7.39}$ (HB) (B). In A, amino acids reported to interact with the allosteric modulator **9**, that is $Y80^{2.61}$, $E172^{ECL2}$, $Y177^{ECL2}$, $N410^{6.58}$, $N419^{7.32}$, $W422^{7.35}$ and $Y426^{7.39}$, are surrounded by transparent cyan surface.[22] (C) Time course of the 3-µs MD simulation of the M_2R bound to **33** showing superimposed snap shots collected every 100 ns. (D) Superimposition of the cluster 1 binding poses of **19** (purple) and **33** (green). HB = hydrogen bonding.

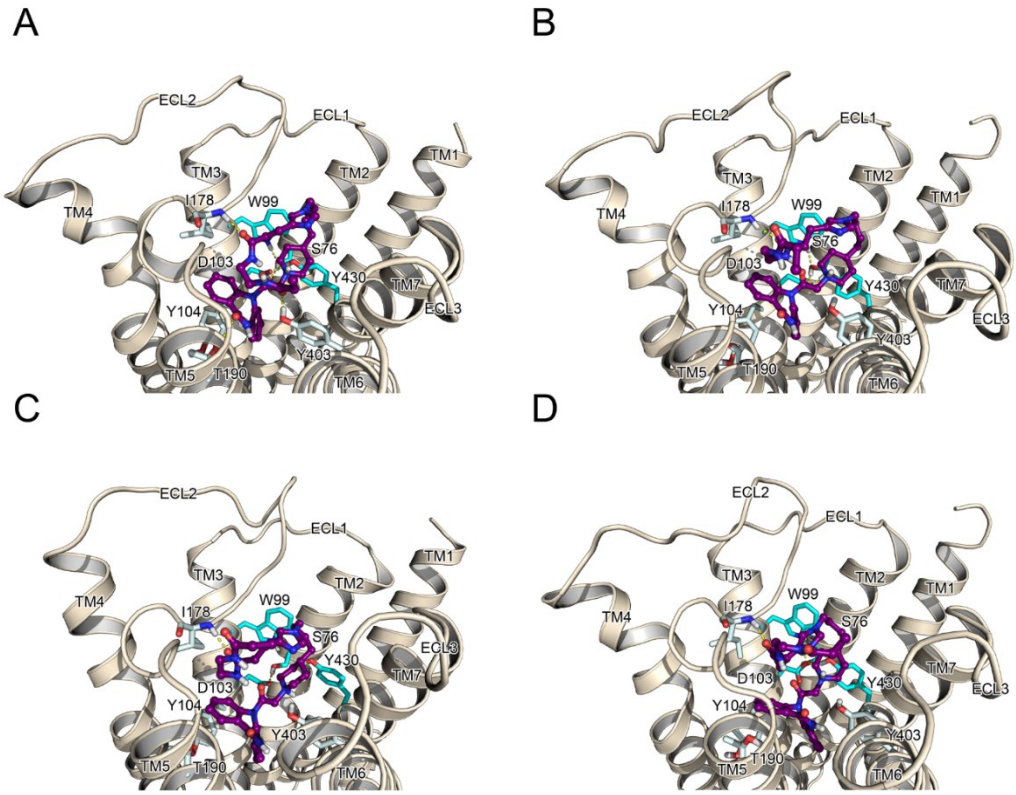

Figure 18. Binding poses of cluster 2 (A), 3 (B), 4 (C) and 5 (D) (*cf.* Table 5) of the monomeric dibenzodiazepinone derivative **19** (shown in purple) obtained from a 2-µs MD simulation of the human M_2R (inactive state, PDB ID 3UON) bound to **19**. The poses and putative interactions of **19** with the M_2R were comparable to that of cluster 1 (see Figure 17A).

As also observed for the monomeric compound **19,** the orientation of the orthosterically bound part of the dimeric ligand **33** varied only marginally during the 3-µs simulation, that is, it remained tightly bound to the orthosteric site. By contrast, the major part of the linker and the second dibenzodiazepinone pharmacophore in **33**, being unbound and located in the 'extracellular space' at the beginning of the simulation (*cf*. Figure 16B and frame 1 (orange) in Figure 17C), showed a high flexibility over the first 2 µs (in part reflected by Figure 17C and Figure 19). Strikingly, in the late phase of the simulation the flexibility of the allosterically interacting part of **33** was much lower resulting in a persistence of the predominant binding pose of **33** (represented by cluster 1, Figure 17D, Table 5) over 1 µs (Figure 17C).

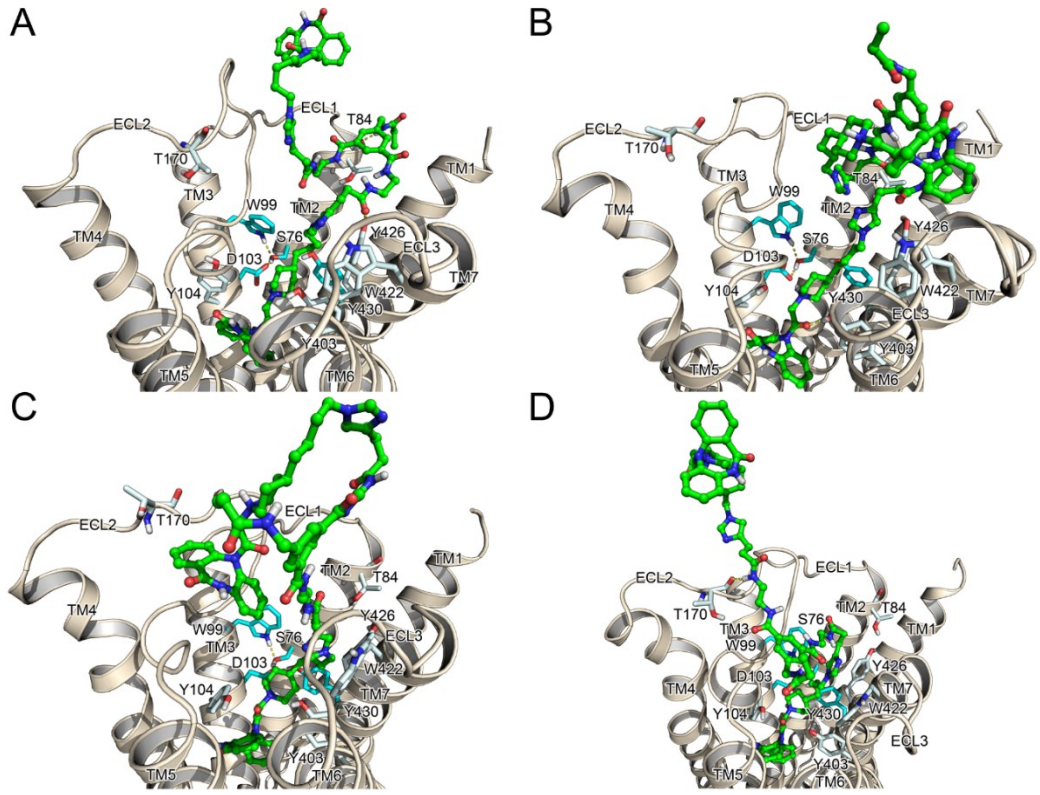

Figure 19. Binding poses of cluster 2 (A), 3 (B), 4 (C) and 5 (D) (*cf*. Table 5) of the homodimeric dibenzodiazepinone derivative **33** (shown in green) obtained from a 3-µs MD simulation of the human M_2R (inactive state, PDB ID 3UON) bound to **33**. Whereas the binding poses of **33** were mostly invariant in the region of the orthosteric binding pocket they markedly differed concerning the allosterically interacting part of **33** (for cluster 1 binding pose of **33** *cf*. Figure 17B**)**

Table 5. Relative occurrence of the clusters 1-5 obtained by the cluster analysis of the MD simulation trajectories (*cf*. experimental section).

Cluster	**19**	**33**
1	92.8 %	95 %
2	4.2 %	2 %
3	1.3 %	1.7 %
4	1.1 %	1.3 %
5	0.6 %	0.1 %

Notably, Asp103$^{3.32}$, which typically forms a salt bridge with basic amine functions of MR agonists as a key interaction for receptor activation[45] and can be involved in the binding of MR antagonists as well,[21] did not show an interaction with the monomeric ligand **19** (Figure 20B). By contrast, an interaction of Asp103$^{3.32}$ was evident with the dimeric compound **33** (Figure 20B). In both simulations, Asp103$^{3.32}$ formed an H-bonding network with Ser76$^{2.57}$ and Trp99$^{3.28}$, in case of the simulation with **19** additionally with Tyr430$^{7.43}$ (*cf*. Figure 20A),

which is characteristic of the inactive receptor conformation.[23] As anticipated, the homodimeric ligand **33** showed more 'allosteric contacts' in the simulation compared to the monomeric ligand **19**. Summarized, the results obtained from the MD simulations were consistent with the results of the aforementioned experiments, which suggested a dualsteric binding mode of the investigated tricyclic MR ligands **19** and **33**.

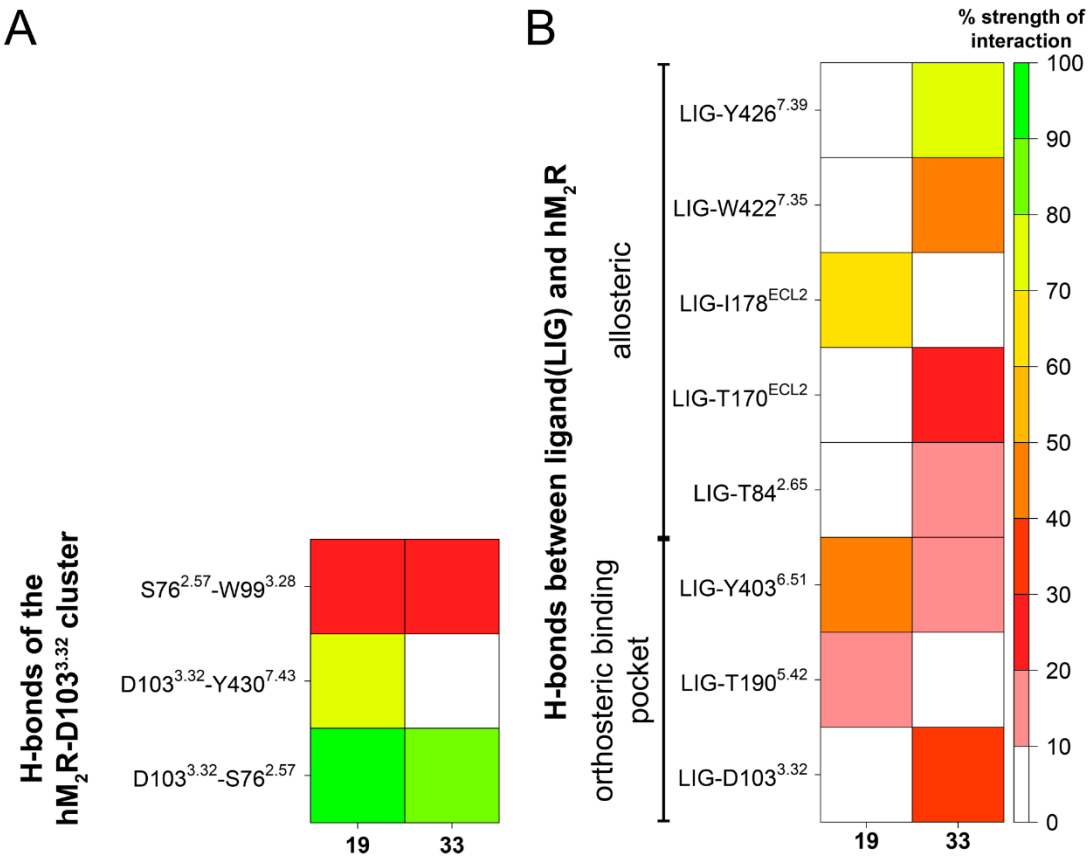

Figure 20. H-bond analysis of the MD simulation trajectories performed for the D103 cluster (comprising D103, W99, S76, Y430) (A) and ligand receptor interactions (B). In case of the homodimeric ligand **33** 'allosteric contacts' were considerably more pronounced compared to the monomeric ligand **19** (B). The % strength of interaction values represent cumulated values taking into account all possible atom to atom combinations of the given amino acid pairs (excluding the backbone) (A) or atom to atom combinations of the respective ligand and the given amino acid (including the backbone).

2.2.9 M_2R binding studies with 50

Compound **50**, representing the allosterically interacting part of the dualsterically binding MR ligand **19**, was investigated with respect to M_2R binding by studying its potential inhibitory effect on M_2R equilibrium binding of [^{3}H]NMS and [^{3}H]**19** at intact CHO-hM_2 cells. **50** could not 'inhibit' M_2R binding of [^{3}H]NMS and [^{3}H]**19** at concentrations below 100 µM (Figure 21) suggesting that the allosteric interactions of **19** are not or only marginally responsible for the high M_2R affinity of the dualsteric ligand **19**.

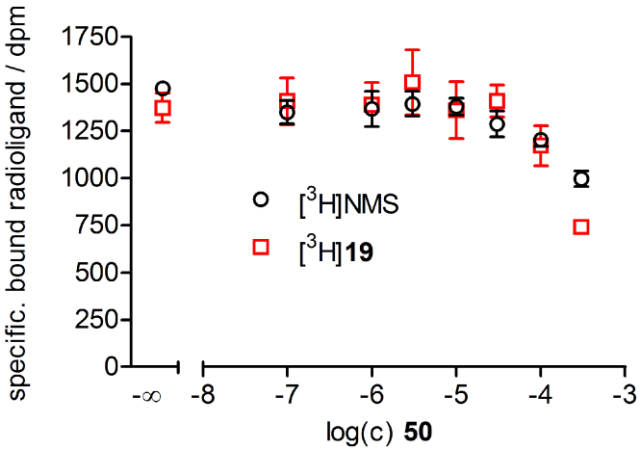

Figure 21. Effect of **50** on M_2R equilibrium binding of [^{3}H]NMS (c = 0.2 nM, K_d = 0.09 nM) and [^{3}H]**19** (c = 2 nM, K_d = 0.87 nM) determined at intact CHO-hM_2 cells. **50** did not 'inhibit' M_2R binding of [^{3}H]NMS and [^{3}H]19 at concentrations below 100 µM. Shown are data of representative experiments performed in triplicate (at least two independent experiments were performed and gave comparable results).

2.3. Conclusion

The presented study comprises the first report on tritium-labeled dibenzodiazepinone-type, M_2R subtype-preferring MR antagonists including the comparison of a homodimeric derivative ([^{3}H]**33**) with its monomeric counterpart ([^{3}H]**19**). With K_d values below 1 nM both radioligands exhibited considerably higher M_2R affinities than the structurally related pyridobenzodiazepinone-type MR antagonist [^{3}H]**10** (K_d = 11 nM, M_2R), that was previously suggested to bind to the allosteric vestibule of the M_2R.[29] The synthesis of the radiolabeled compounds [^{3}H]**19** and [^{3}H]**33** contributed significantly to the elucidation of the M_2R binding mode of the high affinity dibenzodiazepinone derivatives **19** and **33**. The results from various binding experiments with [^{3}H]**19** and [^{3}H]**33**, in particular, saturation binding studies in the absence and in the presence of well characterized allosteric M_2R ligands (compounds **8** and **9**), strongly indicated that the presented type of M_2R antagonists (**19**, **33**, and presumably the reported congeners **20** and **21**, too) interact simultaneously with both the orthosteric and the 'common' allosteric binding site. Therefore, this study demonstrates that the use of radiolabeled analogs can significantly contribute to a better understanding of the binding mode of complex receptor ligands. The dualsteric radioligands [^{3}H]**19** and [^{3}H]**33**, which are synthetically conveniently available and exhibit high M_2R affinity and high chemical stability, represent valuable pharmacological tools complementary to known orthosteric MR radioligands. Moreover, this work suggests dibenzodiazepinone-type MR ligands as privileged structures to develop M_2R selective antagonists according to the dualsteric ligand approach[8, 14, 16-20] by the synthesis of heterodimeric ligands comprising a linkage of the dibenzodiazepinone scaffold to reported allosteric M_2R pharmacophores as well as to newly designed allosterically interacting moieties based on the information from MR crystal structures.

2.4. Experimental Section

2.4.1 General experimental conditions

Chemicals and solvents were purchased from commercial suppliers and were used without further purifications unless otherwise specified. Acetonitrile for HPLC (gradient grade) was obtained from Merck (Darmstadt, Germany). *N*-methyl scopolamine (**1**), atropine (**2**), carbachol (**3**), gallamine (**7**), **8**, **22**, **34**, **39** and **40** were purchased from Sigma-Aldrich (Deisenhofen, Germany). Oxotremorine sesquifumarate (**4**) was from MP Biomedicals (Eschwege, Germany), compound **9** was from Absource Diagnostic (Munich, Germany) and **10** was purchased from Abcam (Cambridge, UK). [^{3}H]NMS (specific activity = 80 Ci/mmol) was purchased from American Radiolabeled Chemicals Inc. (St. Louis, MO) via Hartman Analytics GmbH (Braunschweig, Germany). The syntheses of dibenzodiazepinone derivative **30** and urocanic acid derivative **48** were described previously.[31] Xanomeline (**5**) and compound **36** were synthesized according to described procedures.[46, 47] Technical grade solvents (CH_2Cl_2, ethyl acetate, light petroleum) were distilled before use. For solvent dehydration THF and diethyl ether were distilled over sodium, and CH_2Cl_2 was distilled over P_2O_5 after predrying over $CaCl_2$. Millipore water was used throughout for the preparation of buffers and HPLC eluents. Polypropylene reaction vessels (1.5 or 2 mL) with screw cap (Süd-Laborbedarf, Gauting, Germany) were used for the synthesis of radioligands ([^{3}H]**19**, [^{3}H]**33**, [^{3}H]**47**), for small scale reactions, for the investigation of chemical stabilities (**19**, **47**) and for the preparation and storage of stock solutions. The chemical stability of **33** was investigated in a flat-bottom glass tube (40 × 8.2 mm) (Altmann Analytik GmbH, Munich, Germany), which was siliconized before use using Sigmacote (Sigma-Aldrich). Thin layer chromatography (TLC) was performed on Merck silica gel 60 F_{254} TLC aluminum plates. Visualization was accomplished by UV irradiation (λ = 254 or 366 nm) and by staining with ninhydrin or potassium permanganate. Silica Gel 60 (40-60 µm, Merck) was used for column chromatography. A Biotage Initiator microwave synthesizer (Biotage, Uppsala, Sweden) was used for microwave driven reactions. NMR spectra were recorded on a Bruker Avance 300 (7.05 T, ^{1}H: 300.1 MHz, ^{13}C: 75.5 MHz), Bruker Avance III HD 400 (9.40 T, ^{1}H: 400 MHz, ^{13}C: 100 MHz) or a Bruker Avance III HD 600 equipped with a cryogenic probe (14.1 T ^{1}H: 600.1 MHz, ^{13}C: 150.9 MHz) (Bruker, Karlsruhe, Germany) with TMS as external standard. IR spectra were measured with a NICOLET 380 FT-IR spectrophotometer (Thermo Electron Corporation). Low-resolution mass spectrometry (MS) was performed on a Finnigan SSQ 710A instrument (CI-MS) (Thermo Finnigan, San Jose, CA). High-resolution mass spectrometry (HRMS) analysis was performed on an Agilent 6540 UHD Accurate-Mass Q-TOF LC/MS system (Agilent Technologies, Santa Clara, CA) using an ESI source. Preparative HPLC was performed with a system from Knauer (Berlin, Germany)

consisting of two K-1800 pumps and a K-2001 detector. A Kinetex-XB C18 (5 µm, 250 mm × 21 mm; Phenomenex, Aschaffenburg, Germany) or an Actus Triart C18 (5 µm, 150 mm × 21 mm; YMC Europe GmbH, Dinslaken, Germany) were used as stationary phases at a flow rate of 18 mL/min. Mixtures of acetonitrile and 0.1% aq TFA and mixtures of acetonitrile and 0.1% aq ammonia, respectively, were used as mobile phase. The detection wavelength was set to 220 nm throughout. The solvent of the collected fractions was removed by lyophilization using an Alpha 2-4 LD apparatus (Martin Christ, Osterode am Harz, Germany) equipped with a RZ 6 rotary vane vacuum pump (Vacuubrand, Wertheim, Germany). Analytical HPLC analysis of compounds **19**, **33** and **47** (concentrations between 25 and 50 µM) was performed with a system from Agilent Technologies composed of a 1290 Infinity binary pump equipped with a degasser, a 1290 Infinity autosampler, a 1290 Infinity thermostated column compartment, a 1260 Infinity diode array detector, and a 1260 Infinity fluorescence detector. A Kinetex-XB C18 (2.6 µm, 100 × 3 mm; Phenomenex) served as stationary phase at a flow rate of 0.5 mL/min except for the analysis of **50**. Mixtures of 0.04% aq TFA (A) and acetonitrile (B) were used as mobile phase. The following linear gradient was applied: 0-20 min: A/B 90:10-68:32, 20-22 min: 68:32-5:95, 22-28 min: 5:95. Analytical HPLC analysis of compound **50** was performed using an Actus Triart C18 (3 µm, 150 × 2 mm; YMC Europe) as stationary, and mixtures of 0.1% aq ammonia (C) and acetonitrile (B) as mobile phase (flow rate: 0.5 mL/min). The following linear gradient was applied: 0−10 min: C/B 95:5-90:10, 10-20 min: 90:10-10:90, 20-28 min: 10:90. For all analytical HPLC runs the oven temperature was set to 25 °C, the injection volume was 20 µL and detection was performed at 220 nm. Melting points were determined with a Büchi 510 apparatus (Büchi, Essen, Germany) and are uncorrected.

Annotation concerning the NMR spectra (^{1}H, ^{13}C) of the dibenzodiazepinone derivatives (**31**, **33**, **37**, **38**, **46**, **47**): due to a slow rotation about the exocyclic amide group on the NMR time scale, two isomers (ratios provided in the experimental protocols) were evident in the ^{1}H- and ^{13}C-NMR spectra.

2.4.2 Compound characterization

New organic compounds were characterized by ^{1}H- and ^{13}C-NMR spectroscopy, HRMS and melting point (if applicable). In addition, the target compounds **31**, **33**, **46**, **47, 50** and **52** were characterized by 2D-NMR spectroscopy (^{1}H-COSY, HSQC, HMBC) and RP-HPLC analysis. Furthermore, IR spectra were acquired for the homodimeric ligands **33** and **47**. The purity of final compounds, determined by RP-HPLC (220 nm), was ≥97% throughout (chromatograms shown in Appendix).

2.4.3 Chemistry: experimental protocols and analytical data

Trimethyl 1,3,5-benzenetricarboxylate (23)[48] Trimesic acid (**22**) (16 g, 76.1 mmol) was dissolved in MeOH (280 mL) and concentrated H_2SO_4 (4 mL, ca 75 mmol) was added dropwise under stirring. The mixture was refluxed for 24 h. Cooling to rt resulted in a partial precipitation of **23** as a white solid that was collected by vacuum filtration. The filtrate was evaporated to dryness to yield a white solid, which was dissolved in CH_2Cl_2 (40 mL) followed by washing with saturated aq $NaHCO_3$ (2 × 15 mL) and drying over Na_2SO_4. Removal of the solvent under reduced pressure yielded **23** as a white solid that was combined with the above mentioned precipitated product (19.1 g, 75.8 mmol, 99%), mp 145 °C (lit.[49] 144-145 °C). ^{1}H-NMR (300 MHz, DMSO-d_6): δ (ppm) 3.92 (s, 9H), 8.56 (s, 3H). ^{13}C-NMR (75 MHz, DMSO-d_6): δ (ppm) 48.64, 130.97, 133.43, 164.56. MS (CI, NH_3): *m/z* (%) 252 (25) $[M]^{\bullet+}$, 221 (100) $[M\text{-}OCH_3]^{\bullet+}$. $C_{12}H_{12}O_6$ (252.22).

3,5-Di(methoxycarbonyl)benzoic acid (24)[33] 1 N aq NaOH (19.8 mL, 19.8 mmol) was added dropwise to a suspension of **23** (5.55 g, 22.0 mmol) in MeOH (500 mL) over a period of 5 min and the mixture was stirred vigorously at rt for 18 h (after 8 h solid material had completely disappeared). The volatiles were removed under reduced pressure. The residue was dissolved in CH_2Cl_2 (75 mL) and the product was extracted with saturated aq $NaHCO_3$ (2 × 75 mL). The organic phase was dried over Na_2SO_4 and the solvent was evaporated to give non-converted starting material **23**. The aqueous phase was acidified (pH 2) by the addition of concentrated aq hydrochloric acid to yield a white precipitate. Solid material was collected by vacuum filtration, washed with EtOAc (2 × 75 mL) and dried *in vacuo* to give **24** as a white solid (3.95 g, 16.6 mmol, 75%), mp 145-147°C (lit.[50] 145-147 °C). ^{1}H-NMR (300 MHz, $CDCl_3$): δ (ppm) 4.00 (s, 6H), 8.90-8.94 (m, 3H). ^{13}C-NMR (75 MHz, $CDCl_3$): δ (ppm) 53.89, 130.44, 131.53, 135.28, 135.59, 165.41, 170.28. HRMS (ESI): *m/z* $[M+H]^+$ calcd. for $[C_{11}H_{12}O_6]^+$ 239.0550, found 239.0549. $C_{11}H_{11}O_6$ (238.20).

Dimethyl 5-(hydroxymethyl)isophthalate (25)[33] Carboxylic acid **24** (3.40 g, 14.3 mmol) was dissolved in anhydrous THF (24 mL). Borane dimethyl sulfide complex (2 M in THF, 14.3 mL, 28.6 mmol) was added dropwise over a period of 20 min (effervescence occurred). The solution was stirred at room temperature for 24 h. MeOH (50 mL) was added and stirring was continued at rt for 30 min. The volatiles were removed *in vacuo* to yield a white solid, which was dissolved in EtOAc (75 mL) followed by washing with H_2O (75 mL), saturated aq $NaHCO_3$ (75 mL) and brine (50 mL). The organic phase was dried over Na_2SO4 and the solvent was evaporated under reduced pressure to afford **25** as a white solid (2.79 g, 12.4 mmol, 87%), mp 102-104 °C (lit.[33] 104 °C). ^{1}H-NMR (300 MHz, $CDCl_3$): δ (ppm) 3.94 (s, 6H), 4.79 (d, 2H, *J* 0.7 Hz), 8.20-8.22 (m, 2H), 8.56 (t, 1H, *J* 1.7 Hz). ^{13}C-

NMR (75 MHz, $CDCl_3$): δ (ppm) 52.58, 64.29, 129.91, 130.89, 132.12, 142.03, 166.33. MS (CI, NH_3): *m/z* (%) 224 (40) $[M]^{\bullet+}$, 193 (100) $[M\text{-}OCH_3]^{\bullet+}$. $C_{11}H_{12}O_5$ (224.21).

Dimethyl 5-(chloromethyl)isophthalate (26)[33] Alcohol **25** (2.0 g, 8.9 mmol) was dissolved in thionyl chloride (1.3 mL, 17.9 mmol) and the mixture was refluxed under an atmosphere of argon for 1.5 h. $CHCl_3$ (40 mL) was added and the solution was washed with 1 N aq NaOH (2 × 50 mL) and brine (2 × 50 mL). The organic phase was dried over Na_2SO_4 and the volatiles were removed under reduced pressure to yield **26** as a white solid (2.13 g, 8.8 mmol, 98%), mp 119-121 °C (lit.[33] 118-120 °C). ^{1}H-NMR (300 MHz, $CDCl_3$): δ (ppm) 3.95 (s, 6H), 4.65 (s, 2H), 8.25 (d, 2H, *J* 1.6 Hz), 8.63 (t, 1H, *J* 1.6 Hz). ^{13}C-NMR (75 MHz, $CDCl_3$): δ (ppm) 45.00, 52.67, 130.71, 131.34, 133.90, 138.58, 165.87. MS (CI, NH_3): *m/z* (%) 244/242 (10/25) $[M]^{\bullet+}$, 213/211 (30/70) $[M\text{-}OCH_3]^{\bullet+}$. $C_{11}H_{11}ClO_4$ (242.66).

Dimethyl 5-(azidomethyl)isophthalate (27)[33] Compound **26** (2.0 g, 8.2 mmol) was dissolved in acetone/water (3:1 v/v) (40 mL). Sodium azide (3.21 g, 49.5 mmol) was added and the mixture was refluxed for 18 h. The volatiles were removed *in vacuo*, the residue was dissolved in $CHCl_3$ (75 mL) and the solution was washed with brine (2 × 50 mL). The organic phase was dried over Na_2SO_4 and the solvent removed under reduced pressure to yield **27** as a pale yellow solid (1.98 g, 7.9 mmol, 96%), mp 74-76 °C (lit.[33] 74-75 °C). ^{1}H-NMR (300 MHz, $CDCl_3$): δ (ppm) 3.96 (s, 6H), 4.48 (s, 2H), 8.19 (d, 2H, *J* 1.6 Hz), 8.65 (t, 1H, *J* 1.7 Hz). ^{13}C-NMR (75 MHz, $CDCl_3$): δ (ppm) 52.68, 54.03, 130.61, 131.38, 133.33, 136.72, 165.94. HRMS (ESI): *m/z* $[M+H]^+$ calcd. for $[C_{11}H_{12}N_3O_4]^+$ 250.0823, found 250.0822. $C_{11}H_{11}N_3O_4$ (249.23).

5-(Aminomethyl)isophthalic acid hydrochloride (28)[34] H_2O (10 mL) and triphenylphosphine (1.89 g, 7.2 g) were added to a solution of **27** (1.6 g, 6.42 mmol) in THF (30 mL) and the mixture was stirred at room temperature for 10 h. 1 M aq NaOH (24.6 mL, 24.6 mmol) was added and stirring was continued for 8 h. H_2O (30 mL) was added followed by treatment with CH_2Cl_2 (1 × 100 mL) and EtOAc (1 × 100 mL). The aqueous phase, containing the product, was acidified (pH 5) by the addition of 1 N HCl. THF (100 mL) was added and the mixture was kept at −20 °C overnight yielding a white precipitate that was collected by filtration, washed with ethanol (2 × 30 mL) and dried to afford **28** as a white solid (0.89 g, 4.6 mmol, 71%). ^{1}H-NMR (300 MHz, D_2O): δ (ppm) 4.14 (s, 2H), 8.08 (d, 2H, *J* 1.7 Hz), 8.28 (t, 1H, *J* 1.6 Hz). ^{13}C-NMR (75 MH, D_2O): δ (ppm) 57.35, 131.07, 131.16, 133.65, 134.44, 168.44. HRMS (ESI): *m/z* $[M+H]^+$ calcd. for $[C_9H_{10}NO_4]^+$ 196.0605, found 196.0613. $C_9H_9NO_4 \cdot HCl$ (195.17 + 36.46).

***N-tert*-Butoxycarbonyl-5-(aminomethyl)isophthalic acid (29)**[51] Triethylamine (323 µL, 2.31 mmol) and di-*tert*-butyl-dicarbonate (202 mg, 0.92 mmol) were added to a suspension of **28** (150 mg, 0.77 mmol) in H_2O/dioxane (1:1 v/v) (16 mL) and the mixture was vigorously stirred at rt for 24 h. 1 N HCl was added (pH 2) and the mixture was kept at −78 °C overnight. Removal of the solvent by lyophilization yielded a white residue which was suspended in EtOAc (30 mL) followed by treatment with 0.1 M aq $NaHSO_4$ (30 mL) and brine (30 mL). The organic phase was dried over Na_2SO_4 and the volatiles were removed under reduced pressure to give **29** as a white powder (140 mg, 0.47 mmol, 61%), mp >300 °C (decomp.). ^{1}H-NMR (300 MHz, MeOH-d_4): δ (ppm) 1.47 (s, 9H), 4.34 (s, 2H), 8.16 (br s, 2H), 8.53 (br s, 1H). ^{13}C-NMR (75 MHz, MeOH-d_4): δ (ppm) 28.74, 44.38, 80.47, 130.52, 132.64, 133.39, 158.61, 168.73. HRMS (ESI): *m/z* $[M-H]^-$ calcd. for $[C_{14}H_{16}NO_6]^-$, 294.0983, found 294.1008. $C_{14}H_{17}NO_6$ (295.29).

5-(Aminomethyl)-*N*^{1},*N*^{3}-bis(2-(3-(1-(4-(1-(2-oxo-2-(11-oxo-10,11-dihydro-*5H*-dibenzo[*b,e*][1,4]diazepin-5-yl)ethyl)piperidin-4-yl)butyl)-1H-imidazol-4-yl)propanamido)ethyl) isophthalamide pentakis(hydrotrifluoroacetate) (31) HOBt (39 mg, 0.29 mmol), TBTU (188 mg, 0.584 mmol) and DIPEA (132 µL, 0.75 mmol) were added to a solution of **29** (43 mg, 0.15 mmol) in DMF and the mixture was stirred at rt for 15 min. Amine **30** (tris(hydrotrifluoroacetate))[31] was added and stirring was continued at 60 °C for 3 h. The volatiles were removed under reduced pressure, the residue was dissolved in CH_2Cl_2/TFA/H_2O 1:1:0.1 (v/v/v, 8 mL) and the mixture was stirred at rt for 2 h followed by evaporation of the volatiles. Purification by preparative HPLC (column: Kinetex-XB C18, gradient: 0-25 min: 0.1% aq TFA/acetonitrile 90:10-60:40, t_R = 16 min) yielded **31** as a white fluffy solid (89 mg, 0.048 mmol, 32%). Ratio of configurational isomers evident in the NMR spectra: ca 1.6:1. ^{1}H-NMR (600 MHz, MeOH-d_4): δ (ppm) 1.30-1.36 (m, 8H), 1.40-1.58 (m, 6H), 1.80-1.98 (m, 8H), 2.60 (t, 4H, *J* 7.2 Hz), 2.85-2.94 (m, 2H), 2.97 (t, 4H, *J* 7.2 Hz), 3.00-3.11 (m, 2H), 3.41 (t, 4H, *J* 6.2 Hz), 3.43-3.49 (m, 2H), 3.50 (t, 4H, *J* 6.1 Hz), 3.73 (d, 3H, *J* 16.4 Hz), 3.80 (d, 1H, *J* 16.6 Hz), 4.15 (t, 4H, *J* 7.3 Hz), 4.24 (s, 2H), 4.41 (d, 1H, *J* 16.6 Hz), 4.45 (d, 1H, *J* 16.6 Hz), 7.22-7.42 (m, 7H), 7.44-7.56 (m, 4H), 7.59-7.72 (m, 4H), 7.75 (t, 1H, *J* 1.6 Hz), 7.90 (d, 1H, *J* 8.1 Hz), 7.96 (d, 1H, *J* 7.9 Hz), 8.06 (d, 2H, *J* 1.5 Hz), 8.28 (t, 1H, *J* 1.7 Hz), 8.80 (d, 2H, *J* 1.5 Hz). ^{13}C-NMR (150.9 MHz, MeOH-d_4): δ (ppm) 21.51, 24.17, 30.39, 31.08, 34.26, 34.88, 36.00, 40.08, 40.93, 43.79, 50.34, 54.87, 55.23, 58.08, 119.78, 123.08, 123.65, 126.85, 127.52, 127.89, 128.48, 128.87, 129.44, 130.11, 130.55, 130.88, 131.21, 131.71, 131.87, 131.95, 132.34, 133.00, 133.40, 134.57, 134.92, 135.26, 135.47, 135.52, 135.72, 137.02, 141.00, 142.67, 164.98, 165.48, 168.81, 168.84, 174.02. HRMS (ESI): *m/z* $[M+4H]^{4+}$ calcd. for $[C_{73}H_{91}N_{15}O_8]^{4+}$ 326.4289, found 326.4305. RP-HPLC (220 nm): 98% (t_R = 11.7 min, *k* = 11.6). $C_{73}H_{87}N_{15}O_8 \cdot C_{10}H_5F_{15}O_{10}$ (1302.60 + 570.12).

***N*¹,*N*³-Bis(2-(3-(1-(4-(1-(2-oxo-2-(11-oxo-10,11-dihydro-5H-dibenzo[b,e][1,4]diazepin-5-yl)ethyl)piperidin-4-yl)butyl)-1H-imidazol-4-yl)propanamido)ethyl)-5-(propionamidomethyl)isophthalamide tetrakis(hydrotrifluoroacetate) (33)** Succinimidyl proprionate (**32**) (3.28 mg, 19 µM) was added to a solution of **31** (30 mg, 0.016 mM) and DIPEA (22 µL, 0.128 mmol) in anhydrous DMF (0.45 mL) and the mixture was stirred at rt for 45 min. 10% aq TFA (1 mL) was added and the product was purified by preparative HPLC (column: Kinetex-XB C18, gradient: 0-25 min: 0.1% aq TFA/acetonitrile 90:10-60:40, t_R = 18 min). **33** was obtained as a white fluffy solid (28 mg, 0.015 mmol, 95%). IR (KBr): 3310, 3130, 3065, 2940, 2865, 1665, 1550, 1505, 1460, 1365, 1200, 1135, 800, 720 cm^{-1}. Ratio of configurational isomers evident in the NMR spectra: ca 1.7:1. ^{1}H-NMR (600 MHz, MeOH-d_4): δ (ppm) 1.15 (t, 3H, *J* 7.6 Hz), 1.30-1.33 (m, 8H), 1.38-1.57 (m, 6H), 1.77-1.98 (m, 8H), 2.30 (q, 2H, *J* 7.6 Hz), 2.59 (t, 4H, *J* 7.1 Hz), 2.88-2.95 (m, 2H), 2.97 (t, 4H, *J* 7.1 Hz), 3.01-3.08 (m, 2H), 3.40 (t, 4H, *J* 6.0 Hz), 3.42-3.47 (m, 2H), 3.48 (t, 4H, *J* 6.0 Hz), 3.73 (d, 3H, *J* 16.3 Hz), 3.80 (d, 1H, *J* 16.6 Hz), 4.13 (t, 4H, *J* 7.3 Hz), 4.41 (d, 1H, *J* 16.7 Hz), 4.44 (s, 2H), 4.45 (d, 1H, *J* 16.6 Hz), 7.24-7.40 (m, 7H), 7.45-7.55 (m, 4H), 7.60-7.71 (m, 4H), 7.74 (t, 1H, *J* 1.6 Hz), 7.86 (d, 2H, *J* 1.6 Hz), 7.90 (d, 1H, *J* 8.1 Hz), 7.96 (d, 1H, *J* 7.8 Hz), 8.12 (t, 1H, *J* 1.7 Hz), 8.77 (d, 2H, *J* 1.5 Hz). ^{13}C-NMR (150.9 MHz, MeOH-d_4): δ (ppm) 10.39, 21.50, 24.15, 30.13, 30.38, 31.06, 34.25, 34.81, 36.00, 40.14, 40.93, 43.67, 50.33, 54.90, 55.31, 58.02, 119.77, 123.08, 123.65, 126.22, 126.84, 127.52, 127.88, 128.48, 128.88, 129.44, 130.11, 130.15, 130.55, 130.89, 131.21, 131.71, 131.95, 132.35, 133.00, 133.40, 134.57, 134.91, 135.24, 135.42, 135.72, 136.38, 137.02, 141.61, 142.67, 165.48,169.36, 174.03, 177.21. HRMS (ESI): *m/z* $[M+4H]^{4+}$ calcd. for $[C_{73}H_{95}N_{15}O_9]^{4+}$ 340.4354, found 340.4367. RP-HPLC (220 nm): 98% (t_R = 13.4 min, *k* = 13.6). $C_{73}H_{91}N_{15}O_9 \cdot C_8H_4F_{12}O_8$ (1358.66 + 456.09).

4-(Piperidin-4-yl)butan-1-ol (35)[52] Under an atmosphere of argon piperidine derivative **34** (800 mg, 3.9 mmol) was suspended in anhydrous THF (15 mL) and the mixture was cooled in an ice-bath. $LiAlH_4$ (365 mg, 9.6 mmol) was added portionwise over a period of 10 min. The resulting suspension was stirred at 0 °C for 1 h and under reflux for 12 h. The mixture was cooled to rt and 20% aq NaOH (w/w, 10 mL) was added and the suspension was vigorously stirred for 1 h. Solid material was removed by filtration through a pad of celite and the volatiles of the filtrate were removed under reduced pressure to yield **35** as a pale yellow oil (539 mg, 3.4 mmol, 89%), which was used without purification. HRMS (ESI): *m/z* $[M+H]^+$ calcd. for $[C_9H_{20}NO]^+$ 158.1540, found 158.1541. $C_9H_{19}NO$ (157.26).

5-(2-(4-(4-Hydroxybutyl)piperidin-1-yl)acetyl)-5,10-dihydro-11H-dibenzo[b,e][1,4] diazepin-11-one (37) Freshly grained K_2CO_3 (3.19 g, 6.9 mmol) was added to a solution of

35 (0.91 g, 5.8 mmol) and dibenzodiazepinone derivative **36**[53] in acetonitrile (30 mL) and the mixture was vigorously stirred under reflux for 5 h. Solid material was removed by filtration, the filtrate collected and the volatiles evaporated under reduced pressure. The residue was dissolved in EtOAc (30 mL) and the solution was washed with H_2O (3 × 30 mL). The organic phase was dried over Na_2SO_4 and the solvent was removed under reduced pressure. Purification by column chromatography (eluent: CH_2Cl_2/MeOH/NH_3 (7 M in MeOH) 100:5:1 (R_f = 0.3)) afforded **37** as a colorless glass (1.0 g, 2.5 mmol, 43%). Ratio of configurational isomers evident in the NMR spectra: ca 2.1:1. ^{1}H-NMR (300 MHz, MeOH-d_4): δ (ppm) 0.99-1.41 (m, 7H), 1.42-1.70 (m, 4H), 1.81-2.12 (m, 2H), 2.46-2.70 (m, 1H), 2.83 (t, 1H, *J* 11.4 Hz*),* 2.97-3.29 (m, 2H), 3.52 (t, 2H, *J* 6.5 Hz), 7.16-7.73 (m, 7H), 7.88 (t, 1H, *J* 9.3 Hz). ^{13}C-NMR (150 MHz, MeOH-d_4): δ (ppm) 24.05, 30.16, 32.90, 33.84, 36.42, 37.37, 54.82, 54.99, 60.96, 62.91, 122.95, 126.56, 126.94, 127.76, 128.92, 129.46, 129.87, 130.55, 132.01, 132.17, 134.27, 134.68, 135.92, 143.83. HRMS (ESI): *m/z* $[M+H]^+$ calcd. for $[C_{24}H_{30}N_3O_3]^+$ 408.2282, found 408.2290. $C_{24}H_{29}N_3O_3$ (407.51).

5-(2-(4-(4-Bromobutyl)piperidin-1-yl)acetyl)-5,10-dihydro-11H-dibenzo[b,e][1,4]diazepin-11-one (38) In a three-necked round-bottom flask compound **37** (200 mg, 0.49 mmol) and triphenylphosphine (386 mg, 1.47 mmol) were dissolved in CH_2Cl_2 (5 mL) under an atmosphere of argon and the mixture was cooled to −5°C. Tetrabromomethane (1.058 g, 3.19 mmol) in CH_2Cl_2 (10 mL) was added dropwise to over a period of 10 min and the mixture was stirred at 0 °C for 5 h followed by washing with H_2O (2 x 10 mL) and brine (1 x 10 mL). The organic phase was dried over Na_2SO_4 and the solvent was removed under reduced pressure. The residue was subjected to column chromatography (eluent: light petroleum/acetone/25% aq NH_3 (83:16:1 (R_f = 0.5)) to give **38** as a white solid (180 mg, 79%). Ratio of configurational isomers evident in the NMR spectra: ca 2:1. ^{1}H-NMR (600 MHz, MeOH-d_4): δ (ppm) 0.83-1.33 (m, 7H), 1.33-1.67 (m, 4H), 1.86-2.05 (m, 2H), 2.45-2.71 (m, 1H), 2.85 (t, 1H, *J* 12.0 Hz), 2.98-3.30 (m, 2H), 3.42 (t, 2H, *J* 6.7 Hz), 7.18-7.72 (m, 7H), 7.88 (t, 1H, *J* 9.5 Hz). ^{13}C-NMR (150 MHz, MeOH-d_4): δ (ppm) 26.31, 32.83, 34.13, 34.40, 36.27, 36.55, 54.89, 54.94, 60.93, 61.29, 123.00, 126.95, 127.76, 128.89, 129.46, 130.56, 131.93, 132.16, 133.33, 133.75, 133.79, 134.25, 135.89, 143.80. HRMS (ESI): m/z $[M+H]^+$ calcd. for $[C_{24}H_{29}BrN_3O_2]^+$ 470.1438, found: 470.1437. $C_{24}H_{28}BrN_3O_2$ (470.41).

(1,4-Dibenzyl-6-nitro-1,4-diazepan-6-yl)methanol (41)[54] Amine **39** (0.98 mL, 4.16 mmol) and nitroethanol **40** (0.3 mL, 4.16 mmol) were dissolved in toluene/EtOH (1:1 v/v) (40 mL). Paraformaldehyde (450 mg, 14.8 mmol) was added portionwise and the suspension was vigorously stirred under reflux for 6 h. The volatiles were removed under reduced pressure,

the residue was dissolved in CH_2Cl_2 (15 mL) and the solution was washed with H_2O (3 × 10 mL). The organic phase was dried over Na_2SO_4 and the solvent evaporated. Purification by column chromatography (eluent: light petroleum/EtOAc 6:1-4:1 (R_f = 0.3, light petroleum/EtOAc 6:1)) yielded **41** as a pale yellow oil (1.3 g, 3.66 mmol, 87%). ^{1}H-NMR (300 MHz, $CDCl_3$): δ (ppm) 2.57-2.76 (m, 4H), 3.05 (d, 2H, *J* 14.5 Hz), 3.51 (d, 2H, *J* 14.3 Hz), 3.65 (d, 2H, *J* 12.9), 3.68 (s, 2H), 3.74 (d, 2H, *J* 13.1 Hz), 7.29 (m, 10H). ^{13}C-NMR (75 MHz, $CDCl_3$): δ (ppm) 59.06, 60.56, 63.86, 65.82, 94.64, 127.65, 128.56, 129.23, 138.66. HRMS (ESI): *m/z* $[M+H]^+$ calcd. for $[C_{20}H_{26}N_3O_3]^+$ 356.1969, found: 356.1978. $C_{20}H_{25}N_3O_3$ (455.44).

1,4-Dibenzyl-6-nitro-1,4-diazepane (42)[55] Homopiperazine **41** (472 mg, 1.33 mmol) was dissolved in anhydrous THF (3.5 mL), potassium *tert*-butanolate (228 mg, 2.03 mmol) was added and the suspension was vigorously stirred at rt for 30 min. Insoluble material was removed by filtration and the volatiles were evaporated. The residue was dissolved in aqueous H_2NOH × HCl (0.2 mmol, 10 mL) immediately followed by extraction with CH_2Cl_2 (3 × 50 mL). The organic phase was dried over Na_2SO_4 and the volatiles were evaporated to afford compound **42** as a yellow oil (410 mg, 1.26 mmol, 95%), which was used without further purification. ^{1}H-NMR (300 MHz, $CDCl_3$): δ (ppm) 2.68 (s, 4H), 3.21-3.34 (m, 2H), 3.40-3.52 (m, 2H), 3.75 (d, 4H, *J* 5.9 Hz), 4.59 (t, 1H, *J* 5.3 Hz), 7.22-7.36 (m, 10H). ^{13}C-NMR (75 MHz, $CDCl_3$ MHz): δ (ppm) 56.72, 56.93, 62.82, 77.37, 127.48, 128.51, 128.86, 138.69. HRMS (ESI): m/z $[M+H]^+$ calcd. for $[C_{19}H_{24}N_3O_2]^+$ 326.1863, found: 326.1884. $C_{19}H_{23}N_3O_2$ (325.41).

1,4-Dibenzyl-1,4-diazepan-6-amine (43)[56] Homopiperazine **42** (700 mg, 2.15 mmol) was dissolved in EtOH (25 mL). Raney 2800 (slurry in H_2O, ca 5 mL) was carefully added and the suspension was stirred under an atmosphere of hydrogen at rt for 12 h. The catalyst was removed by filtration through a pad of celite and the volatiles were evaporated. The residue was subjected to column chromatography (eluent: CH_2Cl_2/MeOH/NH_3 (7 M in MeOH) 100:10:1 (R_f = 0.2)) to give **43** as a pale yellow oil (278 mg, 0.94 mmol, 44%). ^{1}H-NMR (300 MHz, $CDCl_3$): δ (ppm) 2.46-2.59 (m, 2H), 2.60-2.72 (m, 2H), 2.72-2.82 (m, 2H), 2.81-2.92 (m, 2H), 3.16 (br s, 1H), 3.68 (d, 4H, *J* 5.0 Hz), 7.19-7.40 (m, 10H). ^{13}C-NMR (75 MHz, $CDCl_3$ MHz): δ (ppm) 50.23, 56.43, 61.04, 63.48, 127.19, 128.40, 129.01, 139.26. HRMS (ESI): m/z $[M+H]^+$ calcd. for $[C_{19}H_{26}N_3]^+$ 296.2121, found: 296.2128. $C_{19}H_{25}N_3$ (295.43).

***tert*-Butyl (1,4-dibenzyl-1,4-diazepan-6-yl)carbamate (44)**[57] Amine **43** (333 mg, 1.13 mmol) was dissolved in $CHCl_3$ (10 mL), the solution was cooled in an ice-bath and a solution of di-*tert*-butyldicarbonate (296 mg, 1.35 mmol) in $CHCl_3$ (5 mL) was added dropwise over a period of 10 min. The bath was removed and the mixture was stirred at rt for 5 h followed by washing with H_2O (3 × 15 mL). The organic phase was dried over Na_2SO_4 and the volatiles were removed under reduced pressure. Purification by column chromatography (eluent: CH_2Cl_2/MeOH 100:2.5 (R_f = 0.25)) yielded **44** as a pale yellow oil (361 mg, 0.91 mmol, 81%). ^{1}H-NMR (300 MHz, $CDCl_3$): δ (ppm) 1.39 (s, 9H), 2.35-3.03 (m, 9H), 3.46-3.86 (m, 5H), 7.14-7.48 (m, 10H). ^{13}C-NMR (75 MHz, $CDCl_3$): δ (ppm) 28.56, 48.99, 56.98, 59.47, 63.46, 77.36, 127.22, 128.46, 129.06, 139.41, 155.41. HRMS (ESI): m/z $[M+H]^+$ calcd. for $[C_{24}H_{34}N_3O_2]^+$ 396.2646, found: 396.2666. $C_{24}H_{33}N_3O_2$ (395.55).

***tert*-Butyl (1,4-diazepan-6-yl)carbamate (45)**[58] Under an atmosphere of argon Pd/C (10%) (35 mg) was carefully added to a solution of **44** (70 mg, 0.18 mmol) in 2,2,2-trifluoroethanol (2 mL). The mixture was vigorously stirred under an atmosphere of hydrogen at rt for 12 h. Solid material was removed by filtration thought a pad of celite and the volatiles were evaporated to obtain **45** as a colorless oil (34 mg, 0.16 mmol, 88%), which was used without further purification. ^{1}H-NMR (300 MHz, DMSO-d_6): δ (ppm) 1.37 (s, 9H), 2.52-2.59 (m, 2H), 2.62-2.71 (m, 4H), 2.84-2.90 (m, 2H), 3.43-3.53 (m, 1H). ^{13}C-NMR (75 MHz, DMSO-d_6): δ (ppm) 28.2, 51.9, 53.1, 56.4, 77.3, 154.7. HRMS (ESI): m/z $[M+H]^+$ calcd. for $[C_{10}H_{22}N_3O_2]^+$ 216.1707, found: 216.1707. $C_{10}H_{21}N_3O_2$ (215.30).

5,5'-(2,2'-(((6-Amino-1,4-diazepane-1,4-diyl)bis(butane-4,1-diyl))bis(piperidine-4,1-diyl))bis(acetyl))bis(5,10-dihydro-11*H*-dibenzo[*b,e*][1,4]diazepin-11-one) pentakis(hydrotrifluoroacetate) (46) Dibenzodiazepinone **38** (60 mg, 0.13 mmol) and homopiperazine **45** (13 mg, 0.061 mmol) were dissolved in acetonitrile (1.5 mL). Freshly grained K_2CO_3 (38 mg, 0.24 mmol) was added and the mixture was stirred and heated in a microwave reactor at 120 °C for 1.5 h. The solvent was removed under reduced pressure and the residue was taken up in EtOAc (5 mL) followed by washing with H_2O (3 × 5 mL). The organic phase was dried over Na_2SO_4 and the volatiles were removed *in vacuo*. The residue was dissolved in a mixture formed by CH_2Cl_2/TFA/H_2O 1:1:0.1 (v/v/v, 3 mL) and the solution was stirred at rt for 3 h. The volatiles were evaporated and the residue was taken up in DMF/0.1% aq TFA 1:1 (v/v, 3 mL) and subjected to preparative HPLC (column: Kinetex-XB C18, gradient: 0-25 min: 0.1% aq TFA/acetonitrile 90:10-50:50, t_R = 16 min) to yield **46** as a white fluffy solid (33 mg, 0.023 mmol, 37%). Ratio of configurational isomers evident in the NMR spectra: ca 1.5:1. ^{1}H-NMR (600 MHz, MeOH-d_4): δ (ppm) 1.26-1.57 (m, 14H), 1.57-1.68 (m, 4H), 1.85-2.02 (m, 4H), 2.88-2.98 (m, 6H), 3.00-3.08 (m, 2H), 3.11-3.20

(m, 2H), 3.23-3.30 (m, 4H), 3.36-3.50 (m, 4H), 3.68-3.89 (m, 5H), 4.40 (d, 1.2H, *J* 16.8 Hz), 4.44 (d, 0.8H, *J* 16.8 Hz), 7.24-7.41 (m, 5H), 7.45-7.56 (m, 4H), 7.60-7.71 (m, 4H), 7.75 (t, 1H, *J* 7.7 Hz), 7.90 (d, 1H, *J* 8.4 Hz), 7.97 (d, 1H, *J* 7.8 Hz). ^{13}C-NMR (150.9 MHz, MeOH-d_4): δ (ppm) 24.90, 26.54, 30.58, 34.47, 36.50, 53.81, 55.11, 55.47, 55.96, 58.08, 58.19, 59.83, 123.23, 123.80, 127.00, 127.67, 128.02, 128.63, 129.03, 129.60, 130.26, 130.70, 131.04, 131.36, 131.86, 132.12, 132.50, 133.16, 134.72, 135.09, 135.61, 136.87, 137.19, 141.16, 142.83, 155.56 165.11, 165.59, 168.72, 168.98. HRMS (ESI): m/z $[M+3H]^{3+}$ calcd. for $[C_{53}H_{70}N_9O_4]^{3+}$ 298.8511, found: 298.8520. RP-HPLC (220 nm): 96% (t_R = 12.5 min, *k* = 12.5). $C_{53}H_{67}N_9O_4 \cdot C_{10}H_5F_{15}O_{10}$ (894.18 + 570.12).

***N*-(1,4-Bis(4-(1-(2-oxo-2-(11-oxo-10,11-dihydro-5*H*-dibenzo[*b,e*][1,4]diazepin-5-yl)ethyl)piperidin-4-yl)butyl)-1,4-diazepan-6-yl)propionamide tetrakis(hydrotrifluoroacetate) (47)** Succinimidyl proprionate **32** (2.7 mg, 0.015 mmol) was added to a solution of amine **46** (16 mg, 0.011 mmol) and DIPEA (15 µL, 0.087 mmol) in anhydrous DMF (400 µL) and the mixture was stirred at rt for 1.5 h. 10% aq TFA (20 µL) was added and the mixture was subjected to preparative HPLC (column: Kinetex-XB C18, gradient: 0-25 min: 0.1% aq TFA/acetonitrile 90:10-50:50, t_R = 16 min) to yield **47** as a white fluffy solid (11.5 mg, 0.008 mmol, 72%). IR (KBr): 3435, 3060, 2945, 2865, 1680, 1505, 1460, 1365, 1200, 1130, 800, 720 cm^{-1}. Ratio of configurational isomers evident in the NMR spectra: ca 1.5:1. ^{1}H-NMR (600 MHz, MeOH-d_4): δ (ppm) 1.11 (t, 3H, *J* 7.7 Hz), 1.28-1.58 (m, 14H), 1.66 (m, 4H), 1.86-2.01 (m, 4H), 2.24 (q, 2H, *J* 7.6 Hz), 2.93 (m, 2H), 3.00-3.08 (m, 6H), 3.32-3.39 (m, 4H), 3.40-3.50 (m, 6H), 3.69-3.77 (m, 3H), 3.80 (d, 1H, *J* 16,7 Hz), 4.31-4.37 (m, 1H), 4.40 (d, 1.2H, *J* 16.7 Hz), 4.44 (d, 0.8H, *J* 16.7 Hz), 7.23-7.42 (m, 5H), 7.45-7.57 (m, 4H), 7.60-7.72 (m, 4H), 7.75 (t, 1H, *J* 7.7 Hz), 7.90 (d, 1H, *J* 8.2 Hz), 7.97 (d, 1H, *J* 7.8 Hz). ^{13}C-NMR (150.9 MHz, MeOH-d_4): δ (ppm) 10.03, 24.60, 26.08, 29.86, 30.43, 34.32, 36.25, 52.93, 54.90, 54.96, 55.32, 57.59, 57.95, 58.04, 59.28, 123.08, 123.64, 126.85, 127.50, 127.86, 128.47, 128.87, 129.43, 130.11, 130.55, 130.88, 131.22, 131.71, 131.97, 132.35, 133.01, 133.40, 134.57, 134.93, 135.45, 135.72, 137.04, 141.00, 142.66, 165.43, 168.56, 168.81, 176.89. HRMS (ESI): m/z $[M+3H]^{3+}$ calcd. for $[C_{56}H_{74}N_9O_5]^{3+}$ 317.5266, found: 317.5273. RP-HPLC (220 nm): 98% (t_R = 12.8 min, *k* = 12.9). $C_{56}H_{71}N_9O_5 \cdot C_8H_4F_{12}O_8$ (950.24 + 456.09).

***N*-(2-Aminoethyl)-3-(1*H*-imidazol-4-yl)propanamide bis(hydrotrifluoroacetate) (49)** Urocanic acid derivative **48**[31] (300 mg, 1.07 mmol) was dissolved in MeOH/TFA (1:1 v/v) (8 mL) and a 10% Pd/C catalyst (30 mg) was carefully added under an atmosphere of argon. The mixture was stirred in an autoclave under an atmosphere of hydrogen at 7.9 atm at rt for 12 h. The catalyst was removed by filtration through a pad of celite and the volatiles

were evaporated to yield **49** as colorless oil (299 mg, 1.01 mmol, 95%), which was used without further purification. ^{1}H-NMR (300 MHz, MeOH-d_4): δ (ppm) 2.65 (t, 2H, *J* 7.3 Hz), 2.98-3.09 (m, 4H), 3.46 (t, 2H, *J* 6.0 Hz), 7.31 (br s, 1H), 8.78 (d, 1H, *J* 1.4 Hz). ^{13}C-NMR (75 MHz, MeOH-d_4): δ (ppm) 21.15, 34.97, 38.32, 40.85, 117.10, 134.68, 134.78, 175.05. HRMS (ESI): *m/z* $[M+H]^+$ calcd. for $[C_8H_{16}N_4O_5]^+$ 183.1241, found: 183.1245. $C_8H_{15}N_4O_5 \cdot C_4H_2F_6O_2$ (182.23 + 228.04).

3-(1*H*-Imidazol-4-yl)-*N*-(2-propionamidoethyl)propanamide (50) A solution of succinimidyl proprionate **32** (23 mg, 0.134 mmol) in DMF (0.1 mL) was added to a solution of **49** (110 mg, 0.27 mmol) and DIPEA (0.234 mL, 1.34 mmol) in DMF (0.5 mL) and the mixture was stirred at rt for 30 min. 32% aq NH_3 (0.15 mL) and H_2O (3 mL) were added and the mixture was subjected to preparative HPLC (column: Actus Triart C18, gradient: 0-10 min: 0.1% aq NH_3/acetonitrile 95:5, 10-20 min: 95:5-88:12, t_R = 10 min) to afford **50** as a white solid (27.5 mg, 0.115 mmol, 43%). ^{1}H-NMR (400 MHz, MeOH-d_4): δ (ppm) 1.11 (t, 3H, *J* 7.6 Hz), 2.19 (q, 2H, *J* 7.6 Hz), 2.49 (t, 2H, *J* 7.6 Hz), 2.87 (t, 2H, *J* 7.6 Hz), 3.25 (m, 4H), 6.79 (br s, 1H), 7.56 (d, 1H, *J* 1.2 Hz). ^{13}C-NMR (100 MHz, MeOH-d_4): δ (ppm) 10.37, 23.93, 30.18, 36.86, 39.99, 40.05, 117.2, 135.93, 137.8, 175.46, 177.32. HRMS (ESI): *m/z* $[M+H]^+$ calcd. for $[C_{11}H_{19}N_4O_2]^+$ 239.1503, found: 239.1507. RP-HPLC (220 nm): 99% (t_R = 8.0 min, *k* = 3.0). $C_{11}H_{18}N_4O_2$ (238.29).

5,5'-(2,2'-(Piperazine-1,4-diyl)bis(acetyl))bis(5,10-dihydro-11*H*-dibenzo[*b,e*][1,4]diazepin-11-one) bis(hydrotrifluoroacetate) (52) Dibenzodiazepinone **36** (100 mg, 0.35 mmol) and piperazine (**51**) (14 mg, 0.16 mmol) were dissolved in acetonitrile (2 mL). Freshly grained K_2CO_3 (88 mg, 0.64 mmol) was added and the suspension was stirred in a microwave reactor at 130 °C (approx. 4 bar) for 30 min. Insoluble material was removed by filtration, the volatiles were evaporated and the residue subjected to preparative HPLC (column: Kinetex-XB C18, gradient: 0-25 min: 0.1% aq TFA/acetonitrile 15:85-55:45, t_R = 16 min) to yield **52** as a white fluffy solid (28 mg, 0.034 mmol, 20%). Four isomers were evident in the ^{1}H- and ^{13}C-NMR spectrum and two isomers were evident by RP-HPLC analysis (ratio 1:1). HRMS analysis revealed a uniform sample with respect to the molecular formula. ^{1}H-NMR (600 MHz, MeOH-d_4): δ (ppm) 2.55-3.18 (m, 8H), 3.43-3.56 (m, 1H), 3.56-3.65 (m, 1H), 3.65-3.72 (m, 0.5H), 3.72-3.84 (m, 0.5H), 3.86-3.98 (m, 0.5H), 4.05-4.16 (m, 0.5H) 7.22-7.39 (m, 5H), 7.40-7.53 (m, 4H), 7.53-7.75 (m, 5H), 7.84-7.98 (m, 2H). ^{13}C-NMR (150.9 MHz, MeOH-d_4): δ (ppm). 51.52, 52.08, 52.27, 52.80, 58.19, 58.48, 58.91, 59.46, 123.17, 123.52, 123.63, 123.68, 126.94, 127.49, 127.58, 127.75, 127.87, 128.72, 128.79, 129.04, 129.80, 129.88, 130.02, 130.11, 130.35, 130.44, 130.56, 130.81, 131.06, 131.44, 131.61, 132.35, 132.40, 132.48, 132.65, 134.18, 134.63,

135.19, 135.29, 135.53, 135.76, 135.92, 137.13, 142.44, 143.04, 143.24, 166.99, 168.14, 168.96, 169.14, 169.47. HRMS (ESI): m/z $[M+H]^+$ calcd. for $[C_{34}H_{31}N_6O_4]^+$ 587.2402, found: 587.2423. RP-HPLC (220 nm): 98% (t_R = 15.4, 15.6 min, k = 15.7, 15.9) $C_{34}H_{30}N_6O_4 \cdot C_4H_2F_6O_2$ (586.65 + 228.04).

2.4.4 Investigation of the chemical stability

The chemical stability of **19**, **33** and **47** was investigated in PBS (pH 7.4) at 22 ± 1 °C. The incubation was started by the addition of 2 µL of a 10 mM solution of **19**, **33** or **47** to PBS (198 µL) to yield a final concentration of 100 µM. After 0, 24 and 48 h, aliquots (20 µL) were taken and added to 1% aq TFA (20 µL). The resulting solutions were analyzed by RP-HPLC (analytical HPLC system and conditions see general experimental conditions; t_R 8.8 min (**19**), 13.5 min (**33**), 12.8 min (**47**)).

2.4.5 Synthesis of the radioligands [^{3}H]19, [^{3}H]33 and [^{3}H]47.

The tritiated dibenzodiazepinone derivatives [^{3}H]**19**, [^{3}H]**33** and [^{3}H]**47** were prepared by [^{3}H]propiolynation of the amino-functionalyzed precursors **30**, **31** and **46**, respectively, using a reported protocol with modifications.[59] A solution of succinimidyl [2,3-^{3}H]-proprionate ([^{3}H]**32**) (specific activity: 80 mCi/mmol; from American Radiolabeled Chemicals, St. Louis, MO, via Hartman Analytics, Braunschweig, Germany) (for [^{3}H]**19** and [^{3}H]**47**: 2.5 mCi, 5.5 µg, 31.25 nmol (each), for [^{3}H]**33**: 2 mCi, 4.4 µg, 25 nmol) in hexane/EtOAc 9:1 was transferred into a 1.5-mL reaction vessel with a screw cap and the volatiles were evaporated in a vacuum concentrator (ca 30 min at about 30 °C). A solution of the precursor molecule (**30**: 411 µg, 0.76 µmol; **31**: 870 µg, 0.46 µmol; **46**: 400 µg, 0.27 µmol) in DMF/DIPEA (50:1 v/v) (55 µL) was added and the mixture was shaken at rt for 45 min. In case of [^{3}H]**47** the excess of precursor **46** was 'quenched' by 4-fluorobenzoylation. For that purpose succinimidyl ester **53** (250 µg, 1.05 µmol) was added to the mixture and shaken at rt for one additional hour. After completed incubation and 'precursor quenching', 2% aq TFA (90 µL) and H_2O/acetonitrile (3:1 v/v) (85 µL) were added. [^{3}H]**19**, [^{3}H]**33** and [^{3}H]**47** were purified using an analytical HPLC system (Waters, Eschborn, Germany) consisting of two 510 pumps, a pump control module, a 486 UV/vis detector, and a Flow-one Beta series A-500 radiodetector (Packard, Meriden, CT). A Luna C18 (3 µm, 150 mm × 4.6 mm, Phenomenex, Aschaffenburg, Germany) was used as stationary phase at a flow rate of 0.8 mL/min. Mixtures of 0.05% aq TFA (A) and acetonitrile containing 0.04% TFA (B) were used as mobile phase. The following linear gradients were applied: [^{3}H]**19** and [^{3}H]**33**, 0-20 min: A/B 90:10-68:32, 20-30 min: 68:32-5:95, 30-38 min: 5:95, t_R = 16.4 and 20.0 min, respectively); [^{3}H]**47**, 0-20 min: A/B 90:10-75:25, 20-25 min: 75:25, 25-27 min: 75:25-5:95, 27-35 min:

5:95, t_R = 24.7 min). For each radioligand, two HPLC runs (UV detection: 220 nm; no radiometric detection) were performed. Each radioligand was collected in a 2-mL reaction vessel with screw cap. The volumes of the combined eluates were reduced in a vacuum concentrator to 600 µL and EtOH (600 µL) was added. The solutions were transferred into 3-mL borosilicate glass vials with conical bottom (Wheaton NextGen 3 mL V-vials). The 2-mL reaction vessels were rinsed twice with EtOH/water (50:50 v/v) (various volumes), and the washings were transferred to the 3-mL glass vials to obtain tentative stocks with volumes of 1000 µL ([^{3}H]**19**), 1000 µL ([^{3}H]**33**) or 1200 µL ([^{3}H]**47**). For the quantification, a five-point or four-point calibration was performed with the corresponding 'cold' forms **19** (0.1, 0.2, 0.35, 0.5, 0.75 µM), **33** (0.2, 0.4, 0.7, 1, 1.5 µM) and **47** (0.1, 0.2, 0.5, 1 µM) (injection volume throughout 100 µL, UV detection at 220 nm) using the aforementioned HPLC system and conditions (in case of [^{3}H]**47** the linear gradient was modified: 0-20 min: A/B 90:10-69:31, 20-30 min: 69-31:5:95, 30-38 min: 5:95, t_R = 19.9 min). Aliquots of the tentative stock solutions ([^{3}H]**19**: 2.2 µL, [^{3}H]**33**: 2.2 µL, [^{3}H]**47**: 2 µL) were added to 0.05% aq TFA/acetonitrile (9:1 v/v) (127.8 and 128 µL, respectively), 100 µL of the resulting solutions were analyzed by HPLC, and five times 2 µL were counted in 3 mL of Rotiszint eco plus (Carl Roth, Karlsruhe, Germany) with a LS 6500 liquid scintillation counter (Beckman-Coulter, Munich, Germany). These analyses were repeated. The molarities of the tentative stock solutions were calculated from the mean of the peak areas and the linear calibration curves. In order to determine the radiochemical purities and to confirm the chemical identities, solutions (100 µL) of [^{3}H]**19** (0.23 µM), [^{3}H]**33** (0.20 µM) and [^{3}H]**47**(0.20 µM) spiked with **19** (5 µM), **33** (5 µM) and **47** (3 µM), respectively, were analyzed by HPLC using the conditions as for the quantification and additionally radiometric detection (flow rate of the liquid scintillator (Rotiscint eco plus/acetonitrile (85:15 v/v): 4.0 mL/min). For all radioligands the radiochemical purity was 99%. For [^{3}H]**19** and [^{3}H]**33** this analysis was repeated after 1 year of storage at −20 °C, whereas in case of [^{3}H]**47** it was repeated after 9 months of storage at −20°C (radiochemical purities: [^{3}H]**19**, 96%; [^{3}H]**33**, 97%; [^{3}H]**47**, 96%). Calculated specific activities: [^{3}H]**19**, 2.96 TBq/mmol (72.7 Ci/mmol); [^{3}H]**33**, 1.81 TBq/mmol (49.0 Ci/mmol); [^{3}H]**47**, 2.19 TBq/mmol (59.3 Ci/mmol). The final activity concentration was adjusted to 27.75 MBq/mL ([^{3}H]**19**) or 18.5 MBq/mL ([^{3}H]**33**, [^{3}H]**47**) by the addition of H_2O/EtOH (1:1 v/v) resulting in molarities of 10.3 µM ([^{3}H]**19**), 10.2 µM ([^{3}H]**33**) and 8.44 µM ([^{3}H]**47**). Radiochemical yields: [^{3}H]**19**, 36.0 MBq, 39%; [^{3}H]**33**, 24.0 MBq, 32%; [^{3}H]**47**, 34.7 MBq, 38%.

2.4.6 Cell Culture and preparation of cell homogenates

CHO-K9 cell lines stably transfected with the human M_1-M_5 muscarinic receptors were obtained from the Missouri S&T cDNA Resource Center (Rolla, MO). Cells were cultured in

HAM's F12 medium supplemented with fecal calf serum (Biochrom, Berlin, Germany) (10%) and G418 (Biochrom) (750 µg/mL). CHO-hM_2 cell homogenates were prepared according to a reported procedure with minor modifications.[60] The harvest buffer (50 mM TRIS, 1 mM EDTA) was supplemented with protease inhibitor (SIGMAFAST, Sigma-Aldrich)). Aliquots of 200 µL were transferred to 2-mL cups and stored at −80°C.

2.4.7 Radioligand binding experiments

All radioligand binding experiments were performed at 23 ± 1 °C. Leibovitz L-15 medium (Gibco, Life Technologies GmbH, Darmstadt, Germany) supplemented with 1% BSA (Serva, Heidelberg, Germany) (in the following referred to as L15 medium) was used as binding buffer throughout. The effects of various MR ligands on the equilibrium binding of [^{3}H]NMS (equilibrium competition binding assay) and the effect of **19** on saturation binding of [^{3}H]NMS were determined at intact adherent CHO-hM_xR (x = 1-5) in white 96-well plates with clear bottom (Corning Life Sciences, Tewksbury, MA; Corning cat. no. 3610) using the protocol of previously described MR binding studies with [^{3}H]NMS.[31] The concentration of [^{3}H]NMS was 0.2 nM (M_1, M_2, M_3), 0.1 nM (M_4) or 0.3 nM (M_5) and the incubation time was 3 h throughout. For studying the effect of **8** on the M_2R equilibrium binding of [^{3}H]NMS, the radioligand was additionally applied at concentrations of 0.1 and 2 nM. Unspecific binding was determined in the presence of **2** (500-fold excess to [^{3}H]NMS).

Saturation and competition binding experiments as well as association and dissociation experiments with [^{3}H]**19** were performed at intact adherent CHO-hM_2 cells in white 96-well plates with clear bottom (Corning Life Sciences) using the recently described experimental procedure for saturation and equilibrium competition binding studies with [^{3}H]NMS at CHO-hM_xR (x = 1-5) cells.[31] In case of competition binding studies the concentration of [^{3}H]**19** was 2 nM. For competition binding experiments with **8** additional concentrations of [^{3}H]**19** were applied (4, 8, 15 and 30 nM). For both, saturation and competition binding studies, the incubation time was 2 h. Unspecific binding was determined in the presence of **2** (500-fold excess to [^{3}H]**19**). For M_2R association experiments with [^{3}H]**19** CHO-hM_2 cells were incubated with [^{3}H]**19** (2 nM) and the incubation was stopped after different periods of time (between 1 and 140 min) by suction of the radioligand solution, washing of the cells twice with ice-old PBS and further processing as described previously.[31] Unspecific binding was determined in the presence of **2** (400 nM). In case of dissociation experiments cells were preincubated with [^{3}H]**19** (2 nM) for 105 min. The radioligand solution was removed by suction, the cells were covered with L15 medium (200 µL) containing **2** (400 nM) and the plates were gently shaken. After different periods of time (between 0 and 300 min) the cells were washed twice with ice-cold PBS followed by cell lysis and further processing as reported previously.[31] To determine unspecific binding the same experiment was performed, but **2** (400 nM) was added during the preincubation step.

Saturation binding experiments with [^{3}H]**33** and [^{3}H]**47** at live adherent CHO-hM_2 cells (incubation time: 2 h) were performed using white 96-well plates with clear bottom (Corning Life Sciences) and the experimental protocol as for binding studies with [^{3}H]**19** (see above). M_2R association and dissociation experiments with [^{3}H]**33** were performed at intact adherent CHO-hM_2 cells in Primaria 24-well plates (Corning Life Sciences) using the procedure as for association and dissociation experiments with [^{3}H]**19** with the following modifications: The total volume of L15 medium per well was 250 instead of 200 µL, and the volume of PBS for washing steps was 500 instead of 200 µL. Cell lysis was performed with 200 µL of lysis solution (instead of 25 µL). For activity measurements the lysis solution was transferred into 6-mL scintillation vials filled with 3 mL of Rotiscint eco plus (Carl Roth), which were kept at least 1 h in the dark prior to the measurement using a LS 6500 liquid scintillation counter (Beckman-Coulter). For association experiments the concentration of [^{3}H]**33** was 1 nM. The incubation was stopped after different periods of time (between 1 and 140 min). Unspecific binding was determined in the presence of **2** (200 nM). For dissociation experiments cells were preincubated with [^{3}H]**33** (1 nM) for 90 min. The dissociation was started by covering of the cells with L15 medium (250 µL) containing **2** (200 nM) and was followed over a period of 300 min. Unspecific binding was determined by the addition of **2** (200 nM) during the preincubation period.

For saturation binding experiments with [^{3}H]**33** at intact suspended CHO-hM_2 cells the cell suspension was prepared as follows: Cells (80-100% confluency) were scraped off a 175-cm^2 culture flask and centrifuged at 400 *g* for 5 min. The supernatant was discarded and the cells were re-suspended in L15 medium at a density of 200,000 cells/mL. Saturation binding experiments were performed in Primaria 96-well plates (Corning Life Science) using a final volume of 200 µL per well. For the determination of total binding wells were prefilled with L-15 medium (160 µL) and L15 medium (20 µL) containing [^{3}H]**33** 10-fold concentrated. For the determination of unspecific binding (in the presence of **2**, 500-fold excess to [^{3}H]**33**) wells were prefilled with L-15 medium (140 µL), L15 medium (20 µL) containing **2** 10-fold concentrated and L15 medium (20 µL) containing [^{3}H]**33** 10-fold concentrated. To all wells 20 µL of the CHO-hM_2 cell suspension (200,000 cells/mL) were added and the plates were shaken at 23°C for 2 h. The cell mass was collected on GF/C filter mats (0.26 mm; Whatman, Maidstone, UK) (pretreated with 0.3% polyethylenimine) and washed with cold PBS using a Brandel Harvester (Brandel, Gaithersburg, MD). Filter pieces for each well were punched out and transferred into 1450-401 96-well plates (PerkinElmer). Rotiscint eco plus (Carl Roth) (200 µL) was added and the plates were vigorously shaken for at least 3 h and afterwards kept in the dark for at least 1 h prior to the measurement of radioactivity (dpm) with a MicroBeta2 plate counter (PerkinElmer, Rodgau, Germany).

Saturation and competition binding experiments with [^{3}H]**33** and saturation binding experiments with [^{3}H]**47** at CHO-hM_2 cell homogenates were performed in Primaria 96-well plates (Corning Life Sciences) according to the procedure for saturation binding experiments with [^{3}H]**33** at intact suspended CHO-hM_2 cells (see above) using 10 µL of cell homogenate instead of 20 µL of cell suspension. The total volume per well was 100 µL instead of 200 µL, i.e. in case of total binding wells were prefilled with L-15 medium (80 µL) followed by the addition of L15 medium (10 µL) containing the radioligand 10-fold concentrated and cell homogenate (10 µL). On the day of the experiment CHO-hM_2 cell homogenates were thawed and re-suspended using a 1-mL syringe (Henke-Sass Wolf GmBh, Tuttlingen, Germany) equipped with a needle (0.90 × 40 mm, B. Braun, Melsungen, Germany) followed by centrifugation at 500 *g* at 4°C for 5 min. The supernatant was discarded and the pellets were re-suspended in L15 medium using a 1-mL syringe equipped with a needle (0.45 × 25 mm, B. Braun). The homogenates were stored on ice until use. The total amount of protein per well was between 25 and 30 µg. Unspecific binding was determined in the presence of **2** (500-fold excess to [^{3}H]**33** or [^{3}H]**47**). In case of competition binding studies with various ligands the concentration of [^{3}H]**33** was 0.5 nM. For competition binding experiments with **8** additional concentrations of [^{3}H]**33** were applied (0.4, 1, 2 and 4 nM). For both, saturation ([^{3}H]**33**, [^{3}H]**47**) and competition ([^{3}H]**33**) binding studies, the incubation period was 2 h.

Note: To keep the total volume per well at 200 µL in case of saturation binding experiments performed with [^{3}H]**19** and [^{3}H]NMS in the presence of **8**, **9** or **19**, and at 100 µL in case of saturation binding studies performed with [^{3}H]**33** in the presence of **8**, the addition of L15 medium (20 and 10 µL, respectively) containing **8**, **9** or **19 (**10-fold concentrated) was compensated by an equivalent reduction of the volume of L15 medium added to the wells.

2.4.8 IP1 accumulation assay

The measurement of M_2R stimulated activation of the G-protein mediated pathway was performed by applying the IP-One HTRF® assay (Cisbio, Codolet, France) according to the manufacturer's protocol. In brief, HEK-293 cells were grown to a confluency of approx. 70% and transiently co-transfected with the cDNAs of the human M_2 receptor (Missouri S&T cDNA Rescourse Center) and the hybrid G-protein $G\alpha_{qi5\text{-}HA}$ ($G\alpha_q$ protein with the last five amino acids at the C-terminus replaced by the corresponding sequence of $G\alpha_i$; gift from the J. David Gladstone Institutes, San Francisco, CA),[22, 61] applying TransIT-293 Mirus transfection reagent (MoBiTec, Goettingen, Germany). After one day, cells were detached from the culture dish with Versene (Life Technologies GmbH, Darmstadt, Germany), seeded into black 384-well plates (10,000 cells/well) (Greiner Bio-One, Frickenhausen, Germany) and maintained for 24 h at 37 °C. After incubation with the test compounds,

dissolved in stimulation buffer (final concentration range from 1 pM up to 100 µM), at 37 °C for 1 h, the detection reagents were added (IP1-d2 conjugate and Anti-IP1cryptate TB conjugate, each dissolved in lysis buffer), and incubation was continued at rt for 60 min. Time resolved fluorescence resonance energy transfer (HTRF) was determined using a Clariostar plate reader (BMG, Ortenberg, Germany) measuring fluorescence at 620 (± 10) nm and 670 (± 10) nm (excitation at 330 nm). In the agonist mode, each compound (19, 33) was tested in duplicate in three individual experiments in comparison to the reference compound carbachol (3, eight experiments). Antagonist properties of **2**, **19** and **33** were determined after preincubation of the cells with **2**, **19** or **33** for 30 min, subsequent addition of the MR agonist 3 (at a final concentration of 300 nM) and continued incubation at 37°C for 1 h (five independent experiments each).

2.4.9 Molecular dynamics simulation

The crystal structure of the inactive hM_2R bound to the antagonist QNB (PDB ID: 3UON)[21] was used as template. Minor modifications were performed using the modelling suite SYBYL-X 2.0 (Tripos Inc., St. Louis, MO USA): The ICL3 was reconstituted by insertion of eight alanine residues using the loop search module within SYBYL-X 2.0. Coordinates of non-ligand and non-receptor molecules were removed. The protein preparation wizard (Schrödinger LLC, Portland, OR USA) was used to refine the receptor model: The N- and C-terminus were capped by the introduction of an acetyl and a methylamide group, respectively, and amino acid side chains containing hydrogen bond donors and acceptors were optimized for hydrogen bonding. Histidine residues were simulated in the uncharged form as the N^{ε}-H tautomer. Residues other than histidine were simulated in their dominant protonation state at pH 7. Disulphide bonds were maintained between $C96^{3.25}$ and $C176^{ECL2}$ as well as between $C413^{ECL3}$ and $C416^{ECL3}$, and a sodium ion was placed next to $D69^{2.50}$.[62] Ligand (**19**, **33**) geometries were energetically optimized using the LigPrep module (Schrödinger LLC). Tertiary amine groups in **19** and **33** were protonated resulting in a net charge of +1 and +2, respectively.

'Flexible' docking of **19** and **33** to the hM_2R model was performed using the induced fit docking module (Schrödinger LLC). For initial docking, $Y104^{3.33}$, $Y403^{6.51}$ and $Y426^{7.39}$ were temporarily mutated to alanine, and the ligands **19** and **33** were docked within a box of 30 × 30 × 30 Å and a box of 46 × 46 × 46 Å, respectively, around the crystallographic binding pose of QNB. Prior to redocking, performed in the extended precision mode, a second side chain trimming (mutation of $Y104^{3.33}$, $Y403^{6.51}$ and $Y426^{7.39}$ to alanine) was executed in case of **33**, and, after redocking, a second prime refinement was applied (including a reversion of the alanine mutations). Among the reasonable ligand binding poses, the pose, corresponding to the lowest XP GScore, was selected as template for the MD simulation.

The respective ligand-receptor complexes were aligned to the hM_2R entry (PDB ID: 3UON) in the orientations of proteins in membranes (OPM) database[63] using the protein structure alignment tool (Schrödinger LLC). The CHARMM GUI[64-68] interface was used to insert the prepared ligand-receptor complexes into a hydrated, equilibrated palmitoyloleoylphosphatidylcholine (POPC) bilayer, comprising 180 POPC molecules as well as sodium chloride at a concentration of 150 mM (net charge of the entire system was zero). The system contained about 72,000 (**19**) and 81,000 (**33**) atoms and the box size was approximately 86 × 86 × 106 Å and 86 × 86 × 118 Å, respectively. The CHARMM36 parameter set was used for the protein structure,[69-71] lipid,[72] and inorganic ions,[73] and the CHARMM TIP3P model for water[74] to define the geometry and partial charges. The protein parameters included CMAP terms. Ligand geometry and partial charge parameters were derived from the CHARMM ParamChem web server, version 1.0.0[75-78]. Each simulation was executed on one Nvidia GTX 1080 GPU (approx. 9 TFlops) using the CUDA version of PMEMD,[79, 80] implemented in AMBER16 (AMBER 2016, University of California, San Francisco, CA). After minimization, the system was heated from 0 to 100 K in the NVT ensemble during 50 ps and from 100 to 310 K in the NPT ensemble during 450 ps, applying harmonic restraints of 10 kcal · mol^{-1} · $Å^{-1}$ to protein and ligand atoms as well as 2.5 kcal · mol^{-1} · $Å^{-1}$ to POPC atoms. At the first heating step (0 to 100 K), initial velocities were randomly assigned using Langevin dynamics. The simulation systems were successively equilibrated at 310 K in the NPT ensemble using a Langevin thermostat,[81, 82] a collision frequency of 1.0 ps^{-1} and a Berendsen barostat[83] with semi-isotropic pressure scaling maintaining a target pressure of 1 bar with a pressure relaxation time of 0.5 ps. During the subsequent 10-ns equilibration period harmonic restraints were reduced step-wise (every 2 ns) to 0 kcal · mol^{-1} · $Å^{-1}$. The interaction cut-off was set to 8.0 Å and long-range electrostatics were computed using the particle mesh Ewald (PME) method.[84] Bonds involving hydrogen atoms were constrained using SHAKE[85] to enable a frame step size of 2 fs. The final frame of the equilibration period was used as input for the simulations over 2 µs (**19**) and 3 µs (**33**). The 'production runs' were essentially performed as the equilibration runs, but the Berendsen barostat was replaced by the Monte Carlo Barostat. Data were collected every 100 ps and analyzed by means of cpptraj every ns. For cluster analysis, the average linkage algorithm[86] was applied, setting a cluster size of 5 (*cf*. Table 5). H-bond plots were prepared with the programming language R (R Development Core Team (2008), R: A language and environment for statistical computing, R Foundation for Statistical Computing, Vienna, Austria, http://www.R-project.org; Karline Soetaert (2016), plot3D: Plotting Multi-Dimensional Data, R package version 1.1, https://CRAN.R-project.org/package=plot3D; Philip Johnson (2015), devEMF: EMF Graphics Output Device, R package version 2.0, https://CRAN.R-project.org/package=devEMF). Figures

showing molecular structures of the M_2R in complex with **19** or **33** were generated with PyMOL Molecular Graphics system, version 1.8.2.1 (Schrödinger LLC).

2.4.10 Data processing

Data of the IP1 accumulation assay (agonist mode) were processed by plotting the ratios (emission 670 nm/emission 620 nm) of the HTRF measurements against log(concentration **3**) and analysis by a four-parameter logistic equation (GraphPad Prism Software 6.0, GraphPad Software, San Diego, CA), followed by normalization (0% = 'top' (maximum of IP1 accumulation), 100% = 'bottom' (basal activity)) of the four-parameter logistic fit and analysis of the normalized data by a four-parameter logistic equation (log(agonist) vs. response - variable slope). Data of the IP1 accumulation assay (antagonist mode) were processed by plotting the fluorescence ratio against log(concentration antagonist) and analysis by a four-parameter logistic equation (GraphPad Prism), followed by normalization (0% = 'top' (IP1 accumulation elicited by **3** (0.3 µM)) of the four-parameter logistic fit, 100% = 'bottom' (basal activity)) and analysis of the normalized data by a four-parameter logistic equation (log(inhibitor) vs. response - variable slope). pIC_{50} values were converted into pK_b values according to the Cheng-Prusoff equation[87] (logarithmic form). Specific binding data (DPM) from saturation binding experiments were plotted against the free radioligand concentration and analyzed by a two-parameter equation describing hyperbolic binding (one site-specific binding, GraphPad Prism) to obtain K_d and B_{max} values. The free radioligand concentration (nM) was calculated by subtracting the amount of specifically bound radioligand (nM) (calculated from the specifically bound radioligand in dpm, the specific activity and the volume per well) from the total radioligand concentration. Unspecific binding data from saturation binding experiments were fitted by linear regression. In case of saturation binding experiments with [^{3}H]**19** or [^{3}H]**33** in the presence of compounds **8**, **9** as well as saturation binding experiments with [^{3}H]NMS in the presence of **19**, specific binding data (in DPM) were analyzed by a two-parameter equation describing hyperbolic binding (one site-specific binding, GraphPad Prism) to obtain K_d and B_{max} values. Additionally, specific binding data were normalized to the B_{max} value, specific binding (%) was plotted against log(radioligand concentration) followed by analysis using a four-parameters logistic fit (log(agonist) vs. response-variable slope, GraphPad Prism). Data for the 'Schild' analysis were obtained from the rightward shift (ΔpK_d) of the saturation isotherm and transformation into log(r-1) (where $r = 10^{\Delta pKd}$). Log(r-1) was plotted against log(concentration **8**, **9** or **19**) and the data were analyzed by linear regression to obtain the slope and the 'pA_2' values (intercept with the X axis). Specific binding data from association experiments with [^{3}H]**19** and [^{3}H]**33** were analyzed by a two-parameters equation describing an exponential rise to a maximum (one-phase association, GraphPad Prism) to obtain the

observed association rate constant k_{obs} and the maximum of specifically bound radioligand ($B_{(eq)}$) which was used to calculate specifically bound radioligand ($B_{(t)}$) in %. Data from dissociation experiments (% specifically bound radioligand ($B_{(t)}$) plotted over time) were analyzed by a three-parameter equation (one phase decay, GraphPad Prism) (in case of [^{3}H]**19** 'plateau' was defined as 0) or by a three-parameter equation to obtain the dissociation rate constant k_{off}. The association rate constants (k_{on}) of the radiolabeled dibenzodiazepinone derivatives were calculated from k_{obs}, k_{off} and the radioligand concentration ([RL]) according to the correlation: $k_{on} = (k_{obs}-k_{off})/[RL]$. Total binding data (DPM) from radioligand competition binding experiments (determination of the effect of various MR ligands on the equilibrium binding of [^{3}H]NMS, [^{3}H]**19** or [^{3}H]**33**) were plotted against log(concentration competitor) and analyzed by a four-parameter logistic equation (log(inhibitor) vs. response-variable slope, GraphPad Prism) followed by normalization (100% = 'top' of the four-parameter logistic fit, 0% = unspecifically bound radioligand (DPM) determined in the presence of **2** at 200 or 500-fold excess) and analysis of the normalized data by a four-parameter logistic equation (effect of **8** on the equilibrium binding of [^{3}H]NMS, [^{3}H]**19** or [^{3}H]**33**; *cf.* Fig. 8) or by a four-parameter logistic equation fused to the Cheng-Prusoff equation (logarithmic form) (equation 1) to obtain pIC_{50} and pK_i values, respectively. Statistical significance was assessed by a one-sample *t*-test.

(equation 1)

$$Y = \frac{Top - Bottom}{1 + 10^{(logIC50 - X) * HillSlope}} + Bottom$$

$$logIC50 = \log\left(10^{logKi} * \left(1 + \frac{HotNM}{HotKdNM}\right)\right)$$

HotNM = radioligand concentration in nM, HotKdNM = Dissociation constant (K_d) of the radioligand in nM

2.5. References

(1) Eglen, R. M. Overview of muscarinic receptor subtypes. *Handb. Exp. Pharmacol.* **2012**, 3-28.

(2) Eglen, R. M.; Choppin, A.; Watson, N. Therapeutic opportunities from muscarinic receptor research. *Trends Pharmacol. Sci.* **2001,** *22*, 409-414.

(3) Sheardown, M. J. Muscarinic M1receptor agonists and M2 receptor antagonists as therapeutic targets in Alzheimer's disease. *Expert Opin. Ther. Pat.* **2002,** *12*, 863-870.

(4) Clader, J. W.; Wang, Y. Muscarinic receptor agonists and antagonists in the treatment of Alzheimer's disease. *Curr. Pharm. Des.* **2005,** *11*, 3353-3361.

(5) Citron, M. Alzheimer's disease: strategies for disease modification. *Nat. Rev. Drug Discovery* **2010,** *9*, 387-398.

(6) Conn, P. J.; Christopoulos, A.; Lindsley, C. W. Allosteric modulators of GPCRs: a novel approach for the treatment of CNS disorders. *Nat. Rev. Drug Discovery* **2009,** *8*, 41-54.

(7) Kruse, A. C.; Hu, J.; Pan, A. C.; Arlow, D. H.; Rosenbaum, D. M.; Rosemond, E.; Green, H. F.; Liu, T.; Chae, P. S.; Dror, R. O.; Shaw, D. E.; Weis, W. I.; Wess, J.; Kobilka, B. K. Structure and dynamics of the M3 muscarinic acetylcholine receptor. *Nature* **2012,** *482*, 552-556.

(8) Birdsall, N. J. M.; Lazareno, S. Allosterism at muscarinic receptors: ligands and mechanisms. *Mini. Rev. Med. Chem.* **2005,** *5*, 523-543.

(9) Conn, P. J.; Jones, C. K.; Lindsley, C. W. Subtype-selective allosteric modulators of muscarinic receptors for the treatment of CNS disorders. *Trends Pharmacol. Sci.* **2009,** *30*, 148-155.

(10) Clark, A. L.; Mitchelson, F. The inhibitory effect of gallamine on muscarinic receptors. *Br. J. Pharmacol.* **1976,** *58*, 323-331.

(11) Luellmann, H.; Ohnesorge, F. K.; Schauwecker, G. C.; Wassermann, O. Inhibition of the actions of carbachol and DFP [disopropyl phosphorofluoridate] on guinea pig isolated atria by alkane-bis-ammonium compounds. *Eur. J. Pharmacol.* **1969,** *6*, 241-247.

(12) Croy, C. H.; Schober, D. A.; Xiao, H.; Quets, A.; Christopoulos, A.; Felder, C. C. Characterization of the novel positive allosteric modulator, LY2119620, at the muscarinic M2 and M4 receptors. *Mol. Pharmacol.* **2014,** *86*, 106-115, 110 pp.

(13) Schober, D. A.; Croy, C. H.; Xiao, H.; Christopoulos, A.; Felder, C. C. Development of a radioligand, [(3)H]LY2119620, to probe the human M(2) and M(4) muscarinic receptor allosteric binding sites. *Mol. Pharmacol.* **2014,** *86*, 116-123.

(14) Kruse, A. C.; Kobilka, B. K.; Gautam, D.; Sexton, P. M.; Christopoulos, A.; Wess, J. Muscarinic acetylcholine receptors: novel opportunities for drug development. *Nat. Rev. Drug Discovery* **2014,** *13*, 549-560.

(15) Christopoulos, A.; Changeux, J. P.; Catterall, W. A.; Fabbro, D.; Burris, T. P.; Cidlowski, J. A.; Olsen, R. W.; Peters, J. A.; Neubig, R. R.; Pin, J. P.; Sexton, P. M.; Kenakin, T. P.; Ehlert, F. J.; Spedding, M.; Langmead, C. J. International Union of Basic and Clinical Pharmacology. XC. multisite pharmacology: recommendations for the nomenclature of receptor allosterism and allosteric ligands. *Pharmacol Rev* **2014,** *66*, 918-947.

(16) Antony, J.; Kellershohn, K.; Mohr-Andrae, M.; Kebig, A.; Prilla, S.; Muth, M.; Heller, E.; Disingrini, T.; Dallanoce, C.; Bertoni, S.; Schrobang, J.; Traenkle, C.; Kostenis, E.; Christopoulos, A.; Hoeltje, H.-D.; Barocelli, E.; De Amici, M.; Holzgrabe, U.; Mohr, K. Dualsteric GPCR targeting: a novel route to binding and signaling pathway selectivity. *FASEB J.* **2009,** *23*, 442-450.

(17) De Amici, M.; Dallanoce, C.; Holzgrabe, U.; Trankle, C.; Mohr, K. Allosteric ligands for G protein-coupled receptors: a novel strategy with attractive therapeutic opportunities. *Med. Res. Rev.* **2010,** *30*, 463-549.

(18) Valant, C.; Lane, J. R.; Sexton, P. M.; Christopoulos, A. The best of both worlds? Bitopic orthosteric/allosteric ligands of G protein-coupled receptors. *Annu. Rev. Pharmacol. Toxicol.* **2012,** *52*, 153-178.

(19) Lane, J. R.; Sexton, P. M.; Christopoulos, A. Bridging the gap: bitopic ligands of G-protein-coupled receptors. *Trends Pharmacol. Sci.* **2013,** *34*, 59-66.

(20) Christopoulos, A. Advances in G protein-coupled receptor allostery: from function to structure. *Mol. Pharmacol.* **2014,** *86*, 463-478.

(21) Haga, K.; Kruse, A. C.; Asada, H.; Yurugi-Kobayashi, T.; Shiroishi, M.; Zhang, C.; Weis, W. I.; Okada, T.; Kobilka, B. K.; Haga, T.; Kobayashi, T. Structure of the human M2 muscarinic acetylcholine receptor bound to an antagonist. *Nature* **2012,** *482*, 547-551.

(22) Kruse, A. C.; Ring, A. M.; Manglik, A.; Hu, J.; Hu, K.; Eitel, K.; Hubner, H.; Pardon, E.; Valant, C.; Sexton, P. M.; Christopoulos, A.; Felder, C. C.; Gmeiner, P.; Steyaert, J.; Weis, W. I.; Garcia, K. C.; Wess, J.; Kobilka, B. K. Activation and allosteric modulation of a muscarinic acetylcholine receptor. *Nature* **2013,** *504*, 101-106.

(23) Thal, D. M.; Sun, B.; Feng, D.; Nawaratne, V.; Leach, K.; Felder, C. C.; Bures, M. G.; Evans, D. A.; Weis, W. I.; Bachhawat, P.; Kobilka, T. S.; Sexton, P. M.; Kobilka, B. K.; Christopoulos, A. Crystal structures of the M1 and M4 muscarinic acetylcholine receptors. *Nature* **2016,** *531*, 335-340.

(24) Mohr, M.; Heller, E.; Ataie, A.; Mohr, K.; Holzgrabe, U. Development of a new type of allosteric modulator of muscarinic receptors: hybrids of the antagonist AF-DX 384 and the hexamethonio derivative W84. *J. Med. Chem.* **2004,** *47*, 3324-3327.

(25) Disingrini, T.; Muth, M.; Dallanoce, C.; Barocelli, E.; Bertoni, S.; Kellershohn, K.; Mohr, K.; De Amici, M.; Holzgrabe, U. Design, synthesis, and action of oxotremorine-related

hybrid-type allosteric modulators of muscarinic acetylcholine receptors. *J. Med. Chem.* **2006,** *49*, 366-372.

(26) Steinfeld, T.; Mammen, M.; Smith, J. A.; Wilson, R. D.; Jasper, J. R. A novel multivalent ligand that bridges the allosteric and orthosteric binding sites of the M2 muscarinic receptor. *Mol. Pharmacol.* **2007,** *72*, 291-302.

(27) Bock, A.; Mohr, K. Dualsteric GPCR targeting and functional selectivity: the paradigmatic M(2) muscarinic acetylcholine receptor. *Drug. Discov. Today Technol.* **2013,** *10*, e245-252.

(28) Schmitz, J.; van der Mey, D.; Bermudez, M.; Klockner, J.; Schrage, R.; Kostenis, E.; Trankle, C.; Wolber, G.; Mohr, K.; Holzgrabe, U. Dualsteric muscarinic antagonists--orthosteric binding pose controls allosteric subtype selectivity. *J. Med. Chem.* **2014,** *57*, 6739-6750.

(29) Trankle, C.; Andresen, I.; Lambrecht, G.; Mohr, K. M2 receptor binding of the selective antagonist AF-DX 384: possible involvement of the common allosteric site. *Mol. Pharmacol.* **1998,** *53*, 304-312.

(30) Mitchelson, F. J. The pharmacology of McN-A-343. *Pharmacol. Ther.* **2012,** *135*, 216-245.

(31) Keller, M.; Trankle, C.; She, X.; Pegoli, A.; Bernhardt, G.; Buschauer, A.; Read, R. W. M2 Subtype preferring dibenzodiazepinone-type muscarinic receptor ligands: Effect of chemical homo-dimerization on orthosteric (and allosteric?) binding. *Bioorg. Med. Chem.* **2015,** *23*, 3970-3990.

(32) Eberlein, W. G.; Engel, W.; Mihm, G.; Rudolf, K.; Wetzel, B.; Entzeroth, M.; Mayer, N.; Doods, H. N. Structure-activity relationships and pharmacological profile of selective tricyclic antimuscarinics. *Trends Pharmacol. Sci.* **1989,** *Suppl*, 50-54.

(33) Dimick, S. M.; Powell, S. C.; McMahon, S. A.; Moothoo, D. N.; Naismith, J. H.; Toone, E. J. On the meaning of affinity: cluster glycoside effects and Concanavalin A. *J. Am. Chem. Soc.* **1999,** *121*, 10286-10296.

(34) Park, J.; Wang, Z. U.; Sun, L.-B.; Chen, Y.-P.; Zhou, H.-C. Introduction of Functionalized Mesopores to Metal–Organic Frameworks via Metal–Ligand–Fragment Coassembly. *J. Am. Chem. Soc.* **2012,** *134*, 20110-20116.

(35) Bailey, P. D.; Beard, M. A.; Dang, H. P. T.; Phillips, T. R.; Price, R. A.; Whittaker, J. H. Debenzylation using catalytic hydrogenolysis in trifluoroethanol, and the total synthesis of (-)-raumacline. *Tetrahedron Lett.* **2008,** *49*, 2150-2153.

(36) Copeland, R. A. Conformational adaptation in drug-target interactions and residence time. *Future Med. Chem.* **2011,** *3*, 1491-1501.

(37) Vauquelin, G. Simplified models for heterobivalent ligand binding: when are they applicable and which are the factors that affect their target residence time. *Naunyn. Schmiedebergs Arch. Pharmacol.* **2013,** *386*, 949-962.

(38) Lazareno, S. Quantification of receptor interactions using binding methods. *J. Recept. Signal Transduct. Res.* **2001,** *21*, 139-165.

(39) Christopoulos, A.; Kenakin, T. G protein-coupled receptor allosterism and complexing. *Pharmacol. Rev.* **2002,** *54*, 323-374.

(40) Dei, S.; Bellucci, C.; Buccioni, M.; Ferraroni, M.; Guandalini, L.; Manetti, D.; Martini, E.; Marucci, G.; Matucci, R.; Nesi, M.; Romanelli, M. N.; Scapecchi, S.; Teodori, E. Synthesis, affinity profile, and functional activity of muscarinic antagonists with a 1-methyl-2-(2,2-alkylaryl-1,3-oxathiolan-5-yl)pyrrolidine structure. *J. Med. Chem.* **2007,** *50*, 1409-1413.

(41) Jakubik, J.; El-Fakahany, E. E.; Dolezal, V. Differences in kinetics of xanomeline binding and selectivity of activation of G proteins at M(1) and M(2) muscarinic acetylcholine receptors. *Mol. Pharmacol.* **2006,** *70*, 656-666.

(42) Kenakin, T. P. *A pharmacology primer: theory, applications, and methods*. 3rd ed. Elsevier Academic Press: Burlington, **2009**.

(43) Hulme, E. C.; Trevethick, M. A. Ligand binding assays at equilibrium: validation and interpretation. *Br. J. Pharmacol.* **2010,** *161*, 1219-1237.

(44) Mohr, M.; Heller, E.; Ataie, A.; Mohr, K.; Holzgrabe, U. Development of a New Type of Allosteric Modulator of Muscarinic Receptors: Hybrids of the Antagonist AF-DX 384 and the Hexamethonio Derivative W84. *J. Med. Chem.* **2004,** *47*, 3324-3327.

(45) Suga, H.; Ehlert, F. J. Effects of asparagine mutagenesis of conserved aspartic acids in helix 2 (D2.50) and 3 (D3.32) of M1-M4 muscarinic receptors on the irreversible binding of nitrogen mustard analogs of acetylcholine and McN-A-343. *Biochemistry* **2013,** *52*, 4914-4928.

(46) Cohen, V. I.; Baumgold, J.; Jin, B.; De La Cruz, R.; Rzeszotarski, W. J.; Reba, R. C. Synthesis and structure-activity relationship of some 5-[[[(dialkylamino)alkyl]-1-piperidinyl]acetyl]-10,11-dihydro-5H- benzo[b,e][1,4]diazepin-11-ones as M2-selective antimuscarinics. *J. Med. Chem.* **1993,** *36*, 162-165.

(47) Kane, B. E.; Grant, M. K. O.; El-Fakahany, E. E.; Ferguson, D. M. Synthesis and evaluation of xanomeline analogs—Probing the wash-resistant phenomenon at the M1 muscarinic acetylcholine receptor. *Bioorg. Med. Chem.* **2008,** *16*, 1376-1392.

(48) Ramaswamy, S.; Malaiyandi, M.; Buchanan, G. W. Phase-transfer-catalyzed methylation of hydroxyaromatic acids, hydroxyaromatic aldehydes, and aromatic polycarboxylic acids. *Environ. Sci. Technol.* **1985,** *19*, 507-512.

(49) Castaldi, M. P.; Gibson, S. E.; Rudd, M.; White, A. J. A new approach to enantiopure C3-symmetric molecules. *Chemistry* **2005,** *12*, 138-148.

(50) Kasina, S.; Nematollahi, J. A facile synthesis of acid esters. *Tetrahedron Lett.* **1978**, 1403-1406.

(51) Brellier, M.; Barlaam, B.; Mioskowski, C.; Baati, R. Insight into the Complexation Mode of Bis(nitrilotriacetic acid) (NTA) Ligands with Ni2+ Involved in the Labeling of Histidine-Tagged Proteins. *Chem. Eur. J.* **2009,** *15*, 12689-12701.

(52) Galli, U.; Ercolano, E.; Carraro, L.; Roman, C. R. B.; Sorba, G.; Canonico, P. L.; Genazzani, A. A.; Tron, G. C.; Billington, R. A. Synthesis and biological evaluation of isosteric analogues of FK866, an inhibitor of NAD salvage. *ChemMedChem* **2008,** *3*, 771-779.

(53) Ruger, C.; Rohnert, H.; Lohmann, D. [New derivatives of 5,10-dihydro-11H-dibenzo[b,e][1,4]diazepine-11-ones with anticholinergic activity]. *Pharmazie* **1990,** *45*, 555-559.

(54) Gugliotta, G.; Botta, M.; Giovenzana, G. B.; Tei, L. Fast and easy access to efficient bifunctional chelators for MRI applications. *Bioorg. Med. Chem. Lett.* **2009,** *19*, 3442-3444.

(55) Martinelli, J.; Gugliotta, G.; Tei, L. Synthesis of 6-substituted 6-nitroperhydro-1,4-diazepines via novel tandem retro-Henry and Mannich/Michael reactions. *Org. Lett.* **2012,** *14*, 716-719.

(56) Kon, T.; Kato, S.; Morie, T.; Karasawa, T.; Yoshida, N. Indazole-3-carbonylaminodiazepines as serotonin 5-HT3 antagonists. 1989-113776358903, 19890726., **1990**.

(57) Kato, S.; Harada, H.; Morie, T. Synthesis of 6-amino-1-benzyl-4-methylhexahydro-1H-1,4-diazepine. *J. Heterocycl. Chem.* **1995,** *32*, 637-642.

(58) Himmelsbach, F.; Mark, M.; Eckhardt, M.; Langkopf, E.; Maier, R.; Lotz, R. Preparation of xanthine derivatives as dipeptidylpeptidase-IV inhibitors. WO2002068420A1, **2002**.

(59) Keller, M.; Kuhn, K. K.; Einsiedel, J.; Hubner, H.; Biselli, S.; Mollereau, C.; Wifling, D.; Svobodova, J.; Bernhardt, G.; Cabrele, C.; Vanderheyden, P. M.; Gmeiner, P.; Buschauer, A. Mimicking of Arginine by Functionalized N(omega)-Carbamoylated Arginine As a New Broadly Applicable Approach to Labeled Bioactive Peptides: High Affinity Angiotensin, Neuropeptide Y, Neuropeptide FF, and Neurotensin Receptor Ligands As Examples. *J. Med. Chem.* **2016,** *59*, 1925-1945.

(60) Hübner, H.; Haubmann, C.; Utz, W.; Gmeiner, P. Conjugated Enynes as Nonaromatic Catechol Bioisosteres: Synthesis, Binding Experiments, and Computational Studies of Novel Dopamine Receptor Agonists Recognizing Preferentially the D3 Subtype. *J. Med. Chem.* **2000,** *43*, 756-762.

(61) Conklin, B. R.; Farfel, Z.; Lustig, K. D.; Julius, D.; Bourne, H. R. Substitution of three amino acids switches receptor specificity of Gq alpha to that of Gi alpha. *Nature* **1993,** *363*, 274-276.

(62) Huang, W.; Manglik, A.; Venkatakrishnan, A. J.; Laeremans, T.; Feinberg, E. N.; Sanborn, A. L.; Kato, H. E.; Livingston, K. E.; Thorsen, T. S.; Kling, R. C.; Granier, S.; Gmeiner, P.; Husbands, S. M.; Traynor, J. R.; Weis, W. I.; Steyaert, J.; Dror, R. O.; Kobilka, B. K. Structural insights into micro-opioid receptor activation. *Nature* **2015,** *524*, 315-321.

(63) Lomize, M. A.; Lomize, A. L.; Pogozheva, I. D.; Mosberg, H. I. OPM: orientations of proteins in membranes database. *Bioinformatics* **2006,** *22*, 623-625.

(64) Jo, S.; Kim, T.; Im, W. Automated builder and database of protein/membrane complexes for molecular dynamics simulations. *PLoS One* **2007,** *2*, e880.

(65) Jo, S.; Kim, T.; Iyer, V. G.; Im, W. CHARMM-GUI: a web-based graphical user interface for CHARMM. *J. Comput. Chem.* **2008,** *29*, 1859-1865.

(66) Brooks, B. R.; Brooks, C. L., 3rd; Mackerell, A. D., Jr.; Nilsson, L.; Petrella, R. J.; Roux, B.; Won, Y.; Archontis, G.; Bartels, C.; Boresch, S.; Caflisch, A.; Caves, L.; Cui, Q.; Dinner, A. R.; Feig, M.; Fischer, S.; Gao, J.; Hodoscek, M.; Im, W.; Kuczera, K.; Lazaridis, T.; Ma, J.; Ovchinnikov, V.; Paci, E.; Pastor, R. W.; Post, C. B.; Pu, J. Z.; Schaefer, M.; Tidor, B.; Venable, R. M.; Woodcock, H. L.; Wu, X.; Yang, W.; York, D. M.; Karplus, M. CHARMM: the biomolecular simulation program. *J. Comput. Chem.* **2009,** *30*, 1545-1614.

(67) Wu, E. L.; Cheng, X.; Jo, S.; Rui, H.; Song, K. C.; Davila-Contreras, E. M.; Qi, Y.; Lee, J.; Monje-Galvan, V.; Venable, R. M.; Klauda, J. B.; Im, W. CHARMM-GUI Membrane Builder toward realistic biological membrane simulations. *J. Comput. Chem.* **2014,** *35*, 1997-2004.

(68) Lee, J.; Cheng, X.; Swails, J. M.; Yeom, M. S.; Eastman, P. K.; Lemkul, J. A.; Wei, S.; Buckner, J.; Jeong, J. C.; Qi, Y.; Jo, S.; Pande, V. S.; Case, D. A.; Brooks, C. L., 3rd; MacKerell, A. D., Jr.; Klauda, J. B.; Im, W. CHARMM-GUI Input Generator for NAMD, GROMACS, AMBER, OpenMM, and CHARMM/OpenMM Simulations Using the CHARMM36 Additive Force Field. *J. Chem. Theory Comput.* **2016,** *12*, 405-413.

(69) MacKerell, A. D.; Bashford, D.; Bellott, M.; Dunbrack, R. L.; Evanseck, J. D.; Field, M. J.; Fischer, S.; Gao, J.; Guo, H.; Ha, S.; Joseph-McCarthy, D.; Kuchnir, L.; Kuczera, K.; Lau, F. T.; Mattos, C.; Michnick, S.; Ngo, T.; Nguyen, D. T.; Prodhom, B.; Reiher, W. E.; Roux, B.; Schlenkrich, M.; Smith, J. C.; Stote, R.; Straub, J.; Watanabe, M.; Wiorkiewicz-Kuczera, J.; Yin, D.; Karplus, M. All-atom empirical potential for molecular modeling and dynamics studies of proteins. *J. Phys. Chem. B* **1998,** *102*, 3586-3616.

(70) Mackerell, A. D., Jr.; Feig, M.; Brooks, C. L., 3rd. Extending the treatment of backbone energetics in protein force fields: limitations of gas-phase quantum mechanics in

reproducing protein conformational distributions in molecular dynamics simulations. *J. Comput. Chem.* **2004,** *25*, 1400-1415.

(71) Best, R. B.; Zhu, X.; Shim, J.; Lopes, P. E.; Mittal, J.; Feig, M.; Mackerell, A. D., Jr. Optimization of the additive CHARMM all-atom protein force field targeting improved sampling of the backbone phi, psi and side-chain chi(1) and chi(2) dihedral angles. *J. Chem. Theory Comput.* **2012,** *8*, 3257-3273.

(72) Klauda, J. B.; Venable, R. M.; Freites, J. A.; O'Connor, J. W.; Tobias, D. J.; Mondragon-Ramirez, C.; Vorobyov, I.; MacKerell, A. D., Jr.; Pastor, R. W. Update of the CHARMM all-atom additive force field for lipids: validation on six lipid types. *J. Phys. Chem. B* **2010,** *114*, 7830-7843.

(73) Beglov, D.; Roux, B. Finite representation of an infinite bulk system: Solvent boundary potential for computer simulations. *J. Chem. Phys.* **1994,** *100*, 9050-9063.

(74) Jorgensen, W. L.; Chandrasekhar, J.; Madura, J. D.; Impey, R. W.; Klein, M. L. Comparison of simple potential functions for simulating liquid water. *J. Chem. Phys.* **1983,** *79*, 926-935.

(75) Vanommeslaeghe, K.; Hatcher, E.; Acharya, C.; Kundu, S.; Zhong, S.; Shim, J.; Darian, E.; Guvench, O.; Lopes, P.; Vorobyov, I.; Mackerell, A. D., Jr. CHARMM general force field: A force field for drug-like molecules compatible with the CHARMM all-atom additive biological force fields. *J. Comput. Chem.* **2010,** *31*, 671-690.

(76) Vanommeslaeghe, K.; MacKerell, A. D., Jr. Automation of the CHARMM General Force Field (CGenFF) I: bond perception and atom typing. *J. Chem. Inf. Model.* **2012,** *52*, 3144-3154.

(77) Vanommeslaeghe, K.; Raman, E. P.; MacKerell, A. D., Jr. Automation of the CHARMM General Force Field (CGenFF) II: assignment of bonded parameters and partial atomic charges. *J. Chem. Inf. Model.* **2012,** *52*, 3155-3168.

(78) Yu, W.; He, X.; Vanommeslaeghe, K.; MacKerell, A. D., Jr. Extension of the CHARMM General Force Field to sulfonyl-containing compounds and its utility in biomolecular simulations. *J. Comput. Chem.* **2012,** *33*, 2451-2468.

(79) Salomon-Ferrer, R.; Gotz, A. W.; Poole, D.; Le Grand, S.; Walker, R. C. Routine Microsecond Molecular Dynamics Simulations with AMBER on GPUs. 2. Explicit Solvent Particle Mesh Ewald. *J. Chem. Theory Comput.* **2013,** *9*, 3878-3888.

(80) Le Grand, S.; Götz, A. W.; Walker, R. C. SPFP: Speed without compromise—A mixed precision model for GPU accelerated molecular dynamics simulations. *Comput. Phys. Commun.* **2013,** *184*, 374-380.

(81) Uberuaga, B. P.; Anghel, M.; Voter, A. F. Synchronization of trajectories in canonical molecular-dynamics simulations: observation, explanation, and exploitation. *J. Chem. Phys.* **2004,** *120*, 6363-6374.

(82) Sindhikara, D. J.; Kim, S.; Voter, A. F.; Roitberg, A. E. Bad Seeds Sprout Perilous Dynamics: Stochastic Thermostat Induced Trajectory Synchronization in Biomolecules. *J. Chem. Theory Comput.* **2009,** *5*, 1624-1631.

(83) Berendsen, H. J. C.; Postma, J. P. M.; van Gunsteren, W. F.; DiNola, A.; Haak, J. R. Molecular dynamics with coupling to an external bath. *J. Chem. Phys.* **1984,** *81*, 3684-3690.

(84) Darden, T.; York, D.; Pedersen, L. Particle mesh Ewald: An N·log(N) method for Ewald sums in large systems. *J. Chem. Phys.* **1993,** *98*, 10089-10092.

(85) Ryckaert, J.-P.; Ciccotti, G.; Berendsen, H. J. C. Numerical integration of the cartesian equations of motion of a system with constraints: molecular dynamics of n-alkanes. *J. Comput. Phys.* **1977,** *23*, 327-341.

(86) Sokal R. R. , M. C. D. *The University of Kansas Science Bulletin* **1958,** *38*, 1409-1438.

(87) Cheng, Y.-C.; Prusoff, W. H. Relation between the inhibition constant K1) and the concentration of inhibitor which causes fifty per cent inhibition (I50) of an enzymic reaction. *Biochem. Pharmacol.* **1973,** *22*, 3099-3108.

Chapter 3

Fluorescently labeled monomeric and dimeric dibenzodiazepinone-type muscarinic M_2R ligands

3.1. Introduction

In the last decades, fluorescence-based techniques have been increasingly used for studying ligand-receptor interactions; hence there is a growing demand for suitable fluorescent probes. In contrast to radiolabeled probes, fluorescent ligands harbor less problems concerning safety precautions and waste disposal. Moreover, they are applicable to fluorescent microscopy and flow cytometry, techniques which have become routine in many laboratories. A general issue regarding the design of small-molecule fluorescent ligands is the impairment of the bioactivity caused by the conjugation to the bulky fluorophore. Usually, the pharmacophore (ligand) and the fluorophore are hold apart by some form of linker or spacer moiety.[1] Numerous fluorescent probes have been reported for GPCRs, for instance for neuropeptide Y[2-6], histamine[7-11], opioid[12-14], dopamine[15], neurotensin[16] and adenosine[17] receptors. Concerning muscarinic receptors, several reports on fluorescently labeled M_1R derivatives based on the structure of the antagonist pirenzepine (Figure 1) were published; for instance, compound **55** (BODIPY FL-labeled ligand) (Figure 1), studied by Ilien and coworkers in FRET-based assays, the lissamine-rhodamine B-labeled ligand **56** and the Cy3-labeled compound **57** (Figure 1), which were shown to bind bitopically/dualsterically at the EGFP-fused hM_1R.[18] Notably, the length of the linker and the nature of the fluorophore had a significant impact on the M_1R affinity of pirenzepine derived analogs of **55**-**57**.[18, 19] Furthermore, a fluorescent derivative of the M_1R allosteric modulator AC-42 (Figure 1), bearing a lissamine-rhodamine B fluorophore (**58**) (Figure 1) was prepared and investigated by FRET-based techniques.[19] In contrast to the M_1R, reports on M_2R-M_5R fluorescent probes are rare.

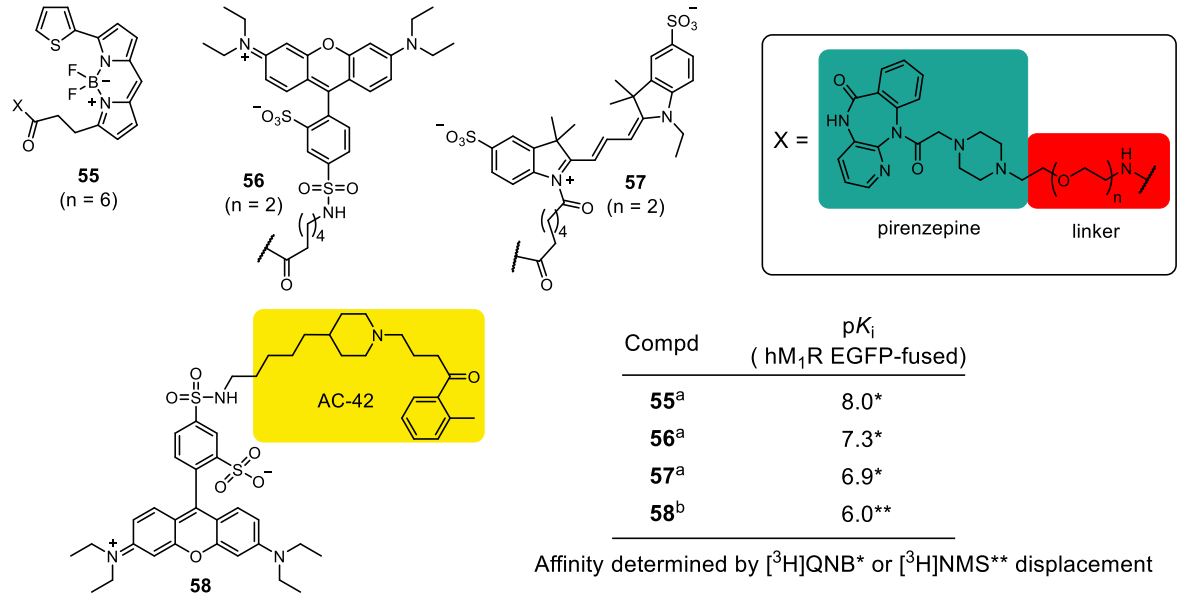

Compd	pK_i (hM_1R EGFP-fused)
55[a]	8.0*
56[a]	7.3*
57[a]	6.9*
58[b]	6.0**

Affinity determined by [^{3}H]QNB* or [^{3}H]NMS** displacement

Figure 1. Structures and M_1R binding affinity of the fluorescently labeled M_1R ligands **55-58**, which were suggested to exhibit a bitopic/dualsteric binding mode.[18, 19] (a) Tahtauoi *et al.*[18] (b) Daval *et al.*[19]

The tricyclic dibenzodiazepinone-type MR ligand **19**[20], derived from the M_2R-preferring antagonist DIBA (*cf.* Chapter 1, Figure 4), was recently prepared as a tritium-labeled ligand, and, by various binding studies with [^{3}H]**19**, this molecular tool was proven to interact dualsterically with the hM_2R (*cf.* Chapter 2). Aiming at fluorescent molecular tools for the M_2R, fluorescently labeled analogs of the monomeric ligand **19** as well as fluorescently labeled homo- and heterodimeric dibenzodiazepinone-type MR ligands were prepared using red-emitting cyanine dyes, and investigated with respect to their M_1R-M_5R affinity. Selected compounds were characterized by flow cytometry and high-content imaging based binding studies as well as by confocal microscopy.

3.2. Results and discussion

3.2.1 Chemistry

The fluorescent monomeric and dimeric dibenzodiazepinone-type MR ligands were prepared using red emitting cyanine dyes in order to have low background fluorescence when applying the fluorescent ligands at cells. Two commercially available cyanine dyes (purchased as *N*-succinimidyl ester), i.e. S 0536 (**59**) and S 0586 (**60**) (emission maximum > 650 nm) (Figure 2A) were used. Treatment of the DIBA-derived amine precursors **30**[20], **31** (*cf.* Chapter 2) and **65**[21] with **59** or **60** (Figure 2A) resulted in the fluorescently labeled DIBA derivatives **61**-**64** and **66** (Figure 2B).

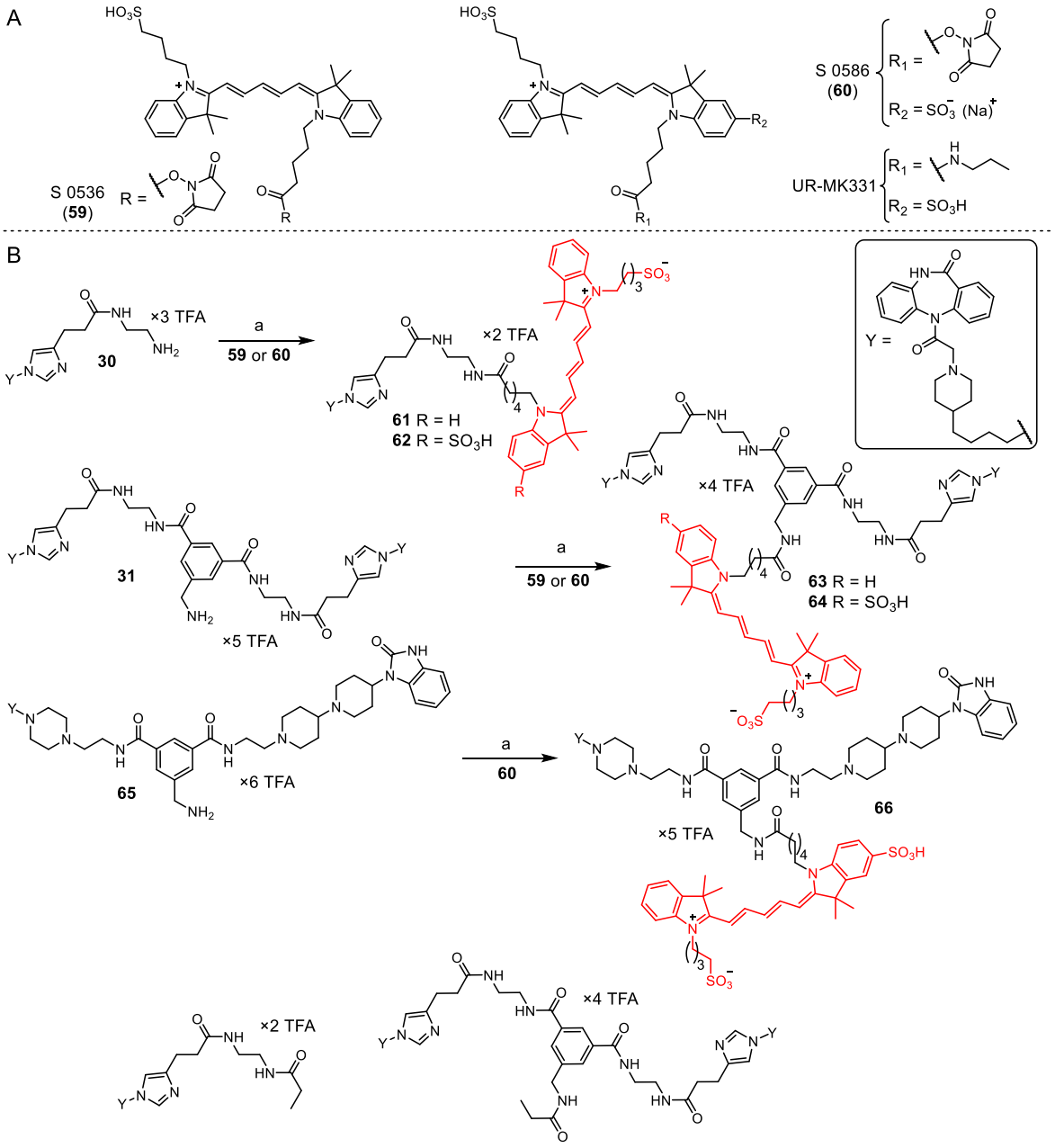

Figure 2. (A) Structures of the fluorescent dyes (succinimidyl esters **59** and **60**), which were used for the labeling of dibenzodiazepinone-type MR ligands. (B) Synthesis of the fluorescently labeled MR ligands **61-64** and **66**. Reagents and conditions: (a) DIPEA, DMF, rt, 1 h, 34% (**61**), 41% (**62**), 36% (**63**), 26% (**64**), 34% (**66**).

Fluorescent ligands **62** and **64** were investigated with respect to their stability under assay-like conditions (PBS pH 7.4) (Figure 3).

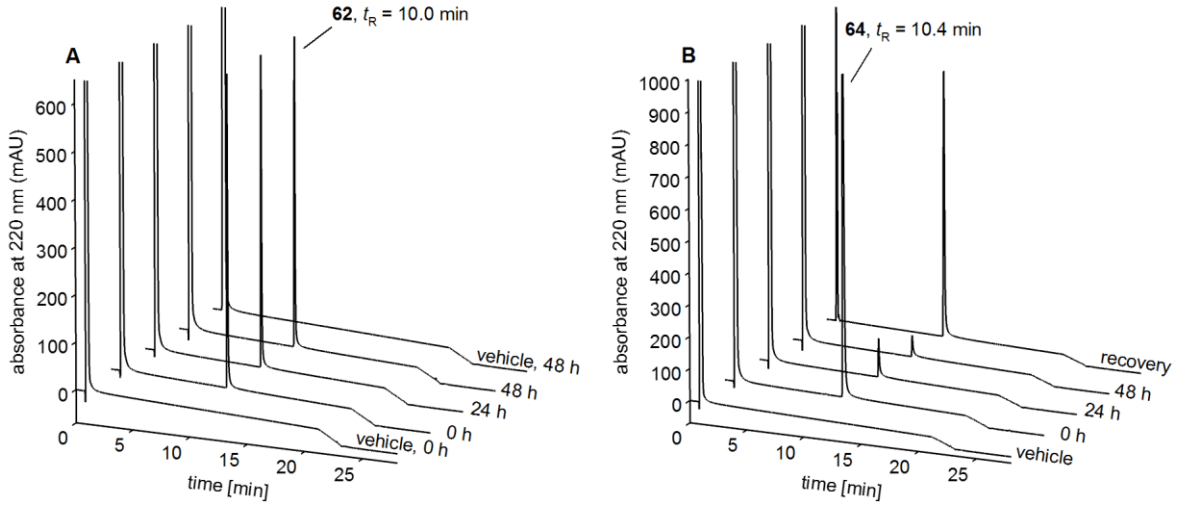

Figure 3. HPLC analysis of **62** (A) and **64** (B) after incubation in PBS (pH 7.4) at 23 °C for up to 48 h. HPLC conditions see experimental section.

No decomposition was observed for both **62** and **64** within the incubation period of 48 h (Figure 3A and Figure 3B). Interestingly, compound **64** adsorbed strongly to the vessel material (siliconized (Sigmacote) glass tubes) resulting in a reduction of the peak area by approx. 90% after 24 h (Figure 3B). The use of other materials (polypropylene and "siliconized" polypropylene tubes) did not result in a lower adsorption of **64** (data not shown). Notably, after removal of the aqueous solution after 48 h, most of the intact fluorescently-labeled ligand could be desorbed and recovered by rinsing of the tube with acetonitrile/0.1% aq TFA (1:1 v/v) (Figure 3B, recovery).

3.2.2 Radioligand binding studies with [^{3}H]NMS

The MR affinities of the fluorescently labeled dibenzodiazepinone derivatives **61-64** and **66** were determined at live CHO-hM_xR cells (x = 1-5) using the orthosteric antagonist [^{3}H]NMS as radioligand. All the fluorescent ligands exhibited high M_2R binding with pK_i values > 8.8 (Table 1), i.e. their M_2R affinities were comparable to those of the structurally closely related, but not fluorescently labeled compounds **19**[20], **33** (*cf.* Chapter 2 Table 1) and **65**.[21] The complete MR selectivity profile was determined for compounds **62** and **64** (Table 1, Figure 4). While both fluorescent ligands exhibited an excellent M_2/M_3 and M_2/M_5 selectivity, no preference for the M_2R over the M_1 and M_4 receptor subtype became evident. Thus, a putative dualsteric binding mode of this type of fluorescent ligands does not result in an improved selectivity profile as also reported for other dualsteric MR ligands.[22, 23]

Table 1. M_1-M_5 receptor affinities (pK_i values) of the dibenzodiazepinone-type fluorescent ligands **62**-**64** and **66**, obtained from equilibrium competition binding studies with [^{3}H]NMS at live CHO-hM_xR cells (x = 1-5).

compd.	dye[a]	pK_i[b]				
		M_1R	M_2R	M_3R	M_4R	M_5R
61	S 0536	n.d.	9.03 ± 0.08	n.d.	n.d.	n.d.
62	S 0586	8.28 ± 0.17	9.10 ± 0.04	6.30 ± 0.05	8.35 ± 0.19	6.91 ± 0.24
63	S 0536	n.d.	8.85 ± 0.07	n.d.	n.d.	n.d.
64	S 0586	8.64 ± 0.03	9.20 ± 0.03	6.61 ± 0.02	8.54 ± 0.16	6.52 ± 0.07
66	S 0586	n.d.	9.59 ± 0.03	n.d.	n.d.	n.d.

[a]Provided are the code numbers of the succinimidyl esters of the fluorescent dyes used for the preparation of the fluorescent ligands (*cf.* Figure 2A). [b]Mean values ± SEM from 3-4 independent experiments (each performed in triplicate). K_d values / applied concentrations of [^{3}H]NMS: M_1: 0.12 / 0.2 nM, M_2: 0.090 / 0.2 nM, M_3: 0.089 / 0.2 nM, M_4: 0.040 / 0.1 nM, M_5: 0.24 / 0.3 nM.

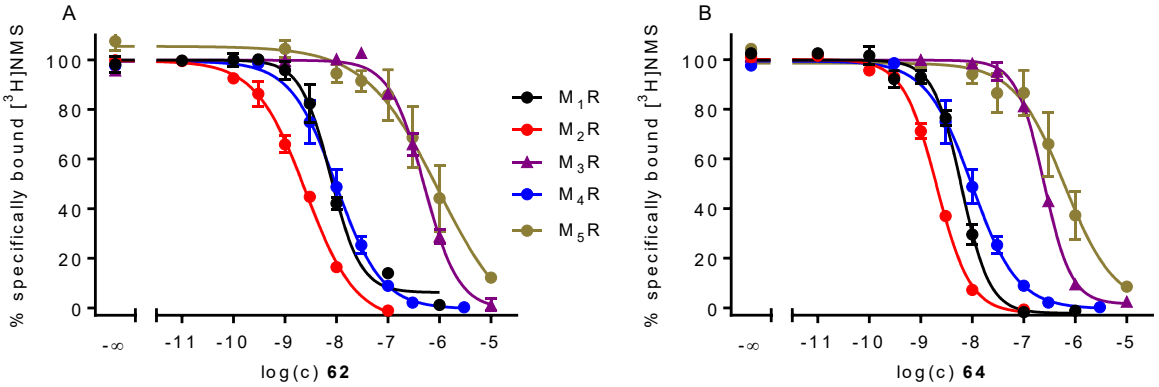

Figure 4. Effect of the dibenzodiazepinone-type MR ligands **62** (A) and **64** (B) on M_xR equilibrium binding of [^{3}H]NMS determined at CHO-hM_xR cells (x = 1-5). Data represent mean values ± SEM from at least three independent experiments (each performed in triplicate).

3.2.3 Fluorescence properties of compounds 61, 62 and 64

The fluorescence quantum yields were determined (reference: cresyl violet perchlorate) for monomeric fluorescent ligands **61** and **62**, and for the homodimeric ligand **64** in PBS (pH 7.4) and in PBS supplemented with 1% bovine serum albumin (BSA) to study the influence of proteins on the quantum yield (Table 2). By selecting compounds **61**, **62** and **64** both types of fluorophores, used in this work, were covered.

Table 2. Fluorescence properties of the fluorescent ligands **61**, **62** and **64** in PBS and PBS containing 1% BSA: excitation/emission maxima and fluorescent quantum yields Φ (reference: cresyl violet perchlorate).

Compound	Dye[a]	PBS		PBS+1% BSA	
		$\lambda_{ex}/\lambda_{em}$	Φ (%)	$\lambda_{ex}/\lambda_{em}$	Φ (%)
61	S 0536	645/666	24.4	663/676	51.1
62	S 0586	651/669	21.6	658/673	36.8
64	S 0586	650/668	4.1	658/673	43.4

[a]Provided are the code numbers of the succinimidyl esters of the fluorescent dyes used for the preparation of the fluorescent ligand (*cf*. Figure 2A).

The investigated fluorescent ligands (**61**, **62**, **64**) showed a higher quantum yield in PBS supplemented with 1% BSA compared to PBS alone (Table 2). This phenomenon was previously observed for fluorescently labeled NPY Y_1 antagonists,[4] too, and can be explained by interactions (hydrophobic, electrostatic) of the fluorophores with the protein, resulting in a changed chemical environment and reduced molecular motion (increased rigidity) of the fluorophore. Therefore, when BSA free buffers are used for binding assays with such kind of fluorescent ligands, the fluorescence quantum yield can potentially increase in the receptor bound state. However, this effect may also occur in case of unspecific interactions of the ligand with other membrane proteins or the lipid bilayer. The increase in fluorescence quantum yield by adding BSA was most pronounced for the homodimeric ligand **64** (> 10-fold), as in this case the quantum yield in neat PBS was considerably lower compared to the monomeric ligands **61** and **62** (Table 2). It can be speculated that in case of the dimeric ligand **64** there is a “cross-talk” between the fluorophore and the two dibenzodiazepinone moieties, which is absent in the presence of proteins.

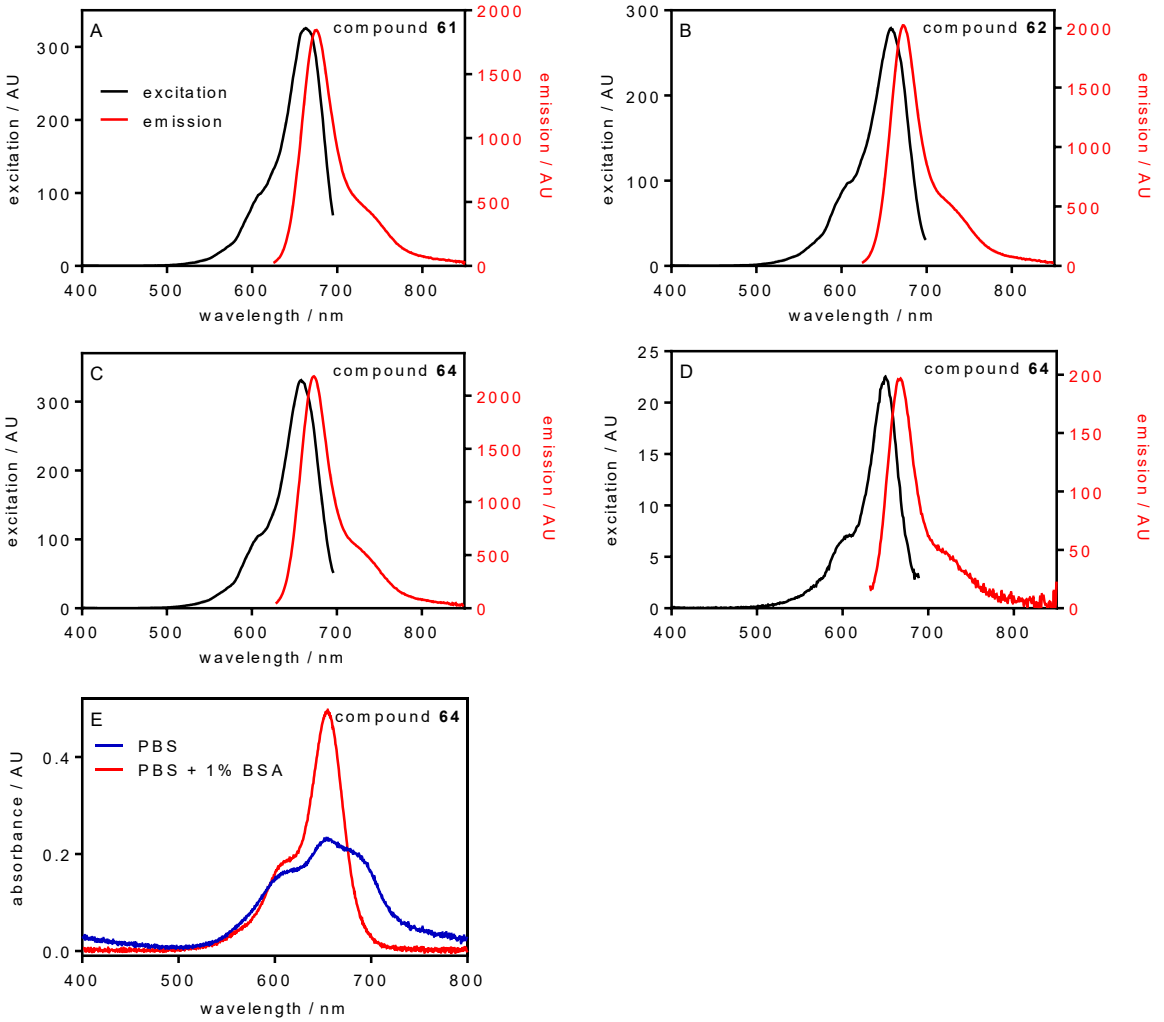

Figure 5. Excitation and corrected emission spectra (recorded at 22 °C) of the fluorescent ligands **61** (A), **62** (B) and **64** (C) at a concentration of 2.5 µM in PBS supplemented with 1% BSA and of fluorescent ligand **64** (D) in neat PBS. (E) Absorption spectra (400-800 nm) of the dimeric compound **64** (2.5 µM) in PBS and PBS supplemented with 1% BSA (recorded at 22 °C).

Excitation and corrected emission spectra of **61**, **62** and **64** in PBS containing 1% BSA appeared to be very similar (Figure 5A-C). All fluorescent ligands are suited for an excitation with the red diode laser (635 nm), which usually belongs to the standard equipment of flow cytometers and confocal microscopes. Notably, whereas in case of the monomeric ligands **61** and **62** the shape of the excitation and absorption spectra was similar (data not shown), the shape of the absorption spectrum of the dimeric ligand **64** was different (bathochromic shift, decreased absorption coefficient) (excitation spectrum in PBS shown in Figure 5D, absorption spectrum shown in Figure 5E). It is a matter of speculation if the dimeric nature of compound **64** has an influence on the spectroscopic properties of the attached fluorophore and/or on the physicochemical properties of the fluorescent probe.

3.2.4 Flow cytometric M_2R saturation binding studies with 62 and 64

The fluorescent ligands **62** and **64**, which showed excellent M_2R affinities (pK_i values > 9.0 nM, *cf*. Table 1) were applied to flow cytometric saturation binding studies using intact CHO-hM_2R cells. The obtained K_d values of 4.6 nM and 3.2 nM, respectively (Figure 6A and Figure 6B, Table 3), were about five times higher than the corresponding K_i values of 0.79 and 0.63 nM (*cf*. Table 1) obtained from competition binding experiments with [^{3}H]NMS at live CHO-hM_2R cells. At concentrations corresponding to the K_d value, unspecific binding was around 10% of the total binding for both fluorescent ligands (Figure 6A and Figure 6B). The orthosteric antagonist atropine (**2**), used to determine unspecific binding, was capable of completely preventing one-site (monophasic) specific binding of the fluorescent ligands, indicating that **62** and **64** bind to the orthosteric binding pocket of the M_2R.

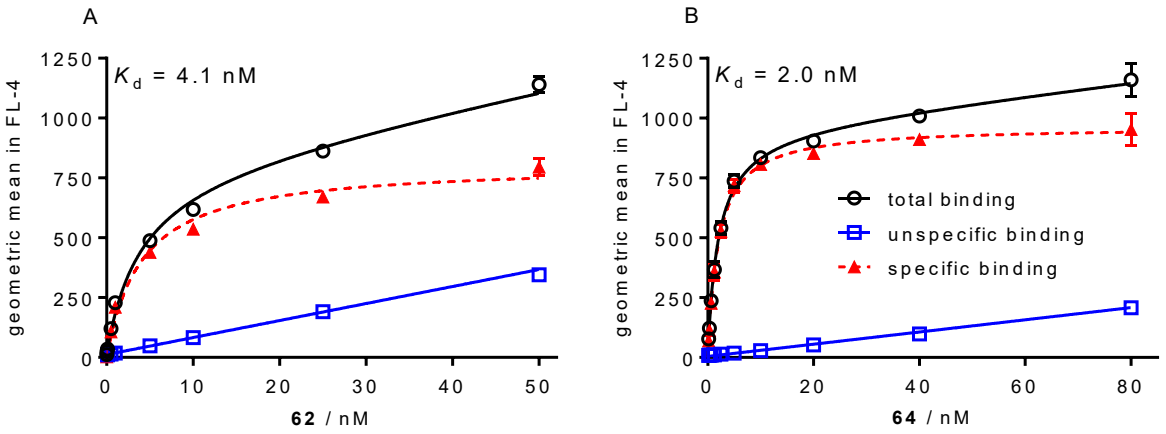

Figure 6. Representative saturation isotherms (specific binding, dashed line) obtained from flow cytometric saturation binding experiments performed with **62** (A) and **64** (B) at intact CHO-hM_2R cells. Unspecific binding was determined in the presence of atropine (**2**) (500-fold excess). Cells were incubated with the fluorescent ligands at 22 °C in the dark for 2 h. Experiments were performed in duplicate. Measurements were performed with a FACSCalibur flow cytometer (Becton Dickinson). Specific binding data were analyzed by an equation describing one-site (monophasic) binding. Error bars of specific binding represent propagated errors calculated according to the Gaussian law of errors. Error bars of total and unspecific binding represent the mean ± SEM from at least two independent experiments (each performed in duplicate).

3.2.5 Application of the fluorescent ligands 62 and 64 to high content imaging

3.2.5.1 Saturation binding

The fluorescent ligands **62** and **64** were also applied to plate reader-based high-content analysis (combination of a microscope and a plate reader for fluorescence detection) using live CHO-hM_1R and CHO-hM_2R cells. In order to find optimal assay conditions, saturation isotherms of **62** at intact CHO-hM_2 cells were recorded using a protocol with and without a washing step (*cf.* general experimental conditions) prior to the measurement of the plate

with an Image Express (IX) Ultra plate reader. A considerable difference in unspecific binding became evident between the non-washed (Figure 7A) and the washed (Figure 7B) plate, suggesting that a washing step after the incubation period (prior to the measurement) is advantageous for the analysis of the data. In fact, without the application of a washing step, it was impossible to calculate a dissociation constant, because a discrimination between total and unspecific binding of the florescent probe **62** at CHO-M_2 cells failed (Figure 7A).

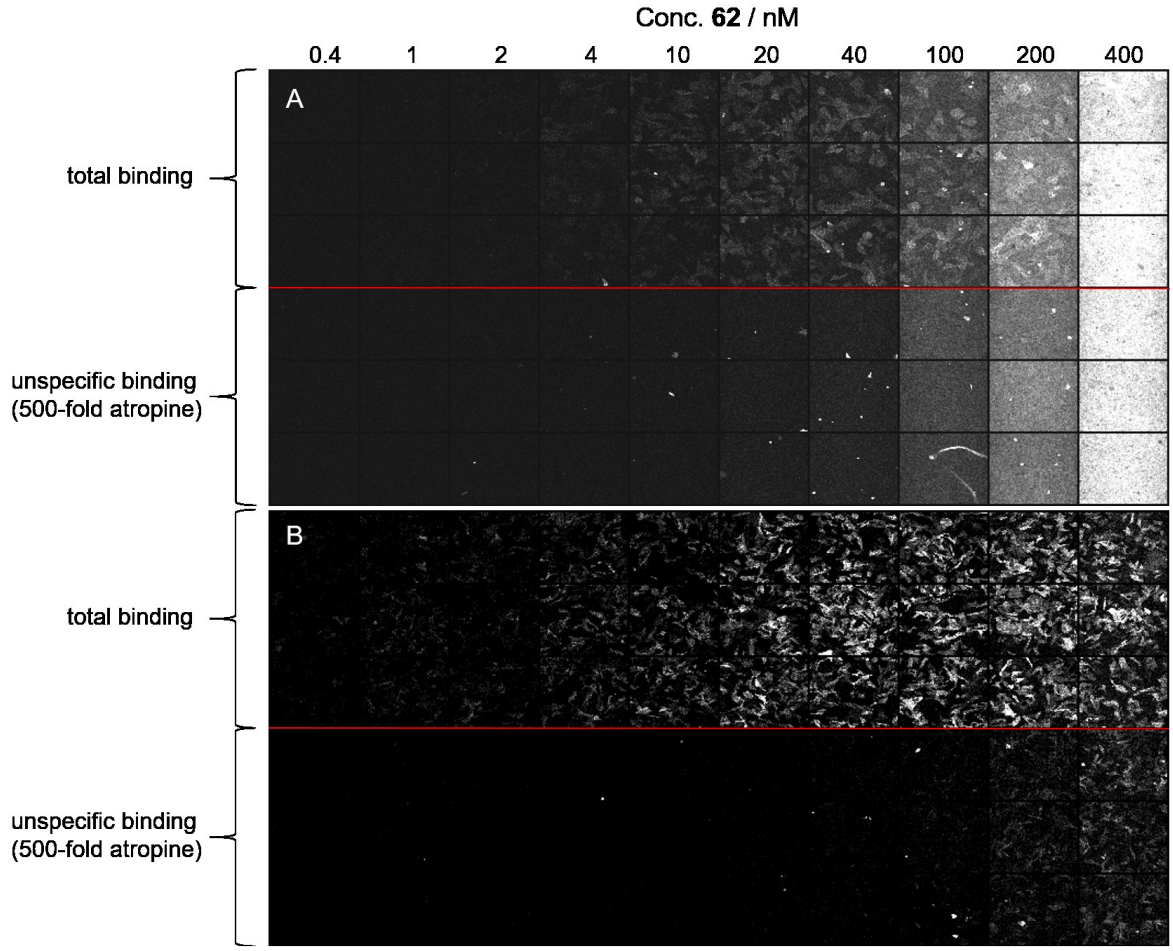

Figure 7. Representative thumbnail fluorescence images acquired with an IX Ultra plate reader of a high-content imaging saturation binding assay performed with the fluorescent ligand **62** at intact CHO-hM_2R cells in a 96-well plate. Omitting a washing step prior to the measurement with the plate reader resulted in considerably higher unspecific binding (A) compared to the assay including a washing step (B).

By contrast, in case of saturation binding experiments with compound **64** at CHO-hM_2R cells almost no differences in unspecific binding and in the resulting K_d values (Figure 8B) were found, regardless whether a washing step was carried out or omitted (thumbnail fluorescence images not shown). In order to use identical protocols for binding studies with **62** and **64**, a washing procedure was always applied before the measurements. The bound fluorescence detected by high-content imaging was quantified by granularity analysis as

reported elsewhere.[24] The K_d values, obtained from M_2R saturation binding experiments including the washing step prior to the measurement, amounted to 14 nM for **62** and 10 nM for **64**, being slightly higher compared to the K_d values obtained from flow cytometric saturation binding studies (Table 3). At concentrations around the K_d value, unspecific binding amounted to around 2% of the total binding (Figure 8A and Figure 8B). In addition, saturation binding experiments with **62** and **64** were performed at CHO-hM_1R cells (Figure 8C and Figure 8D). The K_d values amounted to 19 nM (**62**) and 11 nM (**64**) (Table 3), confirming that the fluorescent ligands **62** and **64** do not exhibit M_2R selectivity. In case of M_2R binding data, the K_d values obtained from high content imaging saturation binding studies at the M_1R were higher compared to the respective K_i values derived from competition binding experiments with [^{3}H]NMS (Table 3). These deviations might be caused by the different assay readouts (radiochemical *vs*. fluorescence-based), and, in case of **62**, by the high adsorption to the plate material (high content imaging) resulting in a considerable decrease in free fluorescent ligand.

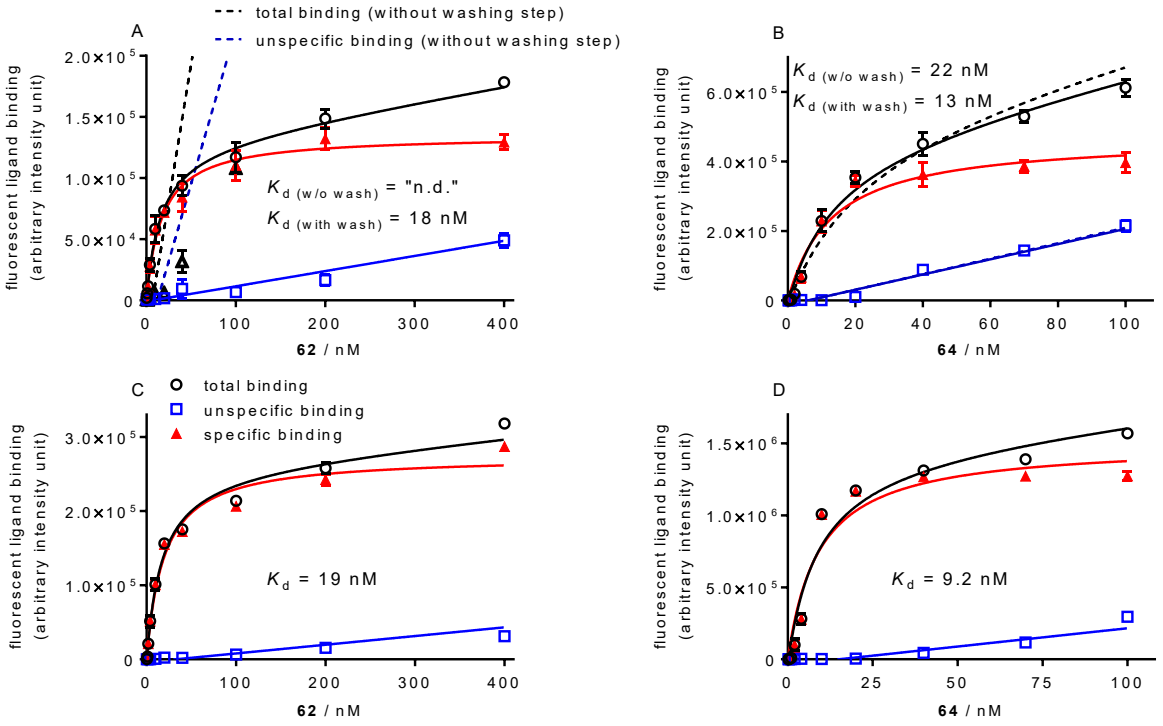

Figure 8. Representative saturation isotherms obtained from high-content imaging saturation binding experiments performed with **62** (A) and **64** (B) at intact CHO-hM_2R cells as well as with **62** (C) and **64** (D) at intact CHO-hM_1R cells. Dashed lines represent total and unspecific binding of **62** (B) and **64** (C) obtained from experiments performed without a washing step prior the measurement of the plate. Unspecific binding was determined in the presence of atropine (**2**) (500-fold excess). Cells were incubated with the fluorescent ligand at 22 °C in the dark for 1 h. Experiments were performed in triplicate. Measurements were performed with an IX Ultra Confocal Plate Reader (Molecular Devices). Specific binding data were analyzed by an equation describing one-site (monophasic) binding. Error bars of specific binding represent propagated errors calculated according to the Gaussian law of errors. Error bars of total and unspecific binding represent the SEM (n = 3).

Table 3. Comparison of M_1R and M_2R binding data of **62** and **64** obtained from various binding assays.

Ligand	CHO-hM_1R cells		CHO-hM_2R cells		
	K_i [nM][a]	K_d [nM][c]	K_i [nM][a]	K_d [nM][b]	K_d [nM][c]
62	5.1 ± 2.4	27 ± 2.6	0.79 ± 0.070	4.6 ± 0.69	14 ± 1.6
64	2.3 ± 0.24	11 ± 1.2	0.64 ± 0.039	3.2 ± 0.58	10 ± 2.0

[a]Dissociation constant determined by equilibrium competition binding with [^{3}H]NMS at intact CHO-hM_2 cells; mean ± SEM from at least three independent experiments (performed in triplicate). [b]Dissociation constant from flow cytometric saturation binding studies at live CHO-hM_2R cells; mean ± SEM from three independent experiments (performed in duplicate). [c]Dissociation constant from high-content imaging saturation binding studies at live CHO-hM_2R cells; mean ± SEM from three independent experiments (performed in triplicate).

In order to investigate if the fluorophore unspecifically stains the cells, saturation binding experiments with UR-MK331, which represents the *N*-propyl amide analog of the fluorescent dye implemented in the structure of **62**, **64** and **66** (*cf*. Figure 2), were performed at the M_2R. As becomes obvious from Figure 9, no binding of this cyanine dye to CHO-hM_2R cells was detected at concentrations of up to 400 nM.

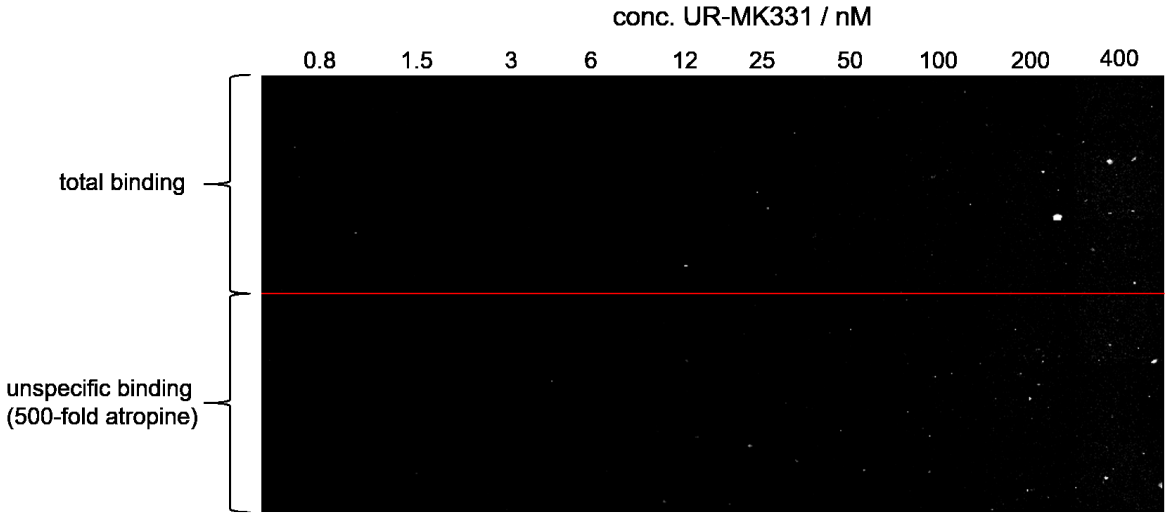

Figure 9. Representative thumbnail fluorescence images acquired with an IX Ultra plate reader of a high-content imaging saturation binding assay performed with the reference compound UR-MK331 at intact CHO-hM_2R cells. A washing step was included prior the measurement of the plate.

3.2.5.2 Competition binding

The effects of various described orthosteric (antagonists **1** and **2**; agonists **4** and **5**), allosteric (**8** and **9**) and dualsteric (**19** and **33**) MR ligands on the equilibrium binding of the monomeric fluorescent ligand **62** and the homodimeric ligand **64** were determined at live CHO-hM_2R cells by means of high content imaging (Figure 10A and Figure 10B). A washing step was applied before measuring the plates with the IX Ultra plate reader. All four-

parameter logistic curves reached 0% specific binding of **62** or **64**, indicating a competitive mechanism between the fluorescent ligand and the investigated MR ligands (Figure 10A and Figure 10B). It should be noted that in case of the allosteric modulators **8** and **9**, a strongly negative cooperativity could also result in sigmoidal "displacement" curves with lower curve plateaus not different from 0% specific fluorescent ligand binding (*cf.* General Introduction, section 1.2.1.1). The obtained pIC_{50} values were converted into the corresponding pK_i values (presented in Table 4) using the logarithmic form of the Cheng-Prusoff equation, and the K_d values (14 nM for **62** and 10 nM for **64**) determined in high-content imaging saturation binding studies (*cf.* Table 3). Generally, the pK_i values were in good agreement with reported data (Table 4), although MR ligand affinities determined with the dimeric fluorescent ligand **64** were lower compared to M_2R affinities obtained from equilibrium competition binding experiments with **62** (Table 4). Interestingly, the same phenomenon was observed in case of equilibrium competition binding studies with the dimeric radioligand [^{3}H]**33** and its monomeric counterpart [^{3}H]**19** (*cf* Chapter 2, Table 3).

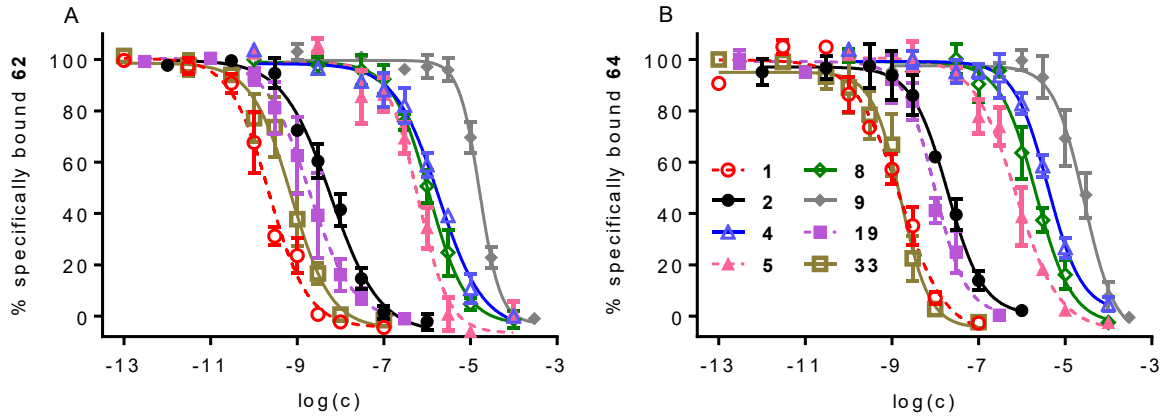

Figure 10. Concentration-dependent effects of various reported orthosteric (**1**, **2**, **4**, **5**), allosteric (**8**, **9**) and dualsteric (**19**, **33**) MR ligands on M_2R equilibrium binding of **62** (c = 10 nM) (A) and **64** (c = 10 nM) (B) determined at intact CHO-hM_2R cells using high-content imaging. Data were analyzed by four parameter logistic fits. Mean values ± SEM from at least three independent experiments (performed in duplicate).

Table 4. M_2R binding data (pK_i or pIC_{50}) of various orthosteric (**1**-**5**), allosteric (**8**-**9**) and dualsteric (**19**, **33**) MR ligands determined by the use of **62**, **64** or [^{3}H]NMS.

Ligand	**62** pK_i [a]	**64** pK_i [a]	[^{3}H]NMS pK_i^* or pIC_{50}^{**} (± SEM)
1	10.1 ± 0.03	9.11 ± 0.08	9.7[*b]
2	8.74 ± 0.12	8.02 ± 0.07	7.8-9.2[*c]
4	6.10 ± 0.03	5.62 ± 0.06	5.0-6.6[*c]
5	6.77 ± 0.15	6.44 ± 0.14	6.5-7.4[*d]
8	6.30 ± 0.16	5.95 ± 0.09	6.32 ± 0.18[**e]
9	5.15 ± 0.06	5.01 ± 0.15	<4.5[**f]
19	9.12 ± 0.28	8.26 ± 0.17	9.12 ± 0.05[*g]
33	9.68 ± 0.23	9.30 ± 0.21	9.39 ± 0.05[*g]

[a]Determined by high-content imaging equilibrium competition binding studies with **62** (c = 10 nM) or with **64** (c = 10 nM) at intact CHO-hM_2R cells; mean values ± SEM from at least three independent experiments (performed in duplicate). [b]Dei *et al*.[25] [c]pK_i values from equilibrium (competition) binding experiments reported in the literature (data taken from the IUPHAR/BPS database (guidetopharmacology.org, (Nov. 2016)). [d]Jakubik *et al*.[26] [e]pIC_{50} value obtained from nonlinear four-parameter logistic curve analyses of data characterizing the inhibition of [^{3}H]NMS (c = 0.2 nM) equilibrium binding at live CHO-hM_2R cells; mean ± SEM from at least three independent experiments (performed in triplicate). [f]Inhibitory effect on M_2R equilibrium binding of [^{3}H]NMS (c = 0.2 nM) at intact CHO-hM_2R cells (*cf.* Chapter 2, Figure 7B). [g]pK_i values taken from Chapter 2, Table 1.

3.2.5.3 M_2R Saturation binding with 62 and 64 in the presence of the allosteric modulator 8 (Schild-like analysis)

In order to unveil a putative involvement of the allosteric vestibule in M_2R binding of the fluorescent ligands **62** and **64**, saturation binding experiments were performed in the presence the allosteric modulators **8** applied at increasing concentrations (Schild-like analysis Figure 11).[27-29] This kind of experiment is equivalent to the Schild analysis used to investigate the inhibiting effect of a receptor antagonist on the response elicited by an agonist, and was applied, for instance, to prove the dualsteric binding mode of [^{3}H]**19** and [^{3}H]**33** at the M_2R (*cf.* Chapter 2, Figure 15) as well as of a fluorescent pirenzepine derivative at the M_1R.[30] In the presence of **8**, the saturation isotherms of both, the monomeric ligand **62** and the homodimeric ligand **64**, were rightward shifted resulting in linear 'Schild' regressions with a slope not different from unity (Figure 11A and Figure 11B, Table 5). These results were indicative of a competitive mechanism between the allosteric M_2R ligand **8** and the fluorescent dibenzodiazepinone-type ligands **62** and **64**. The 'pA_2' values of **8** derived from the 'Schild' regressions were in good agreement with the pK_i values of **8** from equilibrium competition binding studies with **62** and **64** as well as with reported M_2R affinities (pK_A) of **8** (Table 5). With regard to the fact that **62** and **64** address the orthosteric binding site of the M_2R (concluded from experimental data presented in Figure 6, Figure 8 and Figure 10) the results of the Schild-like analyses strongly suggested, as already reported

for the dibenzodiazepinone-type MR ligands **19** and **33** (*cf*. Chapter 2), a dualsteric binding mode of **62** and **64** at the M_2R, that is, a simultaneous binding to the orthosteric site and the allosteric vestibule.

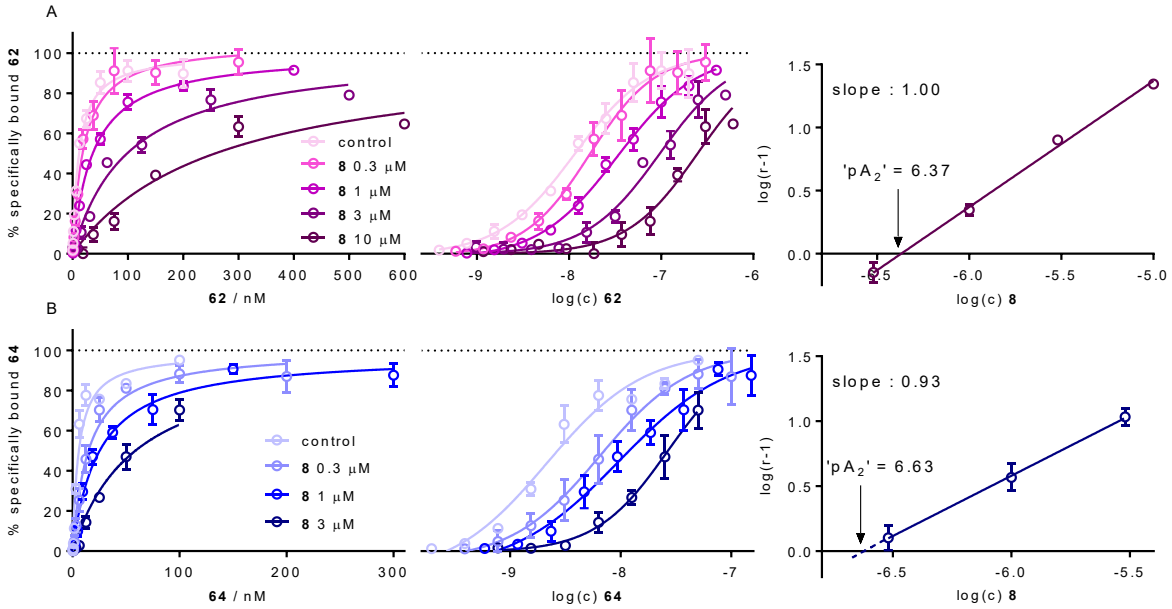

Figure 11. Saturation binding of **62** (A) and **64** (B) in the presence of **8** at increasing concentrations. Presented are saturation isotherms of specific fluorescent ligand binding to the M_2R in linear scale (left) and semi-logarithmic scale (middle), and 'Schild' regressions (right) resulting from the rightward shifts (ΔpK_d) of the saturation isotherms (log(r−1) plotted vs. log(concentration allosteric modulator), where $r = 10^{\Delta pKd}$). The presence of the allosteric modulator **8** led to a parallel rightward shift of the saturation isotherms of both, the monomeric (**62**) and the homodimeric (**64**) fluorescently labeled dibenzodiazepinone derivative. In both cases the slope of the linear 'Schild' regression was nearly equal to unity, indicating a competitive interaction between the fluorescent ligands and the allosteric ligand **8**. Experiments were performed at intact CHO-hM_2R cells. Data represent mean values ± SEM from at least three independent experiments (each performed in triplicate).

Table 5. Summary of M_2R binding data of the allosteric M_2R modulator **8** determined by the use of the fluorescently labeled dibenzodiazepinone derivatives **62** and **64**.

Florescent ligand	Slope[a]	'pA_2'[b]	pK_i[c]	pK_A[d]
62	1.00 ± 0.05	6.38 ± 0.04	6.22 ± 0.16	6.00*/6.53**
64	0.93 ± 0.09	6.67 ± 0.12	5.95 ± 0.09	

[a]Slope of the 'Schild' regression constructed based on fluorescent ligand binding data from saturation binding experiments with **62** or **64** in the presence of increasing fixed concentrations of the allosteric ligands **8**; mean values ± SEM from at least three sets of independent saturation binding experiments (performed in triplicate). The slope of the linear 'Schild' regression was not different from unity (P >0.2). [b]The 'pA_2' value corresponds to the X-axis intercept of the linear 'Schild' regression (*cf.* Figure 11) and reflects the affinity of the investigated allosteric ligand **8**. [c]pK_i values taken from Chapter 2 Table 3. [d]Mohr *et al*.[31] (pK_A determined by [^{3}H]NMS* or [^{3}H]AF-DX 384** displacement.

3.2.6 Application of the fluorescent ligand 62 and 64 to confocal microscopy

The fluorescent probes **62** and **64** were also applied to confocal microscopy using live CHO-hM_2R cells. A significant difference between total and unspecific binding was evident for both ligands (Figure 12 and Figure 13) after different incubation times (5-45 min). Unspecific binding was determined in the presence of the MR antagonist atropine (**2**). The major fraction of detected fluorescence appeared to be associated to the cell membrane. An increase in intracellular fluorescence over time was not observed.

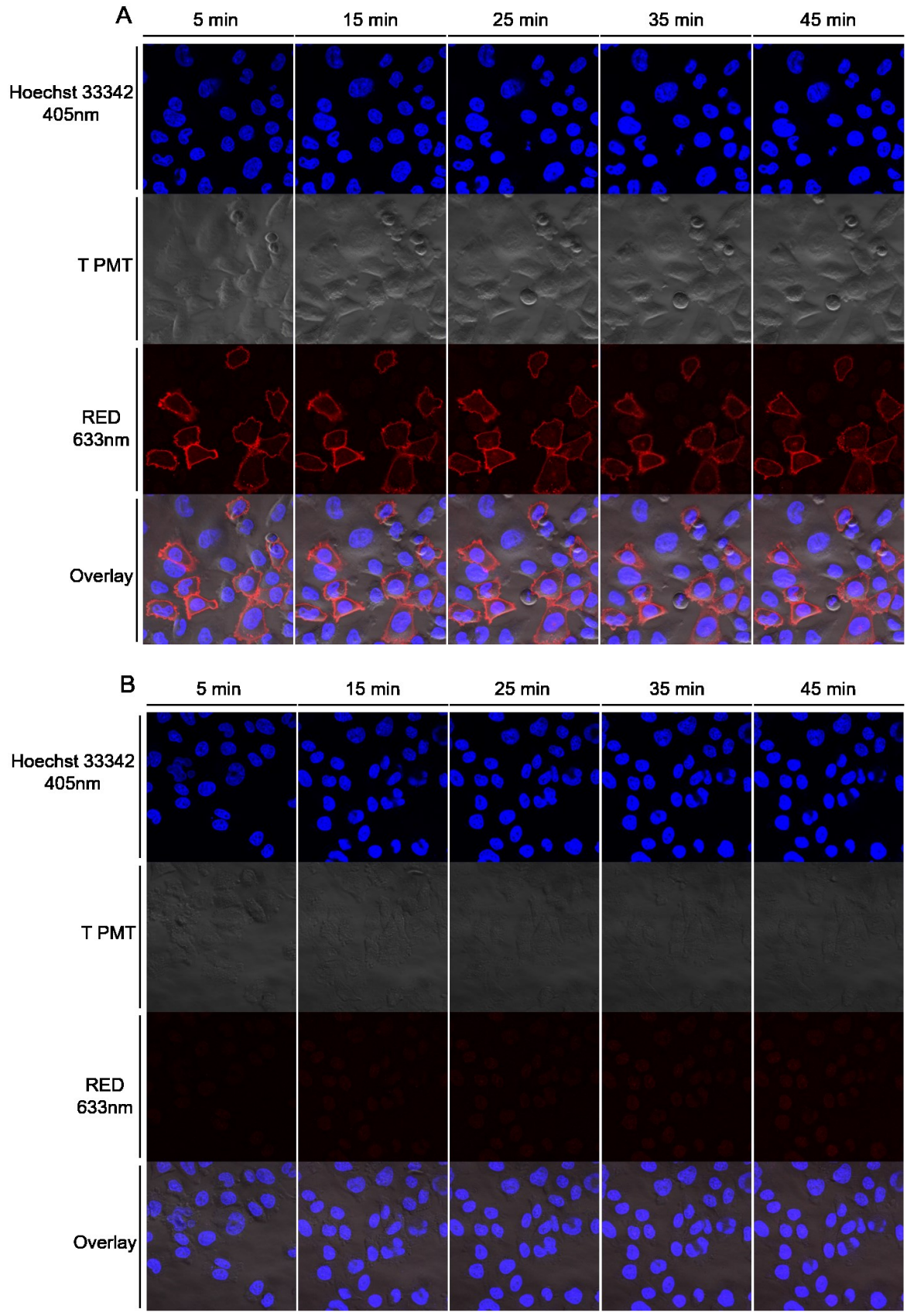

Figure 12. Binding of the fluorescent ligand **62** to CHO-hM_2R cells at 30 °C, visualized by confocal microscopy after 5, 15, 25, 35 and 45 min. (A) Total binding of **62** (30 nM). (B) Unspecific binding of **62** (30 nM) determined in the presence of atropine (10 µM). Images were acquired with a Zeiss LSM 710 confocal microscope. T PMT = transmitted light detector/photomultiplier tube.

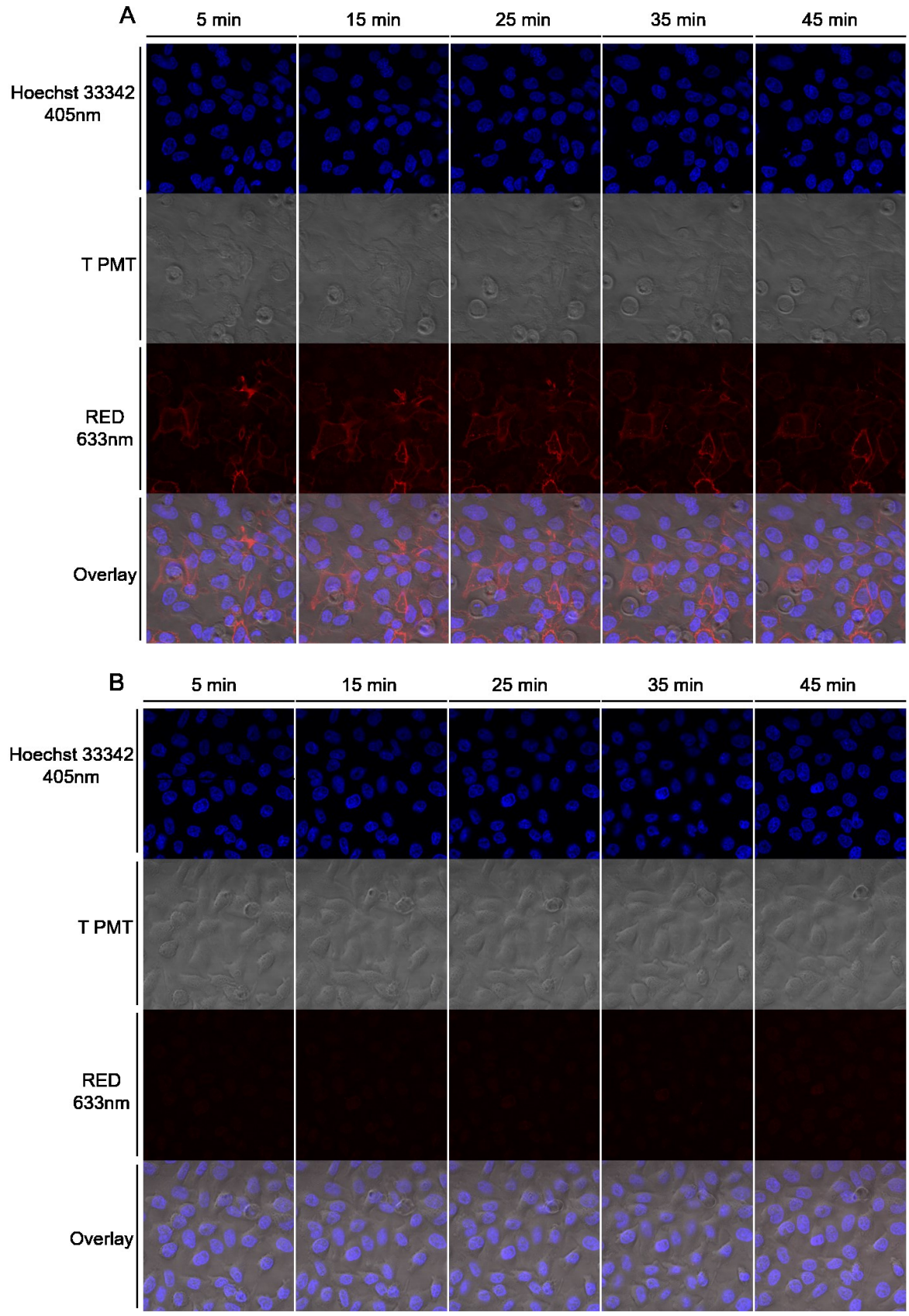

Figure 13. Binding of the fluorescent ligand **64** to CHO-hM_2R cells at 30 °C, visualized by confocal microscopy after 5, 15, 25, 35 and 45 min. (A) Total binding of **64** (30 nM). (B) Unspecific binding of **64** (30 nM) determined in the presence of atropine (10 µM). Images were acquired with a Zeiss LSM 710 confocal microscope. T PMT = transmitted light detector/photomultiplier tube.

3.3. Summary and conclusion

The high-affinity cyanine dye-labeled dibenzodiazepinone-type MR ligands comprising two monomeric (**61** and **62**), two homodimeric (**63** and **64**) and one heterodimeric (**66**) fluorescent ligand are presented. Equilibrium binding studies with [^{3}H]NMS at CHO-hM_2R cells yielded low K_i values (< 1 nM) for **61-64** and **65** (Table 1). Complete MR selectivity profiles, determined for **62** and **64**, revealed a lack of M_2R selectivity towards the M_1 and the M_4 subtype (Table 1). Saturation isotherms of the homodimeric ligand **64** and its monomeric counterpart **62** derived from flow cytometric and high-content imaging M_2R binding experiments gave comparable K_d values (flow cytometry: 4.6 nM (**62**) and 3.2 nM (**64**); high-content imaging analysis: 14 nM (**62**) and 10 nM (**64**)), proving that this type of fluorescent probes represents useful molecular tools suited for such techniques. Competition binding studies with **62** or **64** and reported orthosteric, allosteric and dualsteric MR ligands afforded K_i values, which were in good agreement with literature data (Table 4). In order to unmask a putative dualsteric binding mode of **62** and **64** at the M_2R, Schild-like analyses were performed with the allosteric modulator **8**. The resulting linear “Schild” regressions, showing slopes not different from unity, strongly suggested that both ligands, the monomeric compound **62** and the homodimeric ligand **64**, interact in a competitive manner with **8**, indicating an allosteric interaction of **62** and **64** additional to the occupation of the orthosteric binding site of the M_2R (dualsteric binding mode). Application of **62** and **64** to confocal microscopy showed that both probes were able to label the cell membrane specifically via binding to M_2Rs. In conclusion, this study demonstrated that dibenzodiazepinone-type MR ligands are suited to prepare dualsterically binding, high-affinity fluorescent MR ligands. However, the development of fluorescent MR ligands, which bind selectively to one MR subtype such as the M_2R, requires structural optimizations of the presented type of compounds to be addressed in future studies.

3.4. Experimental section

3.4.1 General experimental conditions

Chemicals and solvents were purchased from commercial suppliers and were used without further purifications unless otherwise specified. Acetonitrile for HPLC (gradient grade) was obtained from Merck (Darmstadt, Germany). *N*-methyl scopolamine (**1**), atropine (**2**), W84 (**8**) and H33342 were purchased from Sigma-Aldrich (Deisenhofen, Germany). Oxotremorine sesquifumarate (**4**) was from MP Biomedicals (Eschwege, Germany) and compound **9** was purchased from Absource Diagnostic (Munich, Germany). The fluorescent dye succinimidyl esters **59** (S 0536) and **60** (S 0586) were obtained from FEW Chemicals (Bitterfeld-Wolfen, Germany). [^{3}H]NMS (specific activity = 80 Ci/mmol) was purchased from American Radiolabeled Chemicals Inc. (St. Louis, MO) via Hartman Analytics GmbH (Braunschweig, Germany). UR-MK331 was kindly provided by Dr. M. Keller (Institute of Pharmacy, University of Regensburg). Xanomeline (**5**) was synthesized according to described procedures.[32] The synthesis of compounds **19** and **30** was reported previously.[20] The synthesis of the homodimeric ligand **31** is described in Chapter 2 and the preparation of **65** is described elsewhere[21]. Millipore water was used throughout for the preparation of buffers and HPLC eluents. Polypropylene reaction vessels (1.5 or 2 mL) with screw cap (Süd-Laborbedarf, Gauting, Germany) were used for the synthesis of the fluorescent ligands (**61**-**64** and **66**) and for the preparation and storage of stock solutions. The chemical stability of **62** and **64** was investigated in a flat-bottom glass tube (40 × 8.2 mm) (Altmann Analytik GmbH, Munich, Germany), which was siliconized before use using Sigmacote (Sigma-Aldrich). High-resolution mass spectrometry (HRMS) analysis was performed on an Agilent 6540 UHD Accurate-Mass Q-TOF LC/MS system (Agilent Technologies, Santa Clara, CA) using an ESI source. Preparative HPLC was performed with a system from Knauer (Berlin, Germany) consisting of two K-1800 pumps and a K-2001 detector. A Kinetex-XB C18 (5 µm, 250 mm × 21 mm; Phenomenex, Aschaffenburg, Germany) was used as stationary phase at a flow rate of 18 mL/min. Mixtures of acetonitrile and 0.1% aq TFA were used as mobile phase. The detection wavelength was set to 220 nm throughout. The solvent of the collected fractions was removed by lyophilization using an Alpha 2-4 LD apparatus (Martin Christ, Osterode am Harz, Germany) equipped with a RZ 6 rotary vane vacuum pump (Vacuubrand, Wertheim, Germany). Analytical HPLC analysis of compounds **61**-**64** and **66** (concentrations between 25 and 50 µM) was performed with a system from Agilent Technologies composed of a 1290 Infinity binary pump equipped with a degasser, a 1290 Infinity autosampler, a 1290 Infinity thermostated column compartment, a 1260 Infinity diode array detector, and a 1260 Infinity fluorescence detector. A Kinetex-XB C18 (2.6 µm, 100 × 3 mm; Phenomenex) served as stationary phase at a flow rate of 0.5 mL/min.

Mixtures of 0.04% aq TFA (A) and acetonitrile (B) were used as mobile phase. The following linear gradient was applied: 0-20 min: A/B 90:10-68:32, 20-22 min: 68:32-5:95, 22-28 min: 5:95. For all analytical HPLC runs the oven temperature was set to 25 °C, the injection volume was 20 µL and detection was performed at 220 nm. The stock solutions (final concentration 1 mM) of fluorescent ligands were prepared in DMSO and were stored at -78 °C.

3.4.2 Chemistry: experimental protocols and analytical data

4-(2-((1E,3E)-5-((E)-3,3-dimethyl-1-(6-oxo-6-((2-(3-(1-(4-(1-(2-oxo-2-(11-oxo-10,11-dihydro-5*H*-dibenzo[*b,e*][1,4]diazepin-5-yl)ethyl)piperidin-4-yl)butyl)-1*H*-imidazol-4-yl)propanamido)ethyl)amino)hexyl)indolin-2-ylidene)penta-1,3-dien-1-yl)-3,3-dimethyl-3*H*-indol-1-ium-1-yl)butane-1-sulfonate bis(hydrotrifluoroacetate) (61) The reaction was carried out in a 1.5-mL polypropylene reaction vessel equipped with a micro stir bar. Compound **30** (7.0 mg, 7.6 µmol) and DIPEA (6.6 mg, 9.0 µL, 51 µmol) were dissolved in anhydrous DMF (50 µL) followed by the addition of **59** (3.6 mg, 5.1 µmol) in anhydrous DMF (50 µL) and stirring was continued at room temperature in the dark for 1 h. 10% aq TFA (100 µL) was added and purification by preparative HPLC (gradient: 0-25 min: 0.1% aq TFA/acetonitrile 85:15-55:45, t_R = 18 min) afforded **61** as a blue fluffy solid (2.4 mg, 1.7 µmol, 34%). HRMS (ESI): m/z $[M+2H]^{2+}$ calcd. for $[C_{67}H_{85}N_9O_7S]^{2+}$ 579.8146, found: 579.8153. RP-HPLC (220 nm): 99% (t_R = 14.5, k = 14.8). $C_{67}H_{83}N_9O_7S \cdot C_4H_2F_6O_4$ (1158.52 + 228.05).

4-(2-((1E,3E)-5-((E)-3,3-dimethyl-1-(6-oxo-6-((2-(3-(1-(4-(1-(2-oxo-2-(11-oxo-10,11-dihydro-5*H*-dibenzo[*b,e*][1,4]diazepin-5-yl)ethyl)piperidin-4-yl)butyl)-1*H*-imidazol-4-yl)propanamido)ethyl)amino)hexyl)-5-sulfoindolin-2-ylidene)penta-1,3-dien-1-yl)-3,3-dimethyl-3*H*-indol-1-ium-1-yl)butane-1-sulfonate bis(hydrotrifluoroacetate) (62) Compound **62** was prepared from amine **30** (3.2 mg, 3.5 µmol) and compound **60** (1.9 mg, 2.3 µmol) according to the procedure for the synthesis of **61**. DIPEA: 3.0 mg, 4.0 µL, 23 µmol. Purification by preparative HPLC (gradient: 0-25 min: 0.1% aq TFA/acetonitrile 85:15-55:45, t_R = 14 min) afforded **62** as a blue fluffy solid (1.4 mg, 0.95 µmol, 41%). HRMS (ESI): m/z $[M+2H]^{2+}$ calcd. for $[C_{67}H_{85}N_9O_{10}S_2]^{2+}$ 619.7930, found: 619.7925. RP-HPLC (220 nm): 98% (t_R = 10.0, k = 9.9) $C_{67}H_{83}N_9O_{10}S_2 \cdot C_4H_2F_6O_4$ (1238.57 + 228.05).

4-(2-((1E,3E)-5-((E)-1-(6-((3,5-bis((2-(3-(1-(4-(1-(2-oxo-2-(11-oxo-10,11-dihydro-5*H*-dibenzo[*b,e*][1,4]diazepin-5-yl)ethyl)piperidin-4-yl)butyl)-1*H*-imidazol-4-yl)propanamido)ethyl)carbamoyl)benzyl)amino)-6-oxohexyl)-3,3-dimethylindolin-2-ylidene)penta-1,3-dien-1-yl)-3,3-dimethyl-3*H*-indol-1-ium-1-yl)butane-1-sulfonate tetrakis(hydrotrifluoroacetate) (63) Compound **63** was prepared from amine **31** (6.0 mg, 4.6 µmol) and compound **59** (2.2 mg, 3.1 µmol) according to the procedure for the synthesis of **61**. DIPEA: 4.0 mg, 5.4 µL, 31 µmol. Purification by preparative HPLC (gradient: 0-25 min: 0.1% aq TFA/acetonitrile 85:15-40:60, t_R = 16 min) afforded **63** as a blue fluffy solid (2.6 mg, 1.1 µmol, 36%). HRMS (ESI): m/z $[M+4H]^{4+}$ calcd. for $[C_{108}H_{133}N_{17}O_{12}S]^{4+}$ 473.0010, found: 473.0005. RP-HPLC (220 nm): 99% (t_R = 13.3, k = 13.5) $C_{108}H_{129}N_{17}O_{12}S \cdot C_8H_4F_{12}O_8$ (1889.39 + 456.09).

4-(2-((1E,3E)-5-((E)-1-(6-((3,5-Bis((2-(3-(1-(4-(1-(2-oxo-2-(11-oxo-10,11-dihydro-5*H*-dibenzo[*b,e*][1,4]diazepin-5-yl)ethyl)piperidin-4-yl)butyl)-1*H*-imidazol-4-yl)propanamido)ethyl)carbamoyl)benzyl)amino)-6-oxohexyl)-3,3-dimethyl-5-sulfoindolin-2-ylidene)penta-1,3-dien-1-yl)-3,3-dimethyl-3*H*-indol-1-ium-1-yl)butane-1-sulfonate tetrakis(hydrotrifluoroacetate) (64) Compound **64** was prepared from amine **31** (6.0 mg, 4.6 µmol) and **60** (7.6 mg, 3.1 µmol) according to the procedure for the synthesis of **61**. DIPEA: 4.0 mg, 5.4 µL, 31 µmol. Purification by preparative HPLC (gradient: 0-25 min: 0.1% aq TFA/acetonitrile 85:15-55:45, t_R = 15 min) afforded **64** as a blue fluffy solid (2.9 mg, 1.2 µmol, 26%). HRMS (ESI): m/z $[M+3H]^{3+}$ calcd. for $[C_{108}H_{132}N_{17}O_{15}S_2]^{3+}$ 656.9843, found: 656.9838. RP-HPLC (220 nm): 99% (t_R = 10.4, k = 10.3) $C_{108}H_{129}N_{17}O_{15}S_2 \cdot C_8H_4F_{12}O_8$ (1969.44 + 456.09).

4-(2-((1E,3E)-5-((E)-3,3-dimethyl-1-(5-((3-((2-(4-(2-oxo-2,3-dihydro-1H-benzo[*d*]imidazol-1-yl)-[1,4'-bipiperidin]-1'-yl)ethyl)carbamoyl)-5-((2-(3-(1-(4-(1-(2-oxo-2-(11-oxo-10,11-dihydro-5*H*-dibenzo[*b,e*][1,4]diazepin-5-yl)ethyl)piperidin-4-yl)butyl)-1*H*-imidazol-4-yl)propanamido)ethyl)carbamoyl)benzyl)amino)pentyl)-5-sulfoindolin-2-ylidene)penta-1,3-dien-1-yl)-3,3-dimethyl-3*H*-indol-1-ium-1-yl)butane-1-sulfonate pentakis(hydrotrifluoroacetate) (66) Compound **66** was prepared from amine **65** (5.0 mg, 4.9 µmol) and **60** (2.6 mg, 3.3 µmol) according to the procedure used for the synthesis of **61**. DIPEA: 4.3 mg, 6.0 µL, 33 µmol. Purification by preparative HPLC (gradient: 0-25 min: 0.1% aq TFA/acetonitrile 85:15-55:45, t_R = 14 min) afforded **66** as a blue fluffy solid (2.3 mg, 1.0 µmol, 34%). HRMS (ESI): m/z $[M+3H]^{3+}$ calcd. for $[C_{93}H_{121}N_{14}O_{12}S_2]^{3+}$ 563.2910, found: 563.2916. RP-HPLC (220 nm): 97% (t_R = 9.4, k = 9.2) $C_{93}H_{118}N_{14}O_{12}S_2 \cdot C_8H_4F_{12}O_8$ (1688.17 + 470.11).

3.4.3 Compound characterization

The identity of the fluorescent ligands **61**-**64** and **66** was determined by HRMS. Their purity was determined by RP-HPLC (220 nm) and was ≥97% throughout (chromatograms shown in the appendix).

3.4.4 Determination of fluorescence quantum yields

The determination of the fluorescence quantum yields of **61**, **62** and **64** in PBS and PBS containing 1% BSA was performed with a Cary Eclipse spectrofluorimeter and a Cary 100 UV/VIS photometer (Varian Inc., Mulgrave, Victoria, Australia) as described previously with minor modifications.[5] All spectra were recorded using acryl cuvettes (10 × 10 mm, Ref. 67.755, Sarstedt, Nümbrecht, Germany). Fluorescence spectra were recorded at the slit adjustments (excitation/emission) 10/5 nm and 10/10 nm. Table 6 provides an overview of the used concentrations of the fluorescent ligands and the applied excitation wavelengths. The concentration of cresyl violet perchlorate in EtOH was 2 µM. Fluorescence spectra of cresyl violet perchlorate were recorded using an excitation wavelength of 575 nm.

Table 6. Concentrations and excitation wavelengths used for the determination of fluorescence quantum yields.

Compound	concentration [µM]		excitation wavelength [nm]	
	PBS	PBS + 1% BSA	PBS	PBS + 1% BSA
61	2.5	2.5	605	610
62	2.5	2.5	604	609
64	2.5	2.5	617	613

3.4.5 Investigation of the chemical stability

The chemical stability of **62** and **64** was investigated in PBS (pH 7.4) at 22 ± 1 °C. The incubation was started by the addition of 10 µL of a 1 mM solution of **62** or **64** to PBS (100 µL) to yield a final concentration of 100 µM. After 0, 24 and 48 h, aliquots (20 µL) were taken and added to 1% aq TFA/acetonitrile (8:2 v/v) (20 µL). The resulting solutions were analyzed by RP-HPLC (analytical HPLC system and conditions see general experimental conditions; t_R: 10.0 min (**62**), 10.4 min (**64**)). To investigate the adsorption of **62** to the siliconized glass tube, the PBS solution containing (residual) **62** was removed from the tube and 0.1% aq TFA/acetonitrile (1:1 v/v) (100 µL) was added. The solution was gently shaken, an aliquote (20 µL) was taken and added to 1% aq TFA (20 µL), and the resulting solution were analyzed by RP-HPLC (referred to as “recovery” in Figure 3).

3.4.6 Cell Culture

CHO-K9 cell lines stably transfected with the DNA of the human M_1-M_5 muscarinic receptors were obtained from the Missouri S&T cDNA Resource Center (Rolla, MO). Cells were cultured in HAM's F12 medium supplemented with fetal calf serum (Biochrom, Berlin, Germany) (10%) and G418 (Biochrom) (750 µg/mL).

3.4.7 [^{3}H]NMS competition binding experiments

Radioligand binding studies with [^{3}H]NMS were performed at 22 ± 1 °C. Leibovitz L-15 medium (Gibco, Life Technologies GmbH, Darmstadt, Germany) supplemented with 1% BSA (Serva, Heidelberg, Germany) (in the following referred to as L15 medium) was used as binding buffer. The effects of the fluorescent ligands **61**-**64** and **66** on the equilibrium binding of [^{3}H]NMS (equilibrium competition binding assay) were determined at intact adherent CHO-hM_xR cells (x = 1-5) in white 96-well plates with clear bottom (Corning Life Sciences, Tewksbury, MA; Corning cat. no. 3610) using the protocol of previously described MR binding studies with [^{3}H]NMS[20] with the following modification: the total volume of L15 medium per well was 200 µL instead of 188 µL, i.e. the cells were covered with L15 medium (160 µL) followed by the addition of L15 medium (20 µL), neat (to determine total binding) or containing atropine or the studied compound 10-fold concentrated, and L15 medium (20 µL) containing the radioligand 10-fold concentrated. The concentration of [^{3}H]NMS was 0.2 nM (M_1, M_2, M_3), 0.1 nM (M_4) or 0.3 nM (M_5) and the incubation time was 3 h throughout. Unspecific binding was determined in the presence of atropine (**2**) (500-fold excess to [^{3}H]NMS).

3.4.8 Flow cytometric saturation binding experiments

Flow cytometric saturation binding studies with **62** and **64** at live CHO-hM_2R cells were performed with a FACSCalibur™ flow cytometer (Becton Dickinson, Heidelberg, Germany), equipped with an argon laser (488 nm) and a red diode laser (635 nm). Cells were seeded in a 175-cm^2 culture flask 5-6 days prior to the experiment. On the day of the experiment, cells were treated with trypsin, suspended in culture medium and centrifuged. The cell pellet was re-suspended in Leibovitz's L15 culture medium (Gibco, Life Technologies, Darmstadt, Germany) supplemented with 1% BSA (in the following referred to as L15 medium). The cell density was adjusted to 1 × 10^6 cells/mL. 490 µL of the cell suspension were added to 1.5 mL reaction vessels (Sarstedt, Nümbrecht, Germany) containing 5 µL of a solution of the fluorescent ligand (100-fold concentrated) in DMSO/H_2O (1:1 v/v) and 5 µL of DMSO/H_2O (1:1 v/v), to determine total binding. For the determination of unspecific binding

(in the presence of atropine (**2**) at 500-fold access to the fluorescent ligand), 490 µL of the cell suspension were added to reaction vessels containing 5 µL of a solution of the fluorescent ligand (100-fold concentrated) in DMSO/H_2O (1:1 v/v) and 5 µL of a solution of atropine (100-fold concentrated) in DMSO/H_2O (1:1 v/v). Compounds **62** and **64** were used at final concentrations of 0.005-50 nM and 0.15-80 nM, respectively. The samples (prepared in duplicate) were incubated at 22 °C under gentle shaking in the dark. Fluorescence signals were recorded in channel FL-4 (excitation: 635 nm, emission: 661 ± 18 nm, gain: 700-800 V). Measurements were stopped after counting of 20,000 gated events.

3.4.9 High-content imaging based saturation and competition binding assay with 62 and 64

One day prior to the experiment, CHO-hM_2R or CHO-hM_1R cells were seeded at 35,000-40,000 cells per well into the central 60 wells of a black/transparent 96-well plate (Grenier 655090). On the day of the experiment the medium was removed by suction, the cells were washed with HBSS containing 0.1 % BSA[33] (in the following referred to as HBSS-BSA) (50 µL), and covered with HBSS-BSA (80 µL) containing the permeable nuclear dye H33342 (2 µg/mL). To determine total binding, HBSS-BSA (10 µL) and HBSS-BSA (10 µL) containing the fluorescent ligand (10-fold concentrated) were added. For the determination of unspecific binding and to study the effect of a compound of interest on M_2R binding of the fluorescent ligand (competition binding assay) HBSS-BSA (10 µL) containing atropine or the 'competitor' (10-fold concentrated) and HBSS-BSA (10 µL) containing the fluorescent ligand (10-fold concentrated) were added. During incubation at room temperature in the dark for 60 min the plates were gently shaken. After incubation, the cells were washed with HBSS-BSA (50 µL) and covered with HBSS-BSA (50 µL) followed by immediate acquisition of the images using the IX Ultra confocal plate reader (Molecular Devices, Sunnyvale CA). The washing procedure was performed within < 3 min. The excitation laser lines of the Ultra plate reader were 405 nm (Hoechst 33342) and 635 nm (Cy5). Two sites/well were measured throughout. The following final concentrations of **62** and **64** were used for saturation binding studies: 0.4-400 nM (**62**, M_1R), 0.4-400 nM (**62**, M_2R), 0.2-100 nM (**64**, M_1R) and 0.2-100 nM (**64**, M_2R). For competition binding experiments at CHO-hM_2R cells, **62** and **64** were applied at final concentrations of 10 nM. Unspecific binding was determined in the presence of atropine (**2**) (in case of saturation binding experiments 500-fold excess to the fluorescent ligand, in case of competition binding experiments at final concentration of 1 µM) in case of competition binding experiments). Saturation binding experiments were performed in triplicate and competition binding assays were performed in duplicate. M_2R saturation binding experiments with **62** and **64** in the presence of various fixed

concentrations of **8** were performed as described above with the following modification: the cells were covered with 70 µL of HBSS-BSA instead of 80 µL to compensate the extra addition of HBSS-BSA (10 µL) containing **8** (10-fold concentrated). The washing step prior to the measurement was performed.

3.4.10 Confocal microscopy

One day prior to the experiment CHO-hM_2R cells seeded in Nunc LabTekTM II chambered coverglasses with 8 chambers (Thermo fisher scientific) (ca. 80000 cells/well). The culture medium was removed, the cells were washed with HBSS-BSA (*cf*. section 3.4.9) (200 µL) and covered with HBSS-BSA (320 µL). HBSS-BSA (40 µL) and HBSS-BSA (40 µL) containing the fluorescent probe (10 fold concentrated) were added for total binding. For unspecific binding HBSS-BSA (40 µL) containing the competing agent atropine (final concentration: 10 µM) and HBSS-BSA (40 µL) containing the fluorescent probe (10 fold concentrated) were added. Images were acquired after an incubation period of 5-45 min with a Zeiss LSM710 confocal laser scanning microscope (Zeiss, Jena, Germany). The objective was 63x magnification with oil (1.4 NA). The excitation laser lines were 405 nm (2.0%) and 633 nm (10%), filter settings were 410-514 nm (Hoechst 33342 channel) and 638-759 nm (Cy5 channel), and the pinhole setting was 44 µm throughout.

3.4.11 Data processing

Retention (capacity) factors *k* were calculated from retention times (t_R) according to k = (t_R−t_0)/t_0 (t_0 = dead time). Raw data from flow cytometric experiments were processed with the aid of the FlowJo software (FlowJo LLC, Ashland, OR) to obtain geometrical mean values of FL-4. Fluorescence images from high content imaging were analyzed using the granularity analysis (2-3-µm-diameter granules; MetaXpress 5.3, Molecular Devices) to obtain fluorescent arbitrary values. For the granularity algorithm, fluorescent intensity thresholds were adapted to maximize the identification of specifically bound fluorescent ligand (without distinguishing membrane from intracellular localization) by referring to total and unspecific binding. Specific binding data from saturation binding experiments (flow cytometry, high content imaging), obtained by subtracting unspecific binding data from total binding data, were plotted against the fluorescent ligand concentration and analyzed by a two-parameter equation describing hyperbolic binding (one site-specific binding, GraphPad Prism) to obtain K_d values. Unspecific binding data from saturation binding experiments were fitted by linear regression. In case of saturation binding experiments in the presence of compound **8**, specific binding data were analyzed by a two-parameter equation

describing hyperbolic binding (one site-specific binding, GraphPad Prism) to obtain K_d and B_{max} values. Additionally, specific binding data were normalized to the B_{max} value, specific binding (%) was plotted against log(concentration **62** or **64**) followed by analysis using a four-parameter logistic fit (log(agonist) vs. response, applied constraints: bottom = 0%, top = 100%; GraphPad Prism). Data for the 'Schild' plot were obtained from the rightward shift (ΔpK_d) of the saturation isotherm and transformation into log(r-1) (where $r = 10^{\Delta pKd}$). Log(r-1) was plotted against log(concentration of **8**) and the data were analyzed by linear regression to obtain the slope and the 'pA_2' value (intercept with the X axis). Total binding data from competition binding experiments (determination of the effect of **61-64** and **66** on the equilibrium binding of [^{3}H]NMS and the effect of various MR ligands on M_2R binding of **62** and **64**) were plotted against log(concentration competitor) and analyzed by a four-parameter logistic equation (log(inhibitor) vs. response-variable slope, GraphPad Prism) followed by normalization (100% = 'top' of the four-parameter logistic fit, 0% = unspecifically bound radioligand or fluorescent ligand determined in the presence of **2**) and analysis of the normalized data by a four-parameter logistic equation. pIC_{50} values were converted to pK_i values according to the Cheng-Prusoff equation[34] used in its logarithmic form. Statistical significance was assessed by a one-sample t-test.

3.5. References

(1) Middleton, R. J.; Kellam, B. Fluorophore-tagged GPCR ligands. *Curr. Opin. Chem. Biol.* **2005,** *9*, 517-525.

(2) Dumont, Y.; Gaudreau, P.; Mazzuferi, M.; Langlois, D.; Chabot, J. G.; Fournier, A.; Simonato, M.; Quirion, R. BODIPY-conjugated neuropeptide Y ligands: new fluorescent tools to tag Y1, Y2, Y4 and Y5 receptor subtypes. *Br. J. Pharmacol.* **2005,** *146*, 1069-1081.

(3) Ziemek, R.; Brennauer, A.; Schneider, E.; Cabrele, C.; Beck-Sickinger, A. G.; Bernhardt, G.; Buschauer, A. Fluorescence- and luminescence-based methods for the determination of affinity and activity of neuropeptide Y2 receptor ligands. *Eur. J. Pharmacol.* **2006,** *551*, 10-18.

(4) Schneider, E.; Keller, M.; Brennauer, A.; Hoefelschweiger, B. K.; Gross, D.; Wolfbeis, O. S.; Bernhardt, G.; Buschauer, A. Synthesis and characterization of the first fluorescent nonpeptide NPY Y1 receptor antagonist. *Chembiochem* **2007,** *8*, 1981-1988.

(5) Keller, M.; Erdmann, D.; Pop, N.; Pluym, N.; Teng, S.; Bernhardt, G.; Buschauer, A. Red-fluorescent argininamide-type NPY Y1 receptor antagonists as pharmacological tools. *Bioorg. Med. Chem.* **2011,** *19*, 2859-2878.

(6) Liu, M.; Richardson, R. R.; Mountford, S. J.; Zhang, L.; Tempone, M. H.; Herzog, H.; Holliday, N. D.; Thompson, P. E. Identification of a Cyanine-Dye Labeled Peptidic Ligand for Y1R and Y4R, Based upon the Neuropeptide Y C-Terminal Analogue, BVD-15. *Bioconjugate Chem.* **2016,** *27*, 2166-2175.

(7) Li, L.; Kracht, J.; Peng, S.; Bernhardt, G.; Buschauer, A. Synthesis and pharmacological activity of fluorescent histamine H1 receptor antagonists related to mepyramine. *Bioorg. Med. Chem. Lett.* **2003,** *13*, 1245-1248.

(8) Li, L.; Kracht, J.; Peng, S.; Bernhardt, G.; Elz, S.; Buschauer, A. Synthesis and pharmacological activity of fluorescent histamine H2 receptor antagonists related to potentidine. *Bioorg. Med. Chem. Lett.* **2003,** *13*, 1717-1720.

(9) Malan, S. F.; van Marle, A.; Menge, W. M.; Zuliani, V.; Hoffman, M.; Timmerman, H.; Leurs, R. Fluorescent ligands for the histamine H2 receptor: synthesis and preliminary characterization. *Bioorg. Med. Chem.* **2004,** *12*, 6495-6503.

(10) Amon, M.; Ligneau, X.; Schwartz, J. C.; Stark, H. Fluorescent non-imidazole histamine H3 receptor ligands with nanomolar affinities. *Bioorg. Med. Chem. Lett.* **2006,** *16*, 1938-1940.

(11) Xie, S. X.; Petrache, G.; Schneider, E.; Ye, Q. Z.; Bernhardt, G.; Seifert, R.; Buschauer, A. Synthesis and pharmacological characterization of novel fluorescent histamine H2-receptor ligands derived from aminopotentidine. *Bioorg. Med. Chem. Lett.* **2006,** *16*, 3886-3890.

(12) Arttamangkul, S.; Alvarez-Maubecin, V.; Thomas, G.; Williams, J. T.; Grandy, D. K. Binding and internalization of fluorescent opioid peptide conjugates in living cells. *Mol. Pharmacol.* **2000,** *58*, 1570-1580.

(13) Balboni, G.; Salvadori, S.; Dal Piaz, A.; Bortolotti, F.; Argazzi, R.; Negri, L.; Lattanzi, R.; Bryant, S. D.; Jinsmaa, Y.; Lazarus, L. H. Highly selective fluorescent analogue of the potent delta-opioid receptor antagonist Dmt-Tic. *J. Med. Chem.* **2004,** *47*, 6541-6546.

(14) Houghten, R. A.; Dooley, C. T.; Appel, J. R. De novo identification of highly active fluorescent kappa opioid ligands from a rhodamine labeled tetrapeptide positional scanning library. *Bioorg. Med. Chem. Lett.* **2004,** *14*, 1947-1951.

(15) Leopoldo, M.; Lacivita, E.; Passafiume, E.; Contino, M.; Colabufo, N. A.; Berardi, F.; Perrone, R. 4-[omega-[4-arylpiperazin-1-yl]alkoxy]phenyl)imidazo[1,2-a]pyridine derivatives: fluorescent high-affinity dopamine D3 receptor ligands as potential probes for receptor visualization. *J. Med. Chem.* **2007,** *50*, 5043-5047.

(16) Keller, M.; Kuhn, K. K.; Einsiedel, J.; Hubner, H.; Biselli, S.; Mollereau, C.; Wifling, D.; Svobodova, J.; Bernhardt, G.; Cabrele, C.; Vanderheyden, P. M.; Gmeiner, P.; Buschauer, A. Mimicking of Arginine by Functionalized N(omega)-Carbamoylated Arginine As a New Broadly Applicable Approach to Labeled Bioactive Peptides: High Affinity Angiotensin, Neuropeptide Y, Neuropeptide FF, and Neurotensin Receptor Ligands As Examples. *J. Med. Chem.* **2016,** *59*, 1925-1945.

(17) Kozma, E.; Jayasekara, P. S.; Squarcialupi, L.; Paoletta, S.; Moro, S.; Federico, S.; Spalluto, G.; Jacobson, K. A. Fluorescent ligands for adenosine receptors. *Bioorg. Med. Chem. Lett.* **2013,** *23*, 26-36.

(18) Tahtaoui, C.; Parrot, I.; Klotz, P.; Guillier, F.; Galzi, J. L.; Hibert, M.; Ilien, B. Fluorescent pirenzepine derivatives as potential bitopic ligands of the human M1 muscarinic receptor. *J. Med. Chem.* **2004,** *47*, 4300-4315.

(19) Daval, S. B.; Valant, C.; Bonnet, D.; Kellenberger, E.; Hibert, M.; Galzi, J. L.; Ilien, B. Fluorescent derivatives of AC-42 to probe bitopic orthosteric/allosteric binding mechanisms on muscarinic M1 receptors. *J. Med. Chem.* **2012,** *55*, 2125-2143.

(20) Keller, M.; Trankle, C.; She, X.; Pegoli, A.; Bernhardt, G.; Buschauer, A.; Read, R. W. M2 Subtype preferring dibenzodiazepinone-type muscarinic receptor ligands: Effect of chemical homo-dimerization on orthosteric (and allosteric?) binding. *Bioorg. Med. Chem.* **2015,** *23*, 3970-3990.

(21) She, X. Synthesis and pharmacological characterization of dibenzodiazepinone-type heterodimeric and fluorescently labeled muscarinic receptor ligands. Doctoral thesis, University of Regensburg, Regensburg, Germany, **2017**.

(22) Mohr, K.; Trankle, C.; Kostenis, E.; Barocelli, E.; De Amici, M.; Holzgrabe, U. Rational design of dualsteric GPCR ligands: quests and promise. *Br. J. Pharmacol.* **2010,** *159*, 997-1008.

(23) Mohr, K.; Schmitz, J.; Schrage, R.; Trankle, C.; Holzgrabe, U. Molecular alliance-from orthosteric and allosteric ligands to dualsteric/bitopic agonists at G protein coupled receptors. *Angew. Chem. Int. Ed.* **2013,** *52*, 508-516.

(24) Liu, M.; Mountford, S. J.; Richardson, R. R.; Groenen, M.; Holliday, N. D.; Thompson, P. E. Optically Pure, Structural, and Fluorescent Analogues of a Dimeric Y4 Receptor Agonist Derived by an Olefin Metathesis Approach. *J. Med. Chem.* **2016,** *59*, 6059-6069.

(25) Dei, S.; Bellucci, C.; Buccioni, M.; Ferraroni, M.; Guandalini, L.; Manetti, D.; Martini, E.; Marucci, G.; Matucci, R.; Nesi, M.; Romanelli, M. N.; Scapecchi, S.; Teodori, E. Synthesis, affinity profile, and functional activity of muscarinic antagonists with a 1-methyl-2-(2,2-alkylaryl-1,3-oxathiolan-5-yl)pyrrolidine structure. *J. Med. Chem.* **2007,** *50*, 1409-1413.

(26) Jakubik, J.; El-Fakahany, E. E.; Dolezal, V. Differences in kinetics of xanomeline binding and selectivity of activation of G proteins at M(1) and M(2) muscarinic acetylcholine receptors. *Mol. Pharmacol.* **2006,** *70*, 656-666.

(27) Christopoulos, A.; Kenakin, T. G protein-coupled receptor allosterism and complexing. *Pharmacol. Rev.* **2002,** *54*, 323-374.

(28) Hulme, E. C.; Trevethick, M. A. Ligand binding assays at equilibrium: validation and interpretation. *Br. J. Pharmacol.* **2010,** *161*, 1219-1237.

(29) Kenakin, T. *A pharmacology primer: theory, applications and methods. 3rd edition*. Elsevier Academic Press: Burlington: **2009**.

(30) Daval, S. B.; Kellenberger, E.; Bonnet, D.; Utard, V.; Galzi, J. L.; Ilien, B. Exploration of the orthosteric/allosteric interface in human M1 muscarinic receptors by bitopic fluorescent ligands. *Mol. Pharmacol.* **2013,** *84*, 71-85.

(31) Mohr, M.; Heller, E.; Ataie, A.; Mohr, K.; Holzgrabe, U. Development of a new type of allosteric modulator of muscarinic receptors: hybrids of the antagonist AF-DX 384 and the hexamethonio derivative W84. *J. Med. Chem.* **2004,** *47*, 3324-3327.

(32) Kane, B. E.; Grant, M. K.; El-Fakahany, E. E.; Ferguson, D. M. Synthesis and evaluation of xanomeline analogs--probing the wash-resistant phenomenon at the M1 muscarinic acetylcholine receptor. *Bioorg. Med. Chem.* **2008,** *16*, 1376-1392.

(33) Kilpatrick, L. E.; Briddon, S. J.; Holliday, N. D. Fluorescence correlation spectroscopy, combined with bimolecular fluorescence complementation, reveals the effects of beta-arrestin complexes and endocytic targeting on the membrane mobility of neuropeptide Y receptors. *Biochim. Biophys. Acta* **2012,** *1823*, 1068-1081.

(34) Cheng, Y.-C.; Prusoff, W. H. Relation between the inhibition constant K1) and the concentration of inhibitor which causes fifty per cent inhibition (I50) of an enzymic reaction. *Biochem. Pharmacol.* **1973,** *22*, 3099-3108.

Chapter 4

Conjugation of dibenzodiazepinone-type muscarinic receptor antagonists to short peptides: a new avenue to highly selective M_2R ligands

4.1. Introduction

Over the last decades, extensive efforts have been made to design molecules, which selectively bind to one of the five muscarinic receptor (MR) subtypes.[1] In fact, due to the high sequence homology of the MRs orthosteric binding site[2], potent and selective therapeutics without side effects, attributed to “MR promiscuity”, are still an unfulfilled need. For instance, antagonism at presynaptic M_2R in the CNS has been suggested as an approach to increase cholinergic function in Alzheimer’s patients.[3-6] However, for that purpose, highly selective M_2R antagonists are required because concomitant blocking of postsynaptic M_1R must be strictly prevented.

As the M_2R exhibits various accessory (allosteric) sites several compounds addressing these less conserved allosteric binding sites have been developed (*cf* Chapter 2);[7-9] however, high-affinity M_2R modulators are still lacking.[10] The dualsteric ligand approach, which means connecting an orthosteric ligand with an allosteric modulator through a linker in order to increase receptor selectivity, has emerged as a promising strategy to design novel MR ligands.[10-16] However, no reports on highly selective (dualsteric) M_2R ligands can be found in the literature to date. Due to their relatively high affinity for the hM_2R, pyridobenzodiazepinone-type (**10**, **67** and **68**) (Figure 1) and dibenzodiazepinone-type (**17**, **19** and **69**) (Figure 1) MR ligands were described[17-19] as preferred scaffolds to develop highly potent and selective M_2R antagonists. For instance, compounds **17**, **19** and **68** exhibit high M_2R affinity with K_i values in the low nanomolar range (≤ 0.8 nM), but a poor selectivity towards the other receptor subtypes (especially the M_1R and M_4R) (Figure 1). Worth mentioning, compounds **10**, **19** and **68** were suggested to interact with both, the orthosteric and an allosteric binding site.[20, 21] Over the past decades, only a few new chemical scaffolds were described as candidates for designing selective M_2R antagonists. Piperidinyl-piperazine derivative **70**, for instance, exhibits high M_2R affinity (K_i = 0.1 nM) and a remarkable M_2R/M_1R selectivity (330-fold) (Figure 1). Nevertheless, the M_2R/M_4R selectivity was still unsatisfactory (12-fold). Indene-derivative **71** (Figure 1), which was designed based on the structure of the H_1R-antagonist dimethindene, exhibits moderate M_2R affinity and no selectivity at all (Figure 1).

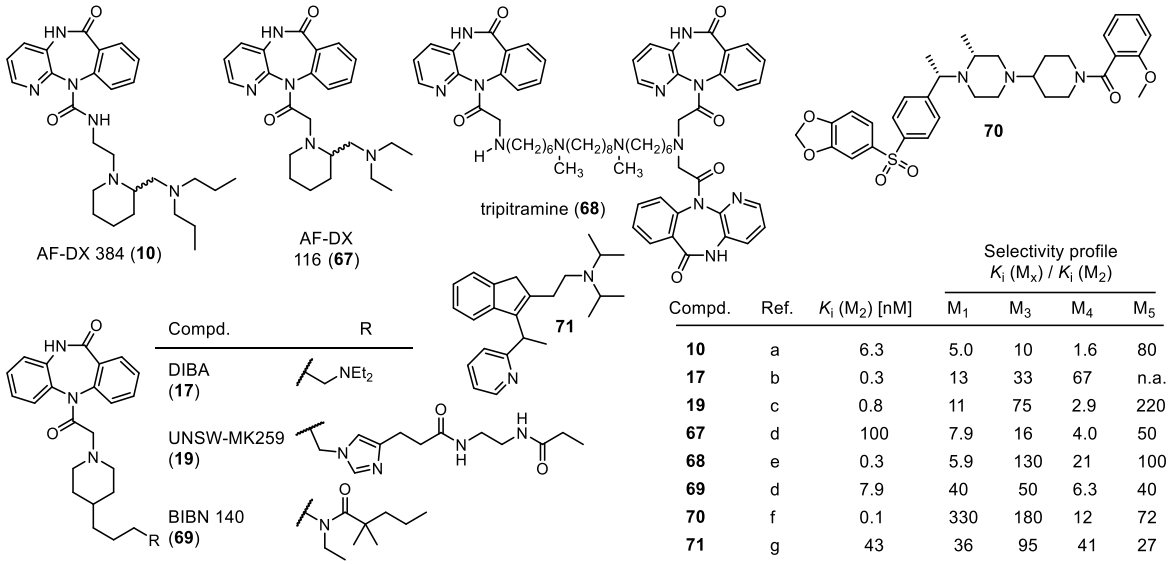

Compd.	Ref.	K_i (M_2) [nM]	Selectivity profile K_i (M_x) / K_i (M_2)			
			M_1	M_3	M_4	M_5
10	a	6.3	5.0	10	1.6	80
17	b	0.3	13	33	67	n.a.
19	c	0.8	11	75	2.9	220
67	d	100	7.9	16	4.0	50
68	e	0.3	5.9	130	21	100
69	d	7.9	40	50	6.3	40
70	f	0.1	330	180	12	72
71	g	43	36	95	41	27

Figure 1. Structure and selectivity profile of a selection of (selective) M_2R antagonist described in literature. n.a.: no data available. References: (a) Dörje *et al.*[22] (b) Gitler *et al.*[17] (c) Keller *et al.*[23] (d) Doods *et al.*[24] (e) Maggio et al.[25] (f) McCombie et al.[26] (g) Boehme et al.[27]

Recently, a series of high-affinity, M_2 subtype-preferring (weakly selective) MR antagonists derived from the dibenzodiazepinone **17**, including compound **19** and two homodimeric analogs, was reported.[23] Aiming at a better understanding of the binding mode of such dibenzodiazepinone-type MR ligands, the tritiated form of **19** and of the homodimeric congener of **19** (**33**, *cf*. Chapter 2) were synthesized ([^{3}H]**19**, [^{3}H]**33**) and pharmacologically characterized (*cf.* Chapter 2). Compounds **19** and **33** were shown to interact dualsterically with the hM_2R (*cf.* Chapter 2). Prompted by these studies, as well as by the fact that conjugation of dibenzodiazepinone-type MR ligands to fluorescent dyes was well tolerated with respect to M_2R binding, the dibenzodiazepinone pharmacophore as in **17** was linked to di- or tripeptides in order to obtain dualsteric ligands (in the following referred to as DIBA-peptide conjugates) with improved M_2R selectivity. Two different linkers, which chemical structures were design based on docking simulation and literature reported M_2R models, were used to connect the DIBA pharmacophore with short peptides (Figure 2).

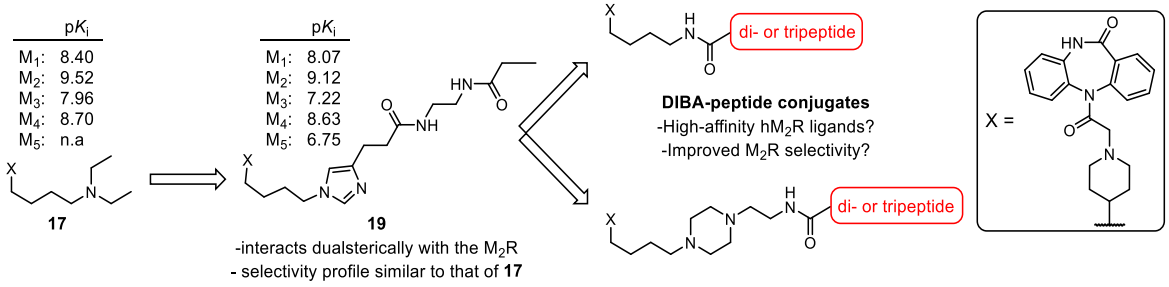

Figure 2. Schematic presentation of the aim of the present chapter. n.a: no data available.

4.2. Results and discussion

4.2.1 Chemistry

Two amino-functionalized dibenzodiazepinone scaffolds, bearing a linear aliphatic linker (**83**)[19] or a linker additionally containing a basic piperazine moiety (**84**)[28] were conjugated to short peptides which design was based on docking simulation experiments (data not shown) and on the M_2R structures available in the literature. The peptide synthesis (compounds **72-82**) was carried out manually on a 2-ClTrt resin according to the Fmoc strategy following a reported protocol ("double" coupling procedure with HBTU/HOBt/DIPEA) (Scheme 1).[29] Prior to the cleavage from the resin the N-terminus of all the peptides was *N*-acetylated by treatment with acetic anhydride to facilitate the coupling of the peptides to the DIBA-derived amine precursors and to prevent a protonation of the N-terminus under assay conditions. After cleavage from the resin, the C-terminus of the peptides was amidated by amine **83** or **84** in order to obtain the protected DIBA-peptide conjugates. Cleavage of the protecting groups using TFA yielded compounds **87**-**108** (Scheme 1). Moreover, propionylation of amine **83** using succinimidyl propionate (**32**) afforded the reference compound **85** (Scheme 1).

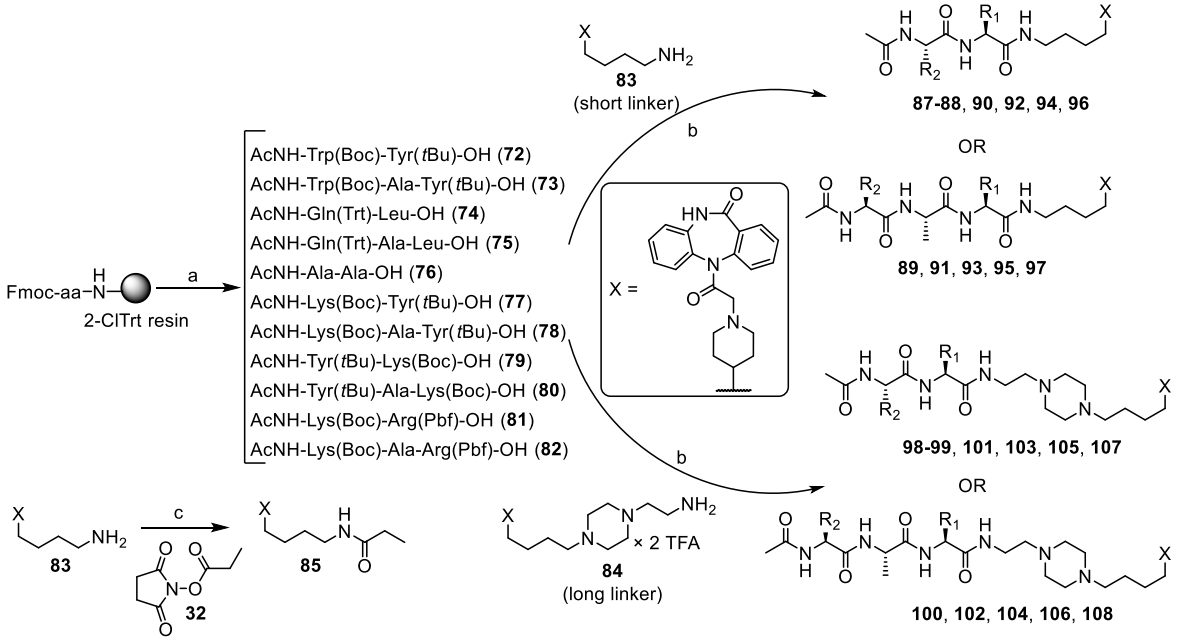

The structures of DIBA-peptides conjugates **87-108** are depicted in Table 1

Scheme 1 Schematic presentation of the synthesis of the DIBA-peptide conjugates. Reagents and conditions: (a) (1) peptide elongation by SPPS (Fmoc strategy), Fmoc-aa/HBTU/HOBt/DIPEA (5/5/5/10 equiv.), solvent DMF/NMP (8:2, v/v), "double" coupling at rt, 60 min. Fmoc deprotection was carried out with 20% piperidine in DMF/NMP (8:2, v/v), rt, 2 × 10 min; (2) acetic anhydride, DIPEA, rt, 30 min; (3) CH_2Cl_2/HFIP (3:1, v/v), rt, 2 × 20 min, 47-98%; (b) (1) EDC × HCl (added to a stirred mixture of the respective peptide, **83** or **84** and HOBt in DMF), HOBt, DMF, 5 °C, 2 h, in case of **84** (provided as tris(hydrotrifluoroacetate) DIPEA (2 equiv.) was added; (2) TFA/CH_2Cl_2/H_2O (1:1:0.1, v/v/v) or with TFA/H_2O (95:5, v/v), rt, 3 h, 27-75%; (c) DIPEA, DMF, rt, 1 h, 99%.

The conditions used for amide coupling between the amines **83** or **84** and the side-chain protected peptides (**72-82**) were crucial with regard to the retention of the stereochemistry at Cα of the C-terminal amino acid of the peptides. For example, when amine **83** was coupled with tripeptide **82** applying a preactivation step of **82** with HBTU/HOBt in the presence of DIPEA for 10 min, a diastereomeric mixture of the product was obtained (Figure 3A). The epimerization at Cα occurs due to the intramolecular cyclization of the activated C-terminal α-amino acid affording a 5(4*H*)-oxazolone[30] which, under basic conditions, undergoes a keto-enol tautomerism provoking the formation of the epimerized product (*S,S,R*)-**86** (Figure 3A). The formation of two diastereomers was confirmed by RP-HPLC (Figure 3B). By contrast, when EDC × HCl/HOBt was used as coupling reagent (without the preactivation of **82**) and no base was added, the reaction led to the formation of the enantiomerically pure product (*S,S,S*)-**86** (Figure 3A and Figure 3C).

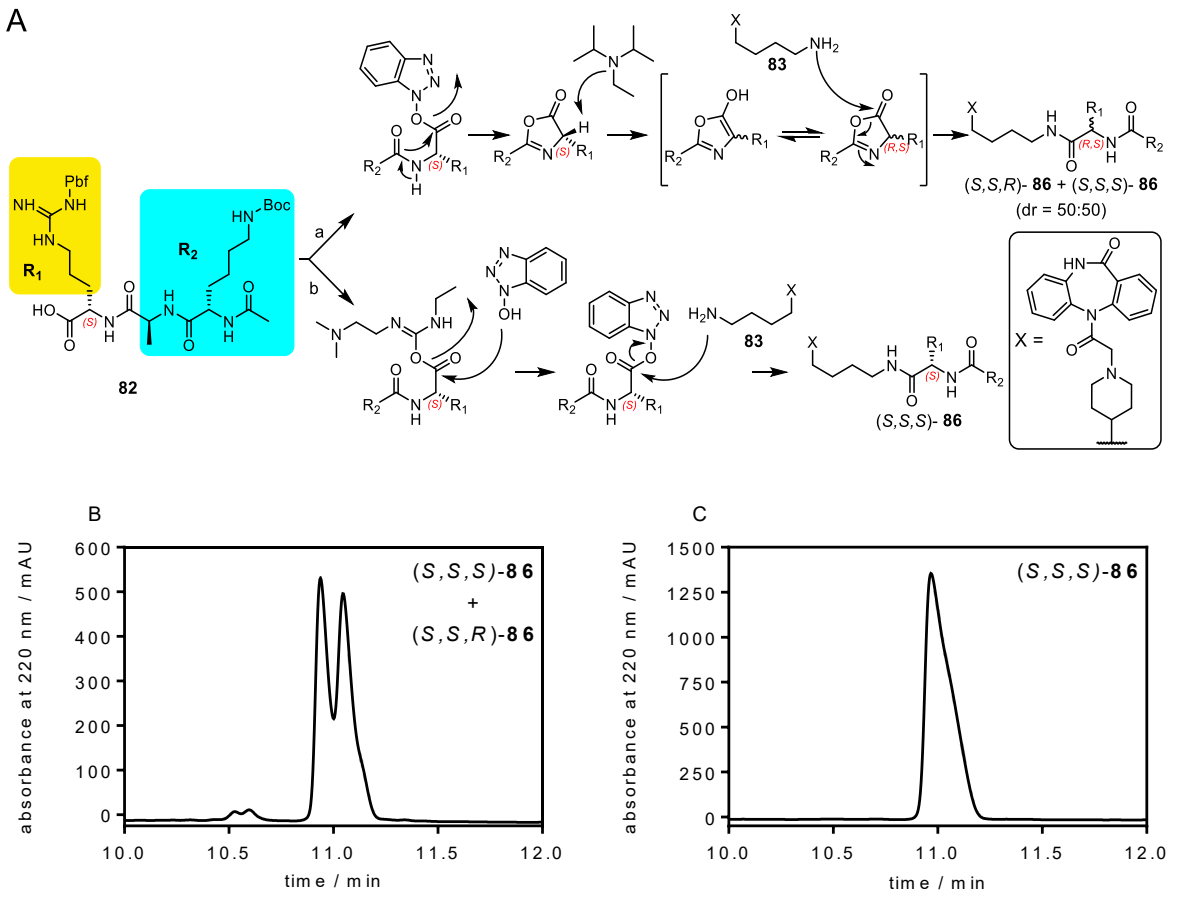

Figure 3. (A) Coupling of peptide **82** to amine **83** using different conditions. (a) HBTU, (added to a mixture of **82**, DIPEA and HOBt in DMF. The resulting mixture was stirred at rt for 10 min before the addition of amine **83**) DMF, rt, 3 h; (b) EDC × HCl, HOBt, DMF, 5 °C, 3 h. Amine **83** was immediately added to the reaction mixture (no preactivation step was applied, see experimental section); (C/D) RP-HPLC analysis (conditions see experimental section) of the reaction mixtures of the coupling reactions presented under (A).

An overview of the chemical structure of all DIBA-peptide conjugates is given in Table 1 together with the RP-HPLC purities after purification by preparative HPLC.

Table 1. Structures and RP-HPLC purities of the DIBA-peptide conjugates **87-108**.

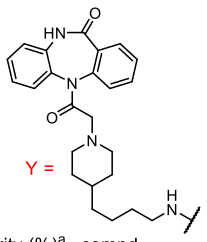

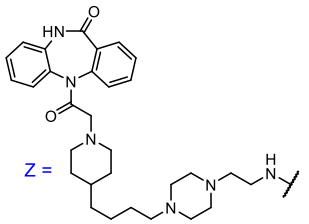

compd.	structure	purity (%)[a]	compd.	structure	purity (%)[a]	compd.	structure	purity (%)[a]	compd.	structure	purity (%)[a]
87	× 1 TFA	96%	**93**	× 2 TFA	97%	**98**	× 3 TFA	95%	**104**	× 4 TFA	95%
88	× 1 TFA	96%	**94**	× 2 TFA	99%	**99**	× 3 TFA	97%	**105**	× 4 TFA	98%
89	× 1 TFA	98%	**95**	× 2 TFA	99%	**100**	× 3 TFA	99%	**106**	× 4 TFA	98%
90	× 1 TFA	95%	**96**	× 3 TFA	99%	**101**	× 3 TFA	97%	**107**	× 5 TFA	98%
91	× 1 TFA	95%	**97**	× 3 TFA	99%	**102**	× 3 TFA	96%	**108**	× 5 TFA	98%
92	× 2 TFA	99%				**103**	× 4 TFA	97%			

[a]Purities determined by analytical RP-HPLC (λ = 220 nm).

4.2.2 Equilibrium competition binding at hM_1-hM_5R.

The M_1-M_5 receptor affinities of the DIBA-peptide conjugates (**87**-**108**) and reference compound **85** were determined by radioligand equilibrium competition binding using stably transfected CHO-cells and the orthosteric MR antagonist [^{3}H]NMS as radioligand. As the dibenzodiazepinone-type MR ligands **19** (monomeric derivative) and **33** (homodimeric ligand) were shown to interact simultaneously with the orthosteric and with the allosteric binding site of the hM_2R (*cf.* Chapter 2), the DIBA-peptide derivatives presented in this chapter were anticipated to bind to the orthosteric site of MRs via the dibenzodiazepinone pharmacophore, being competitive with [^{3}H]NMS. The peptide moieties potentially interact with an allosteric site of the receptor. Therefore, data from equilibrium competition binding with [^{3}H]NMS were analyzed by four-parameter logistic curve fitting and pIC_{50} values were converted to pK_i values. An overview of the MR binding data of **85** and **87**-**108** together with their MR selectivity profile is provided in Table 2. The subset of compounds bearing a short linker (**85**, **87**-**97**) exhibited lower affinities at all MR subtypes (M_1-M_5) compared to the subset of derivatives containing the longer linker with a basic piperazine moiety (Figure 4 and Figure 5, Table 2). Compounds **90** and **91**, both containing a leucine and a glutamine in their structure (*cf*. Table 1), displayed the lowest affinity at the five MR subtypes (Figure 4, Table 2). Interestingly, compound **85**, containing a propionyl residue instead of the peptide moiety (*cf*.Table 1), and compound **87** ("Ala-Ala-DIBA"), which has only methyl groups as amino acid side chains, showed an increased affinity at M_1-M_4 receptors compared to the leucine/glutamine-containing derivatives **90** and **91**. Within the "short-linker" subset of DIBA-peptide derivatives, the range of pK_i values determined for M_2R binding was 6.4-9.0 (Table 2). Compounds containing one or two basic amino acids (**92**, **93**, **95-97**) exhibited the highest M_2R affinities, which was in agreement with previous reports about the importance of basic moieties for ligand binding at the M_2R.[7, 31, 32] By contrast, all "long-linker" DIBA-peptide conjugates exhibited high M_2R affinities (pK_i = 9.42-10.21, Table 2). In case of the subtypes M_1 and M_3-M_5 the situation was similar: whereas the pK_i values of the compounds of the "short-linker" series (**87-97**) varied by approx. two orders of magnitude, pK_i values obtained for the derivatives of the "long-linker" series (**98-108**) varied only by approx. one order of magnitude (Figure 4, Figure 5 and Figure 6; Table 2). The DIBA-peptide derivative with the lowest pronounced M_2R selectivity was evident in the "short-linker" compound subset (**91**, K_i M_1R:M_2R:M_3R:M_4R:M_5R = 1.4:1:44:1.9:2.1, Table 2). The "short-linker" derivative **96** and the "long linker" derivative **108**, containing the peptide sequences Lys-Arg and Lys-Ala-Arg, respectively, exhibited the most pronounced M_2R selectivities (**96**, K_i M_1R:M_2R:M_3R:M_4R:M_5R = 58:1:6900:99:300; **108**, K_i M_1R:M_2R:M_3R:M_4R:M_5R = 49:1:1800:70:3500; Table 2, Figure 6 and Figure 7). As described previously for dibenzodiazepinone- and pyridobenzodiazepinone-type MR ligands[17, 19, 22, 24-27] (for structures *cf*.Figure 1), the M_2 selectivity towards the M_1 subtype was the lowest compared to M_2/M_3-M_5 selectivities. Compounds **96** and **108** showed the highest M_2R affinities within the respective compound subset with pK_i values of 9.00 and 10.21, respectively (Table 1). As both DIBA-peptide

conjugates contain two basic amino acids (Lys and Arg), these results demonstrate that positively charged residues are advantageous for M_2R binding, which is consistent with reports on orthosteric and allosteric M_2R ligands.[7, 31, 32] Notably, the DIBA-peptide conjugates of the "long-linker" subset showed a considerably more pronounced M_2/M_5 receptor selectivity compared to the "short-linker" derivatives (Table 2, Figure 6). The reference compound **85** showed no M_2/M_1 selectivity and only a very low M_2/M_4 selectivity, indicating that the considerable gain in M_2R selectivity as found for **96** and **108** is mediated by the peptide structure. Worth mentioning, compound **97**, which is structurally closely related to **96** (Lys-Ala-Arg *vs*. Lys-Arg; *cf*. Table 1), showed, compared to **96**, a decreased M_2R affinity (pK_i 8.11 *vs*. 9.00, Figure 4B and Table 2) and an impaired selectivity profile (K_i M_1R:M_2R:M_3R:M_4R:M_5R = 11:1:350:15:39) (Table 2). To the best knowledge of the author, compounds **96** and **108** represent the most selective M_2R ligands with K_i values in the low nanomolar and the picomolar range, respectively, which were described to date[33] and represent excellent candidates for the development of highly selective M_2R ligands.

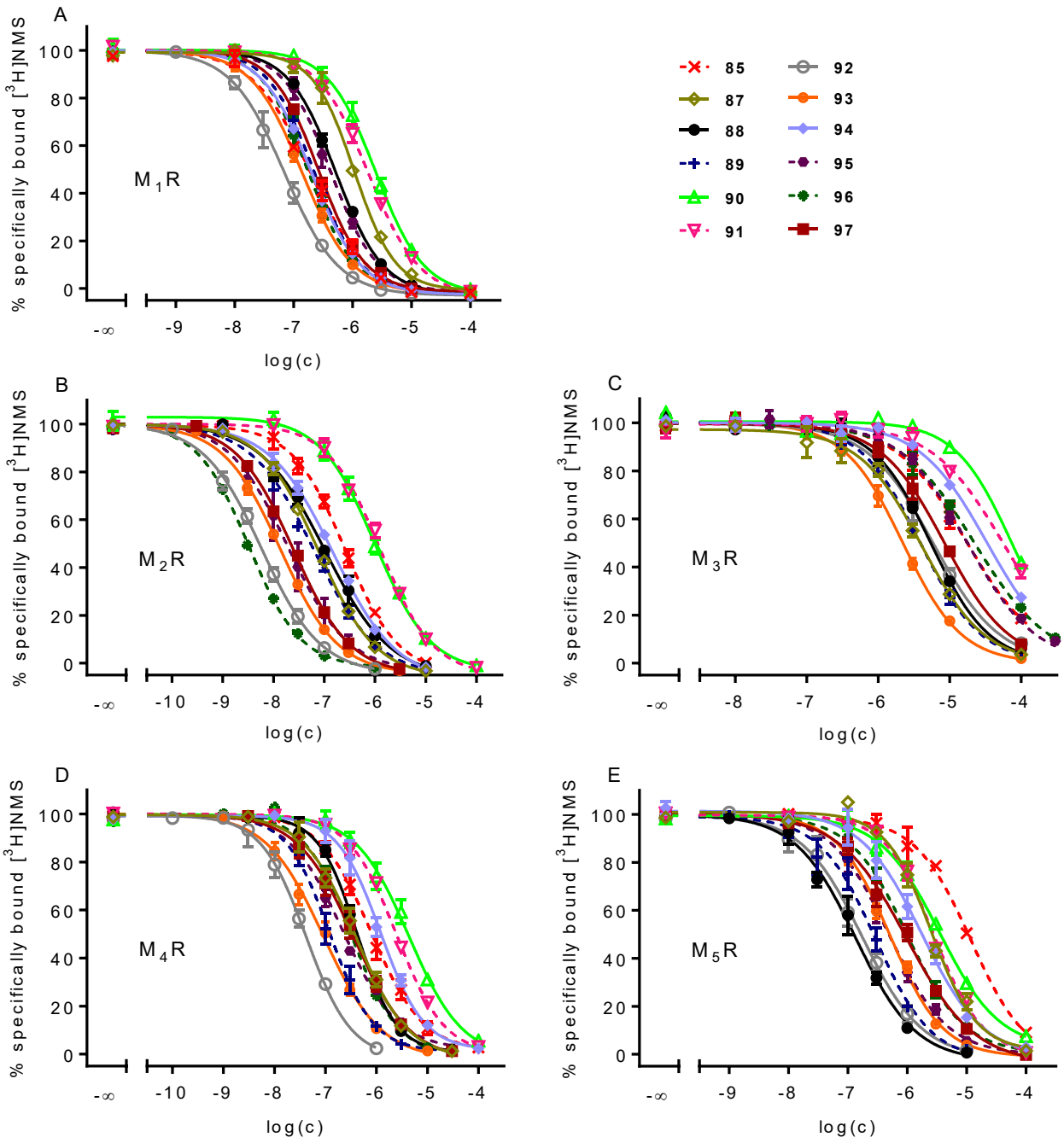

Figure 4. Concentration-dependent effects of the dibenzodiazepinone-type MR ligands containing the "short" tetramethylene linker (**85**, **87-97**) on M_xR equilibrium binding of [^{3}H]NMS (x = 1-5), determined at live CHO-hM_1 (A), CHO-hM_2 (B), CHO-hM_3 (C), CHO-hM_4 (D) and CHO-hM_5 (E). Data were analyzed by four-parameter logistic fits. Mean values ± SEM from at least three independent experiments (performed in triplicate).

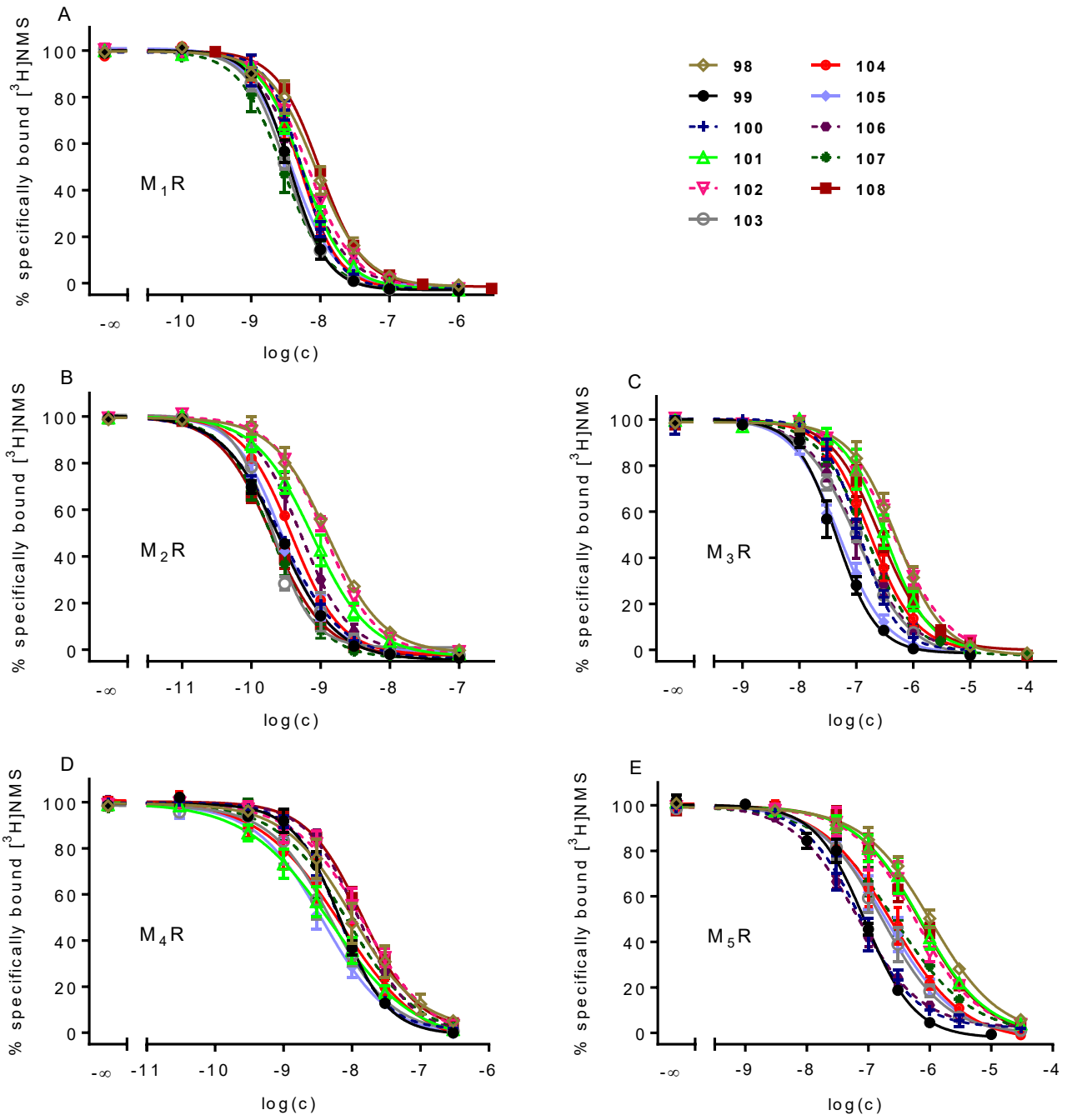

Figure 5. Concentration-dependent effects of the dibenzodiazepinone-type MR ligands containing the "long" piperazinyl linker (**98-108**) on M_xR equilibrium binding of [^{3}H]NMS (x = 1-5) determined at live CHO-hM_1 (A), CHO-hM_2 (B), CHO-hM_3 (C), CHO-hM_4 (D) and CHO-hM_5 (E). Data were analyzed by four-parameter logistic fits. Mean values ± SEM from at least three independent experiments (performed in triplicate).

Table 2. M_1-M_5 receptor affinities of the DIBA-peptide conjugates (**87-108**) and compound **85** obtained from equilibrium competition binding studies with [^{3}H]NMS.

compd.	linker	amino acids sequence	M_1R	M_2R	M_3R	M_4R	M_5R	selectivity toward M_2R (K_i (M_xR)/K_i (M_2R))			
			pK_i	pK_i	pK_i	pK_i	pK_i	M_1R	M_3R	M_4R	M_5R
85	short	/	7.14 ± 0.05	7.10 ± 0.05	5.30 ± 0.08	6.64 ± 0.08	5.14 ± 0.14	0.8	70	3.2	69
87	short	Ala-Ala	6.45 ± 0.03	7.62 ± 0.01	5.90 ± 0.03	6.96 ± 0.09	5.86 ± 0.11	13	58	5.2	42
88	short	Trp-Tyr	6.72 ± 0.04	7.48 ± 0.11	5.84 ± 0.04	6.93 ± 0.05	7.23 ± 0.12	4.6	45	3.6	1.2
89	short	Trp-Ala-Tyr	7.10 ± 0.06	7.70 ± 0.05	5.98 ± 0.04	7.39 ± 0.11	6.91 ± 0.09	3.4	57	2.3	4.4
90	short	Gln-Leu	6.05 ± 0.07	6.51 ± 0.02	4.67 ± 0.03	5.93 ± 0.08	5.81 ± 0.04	2.5	74	4.3	3.4
91	short	Gln-Ala-Leu	6.17 ± 0.03	6.40 ± 0.05	4.80 ± 0.06	6.15 ± 0.02	5.91 ± 0.04	1.4	44	1.9	2.1
92	short	Lys-Tyr	7.70 ± 0.12	8.74 ± 0.08	5.82 ± 0.09	7.93 ± 0.08	7.12 ± 0.12	10	720	7.0	3
93	short	Lys-Ala-Tyr	7.30 ± 0.05	8.37 ± 0.02	6.21 ± 0.05	7.59 ± 0.10	6.64 ± 0.05	10	160	6.9	37
94	short	Tyr-Lys	7.13 ± 0.01	7.33 ± 0.04	5.03 ± 0.01	6.48 ± 0.08	6.14 ± 0.02	1.3	220	7.8	11
95	short	Tyr-Ala-Lys	6.82 ± 0.08	8.03 ± 0.10	5.34 ± 0.05	7.20 ± 0.05	6.67 ± 0.09	14	530	7.1	16
96	short	Lys-Arg	7.17 ± 0.07	9.00 ± 0.02	5.21 ± 0.06	7.04 ± 0.03	6.37 ± 0.07	**58**	**6900**	**99**	**300**
97	short	Lys-Ala-Arg	7.01 ± 0.03	8.11 ± 0.02	5.60 ± 0.06	7.01 ± 0.11	6.37 ± 0.08	11	350	15	39
98	long	Ala-Ala	8.52 ± 0.08	9.42 ± 0.04	6.84 ± 0.09	8.52 ± 0.17	6.33 ± 0.07	6.9	420	10	880
99	long	Trp-Tyr	8.86 ± 0.05	10.10 ± 0.03	7.90 ± 0.09	8.73 ± 0.06	7.40 ± 0.04	15	180	26	350
100	long	Trp-Ala-Tyr	8.71 ± 0.05	10.06 ± 0.03	7.49 ± 0.06	8.75 ± 0.04	7.50 ± 0.10	19	420	22	270
101	long	Gln-Leu	8.69 ± 0.04	9.62 ± 0.10	7.24 ± 0.13	8.88 ± 0.15	6.52 ± 0.13	7.0	270	6.5	920
102	long	Gln-Ala-Leu	8.60 ± 0.07	9.45 ± 0.05	6.85 ± 0.09	8.30 ± 0.11	6.61 ± 0.10	6.1	450	16	500
103	long	Lys-Tyr	8.92 ± 0.02	10.08 ± 0.20	7.59 ± 0.01	8.91 ± 0.16	7.14 ± 0.15	10	270	15	550
104	long	Lys-Ala-Tyr	8.73 ± 0.08	9.93 ± 0.01	7.38 ± 0.07	8.76 ± 0.18	7.01 ± 0.14	14	390	19	630
105	long	Tyr-Lys	8.74 ± 0.17	10.12 ± 0.03	7.82 ± 0.06	8.99 ± 0.12	6.84 ± 0.05	24	220	16	1300
106	long	Tyr-Ala-Lys	8.70 ± 0.10	9.94 ± 0.02	7.58 ± 0.13	8.45 ± 0.03	7.49 ± 0.07	16	290	34	200
107	long	Lys-Arg	8.98 ± 0.10	10.21 ± 0.06	7.34 ± 0.06	8.65 ± 0.17	6.94 ± 0.11	15	800	44	1300
108	long	Lys-Ala-Arg	8.45 ± 0.03	10.21 ± 0.06	6.99 ± 0.07	8.40 ± 0.05	6.52 ± 0.09	**49**	**1800**	**70**	**3500**

Presented are mean values ± SEM from 3-9 independent experiments (each performed in triplicate). K_d values[19] / applied concentrations of [^{3}H]NMS: M_1: 0.12 / 0.2 nM; M_2: 0.090 / 0.2 nM; M_3: 0.089 / 0.2 nM; M_4: 0.040 / 0.1 nM; M_5: 0.24 / 0.3 nM.

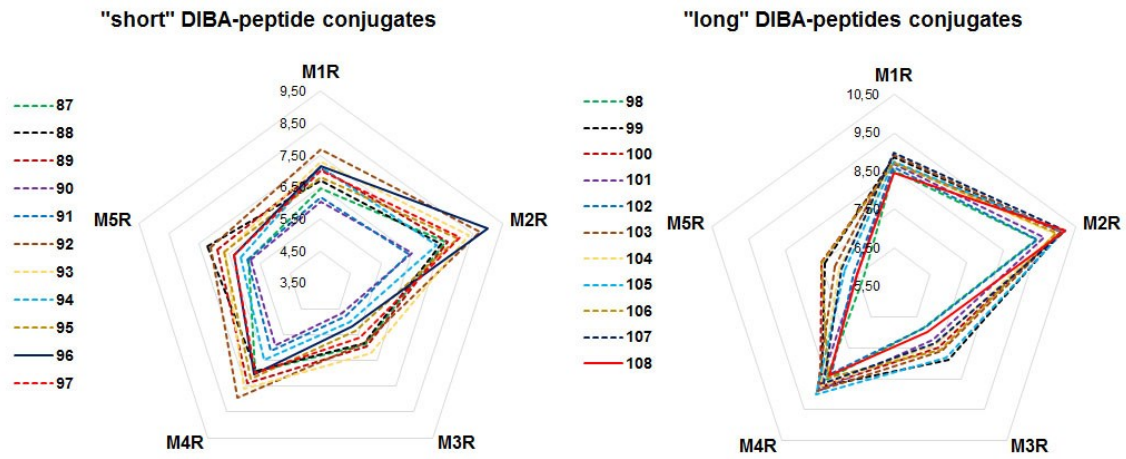

Figure 6. "Radar" charts presenting M_1R-M_5R affinities of reference compound **85** and dibenzodiazepinone derivatives **87**-**97** (DIBA-peptide conjugates containing the short linker) (A), as well as compounds **98**-**108** (DIBA-peptide conjugates containing the long linker) (B). Each vertex of the chart represents a MR subtype (M_1-M_5) plotted against pK_i values (increasing from the center towards the outside). Solid lines indicate the most selective derivatives (**96** in A and **108** in B).

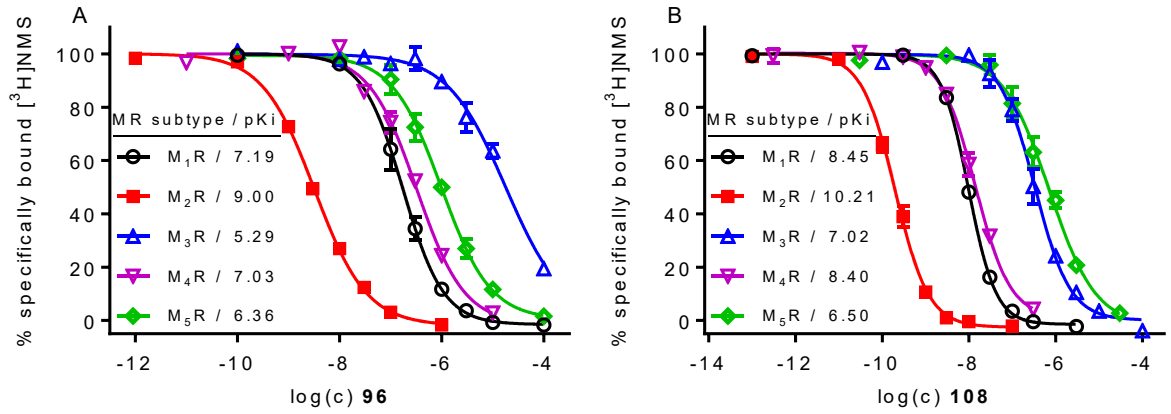

Figure 7. MR selectivity profile of **96** (A) and **108** (B) demonstrated by [^{3}H]NMS displacement curves at MR subtypes M_1-M_5 (extracted from Figure 4A-E and Figure 5A-E, respectively).

4.3. Conclusion

Linkage of two amino-functionalized dibenzodiazepinone-type MR ligands (**83** and **84**, Scheme 1), derived from the M_2R-preferring MR antagonist DIBA (**17**), to di- and tripeptides yielded a series of DIBA-peptide conjugates (22 compounds), comprising two compound subsets according to the type of linker (short/non-basic *vs*. long/basic). M_1-M_5 receptor binding data were determined by equilibrium competition binding with [^{3}H]NMS using intact CHO-hM_xR cells (x = 1-5). For both subsets of DIBA-peptide conjugates, the compound with the highest M_2R affinity exhibited the highest M_2R selectivity, too ("short-linker" subset: **96**, pK_i = 9.00, K_i M_1R:M_2R:M_3R:M_4R:M_5R = 58:1:6900:99:300; "long-linker" subset: **108**, pK_i = 10.21, K_i M_1R:M_2R:M_3R:M_4R:M_5R = 49:1:1800:70:3500). Noteworthily, both hits, **96** and **108**, contained two basic amino acids (Lys, Arg), indicating the importance of polar and positively charged moieties for M_2R binding and selectivity. Compounds **96** and **108**, due to their high M_2R affinity and good selectivity, are considered valuable leads to develop high-affinity and highly selective M_2R antagonists. Both compounds represent the most selective M_2R antagonists described to date with a K_i in the low nanomolar range (**96**) or in the picomolar range (**108**). Investigations on the M_2R binding mode of compounds such as **96** and **108**, supposed to be dualsteric, will be subject of future studies. For that purpose docking studies and MD simulations based on the reported crystal structures of MR receptors, as well as various binding studies involving different radioligands, allosteric modulators and receptor mutants are envisaged.

4.4. Experimental section

4.4.1 General experimental conditions

Chemicals and solvents were purchased from commercial suppliers and were used without further purifications unless otherwise specified. HOBt hydrate, DMF (for peptide synthesis) and NMP (for peptide synthesis) were obtained from Acros Organics/Fischer Scientific (Nidderau, Germany). Dichloromethane (CH_2Cl_2), DIPEA, *N*-(3-Dimethylaminopropyl)-*N*′-ethylcarbodiimide hydrochloride (EDC × HCl), 1,1,1,3,3,3-hexafluoro-2-propanol (HFIP) and trifluoroacetic acid (TFA), were from Sigma-Aldrich (Deisenhofen, Germany). HBTU and piperidine were from Iris Biotech (Marktredwitz, Germany). Acetonitrile for HPLC (gradient grade) was purchased from Merck (Darmstadt, Germany) and [^{3}H]NMS (specific activity = 80 Ci/mmol) was purchased from American Radiolabeled Chemicals Inc. (St. Louis, MO) via Hartman Analytics GmbH (Braunschweig, Germany). Millipore water was used throughout for the preparation of buffers and HPLC eluents. Polypropylene reaction vessels (1.5 or 2 mL) with screw cap (Süd-Laborbedarf, Gauting, Germany) were used for small scale reactions and for the preparation and storage of stock solutions. Temperature-controlled reaction with polypropylene reaction vessels were performed in a Thermocell mixing block from Bioer (Hangzhou, China). Thin layer chromatography (TLC) was performed on Merck silica gel 60 F_{254} TLC aluminum plates. Visualization was accomplished by UV irradiation (λ = 254 or 366 nm) and by staining with ninhydrin or potassium permanganate. NMR spectra were recorded on a Bruker Avance 300 (7.05 T, ^{1}H: 300.1 MHz, ^{13}C: 75.5 MHz) or a Bruker Avance III HD 600 equipped with a cryogenic probe (14.1 T ^{1}H: 600.1 MHz, ^{13}C: 150.9 MHz) (Bruker, Karlsruhe, Germany). High-resolution mass spectrometry (HRMS) analysis was performed on an Agilent 6540 UHD Accurate-Mass Q-TOF LC/MS system (Agilent Technologies, Santa Clara, CA) using an ESI source. Preparative HPLC was performed with a system from Knauer (Berlin, Germany) consisting of two K-1800 pumps and a K-2001 detector. A Kinetex-XB C18 (5 µm, 250 mm × 21 mm; Phenomenex, Aschaffenburg, Germany) was used as stationary phases at a flow rate of 18 mL/min. Mixtures of 0.1% aq TFA and acetonitrile were used as mobile phase. The detection wavelength was set to 220 nm throughout. The solvent of the collected fractions was removed by lyophilization using an Alpha 2-4 LD apparatus (Martin Christ, Osterode am Harz, Germany) equipped with a RZ 6 rotary vane vacuum pump (Vacuubrand, Wertheim, Germany). Analytical HPLC analysis of compounds **85**-**106** (concentrations between 25 and 50 µM) was performed with a system from Agilent Technologies composed of a 1290 Infinity binary pump equipped with a degasser, a 1290 Infinity autosampler, a 1290 Infinity thermostated column compartment, a 1260 Infinity diode array detector, and a 1260 Infinity fluorescence detector. A Kinetex-XB C18 (2.6 µm, 100 × 3 mm; Phenomenex)

served as stationary phase at a flow rate of 0.5 mL/min. Mixtures of 0.04% aq TFA (A) and acetonitrile (B) were used as mobile phase. For HPLC analysis of compounds **87**-**108** the following linear gradient was applied: 0-20 min: A/B 90:10-70:30, 20-22 min: 70:30-5:95, 22-28 min: 5:95. HPLC analysis of **85** was performed using the following gradient: 0-12 min: A/B 90:10-70:30, 12-16 min: 70:30-5:95, 16-20 min: 5:95 whereas for HPLC analysis of compounds **86** the following gradient was used: 0-20 min: A/B 80:20-30:70, 20-22 min: 30:70-5:95, 22-28 min: 5:95. For all analytical HPLC runs the oven temperature was set to 25 °C, the injection volume was 20 µL and detection was performed at 220 nm.
Annotation concerning the NMR spectra (^{1}H, ^{13}C) of the dibenzodiazepinone derivatives (**85**, **87**-**108**): due to a slow rotation about the exocyclic amide group on the NMR time scale, two isomers (ratios provided in the experimental protocols) were evident in the ^{1}H- and ^{13}C-NMR spectra.

4.4.2 Compound characterization

All target compounds (**85**, **87-108**) were characterized by ^{1}H-NMR, ^{13}C-NMR and 2D-NMR (^{1}H-COSY, HSQC, HMBC) spectroscopy, HRMS and RP-HPLC analysis. The purity of the final compounds, determined by RP-HPLC (220 nm), was ≥95% throughout (chromatograms shown in the appendix).

4.4.3 Chemistry: experimental protocols and analytical data

4.4.3.1 Solid-phase peptide synthesis (SPPS)

Peptides were synthesized by manual SPPS applying the Fmoc strategy. 5 mL BD Discardit II syringes (Becton Dickinson, Heidelberg, Germany) equipped with a 35-µm polyethylene frit (Roland Vetter Laborbedarf OHG, Ammerbuch, Germany) served as reaction vessels. Protected standard L-amino acids (Fmoc-Ala-OH, Fmoc-Gln-(Trt)-OH, Fmoc-Lys(Boc)-OH, Fmoc-Trp(Boc)-OH, Fmoc-Tyr(tBu)-OH) and the solid supports H-Ala-2-ClTrt PS resin, H-Arg(Pbf)-2-ClTrt PS resin, H-Leu-2-ClTrt PS resin, H-Lys(Boc)-2-ClTrt PS resin, H-Tyr(tBu)-2-ClTrt PS resin were purchased from Merck Chemicals (Schwalbach am Taunus, Germany). DMF/NMP (8:2 v/v) was used as solvent throughout (ca. 2.2 mL per 1 mmol Fmoc-aa). Standard amino acids (5-fold excess) were preactivated with HBTU/HOBt/DIPEA (5/5/10 equiv.) for 5 min and added to the resin. The vessel was shaken at rt for 60 min. The coupling procedure was repeated (“double coupling”). After coupling of the final Fmoc-aa, the resin was washed with solvent (4×) followed by Fmoc deprotection with 20% piperidine in DMF/NMP (8:2 v/v). For the acetylation of the *N*-terminus a mixture formed by acetic anhydride (5 equiv.) and DIPEA (10 equiv.) in DMF/NMP (8:2 v/v) was added and the vessel was shaken at rt for 30 min. After the acetylation step, the resin was

washed with solvent (4×) and CH_2Cl_2 (treated with K_2CO_3) (6×). The peptides were cleaved off from the 2-ClTrt resin by treatment with CH_2Cl_2/HFIP (3:1 v/v) (rt, 2 × 20 min). The resin was separated by filtration and washed once with CH_2Cl_2/HFIP (3:1) (1 mL). The filtrates were combined, the volatiles evaporated and the resulting residue was used in the next step without any purification. The chemical identity and purity of the protected peptides **72-82** was assessed by high-resolution mass spectrometry and analytical HPLC (data not shown).

4.4.3.2 Synthesis of the DIBA-peptide conjugates 87-108 from amines 83 or 84 and the side-chain protected peptides 72-82

The coupling reaction was performed in polypropylene reaction vessels (1.5 or 2 mL) with screw cap. EDC × HCl (1.2 equiv.) and HOBt (1.2 equiv.) were added to a solution of the respective side-chain protected peptide in DMF (0.1-0.4 mL). In case of compounds derived from **83** 1 equiv. of **83**, dissolved in DMF (0.1 mL), was immediately added and stirring was continued at 5 °C for 3 h. For the synthesis of compounds derived from **84** a solution of **84** × 3 TFA (1 equiv.) and DIPEA (3 equiv.) in DMF (0.1 mL) was immediately added and stirring was continued at 5 °C for 3 h. 1% aq TFA (0.1-0.4 mL, depending on the volume of DMF, final ratio 1:1) was added and the mixture was subjected to preparative HPLC to yield the protected intermediates, which were dissolved in TFA/CH_2Cl_2/H_2O (1:1:0.1 v/v/v) (for the preparation of **88**, **89**, **92**-**95**, **99**, **100**, **103**-**106**) or TFA/H_2O (95:5 v/v) (for the preparation of **90**, **91**, **96**, **97**, **101**, **102**, **107**, **108**). The mixtures were stirred at rt for 3 h, the solvent was removed under reduced pressure and the residue was subjected to preparative HPLC yielding the purified DIBA-peptide conjugates as hydrotrifluoroacetates.

***N*-(4-(1-(2-Oxo-2-(11-oxo-10,11-dihydro-5*H*-dibenzo[*b,e*][1,4]diazepin-5-yl)ethyl)piperidin-4-yl)butyl)propionamide hydrotrifluoroacetate (85)** Purification by preparative HPLC (gradient: 0-25 min: 0.1% aq TFA/acetonitrile 95:5-60:40, t_R = 18 min) yielded **85** as a white fluffy solid (32 mg, 0.055 mmol, 96%). Ratio of configurational isomers evident in the NMR spectra: 1.8:1. ^{1}H-NMR (600 MHz, MeOH-d_4): δ (ppm) 1.11 (t, 3H, *J* 7.7 Hz), 1.27-1.37 (m, 4H), 1.38-1.56 (m, 5H), 1.85-2.00 (m, 2H), 2.17 (q, 2H, *J* 7.6 Hz), 2.87-2.96 (m, 1H), 2.99-3.08 (m, 1H), 3.15 (t, 2H, *J* 7.2 Hz), 3.39-3.49 (m, 1H), 3.67-3.83 (m, 2H), 4.39 (d, 0.6H, *J* 17 Hz), 4.43 (d, 0.4H, *J* 17 Hz), 7.23-7.31 (m, 0.8H), 7.31-7.36 (m, 1.2H), 7.36-7.41 (m, 0.4H), 7.44-7.55 (m, 2.2H), 7.59-7.71 (m, 2H), 7.73-7.78 (m, 0.4H), 7.90 (dd, 0.6H, *J* 1.7 7.7 Hz), 7.97 (d, 0.4H, *J* 7.8 Hz). ^{13}C-NMR (150.9 MHz, MeOH-d_4): δ (ppm) 10.59, 24.66, 30.22, 30.41, 30.47, 34.39, 36.31, 40.07, 54.95, 55.01, 55.37, 57.94, 58.04, 123.08, 123.64, 126.84, 127.51, 127.87, 128.49, 128.89, 129.45, 130.10, 130.54, 130.88, 131.20, 131.70, 131.97, 132.34, 133.01, 133.43, 134.57, 134.94, 135.45, 135.73, 137.04, 141.02, 142.68, 164.96, 165.45, 168.56, 168.81, 177.02. HRMS (ESI): *m/z* $[M+H]^+$

calcd for $[C_{27}H_{35}N_4O_3]^+$ 463.2709, found 463.2729. RP-HPLC (220 nm): 99% (t_R = 8.3 min, k = 8.0). $C_{27}H_{34}N_4O_3 \cdot C_2HF_3O_2$ (462.59 + 114.02).

(*S*)-2-Acetamido-*N*-((*S*)1-oxo-1-((4-(1-(2-oxo-2-(11-oxo-10,11-dihydro-5*H*-dibenzo[*b,e*][1,4]diazepin-5-yl)ethyl)piperidin-4-yl)butyl)amino)propan-2-yl)propanamide hydrotrifluoroacetate (87) Purification by preparative HPLC (gradient: 0-25 min: 0.1% aq TFA/acetonitrile 90:10-70:30, t_R = 11 min) yielded **87** as a white fluffy solid (25 mg, 0.035 mmol, 71%). Ratio of configurational isomers evident in the NMR spectra: ca 1.6:1. ^{1}H-NMR (600 MHz, MeOH-d_4): δ (ppm) 1.26-1.38 (m, 10H), 1.41-1.55 (m, 5H), 1.86-1.97 (m, 2H), 1.98 (s, 3H), 2.87-2.97 (m, 1H), 2.98-3.08 (m, 1H), 3.40-3.49 (m, 1H), 3.68-3.83 (m, 2H), 4.19-4.31 (m, 2H), 4.39 (d, 0.6H, *J* 17 Hz), 4.44 (d, 0.4H, *J* 17 Hz), 7.23-7.31 (m, 0.8H), 7.31-7.42 (m, 1.7H), 7.44-7.55 (m, 2H), 7.60-7.72 (m, 2H), 7.75 (t, 0.5H, *J* 7.8 Hz), 7.90 (dd, 0.6H, *J* 7.9 1.6 Hz), 7.97 (dd, 0.4H, *J* 6.8 1.1 Hz). ^{13}C-NMR (150.9 MHz, MeOH-d_4): δ (ppm) 17.80, 18.11, 22.65, 24.58, 30.34, 30.60, 34.49, 36.34, 40.20, 50.67, 51.25, 55.11, 55.19, 55.53, 58.09, 58.18, 126.99, 127.66, 128.03, 128.64, 129.04, 129.60, 130.25, 130.69, 131.03, 131.34, 131.85, 132.11, 132.50, 133.16, 133.58, 134.72, 135.09, 135.60, 135.87, 137.18, 141.17, 142.83, 162.26, 162.50, 165.13, 165.61, 168.70, 168.96, 173.89, 174.97, 175.20. HRMS (ESI): *m/z* $[M+H]^+$ calcd for $[C_{32}H_{43}N_6O_5]^+$ 591.3295, found 591.3307. RP-HPLC (220 nm): 96% (t_R = 16.7 min, k = 17.2). $C_{32}H_{42}N_6O_5 \cdot C_2HF_3O_2$ (590.72 + 114.02).

(*S*)-2-Acetamido-*N*-((*S*)-3-(4-hydroxyphenyl)-1-oxo-1-((4-(1-(2-oxo-2-(11-oxo-10,11-dihydro-5*H*-dibenzo[*b,e*][1,4]diazepin-5-yl)ethyl)piperidin-4-yl)butyl)amino)propan-2-yl)-3-(1H-indol-3-yl)propanamide hydrotrifluoroacetate (88) Purification by preparative HPLC (gradient: 0-25 min: 0.1% aq TFA/acetonitrile 90:10-43:57, t_R = 14 min) yielded **88** as a white fluffy solid (31 mg, 0.034 mmol, 72%). Ratio of configurational isomers evident in the NMR spectra: 1.4:1. ^{1}H-NMR (600 MHz, MeOH-d_4): δ (ppm) 1.09-1.49 (m, 9H), 1.72-1.86 (m, 2H), 1.87 (s, 3H), 2.61-2.65 (m, 4H), 2.99-3.09 (m, 3H), 3.14-3.22 (m, 1H), 3.32-3.40 (m, 1H), 3.55-3.77 (m, 2H), 4.29-4.41 (m, 2H), 4.54-4.60 (m, 1H), 6.66 (d, 2H, *J* 8.8 Hz), 6.90 (d, 2H, *J* 8.8 Hz), 6.96-7.00 (m, 1H), 7.04 -7.08 (m, 1H), 7.09 (br s, 1H), 7.23-7.40 (m, 3.4H), 7.45-7.56 (m, 3.2H), 7.58-7.70 (m, 2H), 7.70-7.78 (m, 0.4H), 7.90 (d, 0.6H, *J* 7.8 Hz), 7.98 (d, 0.4H, *J* 7.6 Hz). ^{13}C-NMR (150.9 MHz, MeOH-d_4): δ (ppm) 22.54, 24.48, 28.50, 30.06, 30.08, 30.41, 34.26, 36.20, 37.73, 40.01, 55.00, 55.35, 55.94, 56.14, 58.02, 110.83, 112.41, 116.23, 119.33, 119.91, 122.54, 123.09, 123.66, 124.63, 126.86, 127.53, 127.86, 128.47, 128.65, 128.77, 128.87, 129.43, 130.11, 130.55, 130.85, 131.24, 131.38, 131.73, 131.96, 132.36, 133.04, 133.41, 134.58, 134.91, 135.48, 135.69, 137.01, 137.97, 141.00, 142.64, 157.33, 164.89, 165.39, 168.58, 168.83, 173.02, 173.57, 173.66. 138.04, 140.99, 142.64, 157.26, 164.89, 165.38, 168.60, 168.84, 173.28, 173.88, 174.72, 174.94. HRMS

(ESI): *m/z* $[M+H]^+$ calcd for $[C_{46}H_{52}N_7O_6]^+$ 798.3979, found 798.3992. RP-HPLC (220 nm): 96% (t_R = 20.2 min, *k* = 21.0). $C_{46}H_{51}N_7O_6 \cdot C_2HF_3O_2$ (797.96 + 114.02).

(*S*)-2-Acetamido-*N*-((*S*)-1-(((*S*)-3-(4-hydroxyphenyl)-1-oxo-1-((4-(1-(2-oxo-2-(11-oxo-10,11-dihydro-5*H*-dibenzo[*b,e*][1,4]diazepin-5-yl)ethyl)piperidin-4-yl)butyl)amino)propan-2-yl)amino)-1-oxopropan-2-yl)-3-(1H-indol-3-yl)propanamide hydrotrifluoroacetate (89) Purification by preparative HPLC (gradient: 0-25 min: 0.1% aq TFA/acetonitrile 90:10-43:57, t_R = 14 min) yielded **89** as a white fluffy solid (24 mg, 0.024 mmol, 50%). Ratio of configurational isomers evident in the NMR spectra: 1.4:1. ^{1}H-NMR (600 MHz, MeOH-d_4): δ (ppm) 1.11 (d, 3H, *J* 7.3 Hz), 1.18-1.45 (m, 9H), 1.71-1.89 (m, 2H), 1.92-1.96 (m, 3H), 2.58-2.91 (m, 3H), 2.98-3.05 (m, 1H), 3.07-3.20 (m, 3H), 3.21-3.28 (m, 1H), 3.32-3.38 (m, 1H), 3.57-3.70 (m, 2H), 4.11 (q, 1H, *J* 7.3 Hz), 4.30-4.41 (m, 2H), 4.53-4.58 (m, 1H), 6.67 (d, 2H, *J* 8.67 Hz), 6.96-7.01 (m, 3H), 7.04-7.09 (m, 1H), 7.16 (br s, 1H), 7.24-7.41 (m, 3.4H), 7.47-7.54 (m, 2.2H), 7.56 (d, 1H, *J* 7.9 Hz), 7.60-7.70 (m, 2H), 7.73-7.78 (m, 0.4H), 7.90 (d, 0.6H, *J* 7.8 Hz), 7.99 (d, 0.4H, *J* 7.6 Hz). ^{13}C-NMR (150.9 MHz, MeOH-d_4): δ (ppm) 17.23, 22.65, 24.48, 28.44, 30.03, 30.43, 34.23, 36.21, 37.63, 40.16, 51.43, 55.00, 55.35, 56.44, 56.55, 57.95, 58.03, 110.78, 112.44, 116.19, 119.30, 119.91, 122.58, 123.10, 123.66, 124.71, 126.87, 127.54, 127.86, 128.47, 128.77, 128.88, 129.18, 129.43, 130.12, 130.56, 130.86, 131.21, 131.74, 131.98, 132.36, 133.04, 133.41, 134.59, 134.92, 135.48, 135.70, 137.03, 138.04, 140.99, 142.64, 157.26, 164.89, 165.38, 168.60, 168.84, 173.28, 173.88, 174.72, 174.94. HRMS (ESI): *m/z* $[M+H]^+$ calcd for $[C_{49}H_{57}N_8O_7]^+$ 869.4350, found 869.4364. RP-HPLC (220 nm): 98% (t_R = 20.5 min, *k* = 21.3). $C_{49}H_{56}N_8O_7 \cdot C_2HF_3O_2$ (869.04 + 114.02).

(*S*)-2-Acetamido-N^1-((*S*)-4-methyl-1-oxo-1-((4-(1-(2-oxo-2-(11-oxo-10,11-dihydro-5*H*-dibenzo[*b,e*][1,4]diazepin-5-yl)ethyl)piperidin-4-yl)butyl)amino)pentan-2-yl)pentanediamide hydrotrifluoroacetate (90) Purification by preparative HPLC (gradient: 0-25 min: 0.1% aq TFA/acetonitrile 90:10-70:30, t_R = 15 min) yielded **90** as a white fluffy solid (29 mg, 0.036 mmol, 75%). Ratio of configurational isomers evident in the NMR spectra: 1.7:1. ^{1}H-NMR (600 MHz, MeOH-d_4): δ (ppm) 0.90 (d, 3H, *J* 6.6 Hz), 0.94 (d, 3H, *J* 6.6 Hz), 1.25-1.37 (m, 4H), 1.39-1.72 (m, 8H), 1.82-2.00 (m, 6H) 2.00-2.10 (m, 1H), 2.29 (t, 2H, *J* 7.4 Hz), 2.88-2.97 (m, 1H), 3.00-3.08 (m, 1H), 3.13-3.22 (m, 2H), 3.40-3.48 (m, 1H), 3.68-3.83 (m, 2H), 4.25-4.30 (m, 1H), 4.30-4.35 (m, 1H), 4.36-4.46 (m, 1H), 7.24-7.31 (m, 0.8H), 7.31-7.36 (m, 1.2H), 7.36-7.41 (m, 0.4H), 7.46-7.55 (m, 2.2H), 7.59-7.72 (m, 2H), 7.73-7.78 (m, 0.4H), 7.90 (dd, 0.6H, *J* 8.3 1.5 Hz), 7.97 (dd, 0.4H, *J* 7.9 1.0 Hz). ^{13}C-NMR (150.9 MHz, MeOH-d_4): δ (ppm) 21.85, 22.50, 23.43, 24.38, 25.91, 28.68, 30.22, 30.42, 32.49, 34.36, 36.18, 39.98, 41.79, 53.40, 54.60, 54.97, 55.05, 55.41, 57.94, 58.02, 123.09, 123.66, 126.86, 127.52, 127.88, 128.48, 128.89, 129.44, 130.12, 130.55, 130.88, 131.21, 131.71, 131.95, 132.35, 133.01, 133.45, 134.59, 134.94, 135.45, 135.72, 137.02,

141.02, 142.68, 165.04, 165.52, 168.57, 168.83, 173.69, 173.87, 174.68, 177.65, 177.69. HRMS (ESI): *m/z* $[M+H]^+$ calcd for $[C_{37}H_{52}N_7O_6]^+$ 690.3979, found 690.3993. RP-HPLC (220 nm): 95% (t_R = 14.5 min, *k* = 14.8). $C_{37}H_{51}N_7O_6 \cdot C_2HF_3O_2$ (689.86 + 114.02).

(*S*)-2-Acetamido-*N*^{1}-((*S*)-1-(((*S*)-4-methyl-1-oxo-1-((4-(1-(2-oxo-2-(11-oxo-10,11-dihydro-5*H*-dibenzo[*b,e*][1,4]diazepin-5-yl)ethyl)piperidin-4-yl)butyl)amino)pentan-2-yl)amino)-1-oxopropan-2-yl)pentanediamide hydrotrifluoroacetate (91) Purification by preparative HPLC (gradient: 0-25 min: 0.1% aq TFA/acetonitrile 90:10-70:30, t_R = 15 min) yielded **91** as a white fluffy solid (26 mg, 0.030 mmol, 32%). Ratio of configurational isomers evident in the NMR spectra: 1.7:1. ^{1}H-NMR (600 MHz, MeOH-d_4): δ (ppm) 0.90 (d, 3H, *J* 6.4 Hz), 0.95 (d, 3H, *J* 6.4 Hz), 1.23-1.70 (m, 15H), 1.85-2.01 (m, 6H), 2.01-2.09 (m, 1H), 2.33 (t, 2H, *J* 7.8 Hz), 2.87-2.97 (m, 1H), 2.99-3.01 (m, 1H), 3.17 (t, 2H, *J* 6.9 Hz), 3.40-3.49 (m, 1H), 3.69-3.84 (m, 2H), 4.20-4.31 (m, 3H), 4.37-4.46 (m, 1H), 7.24-7.31 (m, 0.8H), 7.32-7.36 (m, 1.2H), 7.37-7.40 (m, 0.4H), 7.46-7.55 (m, 2.2H), 7.60-7.71 (m, 2H), 7.73-7.78 (m, 0.4H), 7.90 (d, 0.6H, *J* 8.32 Hz), 7.97 (d, 0.4H, *J* 8.1 Hz). ^{13}C-NMR (150.9 MHz, MeOH-d_4): δ (ppm) 17.50, 21.75, 22.52, 22.54, 23.47, 24.33, 25.98, 28.45, 30.10, 30.47, 32.41, 34.35, 36.13, 39.94, 39.99, 41.68, 51.20, 53.45, 55.00, 55.13, 55.43, 57.96, 58.05, 123.10, 123.66, 126.86, 127.51, 127.87, 128.48, 128.89, 129.44, 130.13, 130.56, 130.89, 131.22, 131.72, 131.98, 132.37, 133.03, 133.44, 134.59, 134.94, 135.45, 135.74, 137.05, 141.02, 142.67, 165.03, 165.52, 168.55, 168.82, 173.80, 174.38, 174.65, 175.01, 177.63. HRMS (ESI): *m/z* $[M+H]^+$ calcd for $[C_{40}H_{57}N_8O_7]^+$ 761.4350, found 761.4357. RP-HPLC (220 nm): 95% (t_R = 14.5 min, *k* = 14.8). $C_{40}H_{56}N_8O_7 \cdot C_2HF_3O_2$ (760.94 + 114.02).

(*S*)-2-Acetamido-6-amino-*N*-((*S*)-3-(4-hydroxyphenyl)-1-oxo-1-((4-(1-(2-oxo-2-(11-oxo-10,11-dihydro-5*H*-dibenzo[*b,e*][1,4]diazepin-5-yl)ethyl)piperidin-4-yl)butyl)amino)propan-2-yl)hexanamide bis(hydrotrifluoroacetate) (92) Purification by preparative HPLC (gradient: 0-25 min: 0.1% aq TFA/acetonitrile 90:10-67:33, t_R = 11 min) yielded **92** as a white fluffy solid (28 mg, 0.029 mmol, 58%). Ratio of configurational isomers evident in the NMR spectra: 1.6:1. ^{1}H-NMR (600 MHz, MeOH-d_4): δ (ppm) 1.16-1.54 (m, 11H), 1.55-1.71 (m, 4H), 1.85-1.96 (m, 2H), 1.97 (s, 3H), 2.81-2.96 (m, 4H), 2.97-3.09 (m, 3H), 3.14-3.22 (m, 1H), 3.39-3.50 (m, 1H), 3.66-3.84 (m, 2H), 4.15-4.21 (m, 1H), 4.36-4.50 (m, 2H), 6.69 (d, 2H, *J* 8.6 Hz), 7.03 (d, 2H, *J* 8.5 Hz), 7.25-7.31 (m, 0.8H), 7.32-7.36 (m, 1.2H), 7.36-7.40 (m, 0.4H), 7.45-7.55 (m, 2.2H), 7.61-7.71 (m, 2H), 7.73-7.77 (m, 0.4H), 7.90 (d, 0.6H, *J* 8.3 Hz), 7.97 (d, 0.4H, *J* 7.9 Hz). ^{13}C-NMR (150.9 MHz, MeOH-d_4): δ (ppm) 22.51, 23.58, 24.56, 28.08, 30.07, 30.46, 32.05, 34.33, 36.27, 37.99, 40.16, 40.42, 55.05, 55.10, 55.41, 56.23, 57.94, 58.03, 116.24, 123.01, 123.66, 126.85, 127.54, 127.89, 128.49, 128.88, 128.92, 129.45, 130.11, 130.54, 130.87, 131.20, 131.38, 131.71, 131.94, 132.34, 132.99, 133.44, 134.58, 134.93, 135.47, 135.71, 137.00, 141.01, 142.69, 157.28, 164.98, 165.48, 168.57, 168.83, 173.22, 173.84. HRMS (ESI): *m/z* $[M+H]^+$ calcd for $[C_{41}H_{54}N_7O_6]^+$

740.4136, found 740.4134. RP-HPLC (220 nm): 99% (t_R = 13.1 min, k = 13.2). $C_{41}H_{53}N_7O_6 \cdot C_4H_2F_6O_4$ (739.92 + 228.04).

(*S*)-2-Acetamido-6-amino-*N*-((*S*)-1-(((*S*)-3-(4-hydroxyphenyl)-1-oxo-1-((4-(1-(2-oxo-2-(11-oxo-10,11-dihydro-5*H*-dibenzo[*b,e*][1,4]diazepin-5-yl)ethyl)piperidin-4-yl)butyl)amino)propan-2-yl)amino)-1-oxopropan-2-yl)hexanamide bis(hydrotrifluoroacetate) (93) Purification by preparative HPLC (gradient: 0-25 min: 0.1% aq TFA/acetonitrile 90:10-67:33, t_R = 11 min) yielded **93** as a white fluffy solid (31 mg, 0.030 mmol, 63%). Ratio of configurational isomers evident in the NMR spectra: 1.6:1. ^{1}H-NMR (600 MHz, MeOH-d_4): δ (ppm) 1.51-1.26 (m, 4H), 1.27 (d, 3H, *J* 7.2 Hz), 1.35-1.52 (m, 7H), 1.63-1.71 (m, 3H), 1.74-1.81 (m, 1H), 1.83-1.97 (m, 2H), 1.97-2.02 (m, 3H), 2.84-3.00 (m, 5H), 3.00-3.08 (m, 2H), 3.13-3.21 (m, 1H), 3-40-3.49 (m, 1H), 3.67-3.84 (m, 2H), 4.20-4.27 (m, 2H), 4.37-4.47 (m, 2H), 6.69 (d, 2H, *J* 8.4 Hz), 7.03 (d, 2H, *J* 8.5 Hz), 7.24-7.31 (m, 0.8H), 7.32-7.36 (m, 1.2H), 7.36-7.40 (m, 0.4H), 7.45-7.55 (m, 2.2H), 7.60-7.71 (m, 2H), 7.73-7.77 (m, 0.4H), 7.90 (dd, 0.6H, *J* 1.6 7.7 Hz), 7.97 (d, 0.4H, *J* 7.7 Hz). ^{13}C-NMR (150.9 MHz, MeOH-d_4): δ (ppm) 17.64, 22.51, 22.53, 23.70, 24.48, 28.11, 30.05, 30.49, 32.22, 34.35, 36.23, 38.14, 40.04, 40.46, 50.90, 55.02, 55.40, 56.48, 57.96, 58.03, 116.22, 123.09, 123.66, 126.86, 127.54, 127.88, 128.49, 128.89, 128.95, 129.45, 130.11, 130.55, 130.88, 131.21, 131.34, 131.71, 131.94, 132.35, 133.00, 133.43, 134.59, 134.93, 135.47, 135.71, 137.01, 141.00, 142.68, 157.29, 165.00, 165.49, 168.57, 168.83, 173.15, 173.73, 174.43, 174.62. HRMS (ESI): *m/z* $[M+2H]^{2+}$ calcd for $[C_{44}H_{60}N_8O_7]^{2+}$ 406.2292, found 406.2302. RP-HPLC (220 nm): 97% (t_R = 11.1 min, k = 11.1). $C_{44}H_{58}N_8O_7 \cdot C_4H_2F_6O_4$ (811.00 + 228.04).

(*S*)-2-((*S*)-2-Acetamido-3-(4-hydroxyphenyl)propanamido)-6-amino-*N*-(4-(1-(2-oxo-2-(11-oxo-10,11-dihydro-5*H*-dibenzo[*b,e*][1,4]diazepin-5-yl)ethyl)piperidin-4-yl)butyl)hexanamide bis(hydrotrifluoroacetate) (94) Purification by preparative HPLC (gradient: 0-25 min: 0.1% aq TFA/acetonitrile 90:10-70:30, t_R = 11 min) yielded **94** as a white fluffy solid (22 mg, 0.022 mmol, 30%). Ratio of configurational isomers evident in the NMR spectra: 1.1:1. ^{1}H-NMR (600 MHz, MeOH-d_4): δ (ppm) 1.24-1.55 (m, 11H), 1.55-1.70 (m, 3H), 1.79-1.93 (m, 2.4H), 1.94 (s, 3H), 1.95-1.99 (0.6H), 2.82-3.09 (m, 7H), 3.10-3.17 (m, 1H), 3.40-3.48 (m, 1H), 3.67-3.82 (m, 2H), 4.23 (dd, 1H, *J* 9.8, 4.5 Hz), 4.35-4.46 (m, 2H), 6.71 (d, 2H, *J* 8.5 Hz), 7.07 (d, 2H, *J* 8.6 Hz), 7.24-7.31 (m, 0.8H), 7.32-7.35 (m, 1.2H), 7.36-7.41 (m, 0.4H), 7.45-7.55 (m, 2.2H), 7.60-7.71 (m, 2H), 7.72-7.78 (m, 0.4H), 7.90 (d, 0.6H, *J* 8.2 Hz), 7.97 (d, 0.4H, *J* 8.2 Hz). ^{13}C-NMR (150.9 MHz, MeOH-d_4): δ (ppm) 22.37, 22.63, 24.59, 27.89, 30.31, 30.48, 32.30, 34.34, 36.27, 37.65, 40.22, 40.47, 54.29, 55.01, 55.38, 57.09, 58.01, 116.35, 123.08, 123.66, 126.86, 127.54, 127.88, 128.49, 131.33, 134.94, 135.47, 135.71, 137.00, 141.01, 142.68, 157.44, 162.80, 164.97, 165.47, 168.59, 168.84, 173.56, 174.23. HRMS (ESI): *m/z* $[M+H]^+$ calcd for $[C_{41}H_{54}N_7O_6]^+$ 740.4136, found

740.4147. RP-HPLC (220 nm): 99% (t_R = 11.1 min, k = 11.1). $C_{41}H_{53}N_7O_6 \cdot C_4H_2F_6O_4$ (739.92 + 228.04).

(*S*)-2-((*S*)-2-((*S*)-2-Acetamido-3-(4-hydroxyphenyl)propanamido)propanamido)-6-amino-*N*-(4-(1-(2-oxo-2-(11-oxo-10,11-dihydro-5*H*-dibenzo[*b,e*][1,4]diazepin-5-yl)ethyl)piperidin-4-yl)butyl)hexanamide bis(hydrotrifluoroacetate) (95) Purification by preparative HPLC (gradient: 0-25 min: 0.1% aq TFA/acetonitrile 90:10-67:33, t_R = 11 min) yielded **95** as a white fluffy solid (24 mg, 0.023 mmol, 49%). Ratio of configurational isomers evident in the NMR spectra: 1.2:1. ^{1}H-NMR (600 MHz, MeOH-d_4): δ (ppm) 1.25-1.33 (m, 4H), 1.35 (d, 3H, *J* 7.2 Hz), 1.37-1.54 (m, 7H), 1.62-1.74 (m, 3H), 1.80-1.90 (m, 2H), 1.92 (s, 3H), 1.93-1.96 (m, 1H), 2.79-2.85 (m, 1H), 2.85-2.95 (m, 3H), 2.97-3.07 (m, 2H), 3.18 (t, 2H, *J* 6.9 Hz), 3.39-3.48 (m, 1H), 3.67-3.82 (m, 2H), 4.19-4.27 (m, 2H), 4.35-4.45 (m, 2H), 6.70 (d, 2H, *J* 8.7 Hz), 7.06 (d, 2H, *J* 8.5 Hz), 7.24-7.31 (m, 0.8H), 7.32-7.36 (m, 1.2H), 7.36-7.40 (m, 0.4H), 7.45-7.55 (m, 2.2H), 7.61-7.71 (m, 2H), 7.73-7.77 (m, 0.4H), 7.90 (d, 0.6H, *J* 7.8 Hz), 7.97 (d, 0.4H, *J* 7.7 Hz). ^{13}C-NMR (150.9 MHz, MeOH-d_4): δ (ppm) 17.38, 22.51, 23.81, 24.53, 27.92, 30.21, 30.46, 32.22, 34.35, 36.26, 37.61, 40.18, 40.49, 51.09, 54.53, 55.02, 55.39, 57.08, 57.94, 58.03, 116.28, 123.09, 123.66, 126.86, 127.53, 127.88, 128.48, 128.87, 129.44, 130.11, 130.55, 130.88, 131.24, 131.71, 131.96, 132.35, 133.01, 133.43, 134.58, 134.93, 135.47, 135.72, 137.02, 141.01, 142.68, 157.39, 164.97, 165.47, 168.57, 168.84, 173.72, 173.90, 174.39, 174.94. HRMS (ESI): *m/z* $[M+H]^+$ calcd for $[C_{44}H_{59}N_8O_7]^+$ 811.4507, found 811.4508. RP-HPLC (220 nm): 99% (t_R = 13.3 min, k = 13.5). $C_{44}H_{58}N_8O_7 \cdot C_4H_2F_6O_4$ (811.00 + 228.04).

(*S*)-2-Acetamido-6-amino-*N*-((*S*)-5-guanidino-1-oxo-1-((4-(1-(2-oxo-2-(11-oxo-10,11-dihydro-5*H*-dibenzo[*b,e*][1,4]diazepin-5-yl)ethyl)piperidin-4-yl)butyl)amino)pentan-2-yl)hexanamide tris(hydrotrifluoroacetate) (96) Purification by preparative HPLC (gradient: 0-25 min: 0.1% aq TFA/acetonitrile 90:10-70:30, t_R = 8 min) yielded **96** as a white fluffy solid (33 mg, 0.031 mmol, 67%). Ratio of configurational isomers evident in the NMR spectra: 1.8:1. ^{1}H-NMR (600 MHz, MeOH-d_4): δ (ppm) 1.25-1.38 (m, 4H), 1.39-1.56 (m, 7H), 1.57-1.74 (m, 6H), 1.76-1.97 (m, 4H), 1.99 (s, 3H), 2.86-2.97 (m, 3H), 2.99-3.09 (m, 1H), 3.11-3.24 (m, 4H), 3.40-3.50 (m, 1H), 3.67-3.83 (m, 2H), 4.21-4.26 (m, 1H), 4.29-4.34 (m, 1H), 4.37-4.48 (m, 1H), 4.40 (d, 0.6H, *J* 17 Hz), 4.44 (d, 0.4H, *J* 17 Hz), 7.24-7.31 (m, 0.8H), 7.31-7.36 (m, 1.2H), 7.36-7.40 (m, 0.4H), 7.44-7.56 (m, 2.2H), 7.60-7.72 (m, 2.2H), 7.73-7.78 (m, 0.4H), 7.90 (dd, 0.6H, *J* 1.7 7.7 Hz), 7.97 (d, 0.4H, *J* 7.7 Hz). ^{13}C-NMR (150.9 MHz, MeOH-d_4): δ (ppm) 22.44, 23.84, 24.64, 26.36, 28.07, 30.28, 30.36, 30.44, 32.06, 34.38, 36.32, 40.25, 40.45, 41.89, 54.17, 55.00, 55.08, 55.36, 57.95, 58.01, 123.01, 123.66, 126.85, 127.54, 127.89, 128.48, 128.89, 129.44, 130.12, 130.55, 130.89, 131.20, 131.71, 131.95, 132.34, 132.99, 133.45, 134.58, 134.94, 135.47, 135.72, 137.00, 141.01, 142.70, 158.66, 164.99, 165.50, 168.58, 168.85, 173.67, 173.79, 174.46. HRMS (ESI): *m/z* $[M+H]^+$

calcd for $[C_{38}H_{57}N_{10}O_5]^+$ 733.4513, found 733.4512. RP-HPLC (220 nm): 99% (t_R = 6.9 min, k = 6.5). $C_{38}H_{56}N_{10}O_5 \cdot C_6H_3F_9O_6$ (732.93 + 342.07).

(*S*)-2-Acetamido-6-amino-*N*-((*S*)-1-(((*S*)-5-guanidino-1-oxo-1-((4-(1-(2-oxo-2-(11-oxo-10,11-dihydro-5*H*-dibenzo[*b,e*][1,4]diazepin-5-yl)ethyl)piperidin-4-yl)butyl)amino)pentan-2-yl)amino)-1-oxopropan-2-yl)hexanamide tris(hydrotrifluoroacetate) (97) Purification by preparative HPLC (gradient: 0-25 min: 0.1% aq TFA/acetonitrile 90:10-70:30, t_R = 8 min) yielded **97** as a white fluffy solid (24 mg, 0.021 mmol, 60%). Ratio of configurational isomers evident in the NMR spectra: 1.9:1. ^{1}H-NMR (600 MHz, MeOH-d_4): δ (ppm) 1.26-1.36 (m, 4H), 1.37 (d, 3H, *J* 7.1 Hz), 1.38-1.56 (m, 7H), 1.56-1.77 (m, 6H), 1.77-1.97 (m, 4H), 1.98-2.01 (m, 3H), 2.93 (t, 3H, *J* 7.6 Hz), 3.00-3.08 (m, 1H), 3.12-3.24 (m, 4H), 3.41-3.49 (m, 1H), 3.68-3.83 (m, 2H), 4.19-4.24 (m, 1H), 4.24-4.30 (m, 2H) 4.40 (d, 0.6H, *J* 17 Hz), 4.44 (d, 0.4H, *J* 17 Hz), 7.24-7.31 (m, 0.8H), 7.31-7.36 (m, 1.2H), 7.36-7.41 (m, 0.4H), 7.45-7.55 (m, 2.2H), 7.60-7.71 (m, 2H), 7.72-7.78 (m, 0.4H), 7.90 (dd, 0.6H, *J* 1.4 7.9 Hz). ^{13}C-NMR (150.9 MHz, MeOH-d_4): δ (ppm) 17.48, 22.53, 23.77, 24.55, 26.32, 28.11, 30.18, 30.23, 30.46, 32.11, 34.38, 36.26, 40.15, 40.44, 41.90, 51.01, 54.35, 55.01, 55.28, 55.37, 58.02, 118.96, 123.08, 123.67, 126.86, 127.54, 127.89, 128.49, 128.89, 129.44, 130.12, 130.55, 130.89, 131.20, 131.71, 131.95, 132.34, 133.00, 133.44, 134.58, 134.94, 135.47, 135.72, 137.01, 141.01, 142.69, 158.65, 165.00, 165.50, 168.57, 168.84, 173.66, 173.95, 174.64, 175.12. HRMS (ESI): *m/z* $[M+2H]^{2+}$ calcd for $[C_{41}H_{63}N_{11}O_6]^{2+}$ 402.7481, found 402.7484. RP-HPLC (220 nm): 99% (t_R = 7.5 min, k = 7.2). $C_{41}H_{61}N_{11}O_6 \cdot C_6H_3F_9O_6$ (804.01 + 342.07).

(*S*)-2-Acetamido-*N*-((*S*)-1-oxo-1-((2-(4-(4-(1-(2-oxo-2-(11-oxo-10,11-dihydro-5*H*-dibenzo[*b,e*][1,4]diazepin-5-yl)ethyl)piperidin-4-yl)butyl)piperazin-1-yl)ethyl)amino)propan-2-yl)propanamide tris(hydrotrifluoroacetate) (98) Purification by preparative HPLC (gradient: 0-25 min: 0.1% aq TFA/acetonitrile 90:10-77:23, t_R = 9 min) yielded **98** as a white fluffy solid (16 mg, 0.015 mmol, 39%). Ratio of configurational isomers evident in the NMR spectra: 1.6:1. ^{1}H-NMR (600 MHz, MeOH-d_4): δ (ppm) 1.30-1.63 (m, 13H), 1.66-1.76 (m, 2H), 1.86-1.99 (m, 2H), 2.00 (s, 3H), 2.41-2.81 (m, 1H), 2.81-3.23 (m, 10H), 3.32-3.51 (m, 6H), 3.68-3.83 (m, 2H), 4.14-4.27 (m, 2H), 4.40 (d, 0.6H, *J* 17 Hz), 4.44 (d, 0.4H, *J* 17 Hz), 7.23-7.31 (m, 0.8H), 7.31-7.36 (m, 1.2H), 7.36-7.41 (m, 0.4H), 7.45-7.56 (m, 2.2H), 7.60-7.71 (m, 2H), 7.72-7.79 (m, 0.4H), 7.90 (dd, 0.6H, *J* 1.6 8.0 Hz), 7.97 (dd, 0.4H, *J* 1.1 7.8 Hz). ^{13}C-NMR (150.9 MHz, MeOH-d_4): δ (ppm) 17.41, 17.56, 22.39, 22.53, 24.54, 25.27, 30.41, 34.32, 36.16, 36.68, 50.91, 50.96, 51.48, 52.12, 54.94, 55.30, 57.18, 57.76, 58.04, 123.09, 123.65, 126.86, 127.52, 127.87, 128.49, 128.88, 129.45, 130.11, 130.55, 130.89, 131.22, 131.71, 131.97, 132.35, 133.01, 133.41, 134.58, 134.94, 135.46, 135.73, 137.04, 141.01, 142.68, 164.96, 165.45, 168.58, 168.83, 173.91, 175.50, 175.69.

HRMS (ESI): *m/z* $[M+H]^+$ calcd for $[C_{38}H_{55}N_8O_5]^+$ 703.4295, found 703.4296. RP-HPLC (220 nm): 95% (t_R = 7.4 min, *k* = 7.0). $C_{38}H_{54}N_8O_5 \cdot C_4H_2F_6O_4$ (702.90 + 228.04).

(*S*)-2-Acetamido-N-((*S*)-3-(4-hydroxyphenyl)-1-oxo-1-((2-(4-(4-(1-(2-oxo-2-(11-oxo-10,11-dihydro-5*H*-dibenzo[*b,e*][1,4]diazepin-5-yl)ethyl)piperidin-4-yl)butyl)piperazin-1-yl)ethyl)amino)propan-2-yl)-3-(1*H*-indol-3-yl)propanamide tris(hydrotrifluoroacetate) (99) Purification by preparative HPLC (gradient: 0-25 min: 0.1% aq TFA/acetonitrile 90:10-50:50, t_R = 12 min) yielded **99** as a white fluffy solid (24 mg, 0.019 mmol, 53%). Ratio of configurational isomers evident in the NMR spectra: 1.8:1. ^{1}H-NMR (600 MHz, MeOH-d_4): δ (ppm) 1.25-1.55 (m, 8H), 1.60-1.69 (m, 2H), 1.80-1.89 (m, 1H), 1.91 (s, 3H), 1.92-1.96 (m, 1H), 2.74-2.95 (m, 6H), 2.95-3.24 (m, 10H), 3.32-3.47 (m, 4H), 3.67-3.80 (m, 2H), 4.30 (t, 1H, *J* 7.3 Hz), 4.39 (d, 0.6H, *J* 17 Hz), 4.43 (d, 0.4H, *J* 17 Hz), 4.52 (t, 1H, *J* 7.0 Hz), 6.70 (d, 2H, *J* 8.5 Hz), 6.95 (d, 2H, *J* 8.5 Hz), 7.02 (t, 1H, *J* 7.5 Hz), 7.07-7.12 (m, 2H), 7.24-7.31 (m, 0.8H), 7.32-7.36 (m, 2.2H), 7.36-7.40 (m, 0.4H), 7.46-7.55 (m, 3.2H), 7.60-7.71 (m, 2H), 7.73-7.78 (m, 0.4H), 7.91 (d, 0.6H, *J* 8.2 Hz), 7.98 (d, 0.4H, *J* 7.9 Hz). ^{13}C-NMR (150.9 MHz, MeOH-d_4): δ (ppm) 22.57, 24.44, 25.04, 28.45, 30.37, 34.27, 36.07, 36.28, 37.18, 50.66, 51.61, 54.91, 55.27, 56.37, 56.81, 57.05, 57.70, 57.94, 58.04, 110.75, 112.48, 116.34, 119.26, 119.96, 122.61, 123.10, 123.64, 124.67, 126.86, 127.52, 127.87, 128.48, 128.56, 128.73, 128.88, 129.44, 130.12, 130.56, 130.88, 131.23, 131.36, 131.72, 131.97, 132.35, 133.02, 133.40, 134.58, 134.93, 135.47, 135.72, 137.03, 138.01, 141.00, 142.67, 157.47, 164.94, 165.92, 168.59, 168.83, 173.78, 173.93, 174.93. HRMS (ESI): *m/z* $[M+H]^+$ calcd for $[C_{52}H_{64}N_9O_6]^+$ 910.4980, found 910.4972. RP-HPLC (220 nm): 97% (t_R = 14.9 min, *k* = 15.2). $C_{52}H_{63}N_9O_6 \cdot C_4H_2F_6O_4$ (910.13 + 228.04).

(*S*)-2-Acetamido-*N*-((*S*)-1-(((*S*)-3-(4-hydroxyphenyl)-1-oxo-1-((2-(4-(4-(1-(2-oxo-2-(11-oxo-10,11-dihydro-5*H*-dibenzo[*b,e*][1,4]diazepin-5-yl)ethyl)piperidin-4-yl)butyl)piperazin-1-yl)ethyl)amino)propan-2-yl)amino)-1-oxopropan-2-yl)-3-(1*H*-indol-3-yl)propanamide tris(hydrotrifluoroacetate) (100) Purification by preparative HPLC (gradient: 0-25 min: 0.1% aq TFA/acetonitrile 90:10-50:50, t_R = 12 min) yielded **100** as a white fluffy solid (13 mg, 0.010 mmol, 27%). Ratio of configurational isomers evident in the NMR spectra: 1.6:1. ^{1}H-NMR (600 MHz, MeOH-d_4): δ (ppm) 1.13 (d, 3H, *J* 7.4 Hz), 1.26-1.54 (m, 7H), 1.60-1.68 (m, 1H), 1.81-1.97 (m, 2H), 2.01 (s, 3H), 2.80-2.95 (m, 4H), 2.95-3.29 (m, 13H), 3.32-3.49 (m, 4H), 3.66-3.81 (m, 2H), 4.02 (q, 1H, *J* 7.2 Hz), 4.28-4.32 (m, 1H), 4.39 (d, 0.6H, *J* 17 Hz), 4.43 (d, 0.4H, *J* 17 Hz), 4.50 (t, 1H, *J* 7.0 Hz), 6.69 (d, 2H, *J* 8.5 Hz), 6.99-7.03 (m, 3H), 7.10 (t, 1H, *J* 7.5 Hz), 7.27 (br s, 1H), 7.25-7.31 (m, 0.8H), 7.31-7.36 (m, 2.2H), 7.37-7.41 (m, 0.4H), 7.46-7.57 (m, 3.2H), 7.62-7.71 (m, 2H), 7.73-7.78 (m, 0.4H), 7.91 (d, 0.6H, *J* 8.7 Hz), 7.98 (d, 0.4H, *J* 7.9 Hz). ^{13}C-NMR (150.9 MHz, MeOH-d_4): δ (ppm) 16.97, 22.69 24.49, 25.15, 28.42, 30.37, 34.29, 36.12, 36.33, 37.13, 50.64, 51.59, 51.92, 54.92, 55.28, 56.80, 57.04, 57.13, 57.71, 57.96, 58.04, 110.62, 112.53,

116.29, 119.26, 119.96, 122.64, 123.09, 123.65, 124.78, 126.87, 127.52, 127.86, 128.48, 128.80, 128.88, 128.94, 129.44, 130.12, 130.57, 130.88, 131.18, 131.24, 131.98, 132.36, 133.02, 133.40, 134.58, 134.93, 135.47, 135.72, 137.04, 138.04, 141.01, 142.66, 157.41, 164.94, 165.42, 168.59, 168.84,174.16, 174.20, 175.29, 175.47. HRMS (ESI): *m/z* $[M+H]^+$ calcd for $[C_{55}H_{69}N_{10}O_7]^+$ 981.5351, found 981.5366. RP-HPLC (220 nm): 99% (t_R = 14.9 min, *k* = 15.2). $C_{55}H_{68}N_{10}O_7 \cdot C_4H_2F_6O_4$ (981.21 + 228.04).

(*S*)-2-Acetamido-*N*^{1}-((*S*)-3-methyl-1-oxo-1-((2-(4-(4-(1-(2-oxo-2-(11-oxo-10,11-dihydro-5*H*-dibenzo[*b,e*][1,4]diazepin-5-yl)ethyl)piperidin-4-yl)butyl)piperazin-1-yl)ethyl)amino)butan-2-yl)pentanediamide tris(hydrotrifluoroacetate) (101) Purification by preparative HPLC (gradient: 0-25 min: 0.1% aq TFA/acetonitrile 90:10-72:28, t_R = 11 min) yielded **101** as a white fluffy solid (23 mg, 0.020 mmol, 56%). Ratio of configurational isomers evident in the NMR spectra: 1.8:1. ^{1}H-NMR (600 MHz, MeOH-d_4): δ (ppm) 0.91 (d, 3H, *J* 6.5 Hz), 0.96 (d, 3H, *J* 6.5 Hz), 1.30-1.77 (m, 12H), 1.86-1.98 (m, 3H), 2.00 (s, 3H), 2.01-2.09 (m, 1H), 2.33 (t, 2H, *J* 7.5 Hz), 2.88-2.98 (m, 1H), 2.99-3.10 (m, 3H), 3.12-3.18 (m, 2H), 3.21-3.30 (m, 2H), 3.32-3.39 (m, 2H), 3.39-3.59 (m, 7H), 3.69-3.83 (m, 2H), 4.22-4.29 (m, 2H), 4.40 (d, 0.6H, *J* 17 Hz), 4.44 (d, 0.4H, *J* 17 Hz), 7.24-7.31 (m, 0.8H), 7.31-7.36 (m, 1.2H), 7.36-7.41 (m, 0.4H), 7.45-7.55 (m, 2.2H), 7.59-7.72 (m, 2H), 7.72-7.78 (m, 0.4H), 7.90 (dd, 0.6H, *J* 1.7 7.7 Hz), 7.97 (d, 0.4H, *J* 7.9 Hz). ^{13}C-NMR (150.9 MHz, MeOH-d_4): δ (ppm) 21.85, 22.54, 23.33, 24.45, 25.09, 25.88, 28.46, 30.39, 32.39, 34.28, 36.10, 36.20, 41.10, 50.71, 51.35, 53.90, 54.93, 55.08, 55.29, 57.37, 57.74, 57.94, 58.03, 123.08, 123.65, 126.85, 127.52, 127.87, 128.49, 128.88, 129.44, 130.11, 130.55, 130.88, 131.21, 131.71, 131.96, 132.35, 133.00, 133.41, 134.58, 134.94, 135.46, 135.72, 137.03, 141.01, 142.68, 164.97, 165.45, 168.58, 168.83, 173.89, 174.72, 175.52, 177.57. HRMS (ESI): *m/z* $[M+H]^+$ calcd for $[C_{43}H_{64}N_9O_6]^+$ 802.4980, found 802.4982. RP-HPLC (220 nm): 97% (t_R = 9.6 min, *k* = 9.4). $C_{43}H_{63}N_9O_6 \cdot C_4H_2F_6O_4$ (802.03 + 228.04).

(*S*)-2-Acetamido-*N*^{1}-((*S*)1-(((*S*)-4-methyl-1-oxo-1-((2-(4-(4-(1-(2-oxo-2-(11-oxo-10,11-dihydro-5*H*-dibenzo[*b,e*][1,4]diazepin-5-yl)ethyl)piperidin-4-yl)butyl)piperazin-1-yl)ethyl)amino)pentan-2-yl)amino)-1-oxopropan-2-yl)pentanediamide tris(hydrotrifluoroacetate) (102) Purification by preparative HPLC (gradient: 0-25 min: 0.1% aq TFA/acetonitrile 90:10-72:28, t_R = 11 min) yielded **102** as a white fluffy solid (25 mg, 0.021 mmol, 66%). Ratio of configurational isomers evident in the NMR spectra: 1.8:1. ^{1}H-NMR (600 MHz, MeOH-d_4): δ (ppm) 0.91 (d, 3H, *J* 6.5 Hz), 0.96 (d, 3H, *J* 6.4 Hz), 1.33-1.76 (m, 15H), 1.87-1.99 (m, 3H), 2.01 (s, 3H), 2.03-2.12 (m, 1H), 2.34 (t, 2H, *J* 7.5 Hz), 2.88-2.98 (m, 1H), 3.00-3.12 (m, 3H), 3.12-3.18 (m, 2H), 3.22-3.30 (m, 2H), 3.32-3.40 (m, 2H), 3.41-3.57 (m, 7H), 3.68-3.84 (m, 2H), 4.18-4.26 (m, 3H), 4.40 (d, 0.6H, *J* 17 Hz), 4.44 (d, 0.4H, *J* 17 Hz), 7.24-7.31 (m, 0.8H), 7.31-7.36 (m, 1.2H), 7.36-7.40 (m, 0.4H), 7.45-7.55 (m, 2.2H), 7.60-7.72 (m, 2H), 7.72-7.78 (m, 0.4H), 7.90 (dd, 0.6H, *J* 1.7 8.0 Hz), 7.97 (d,

0.4H, *J* 8.1 Hz). ^{13}C-NMR (150.9 MHz, MeOH-d_4): δ (ppm) 17.28, 21.80, 22.58, 23.33, 24.47, 25.11, 25.94, 28.27, 30.39, 32.33, 34.29, 36.11, 36.26, 40.95, 50.71, 51.38, 51.73, 54.02, 54.93, 55.29, 55.37, 57.23, 57.72, 57.94, 58.03, 123.08, 123.65, 126.85, 127.52, 127.87, 128.48, 128.88, 129.44, 130.11, 130.55, 130.88, 131.21, 131.71, 131.96, 132.35, 133.01, 133.41, 134.58, 134.94, 135.46, 135.72, 137.03, 141.01, 142.68, 164.97, 165.45, 168.57, 168.83, 174.05, 174.79, 175.53, 175.93, 177.56. HRMS (ESI): *m/z* $[M+H]^+$ calcd for $[C_{46}H_{69}N_{10}O_7]^+$ 873.5351, found 873.5346. RP-HPLC (220 nm): 96% (t_R = 10.1 min, *k* = 10.0). $C_{46}H_{68}N_{10}O_7 \cdot C_4H_2F_6O_4$ (873.11 + 228.04).

(*S*)-2-Acetamido-6-amino-*N*-((*S*)-3-(4-hydroxyphenyl)-1-oxo-1-((2-(4-(4-(1-(2-oxo-2-(11-oxo-10,11-dihydro-5*H*-dibenzo[*b,e*][1,4]diazepin-5-yl)ethyl)piperidin-4-yl)butyl)piperazin-1-yl)ethyl)amino)propan-2-yl)hexanamide tetrakis(hydrotrifluoroacetate) (103) Purification by preparative HPLC (gradient: 0-25 min: 0.1% aq TFA/acetonitrile 90:10-72:28, t_R = 9 min) yielded **103** as a white fluffy solid (22 mg, 0.017 mmol, 47%). Ratio of configurational isomers evident in the NMR spectra: 1.1:1. ^{1}H-NMR (600 MHz, MeOH-d_4): δ (ppm) 1.22-1.76 (m, 16H), 1.86-1.98 (m, 2H), 1.99 (s, 3H), 2.72-3.16 (m, 14H), 3.32-3.49 (m, 6H), 3.68-3.82 (m, 2H), 4.13-4.17 (m, 1H), 4.37-4.49 (m, 2H), 6.71 (d, 2H, *J* 8.5 Hz), 7.04 (d, 2H, *J* 8.5 Hz), 7.24-7.31 (m, 0.8H), 7.31-7.36 (m, 1.2H), 7.36-7.40 (m, 0.4H), 7.45-7.55 (m, 2.2H), 7.60-7.71 (m, 2H), 7.73-7.77 (m, 0.4H), 7.90 (dd, 0.6H, *J* 1.5 7.7 Hz), 7.97 (d, 0.4H, *J* 7.9 Hz). ^{13}C-NMR (150.9 MHz, MeOH-d_4): δ (ppm) 22.56, 23.59, 24.48, 25.11, 28.12, 30.39, 32.01, 34.29, 36.11, 36.65, 37.55, 40.42, 50.70, 51.93, 54.93, 55.28, 55.37, 56.50, 56.92, 57.73, 58.02, 116.31, 123.08, 123.65, 126.85, 127.52, 127.88, 128.49, 128.88, 128.96, 129.45, 130.10, 130.54, 130.88, 131.20, 131.39, 131.70, 131.95, 132.34, 133.00, 133.41, 134.57, 134.94, 135.46, 135.72, 137.02, 141.00, 142.68, 157.33, 164.96, 165.44, 168.57, 168.83, 173.91, 174.00, 174.24. HRMS (ESI): *m/z* $[M+H]^+$ calcd for $[C_{47}H_{66}N_9O_6]^+$ 852.5136, found 852.5145. RP-HPLC (220 nm): 97% (t_R = 7.9 min, *k* = 7.6). $C_{47}H_{65}N_9O_6 \cdot C_6H_3F_9O_6$ (852.09 + 342.07).

(*S*)-2-Acetamido-6-amino-*N*-((*S*)-1-(((*S*)-3-(4-hydroxyphenyl)-1-oxo-1-((2-(4-(4-(1-(2-oxo-2-(11-oxo-10,11-dihydro-5*H*-dibenzo[*b,e*][1,4]diazepin-5-yl)ethyl)piperidin-4-yl)butyl)piperazin-1-yl)ethyl)amino)propan-2-yl)amino)-1-oxopropan-2-yl)hexanamide tetrakis(hydrotrifluoroacetate) (104) Purification by preparative HPLC (gradient: 0-25 min: 0.1% aq TFA/acetonitrile 90:10-72:28, t_R = 9 min) yielded **104** as a white fluffy solid (27 mg, 0.020 mmol, 54%). Ratio of configurational isomers evident in the NMR spectra: 1.7:1. ^{1}H-NMR (600 MHz, MeOH-d_4): δ (ppm) 1.29 (d, 3H, *J* 7.2 Hz), 1.31-1.60 (m, 10H), 1.63-1.83 (m, 6H), 1.86-2.00 (m, 2H), 2.02 (s, 3H), 2.73-3.17 (m, 14H), 3.26-3.50 (m, 6H), 3.66-3.83 (m, 2H), 4.19-4.27 (m, 2H), 4.35-4.47 (m, 2H), 6.70 (d, 2H, *J* 8.5 Hz), 7.04 (d, 2H, *J* 8.5 Hz), 7.24-7.31 (m, 0.8H), 7.31-7.36 (m, 1.2H), 7.36-7.41 (m, 0.4H), 7.46-7.55 (m, 2.2H), 7.60-7.71 (m, 2H), 7.73-7.78 (m, 0.4H), 7.90 (dd, 0.6H, *J* 1.4 8.5 Hz),

7.97 (d, 0.4H, *J* 7.8 Hz). ^{13}C-NMR (150.9 MHz, MeOH-d_4): δ (ppm) 17.50, 22.55, 23.76, 24.49, 25.12, 28.13, 30.40, 32.15, 34.30, 36.12, 36.64, 37.65, 40.47, 50.72, 51.11, 51.95, 54.93, 55.18, 55.29, 56.82, 56.97, 57.34, 58.04, 116.31, 123.09, 123.65, 126.86, 127.52, 127.87, 128.48, 128.88, 128.91, 129.44, 130.11, 130.55, 130.88, 131.22, 131.26, 131.36, 131.71, 131.97, 132.35, 133.01, 133.41, 134.58, 134.94, 135.46, 135.72, 137.04, 141.01, 142.68, 157.38, 164.96, 165.44, 168.58, 168.83, 173.85, 173.88, 174.62, 175.09. HRMS (ESI): *m/z* $[M+H]^+$ calcd for $[C_{50}H_{71}N_{10}O_7]^+$ 923.5507, found 923.5505. RP-HPLC (220 nm): 95% (t_R = 8.1 min, *k* = 7.8). $C_{50}H_{70}N_{10}O_7 \cdot C_6H_3F_9O_6$ (924.18 + 342.07).

(*S*)-2-((*S*)-2-Acetamido-3-(4-hydroxyphenyl)propanamido)-6-amino-*N*-(2-(4-(4-(1-(2-oxo-2-(11-oxo-10,11-dihydro-5*H*-dibenzo[*b,e*][1,4]diazepin-5-yl)ethyl)piperidin-4-yl)butyl)piperazin-1-yl)ethyl)hexanamide tetrakis(hydrotrifluoroacetate) (105) Purification by preparative HPLC (gradient: 0-25 min: 0.1% aq TFA/acetonitrile 90:10-72:28, t_R = 10 min) yielded **105** as a white fluffy solid (23 mg, 0.017 mmol, 49%). Ratio of configurational isomers evident in the NMR spectra: 1.3:1. ^{1}H-NMR (600 MHz, MeOH-d_4): δ (ppm) 1.28-1.74 (m, 15H), 1.80-1.94 (m, 2.5H), 1.95 (s, 3H), 1.96-1.99 (m, 0.5H), 2.83-3.27 (m, 14H), 3.33-3.51 (m, 6H), 3.68-3.83 (m, 2H), 4.18-4.22 (m, 1H), 4.37-4.47 (m, 2H), 6.73 (d, 2H, *J* 8.5 Hz), 7.09 (d, 2H, *J* 8.5 Hz), 7.24-7.31 (m, 0.8H), 7.31-7.36 (m, 1.2H), 7.36-7.40 (m, 0.4H), 7.45-7.56 (m, 2.2H), 7.59-7.72 (m, 2H), 7.72-7.78 (m, 0.4H), 7.90 (dd, 0.6H, *J* 1.6 8.2 Hz), 7.97 (d, 0.4H, *J* 7.8 Hz). ^{13}C-NMR (150.9 MHz, MeOH-d_4): δ (ppm) 22.42, 23.70, 24.46, 25.07, 27.94, 30.38, 31.82, 34.29, 36.09, 36.45, 37.64, 40.45, 50.73, 51.67, 54.68, 54.93, 55.28, 57.11, 57.36, 57.23, 58.03, 116.37, 123.65, 126.85, 127.52, 127.88, 128.49, 128.73, 128.88, 129.45, 130.10, 130.54. 130.88, 131.21, 121.38, 131.70, 131.95, 132.34, 133.00, 133.41, 134.57, 134.94, 135.46, 135.71, 137.02, 141.00, 142.68, 157.43, 164.96, 165.44, 168.58, 168.83, 173.74, 174.37, 174.62. HRMS (ESI): *m/z* $[M+3H]^{3+}$ calcd for $[C_{47}H_{68}N_9O_6]^{3+}$ 284.8431, found 284.8434. RP-HPLC (220 nm): 98% (t_R = 8.2 min, *k* = 7.9). $C_{47}H_{65}N_9O_6 \cdot C_6H_3F_9O_6$ (852.09 + 342.07).

(*S*)-2-((*S*)-2-((*S*)-2-Acetamido-3-(4-hydroxyphenyl)propanamido)propanamido)-6-amino-*N*-(2-(4-(4-(1-(2-oxo-2-(11-oxo-10,11-dihydro-5*H*-dibenzo[*b,e*][1,4]diazepin-5-yl)ethyl)piperidin-4-yl)butyl)piperazin-1-yl)ethyl)hexanamide tetrakis(hydrotrifluoroacetate) (106) Purification by preparative HPLC (gradient: 0-25 min: 0.1% aq TFA/acetonitrile 90:10-72:28, t_R = 10 min) yielded **106** as a white fluffy solid (28 mg, 0.020 mmol, 56%). Ratio of configurational isomers evident in the NMR spectra: 1.6:1. ^{1}H-NMR (600 MHz, MeOH-d_4): δ (ppm) 1.30-1.36 (m, 4H), 1.37 (d, 3H, *J* 7.2 Hz), 1.39-1.58 (m, 6H), 1.64-1.79 (m, 5H), 1.82-1.94 (m, 2.5H), 1.95 (s, 3H), 1.96-1.98 (m, 0.5H), 2.85-3.22 (m, 14H), 3.34-3.56 (m, 6H), 3.69-3.83 (m, 2H), 4.16-4.22 (m, 2H), 4.35-4.47 (m, 2H), 6.71 (d, 2H *J* 8.5 Hz), 7.06 (d, 2H, *J* 8.5 Hz), 7.24-7.31 (m, 0.8H), 7.31-7.36 (m, 1.2H), 7.36-7.41 (m, 0.4H), 7.45-7.55 (m, 2.2H), 7.61-7.71 (m, 2H), 7.73-7.78 (m, 0.4H), 7.90 (dd,

0.6H, *J* 1.5 8.2 Hz), 7.97 (d, 0.4H, *J* 7.9 Hz). ^{13}C-NMR (150.9 MHz, MeOH-d_4): δ (ppm) 17.14 22.55, 23.82, 24.50, 25.17, 27.97, 30.40, 31.69, 34.31, 36.13, 36.43, 37.61, 40.45, 50.76, 51.59, 51.70, 54.93, 55.14, 55.29, 56.93, 57.66, 57.77, 58.03, 116.31, 123.08, 123.65, 126.86, 127.52, 127.87, 128.48, 128.75, 128.88, 129.44, 130.11, 130.55, 130.88, 131.22, 131.28, 131.71, 131.97, 132.35, 133.01, 133.41, 134.57, 134.94, 135.46, 135.72, 137.04, 141.01, 142.68, 157.44, 164.96, 165.44, 168.59, 168.83, 173.94, 174.66, 174.78, 175.65. HRMS (ESI): *m/z* $[M+3H]^{3+}$ calcd for $[C_{50}H_{73}N_{10}O_7]^{3+}$ 308.5221, found 308.5224. RP-HPLC (220 nm): 98% (t_R = 8.3 min, *k* = 8.0). $C_{50}H_{70}N_{10}O_7 \cdot C_6H_3F_9O_6$ (923.17 + 342.07).

(*S*)-2-Acetamido-6-amino-*N*-((*S*)-5-guanidino-1-oxo-1-((2-(4-(4-(1-(2-oxo-2-(11-oxo-10,11-dihydro-5*H*-dibenzo[*b,e*][1,4]diazepin-5-yl)ethyl)piperidin-4-yl)butyl)piperazin-1-yl)ethyl)amino)pentan-2-yl)hexanamide pentakis(hydrotrifluoroacetate) (107) Purification by preparative HPLC (gradient: 0-25 min: 0.1% aq TFA/acetonitrile 90:10-78:22, t_R = 8 min) yielded **107** as a white fluffy solid (27 mg, 0.019 mmol, 53%). Ratio of configurational isomers evident in the NMR spectra: 1.8:1. ^{1}H-NMR (600 MHz, MeOH-d_4): δ (ppm) 1.30-1.77 (m, 18H), 1.78-1.99 (m, 4H), 2.00 (s, 3H), 2.84-2.98 (m, 5H), 2.99-3.26 (m, 9H), 3.35-3.50 (m, 6H), 3.69-3.83 (m, 2H), 4.20-4.24 (m, 1H), 4.27-4.31 (m, 1H), 4.40 (d, 0.6H, *J* 17 Hz), 4.44 (d, 0.4H, *J* 17 Hz), 7.24-7.31 (m, 0.8H), 7.32-7.36 (m, 1.2H), 7.37-7.41 (m, 0.4H), 7.46-7.55 (m, 2.2H), 7.61-7.71 (m, 2H), 7.73-7.78 (m, 0.4H), 7.90 (dd, 0.6H, *J* 1.6 8.0 Hz), 7.97 (m, 0.4H, *J* 8.0 Hz). ^{13}C-NMR (150.9 MHz, MeOH-d_4): δ (ppm) 22.49, 23.89, 24.49, 25.14, 26.37, 28.09, 29.89, 30.39, 32.02, 34.30, 36.12, 36.69, 40.46, 41.89, 50.79, 51.92, 54.47, 54.93, 55.28, 55.35, 57.08, 57.73, 58.03, 123.08, 123.65, 126.85, 127.52, 127.88, 128.49, 128.88, 129.45, 130.10, 130.55, 130.88, 131.21, 131.71, 131.96, 132.34, 133.00, 133.41, 134.57, 134.94, 135.46, 135.72, 137.03, 141.01, 142.68, 158.67, 164.96, 165.45, 168.58, 168.83, 173.93, 174.29, 174.83. HRMS (ESI): *m/z* $[M+3H]^{3+}$ calcd for $[C_{44}H_{71}N_{12}O_5]^{3+}$ 282.5223, found 282.5232. RP-HPLC (220 nm): 98% (t_R = 5.9 min, *k* = 5.4). $C_{44}H_{68}N_{12}O_5 \cdot C_8H_4F_{12}O_8$ (845.11 + 456.09).

(*S*)-2-Acetamido-6-amino-*N*-((*S*)-1-(((*S*)-5-guanidino-1-oxo-1-((2-(4-(4-(1-(2-oxo-2-(11-oxo-10,11-dihydro-5*H*-dibenzo[*b,e*][1,4]diazepin-5-yl)ethyl)piperidin-4-yl)butyl)piperazin-1-yl)ethyl)amino)pentan-2-yl)amino)-1-oxopropan-2-yl)hexanamide pentakis(hydrotrifluoroacetate) (108) Purification by preparative HPLC (gradient: 0-25 min: 0.1% aq TFA/acetonitrile 90:10-78:22, t_R = 8 min) yielded **108** as a white fluffy solid (35 mg, 0.023 mmol, 65%). Ratio of configurational isomers evident in the NMR spectra: 1.8:1. ^{1}H-NMR (600 MHz, MeOH-d_4): δ (ppm) 1.31-1.57 (m, 12H), 1.58-1.99 (m, 13H), 2.01 (s, 3H), 2.84-2.97 (m, 5H), 3.00-3.25 (m, 9H), 3.35-3.53 (m, 6H), 3.68-3.83 (m, 2H), 4.18-4.22 (m, 1H), 4.23-4.30 (m, 2H), 4.40 (d, 0.6H, *J* 17 Hz), 4.44 (d, 0.4H, *J* 17 Hz), 7.23-7.31 (m, 0.8H), 7.32-7.36 (m, 1.2H), 7.36-7.41 (m, 0.4H), 7.45-7.55 (m, 2.2H), 7.61-7.71 (m, 2H), 7.73-7.78 (m, 0.4H), 7.90 (dd, 0.6H, *J* 1.7 7.6 Hz), 7.97 (d, 0.4H, *J* 7.9

Hz). ^{13}C-NMR (150.9 MHz, MeOH-d_4): δ (ppm) 17.34, 22.57, 23.83, 24.50, 25.16, 26.31, 28.14, 29.72, 30.40, 32.04, 34.31, 36.14, 36.71, 40.44, 41.90, 50.81, 51.25, 52.00, 54.68, 54.92, 55.29, 55.51, 57.06, 57.74, 58.03, 123.09, 123.65, 126.86, 127.52, 127.87, 128.48, 128.88, 129.44, 130.11, 130.55, 130.88, 131.21, 131.71, 131.97, 132.35, 133.01, 133.42, 134.58, 134.94, 135.46, 135.72, 137.04, 141.01, 142.68, 158.67, 164.96, 165.44, 168.58, 168.84, 174.09, 174.28, 174.84, 175.56. HRMS (ESI): *m/z* $[M+3H]^{3+}$ calcd for $[C_{47}H_{76}N_{13}O_6]^{3+}$ 306.2014, found 306.2017. RP-HPLC (220 nm): 98% (t_R = 5.9 min, k = 5.4). $C_{47}H_{73}N_{13}O_6 \cdot C_8H_4F_{12}O_8$ (916.19 + 456.09).

4.4.4 Cell Culture

CHO-K9 cell lines stably expressing the human M_1-M_5 muscarinic receptors were obtained from the Missouri S&T cDNA Resource Center (Rolla, MO). Cells were cultured in HAM's F12 medium supplemented with fetal calf serum (Biochrom, Berlin, Germany) (10%) and G418 (Biochrom) (750 µg/mL).

4.4.5 Radioligand competition binding

Radioligand competition binding experiments at live CHO-hM_xR cells (x = 1-5) were performed in white 96-well plates with clear bottom (Corning Life Sciences, Tewksbury, MA; Corning cat. no. 3610) at 23 ± 1 °C using the protocol of previously described MR binding studies with [^{3}H]NMS.[23] Leibovitz L-15 medium (Gibco, Life Technologies GmbH, Darmstadt, Germany) supplemented with 1% BSA (Serva, Heidelberg, Germany) was used as binding buffer. The concentration of [^{3}H]NMS was 0.2 nM (M_1, M_2, M_3), 0.1 nM (M_4) or 0.3 nM (M_5) and the incubation time was 3 h throughout. Unspecific binding was determined in the presence of atropine (**2**) (500-fold excess to [^{3}H]NMS).

4.4.6 Data processing

Total binding data (DPM) from radioligand competition binding experiments (determination of the effect of compounds **85** and **87-108** on the equilibrium binding of [^{3}H]NMS) were plotted against log(concentration competitor) and analyzed by a four-parameter logistic equation (log(inhibitor) vs. response-variable slope) (GraphPad Prism Software 6.0, GraphPad Software, San Diego, CA) followed by normalization (100% = 'top' of the four-parameter logistic fit, 0% = unspecifically bound radioligand (DPM) determined in the presence of **2**) and analysis of the normalized data by a four-parameter logistic equation

fused to the Cheng-Prusoff equation (logarithmic form) (equation 1) to obtain pIC_{50} and pK_i values.

(equation 1)

$$Y = \frac{Top - Bottom}{1 + 10^{(LogIC50 - X) * HillSlope}} + Bottom$$

$$logIC50 = \log\left(10^{logKi} * \left(1 + \frac{HotNM}{HotKdNM}\right)\right)$$

HotNM = radioligand concentration in nM, HotKdNM = Dissociation constant (K_d) of the radioligand in nM.

4.5. References

(1) Eglen, R. M. Overview of muscarinic receptor subtypes. *Handb. Exp. Pharmacol.* **2012**, 3-28.

(2) Gregory, K. J.; Sexton, P. M.; Christopoulos, A. Allosteric modulation of muscarinic acetylcholine receptors. *Curr. Neuropharmacol.* **2007,** *5*, 157-167.

(3) Eglen, R. M.; Choppin, A.; Watson, N. Therapeutic opportunities from muscarinic receptor research. *Trends Pharmacol. Sci.* **2001,** *22*, 409-414.

(4) Sheardown, M. J. Muscarinic M1receptor agonists and M2 receptor antagonists as therapeutic targets in Alzheimer's disease. *Expert Opin. Ther. Pat.* **2002,** *12*, 863-870.

(5) Clader, J. W.; Wang, Y. Muscarinic receptor agonists and antagonists in the treatment of Alzheimer's disease. *Curr. Pharm. Des.* **2005,** *11*, 3353-3361.

(6) Citron, M. Alzheimer's disease: strategies for disease modification. *Nat. Rev. Drug Discovery* **2010,** *9*, 387-398.

(7) Kruse, A. C.; Ring, A. M.; Manglik, A.; Hu, J.; Hu, K.; Eitel, K.; Hubner, H.; Pardon, E.; Valant, C.; Sexton, P. M.; Christopoulos, A.; Felder, C. C.; Gmeiner, P.; Steyaert, J.; Weis, W. I.; Garcia, K. C.; Wess, J.; Kobilka, B. K. Activation and allosteric modulation of a muscarinic acetylcholine receptor. *Nature* **2013,** *504*, 101-106.

(8) Teller, H.; Straub, A.; Brechmann, M.; Mueller, T.; Meininghaus, M.; Nowak-Reppel, K.; Tinel, H.; Muenter, K.; Fliegner, D.; Mondritzki, T.; Boultadakis Arapinis, M.; Marquardt, T.; Vakalopoulos, A.; Rebstock, A.-S.; Wittwer, M. Naphthyridinecarboxamides as positive allosteric modulators of muscarinic M2 receptor and their preparation. 2016-EP62737 2016198342, 20160606., **2016**.

(9) Miao, Y.; Goldfeld, D. A.; Von Moo, E.; Sexton, P. M.; Christopoulos, A.; McCammon, J. A.; Valant, C. Accelerated structure-based design of chemically diverse allosteric modulators of a muscarinic G protein-coupled receptor. *Proc. Natl. Acad. Sci. U. S. A.* **2016,** *113*, E5675-E5684.

(10) Kruse, A. C.; Kobilka, B. K.; Gautam, D.; Sexton, P. M.; Christopoulos, A.; Wess, J. Muscarinic acetylcholine receptors: novel opportunities for drug development. *Nat. Rev. Drug Discovery* **2014,** *13*, 549-560.

(11) Birdsall, N. J. M.; Lazareno, S. Allosterism at muscarinic receptors: ligands and mechanisms. *Mini-Rev. Med. Chem.* **2005,** *5*, 523-543.

(12) Antony, J.; Kellershohn, K.; Mohr-Andra, M.; Kebig, A.; Prilla, S.; Muth, M.; Heller, E.; Disingrini, T.; Dallanoce, C.; Bertoni, S.; Schrobang, J.; Trankle, C.; Kostenis, E.; Christopoulos, A.; Holtje, H. D.; Barocelli, E.; De Amici, M.; Holzgrabe, U.; Mohr, K. Dualsteric GPCR targeting: a novel route to binding and signaling pathway selectivity. *FASEB J.* **2009,** *23*, 442-450.

(13) De Amici, M.; Dallanoce, C.; Holzgrabe, U.; Trankle, C.; Mohr, K. Allosteric ligands for G protein-coupled receptors: a novel strategy with attractive therapeutic opportunities. *Med. Res. Rev.* **2010,** *30*, 463-549.

(14) Valant, C.; Robert Lane, J.; Sexton, P. M.; Christopoulos, A. The best of both worlds? Bitopic orthosteric/allosteric ligands of g protein-coupled receptors. *Annu. Rev. Pharmacool. Toxicol.* **2012,** *52*, 153-178.

(15) Lane, J. R.; Sexton, P. M.; Christopoulos, A. Bridging the gap: bitopic ligands of G-protein-coupled receptors. *Trends Pharmacol. Sci.* **2013,** *34*, 59-66.

(16) Christopoulos, A. Advances in G protein-coupled receptor allostery: from function to structure. *Mol. Pharmacol.* **2014,** *86*, 463-478.

(17) Gitler, M. S.; Reba, R. C.; Cohen, V. I.; Rzeszotarski, W. J.; Baumgold, J. A novel M2-selective muscarinic antagonist: binding characteristics and autoradiographic distribution in rat brain. *Brain Res.* **1992,** *582*, 253-260.

(18) Martin, J.; Deagostino, A.; Perrio, C.; Dauphin, F.; Ducandas, C.; Morin, C.; Desbene, P. L.; Lasne, M. C. Syntheses of R and S isomers of AF-DX 384, a selective antagonist of muscarinic M2 receptors. *Bioorg. Med. Chem.* **2000,** *8*, 591-600.

(19) Keller, M.; Trankle, C.; She, X.; Pegoli, A.; Bernhardt, G.; Buschauer, A.; Read, R. W. M2 Subtype preferring dibenzodiazepinone-type muscarinic receptor ligands: Effect of chemical homo-dimerization on orthosteric (and allosteric?) binding. *Bioorg Med Chem* **2015,** *23*, 3970-3990.

(20) Chiarini, A.; Burdriesi, R.; Bolognsei, M. L.; Minarini, A.; Melchiorre, C. In vitro characterization of tripitramine, a polymethylene tetraamine displaying high selectivity and affinity for muscarinic M2 receptors. *Br. J. Pharmacol.* **1995,** *114*, 1507-1517.

(21) Trankle, C.; Andresen, I.; Lambrecht, G.; Mohr, K. M2 receptor binding of the selective antagonist AF-DX 384: possible involvement of the common allosteric site. *Mol. Pharmacol.* **1998,** *53*, 304-312.

(22) Doerje, F.; Wess, J.; Lambrecht, G.; Tacke, R.; Mutschler, E.; Brann, M. R. Antagonist binding profiles of five cloned human muscarinic receptor subtypes. *J. Pharmacol. Exp. Ther.* **1991,** *256*, 727-733.

(23) Keller, M.; Trankle, C.; She, X.; Pegoli, A.; Bernhardt, G.; Buschauer, A.; Read, R. W. M2 Subtype preferring dibenzodiazepinone-type muscarinic receptor ligands: Effect of chemical homo-dimerization on orthosteric (and allosteric?) binding. *Bioorg. Med. Chem.* **2015,** *23*, 3970-3990.

(24) Doods, H. N.; Quirion, R.; Mihm, G.; Engel, W.; Rudolf, K.; Entzeroth, M.; Schiavi, G. B.; Ladinsky, H.; Bechtel, W. D.; et al. Therapeutic potential of CNS-active M2 antagonists: novel structures and pharmacology. *Life Sci.* **1993,** *52*, 497-503.

(25) Maggio, R.; Barbier, P.; Bolognesi, M. L.; Minarini, A.; Tedeschi, D.; Melchiorre, C. Binding profile of the selective muscarinic receptor antagonist tripitramine. *Eur. J. Pharmacol.* **1994,** *268*, 459-462.

(26) McCombie, S. W.; Lin, S. I.; Tagat, J. R.; Nazareno, D.; Vice, S.; Ford, J.; Asberom, T.; Leone, D.; Kozlowski, J. A.; Zhou, G.; Ruperto, V. B.; Duffy, R. A.; Lachowicz, J. E. Synthesis and structure-activity relationships of M(2)-selective muscarinic receptor ligands in the 1-[4-(4-arylsulfonyl)-phenylmethyl]-4-(4-piperidinyl)-piperazine family. *Bioorg. Med. Chem. Lett.* **2002,** *12*, 795-798.

(27) Bohme, T. M.; Keim, C.; Kreutzmann, K.; Linder, M.; Dingermann, T.; Dannhardt, G.; Mutschler, E.; Lambrecht, G. Structure-activity relationships of dimethindene derivatives as new M2-selective muscarinic receptor antagonists. *J. Med. Chem.* **2003,** *46*, 856-867.

(28) She, X. Synthesis and pharmacological characterization of dibenzodiazepinone-type heterodimeric and fluorescently labeled muscarinic receptor ligands. Doctoral thesis, University of Regensburg, Regensburg, Germany, **2017**.

(29) Keller, M.; Kuhn, K. K.; Einsiedel, J.; Hubner, H.; Biselli, S.; Mollereau, C.; Wifling, D.; Svobodova, J.; Bernhardt, G.; Cabrele, C.; Vanderheyden, P. M.; Gmeiner, P.; Buschauer, A. Mimicking of Arginine by Functionalized N(omega)-Carbamoylated Arginine As a New Broadly Applicable Approach to Labeled Bioactive Peptides: High Affinity Angiotensin, Neuropeptide Y, Neuropeptide FF, and Neurotensin Receptor Ligands As Examples. *J Med Chem* **2016,** *59*, 1925-1945.

(30) Joullie, M. M.; Lassen, K. M. Evolution of amide bond formation. *ARKIVOC (Gainesville, FL, United States)* **2010**, 189-250.

(31) Haga, K.; Kruse, A. C.; Asada, H.; Yurugi-Kobayashi, T.; Shiroishi, M.; Zhang, C.; Weis, W. I.; Okada, T.; Kobilka, B. K.; Haga, T.; Kobayashi, T. Structure of the human M2 muscarinic acetylcholine receptor bound to an antagonist. *Nature* **2012,** *482*, 547-551.

(32) Dror, R. O.; Green, H. F.; Valant, C.; Borhani, D. W.; Valcourt, J. R.; Pan, A. C.; Arlow, D. H.; Canals, M.; Lane, J. R.; Rahmani, R.; Baell, J. B.; Sexton, P. M.; Christopoulos, A.; Shaw, D. E. Structural basis for modulation of a G-protein-coupled receptor by allosteric drugs. *Nature* **2013,** *503*, 295-299.

(33) Birdsall, N. J. M.; Brown, D. A.; Buckley, N. J.; Christopoulos, A.; Eglen, R. M.; Ehlert, F.; Hammer, R.; Kilbinger, H. J.; Lambrecht, G.; Mitchelson, F.; Mutschler, E.; Nathanson, N. M.; Schwarz, R. D.; Tobin, A. B.; Wess, J. Acetylcholine receptors (muscarinic): M2 receptor. http://www.guidetopharmacology.org/GRAC/ObjectDisplayForward?objectId=14. (Accessed on 13/03/2017).

Chapter 5
Summary

In humans, the family of muscarinic acetylcholine receptors (mAChR, MRs) comprises five subtypes (M_1R-M_5R), which are members of the class A GPCR superfamily and mediate the action of the neurotransmitter acetylcholine in the central and peripheral nervous system. For instance, the M_2R, which binds to $G_{i/o}$ heterotrimeric G-proteins, acts as a presynaptic autoreceptor in the brain and in the periphery. Accordingly, selective M_2R antagonism in the CNS results in an enhanced cholinergic transmission, representing a potential therapeutic approach to increase cholinergic function in Alzheimer patients. The development of high affinity and selective MR ligands has been hampered by the high conservation of the orthosteric (acetylcholine) binding site within the five MR subtypes. Therefore, highly selective molecular tools and therapeutic agents, acting at MRs, are lacking. MRs possess various accessory (allosteric) binding sites, which are less conserved. This prompted the design of numerous allosteric MR ligands. However, allosteric modulators with high MR affinity (K_i < 0.1 µM) are not described to date. The dualsteric ligand approach, that means, the design of ligands, which simultaneously bind to the orthosteric pocket and an allosteric site, was suggested as a promising strategy to develop high-affinity and highly selective MR ligands.

In order to investigate the binding mode of dibenzodiazepinone-type MR antagonists at the M_2R, three radiolabeled compounds, a monomeric ([^{3}H]**19**) and two homodimeric ([^{3}H]**33**, [^{3}H]**47**) derivatives, were prepared. The results from various detailed experiments performed with [^{3}H]**19** and [^{3}H]**33**, in particular saturation binding studies in the absence and in the presence of reported allosteric M_2R ligands, strongly suggested that the studied type of M_2R antagonists bind dualsterically to the M_2R, interacting simultaneously with both, the orthosteric and the 'common' allosteric binding site. The results from molecuclar dynamics (MD) simulations, performed with the M_2R (inactive state) bound to **19** or **33**, were consistent with the conclusions drawn from radioligand binding studies. Interestingly, the homodimeric ligand **33**, in contrast to the monomeric ligand **19**, showed a long residence time at the M_2R, which might be attributed, as also suggested by MD simulations, to additional contacts of **33** with amino acids constituting the allosteric vestibule.

Moreover, five fluorescently labeled dibenzodiazepinone-type MR ligands (including two homodimeric and one heterodimeric derivative) were prepared using red-emitting cyanine dyes. Equilibrium competition binding studies with the orthosteric antagonist [^{3}H]NMS revealed high M_2R affinities for all fluorescent ligands (pK_i = 8.85-9.59). Flow cytometric and high-content imaging-based binding experiments with a monomeric (**62**) and a homodimeric (**64**) fluorescent ligand in the presence of the reported allosteric modulator W84 (**8**) suggested that the fluorescent dibenzodiazepinone-type MR ligands bind dualsterically to the M_2R, as also concluded for the tritium-labeled analogs [^{3}H]**19** and [^{3}H]**33**. Confocal microscopy with **62** and **64** at CHO-hM_2R cells revealed that binding of the fluorescent probes occurred mainly at the cell membrane, and an increase of intracellular fluorescence was not observed with increasing incubation time.

Finally, aiming at MR ligands with improved M_2R selectivity, the dibenzodiazepinone pharmacophore was conjugated to several di- and tripeptides via two different linkers yielding a series of non-peptide/peptide hybrid ligands (DIBA-peptide conjugates). The affinity and the selectivity profile of these compounds was assessed by radioligand competition binding at CHO-hM_xR cells (x = 1-5) using [^{3}H]NMS. The introduction of two basic amino acids (Arg, Lys) yielded the DIBA-peptide conjugates with the highest M_2R selectivity (compound **96** (aliphatic linker, peptide sequence Lys-Arg): K_i M_1R:M_2R:M_3R:M_4R:M_5R = 58:1:6900:99:300; compound **108** (basic linker, peptide sequence Lys-Ala-Arg): K_i M_1R:M_2R:M_3R:M_4R:M_5R = 49:1:1800:70:3500). The DIBA-peptide conjugates **96** and **108** represent the most selective M_2R antagonists reported to date with M_2R binding constants in the low nanomolar (**96**, pK_i = 9.00) and in the picomolar (**108**, pK_i = 10.21) range. Thus, this new class of compounds represents a valuable basis for the development of high affinity and highly selective M_2R antagonists.

Taken together, the present work afforded new radio- and fluorescence labeled molecular tools, which bind with high affinity to the M_2R. Moreover, the conjugation of the dibenzodiazepinone pharmacophore to short peptides yielded high affinity M_2R ligands with improved M_2R selectivity compared to previously reported M_2 subtype preferring MR ligands.

Chapter 6
Appendix

6.1 NMR spectra

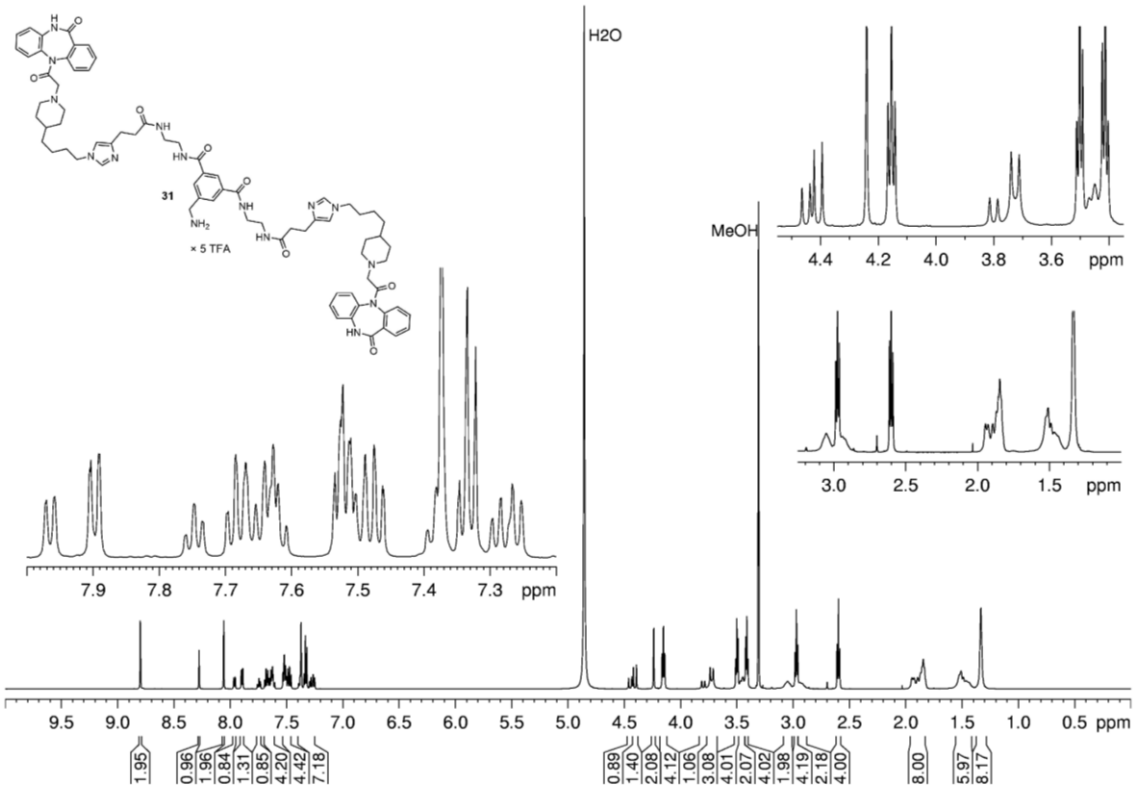

^{1}H-NMR spectrum (600 MHz, MeOH-d_4) of compound **31**.

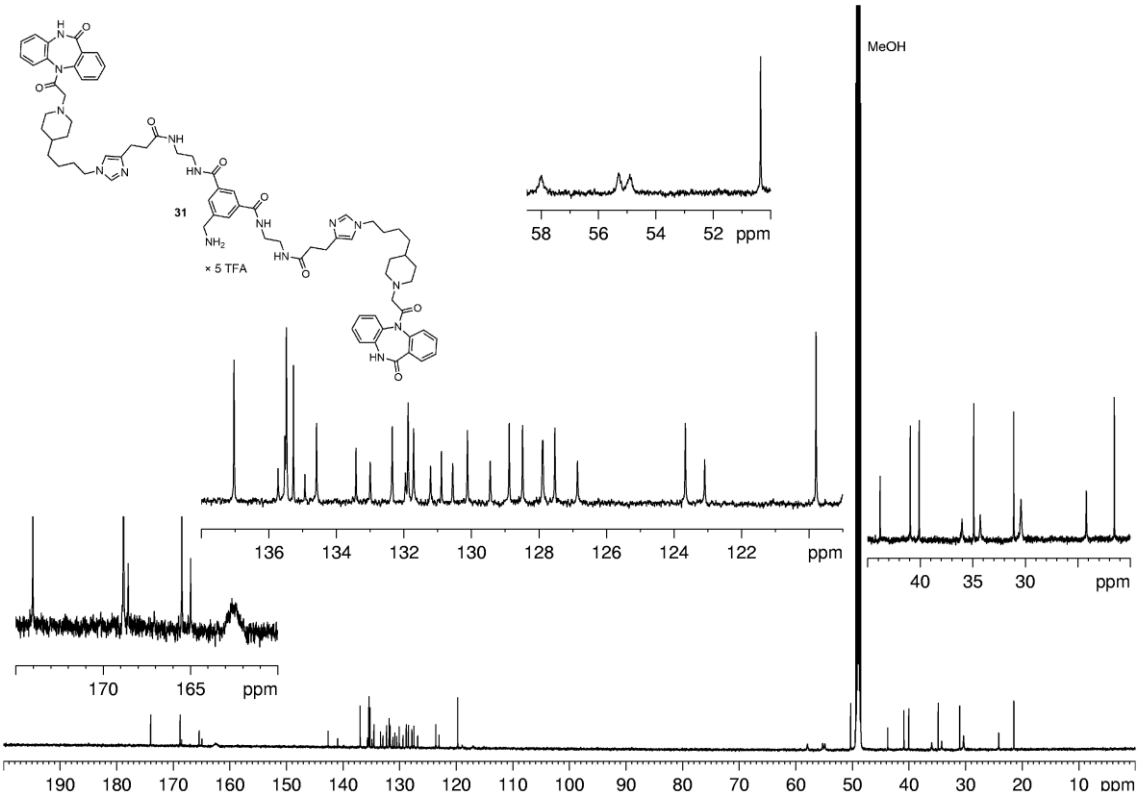

^{13}C-NMR spectrum (150 MHz, MeOH-d_4) of compound **31**.

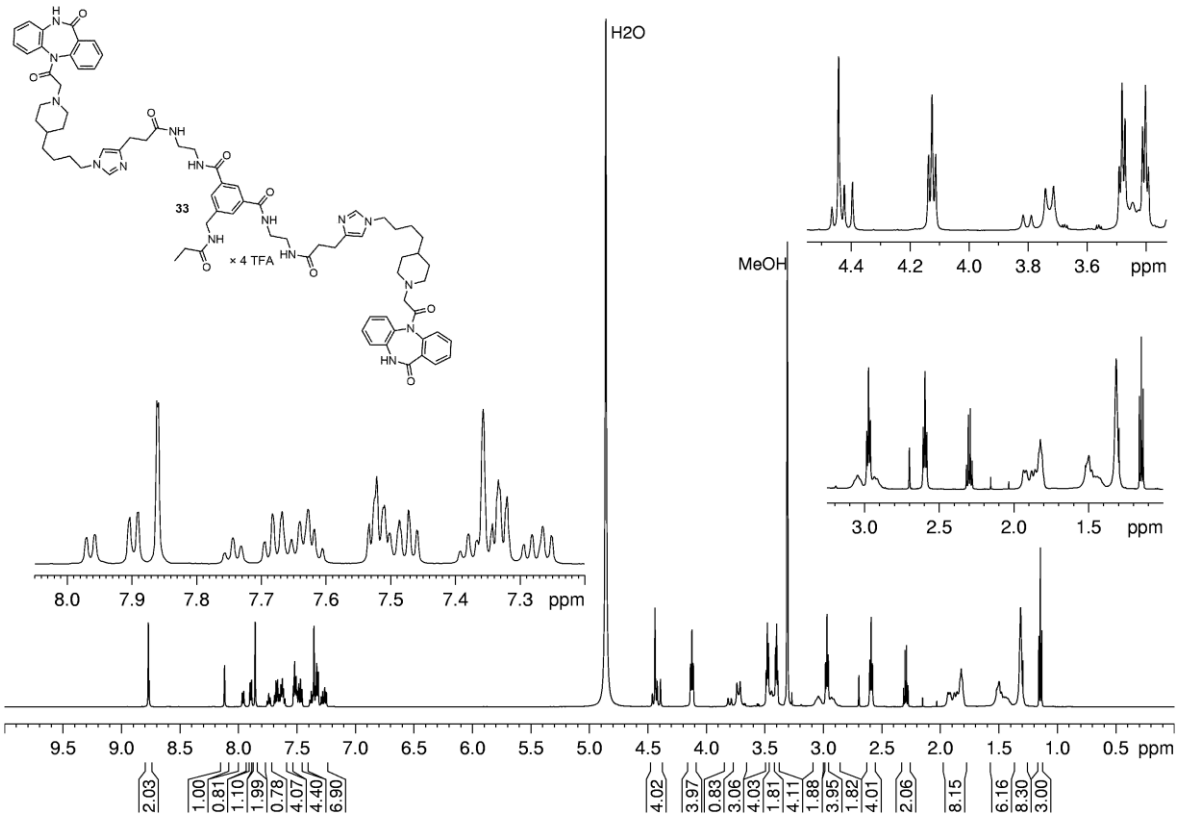

^{1}H-NMR spectrum (600 MHz, MeOH-d_4) of compound **33**.

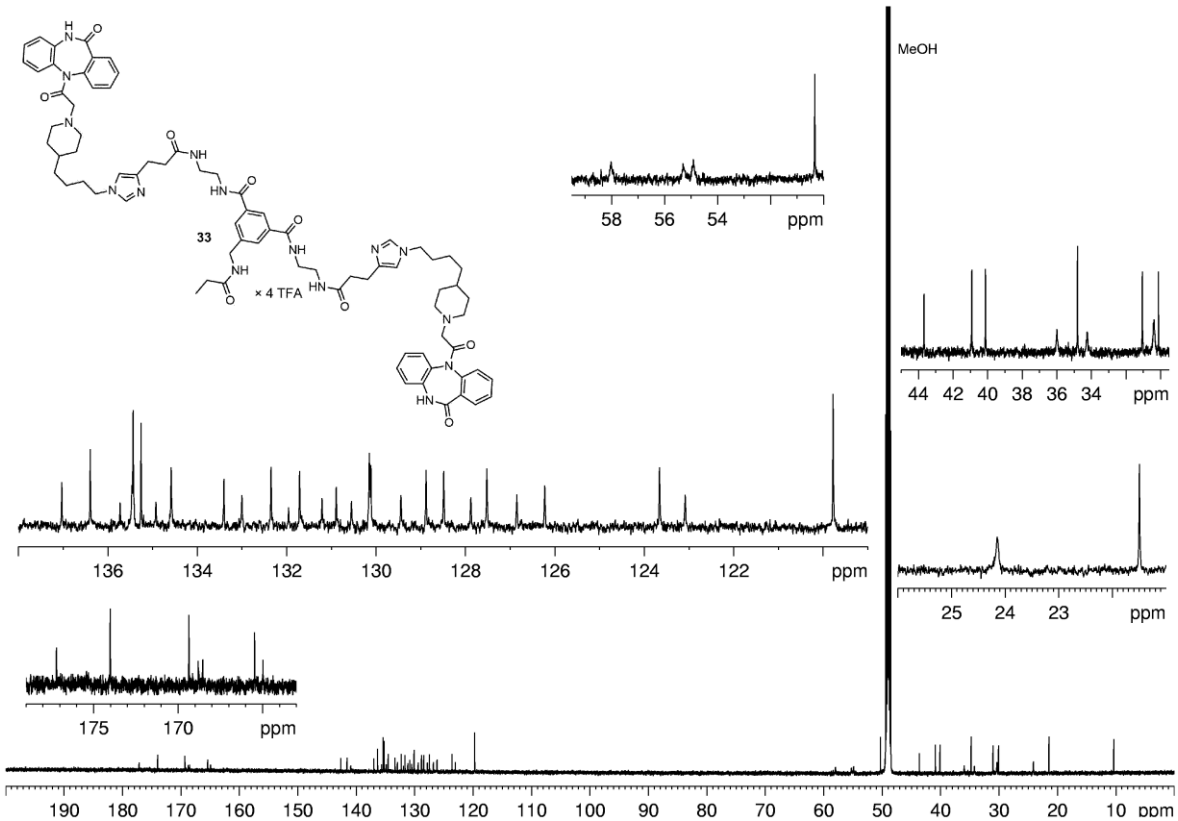

^{13}C-NMR spectrum (150 MHz, MeOH-d_4) of compound **33**.

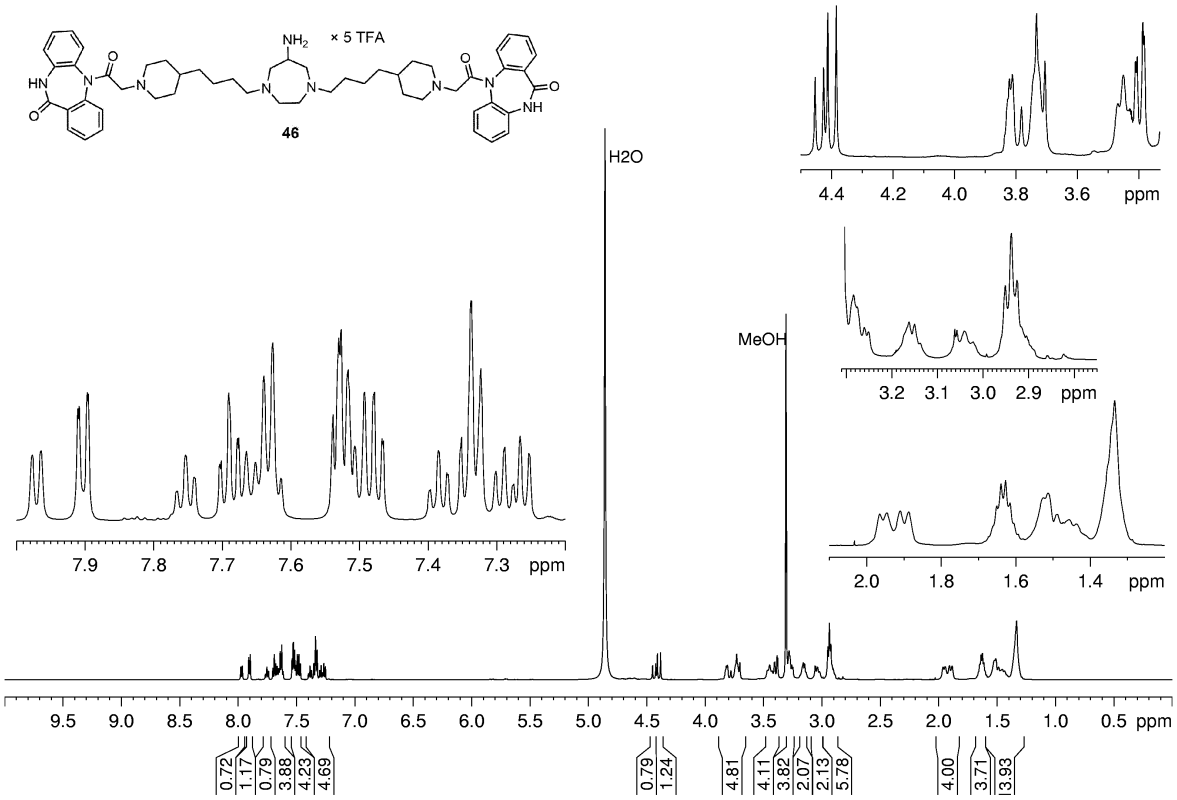

^{1}H-NMR spectrum (600 MHz, MeOH-d_4) of compound **46**.

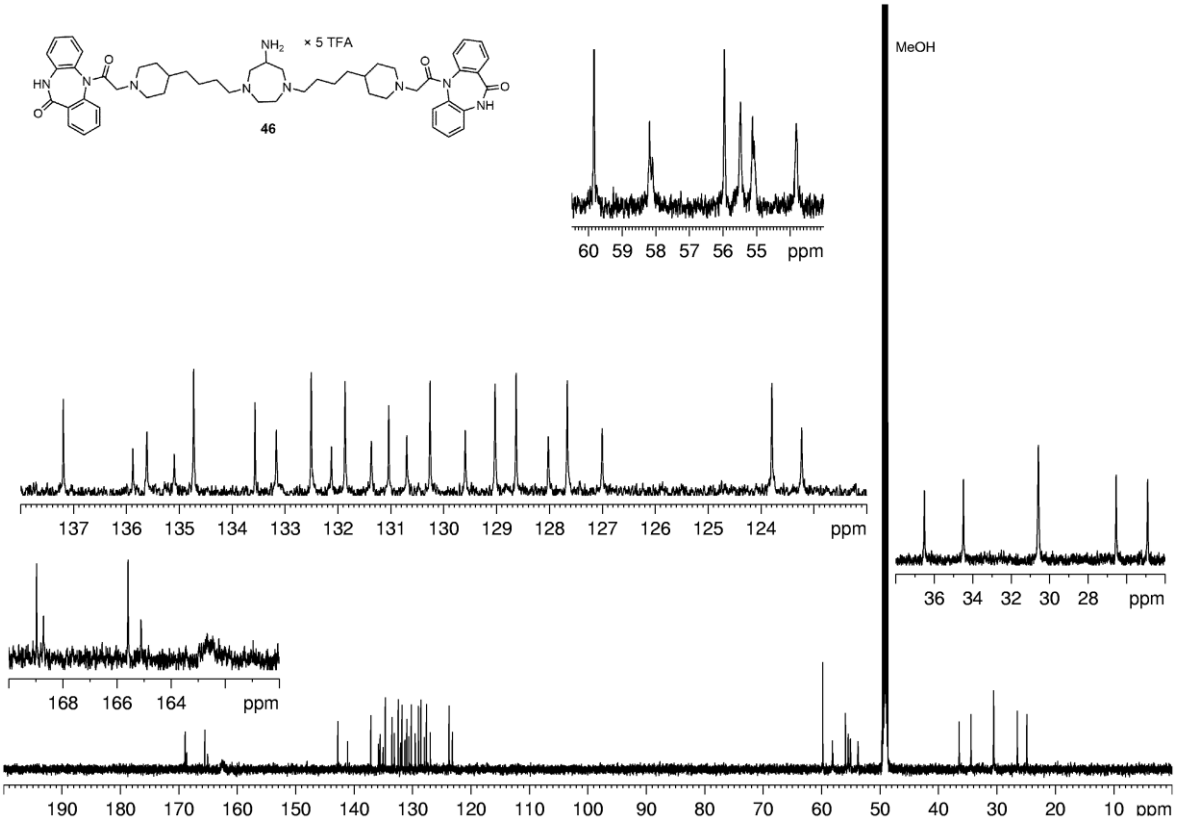

^{13}C-NMR spectrum (150 MHz, MeOH-d_4) of compound **46**.

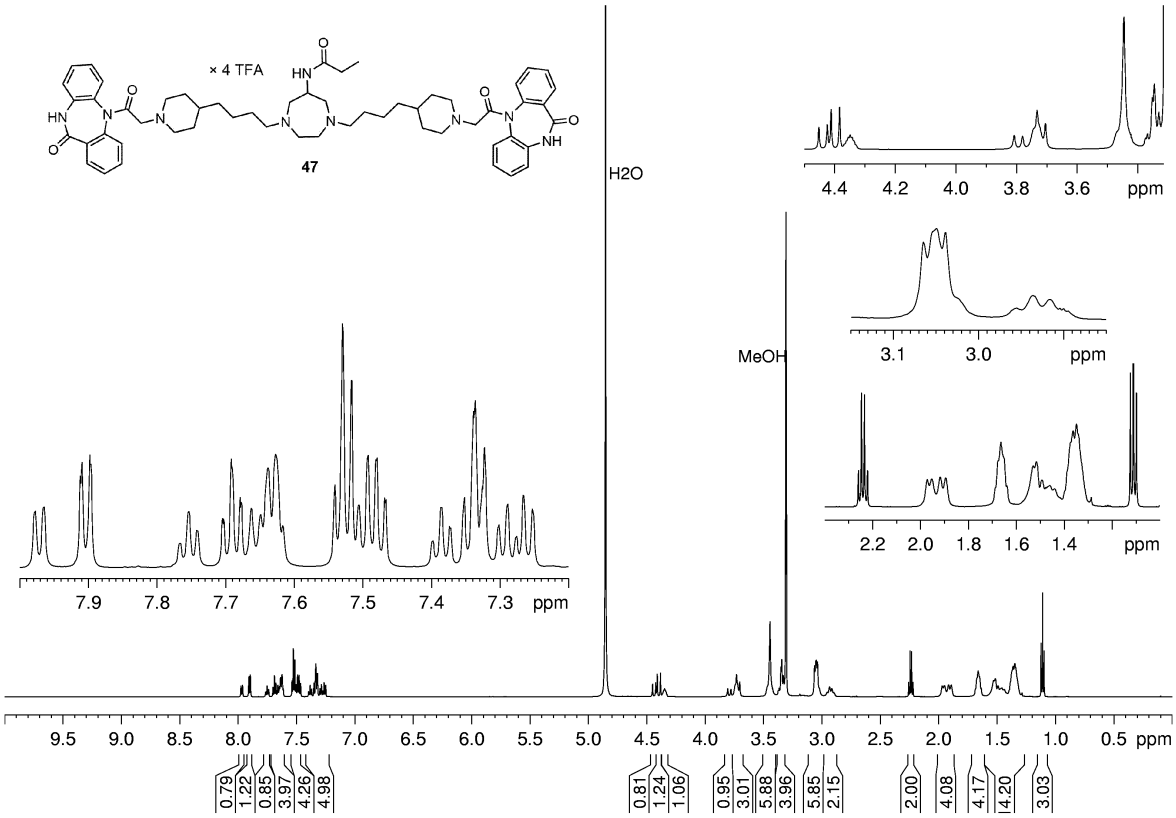

^{1}H-NMR spectrum (600 MHz, MeOH-d_4) of compound **47**.

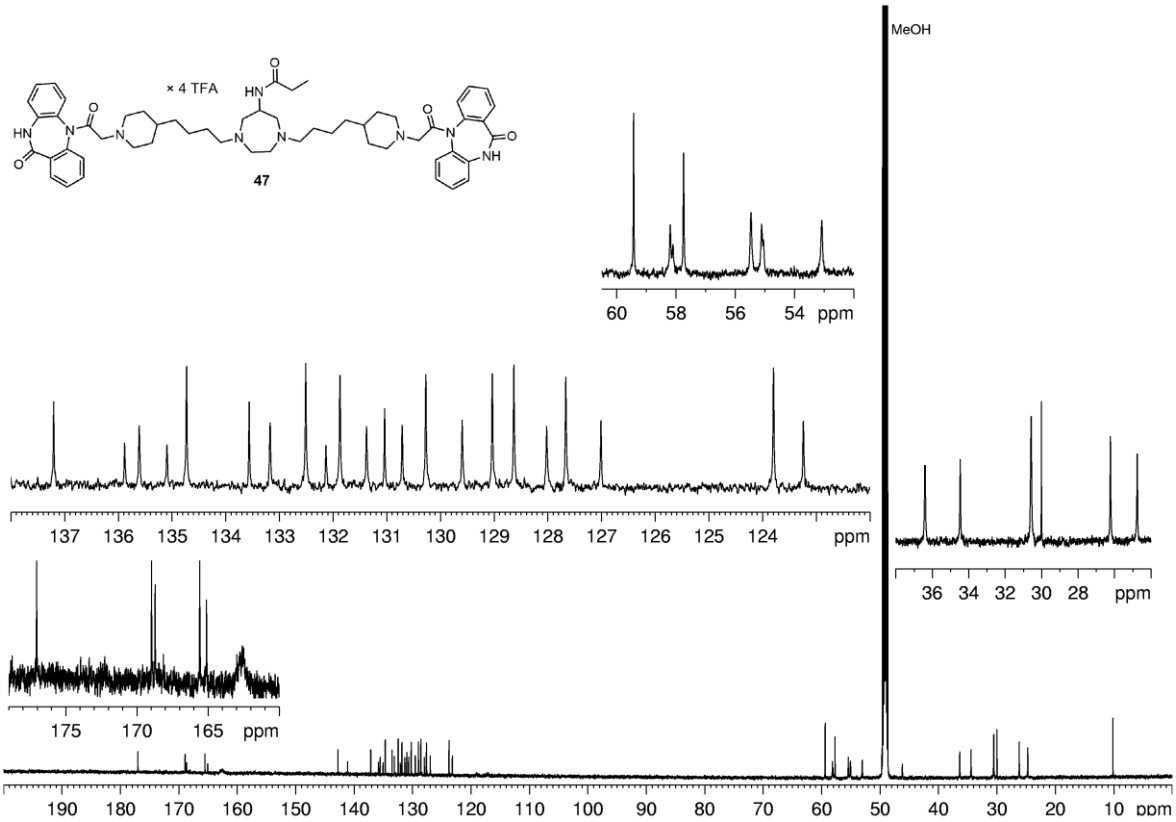

^{13}C-NMR spectrum (150 MHz, MeOH-d_4) of compound **47**.

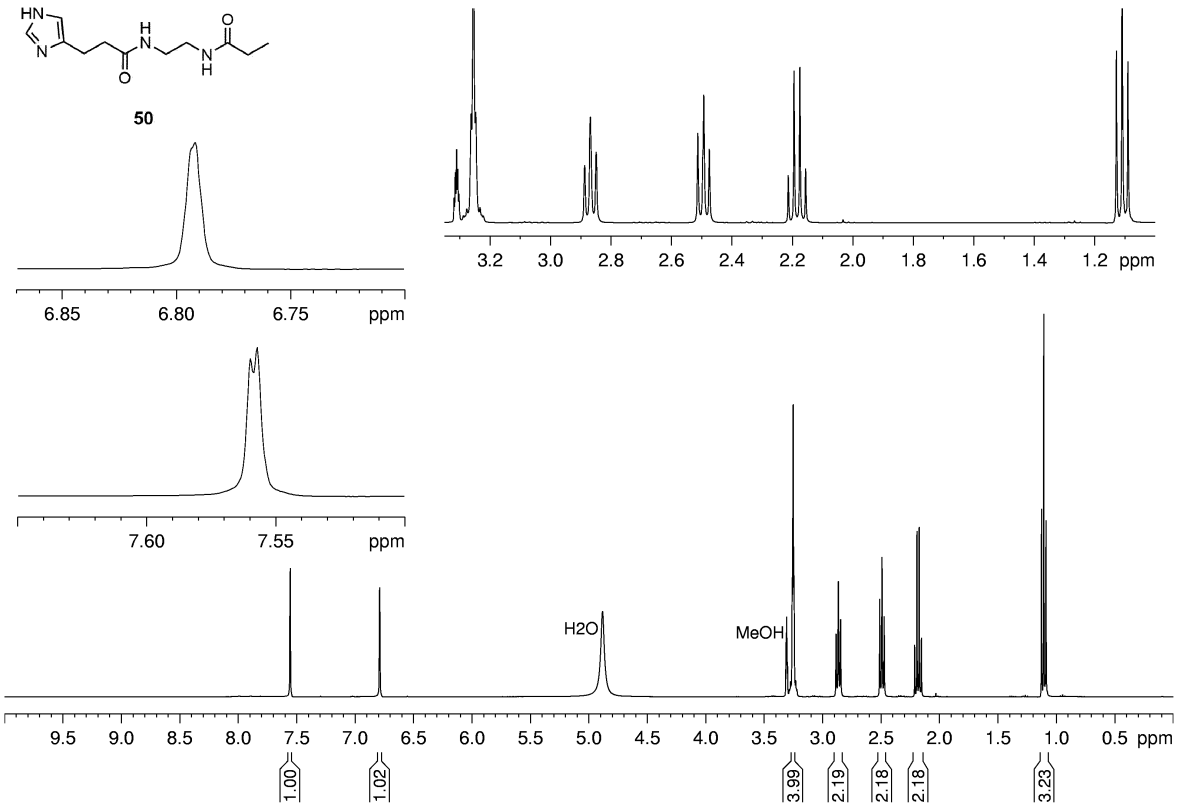

^{1}H-NMR spectrum (400 MHz, MeOH-d_4) of compound **50**.

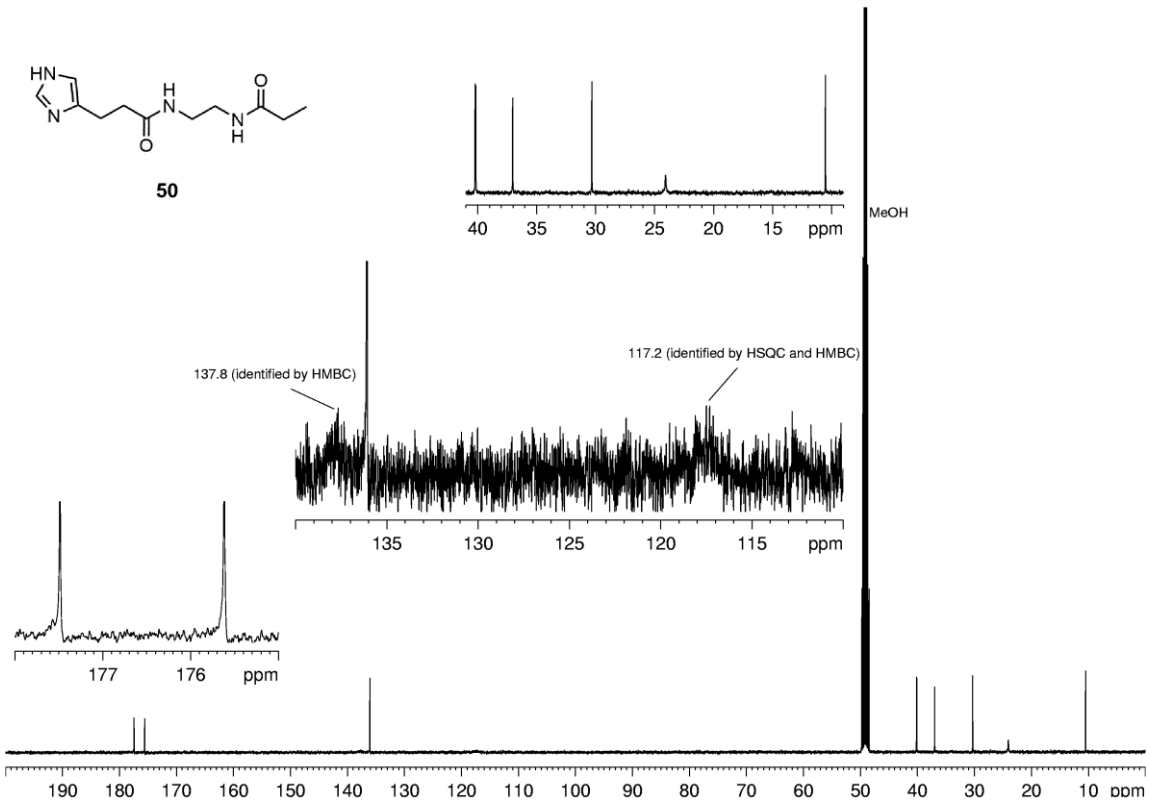

^{13}C-NMR spectrum (100 MHz, MeOH-d_4) of compound **50**.

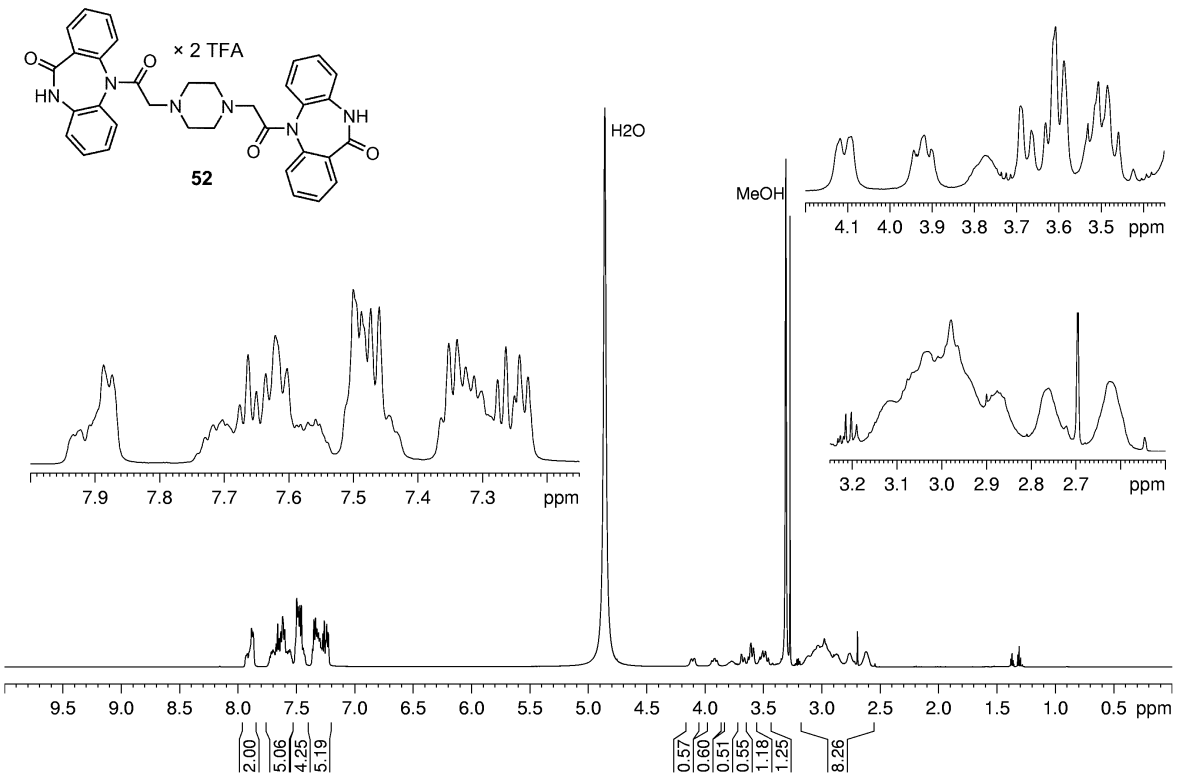

^{1}H-NMR spectrum (600 MHz, MeOH-d_4) of compound **52**.

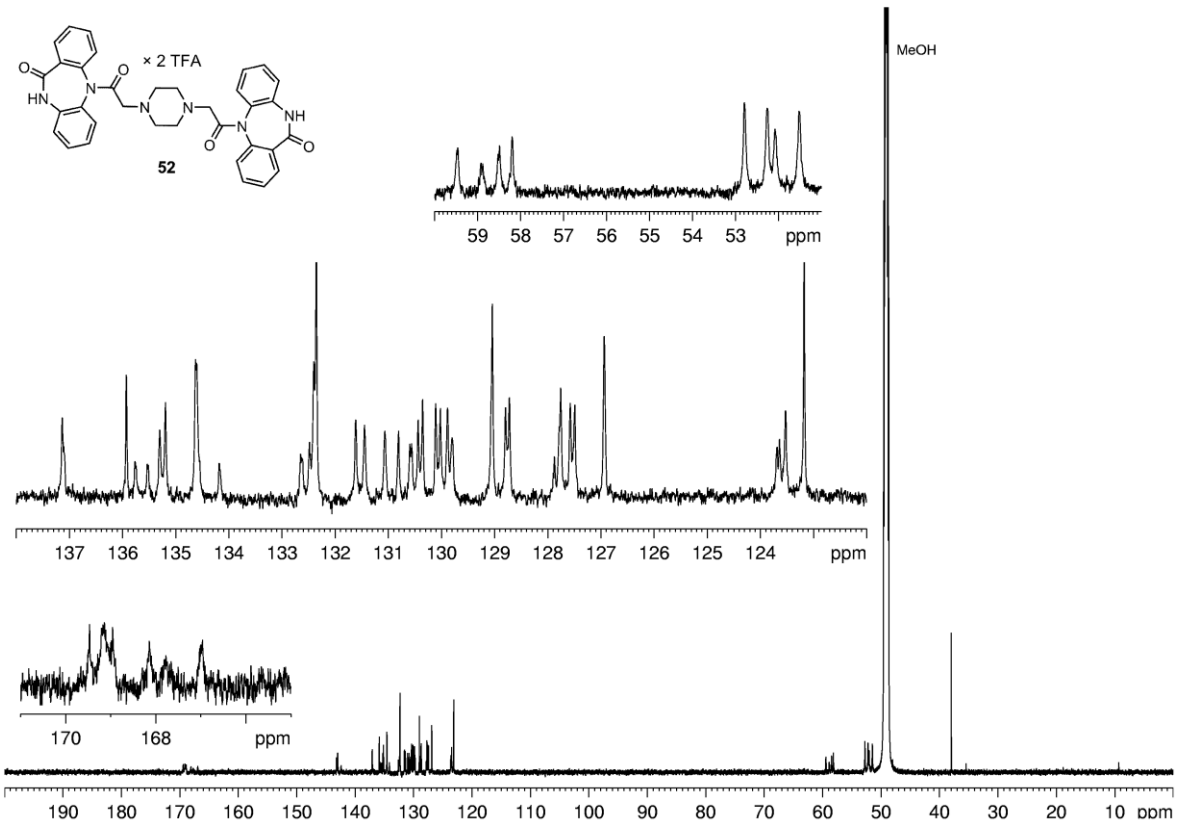

^{13}C-NMR spectrum (150 MHz, MeOH-d_4) of compound **52**.

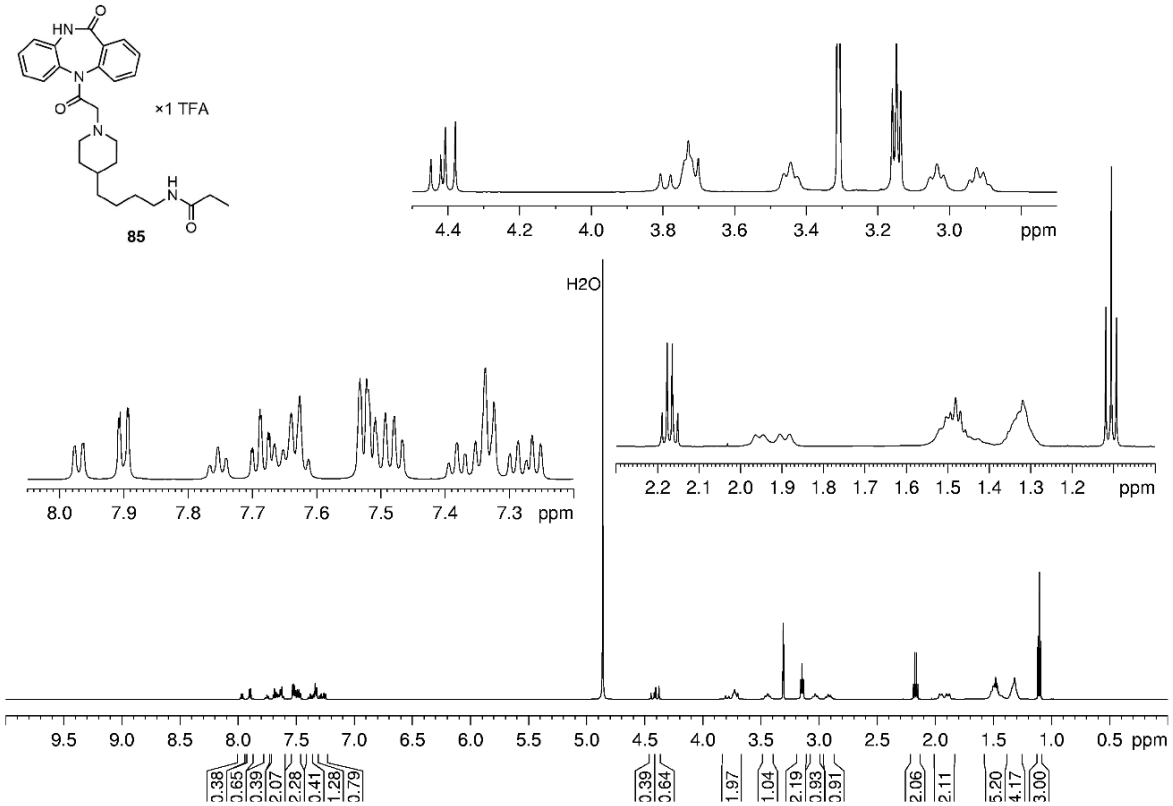

^{1}H-NMR spectrum (600 MHz, MeOH-d$_4$) of compound **85**.

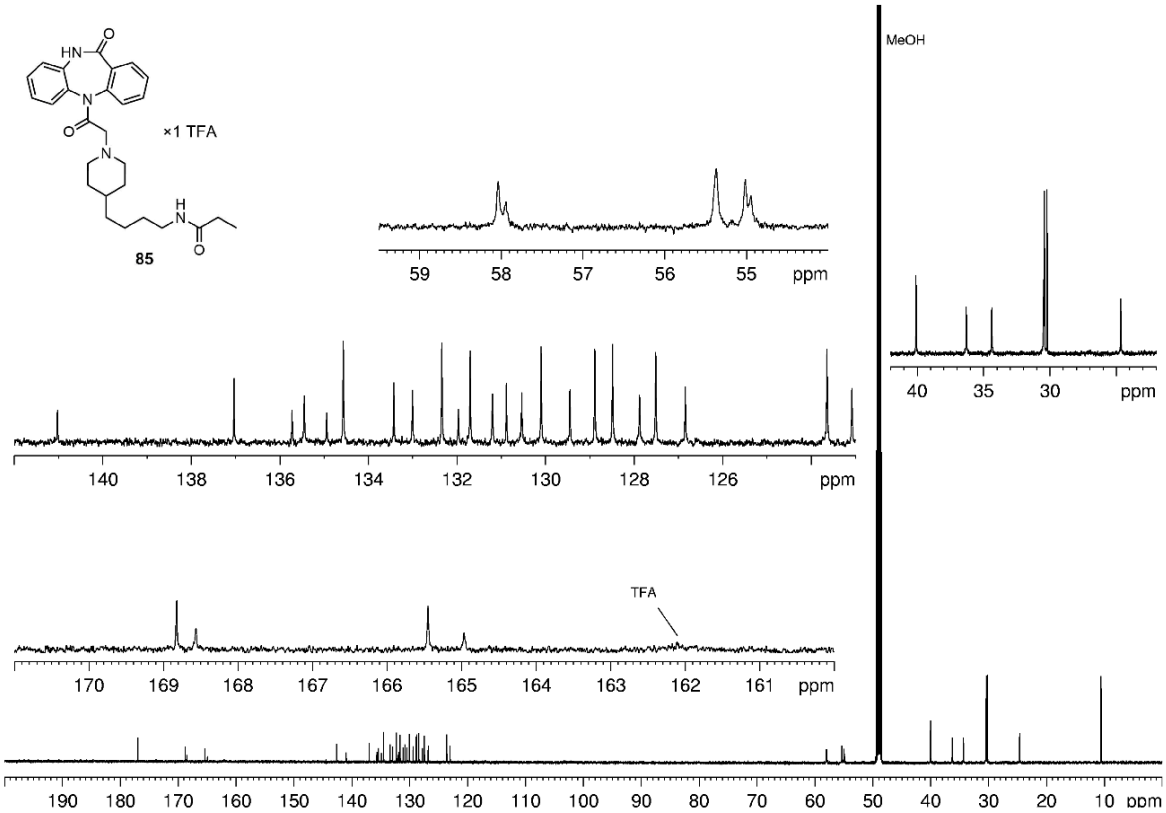

^{13}C-NMR spectrum (150 MHz, MeOH-d$_4$) of compound **85**

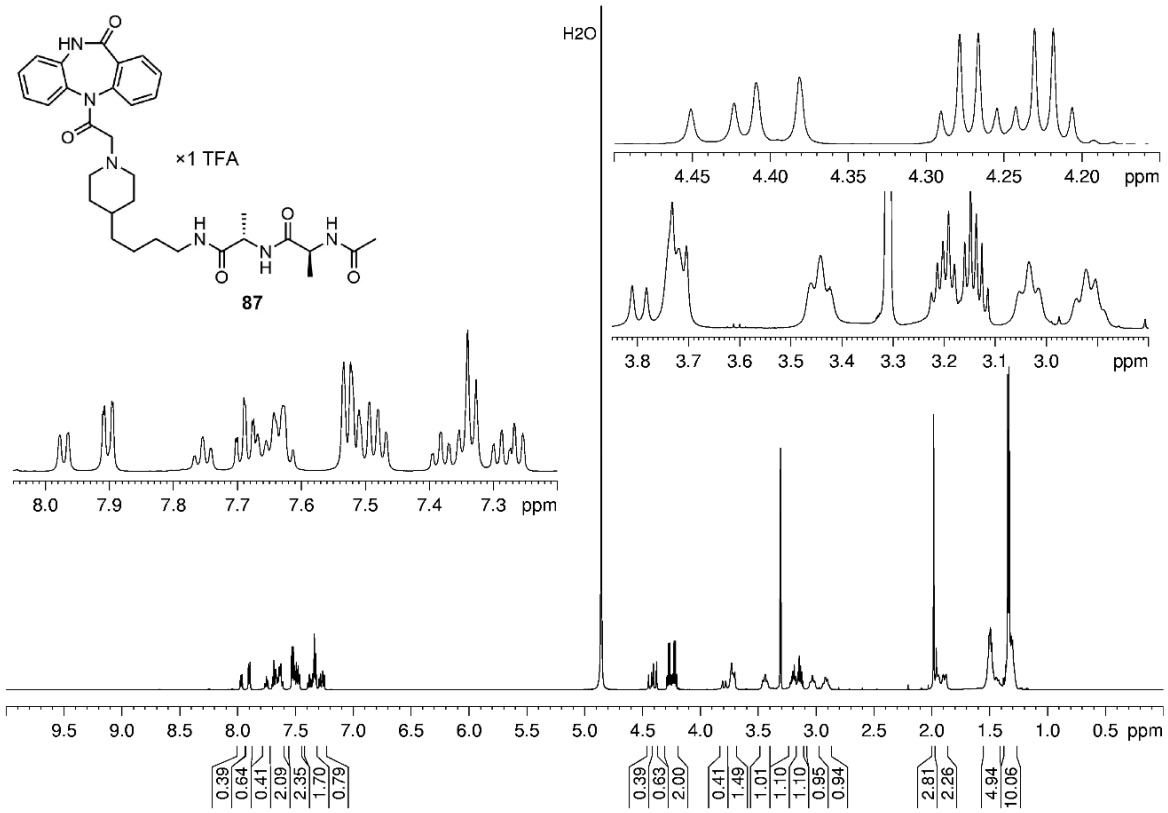

^{1}H-NMR spectrum (600 MHz, MeOH-d_4) of compound **87**.

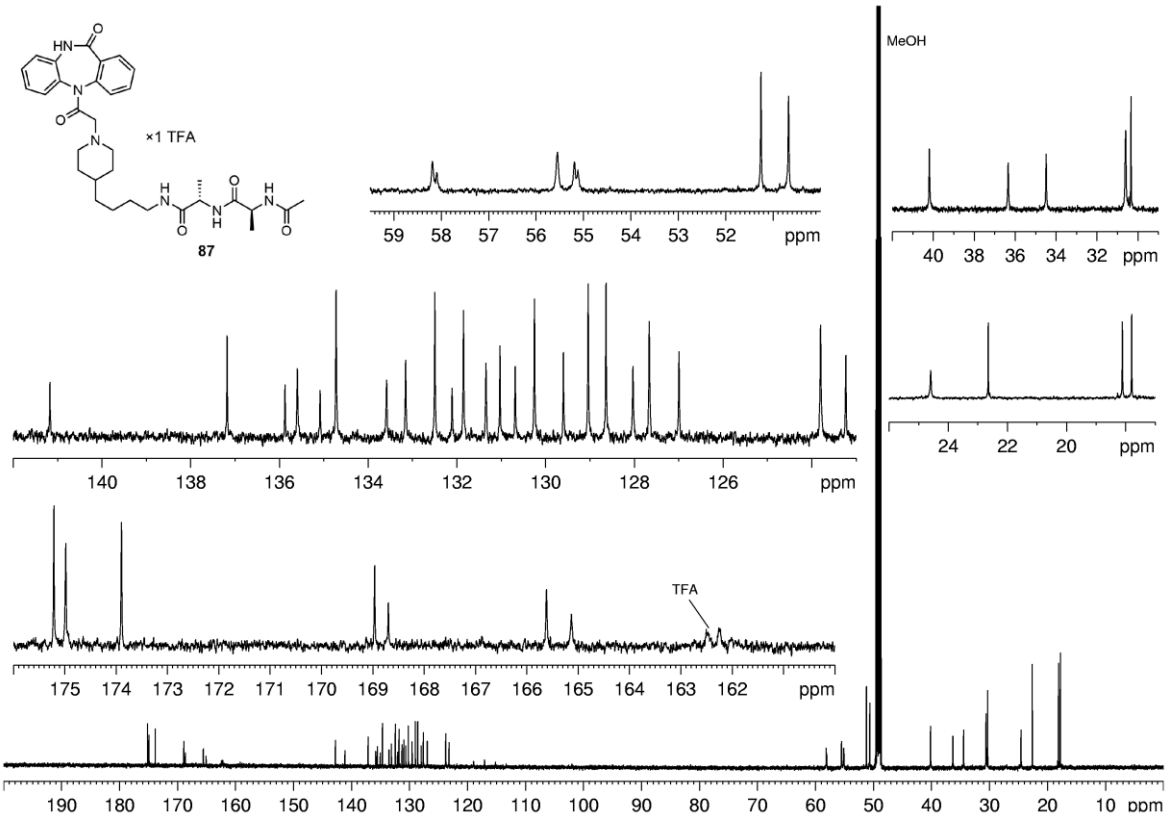

^{13}C-NMR spectrum (150 MHz, MeOH-d_4) of compound **87**.

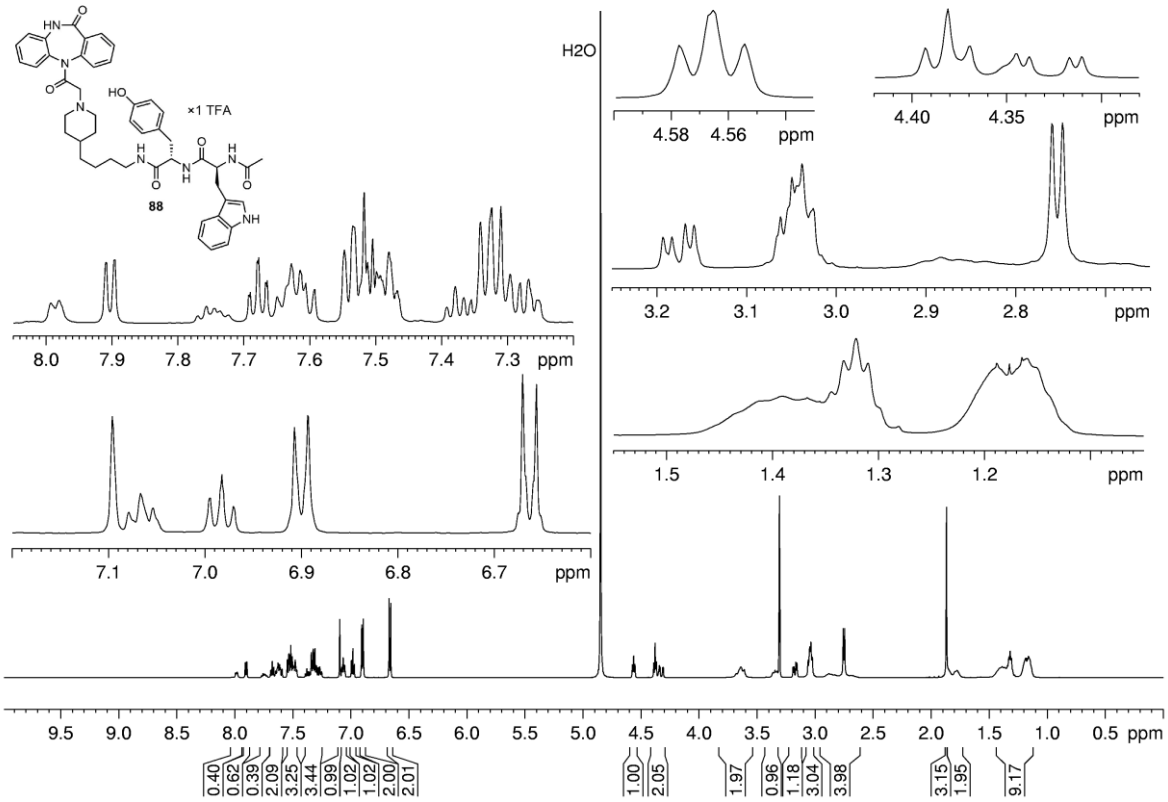

^{1}H-NMR spectrum (600 MHz, MeOH-d_4) of compound **88**.

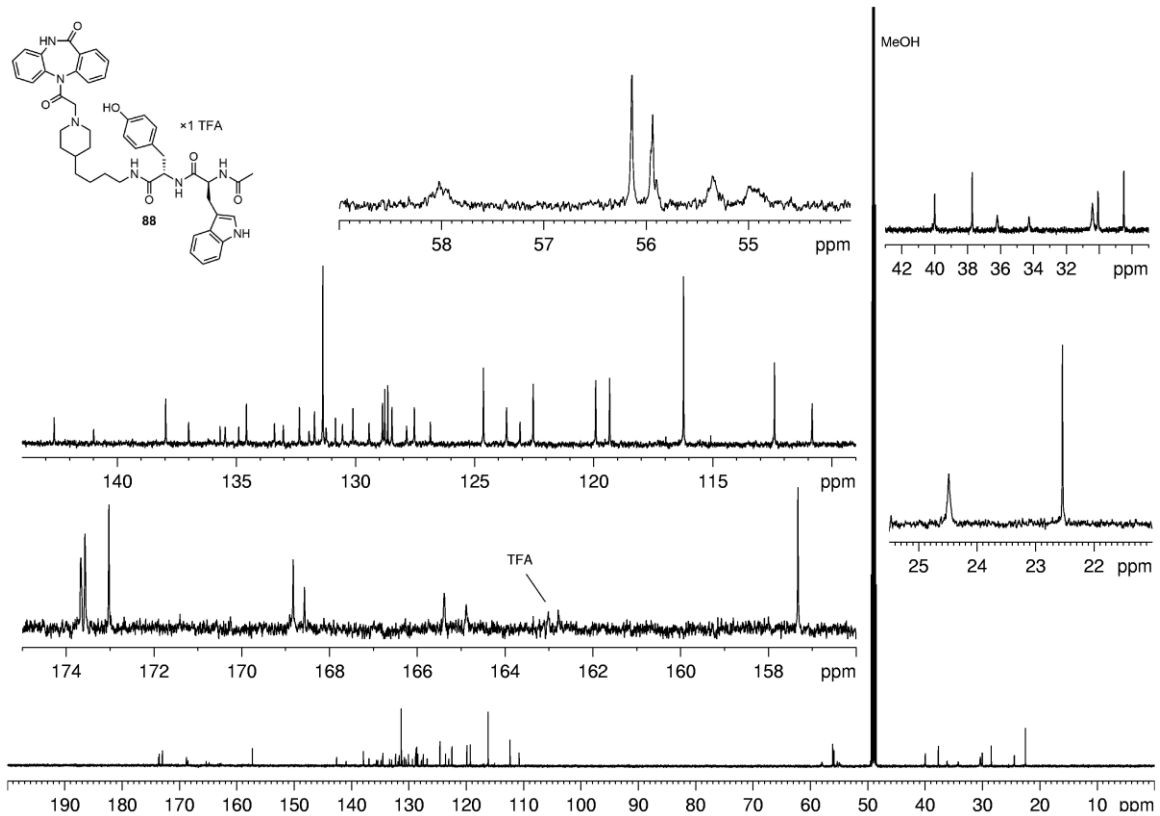

^{13}C-NMR spectrum (150 MHz, MeOH-d_4) of compound **88**.

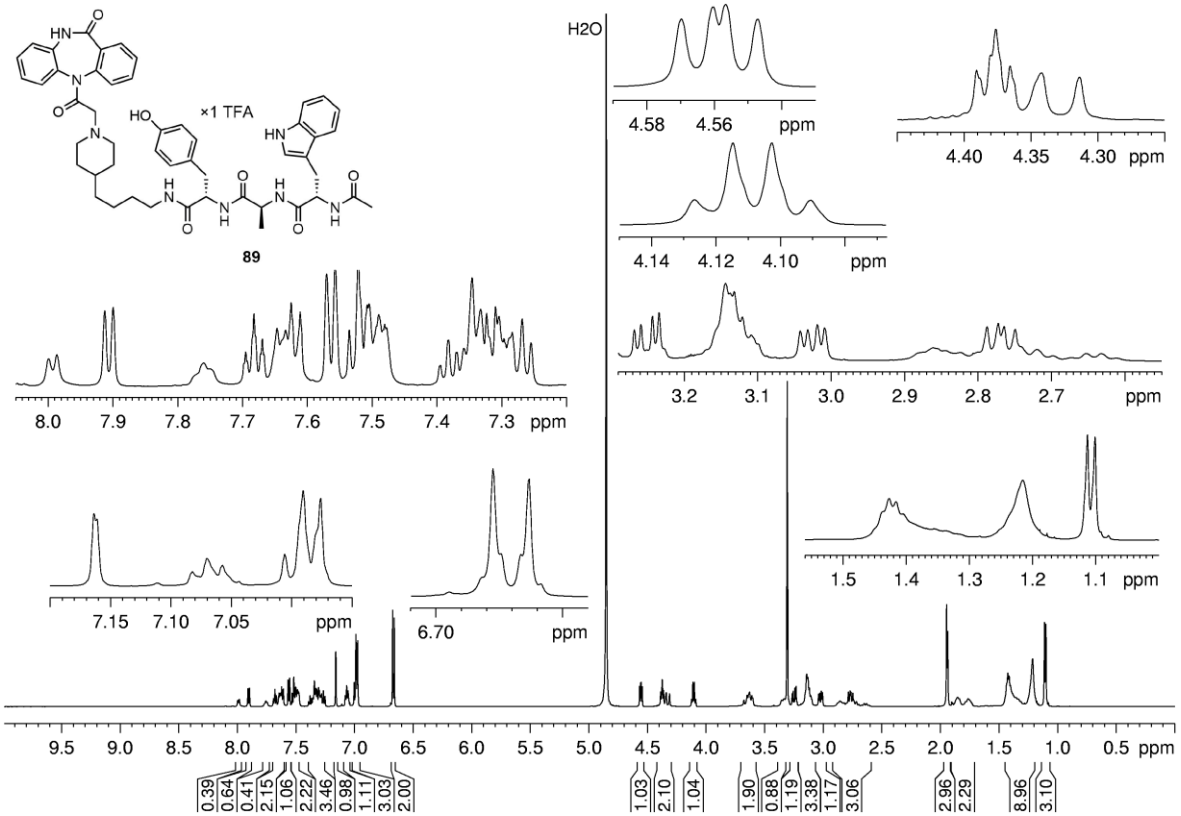

^{1}H-NMR spectrum (600 MHz, MeOH-d_4) of compound **89**.

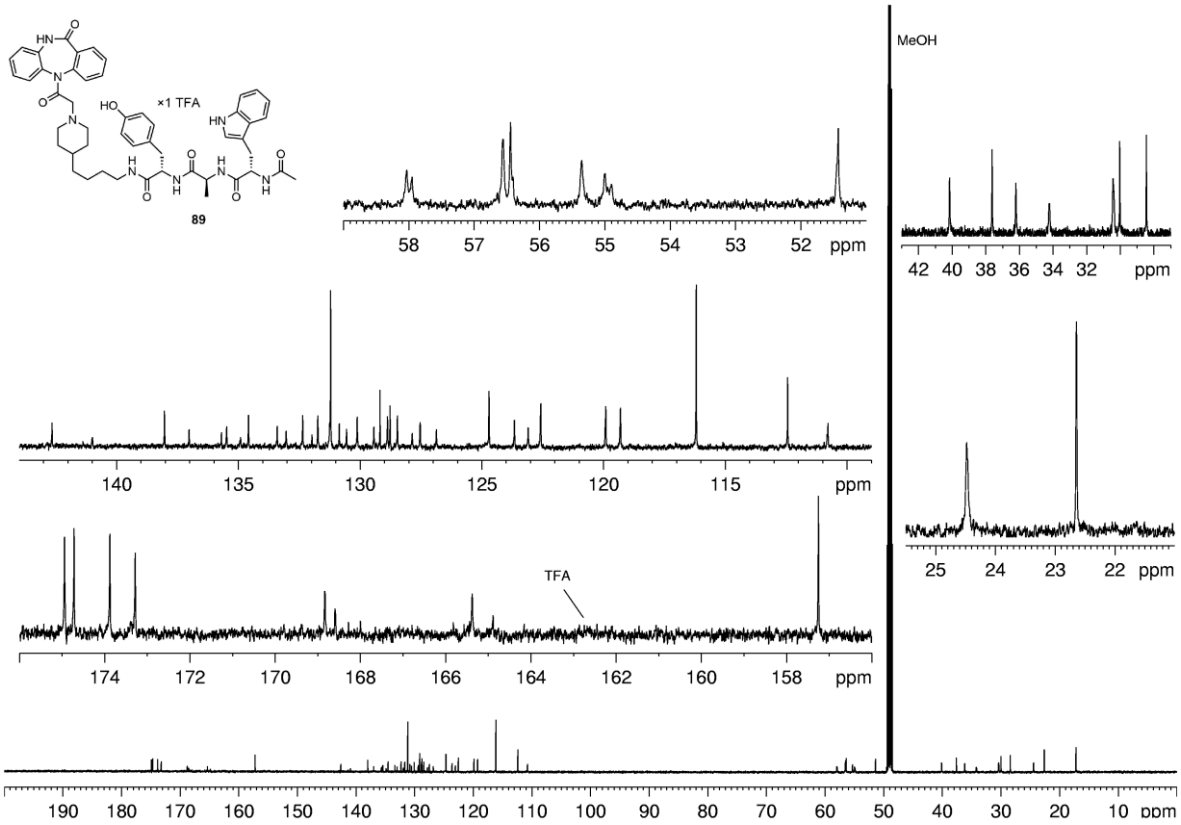

^{13}C-NMR spectrum (150 MHz, MeOH-d_4) of compound **89**.

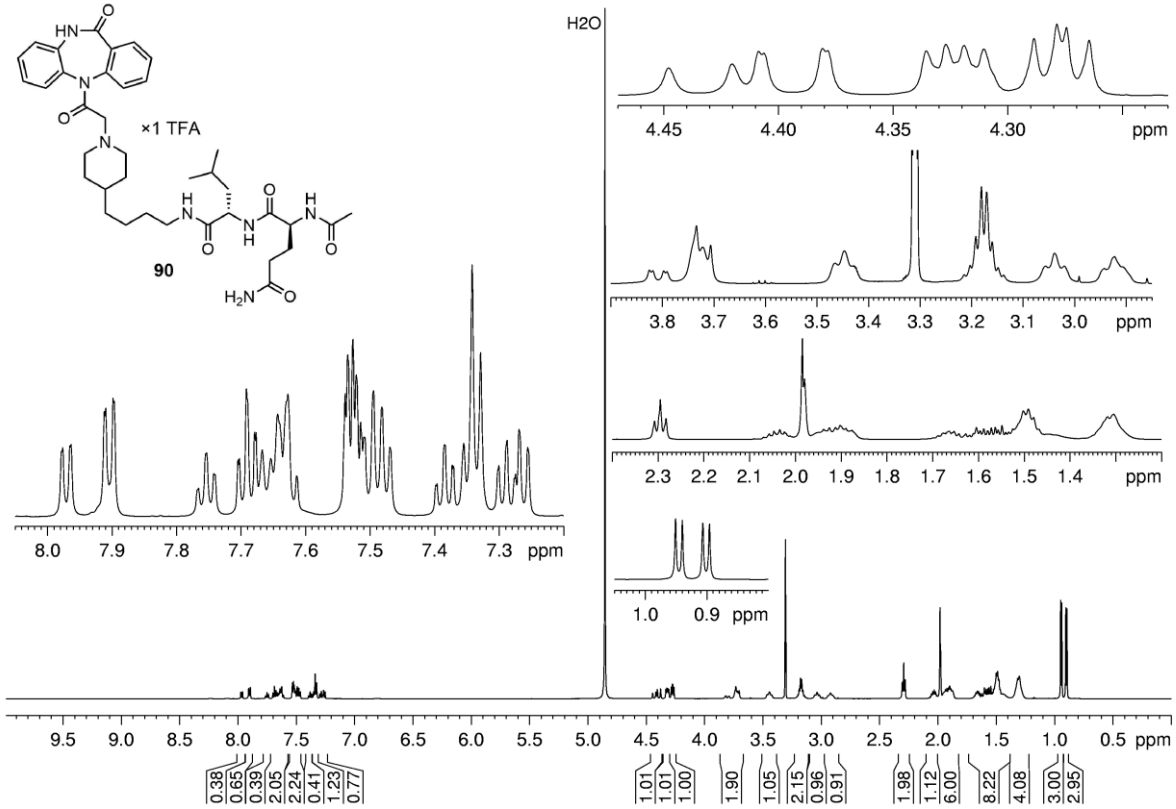

^{1}H-NMR spectrum (600 MHz, MeOH-d_4) of compound **90**.

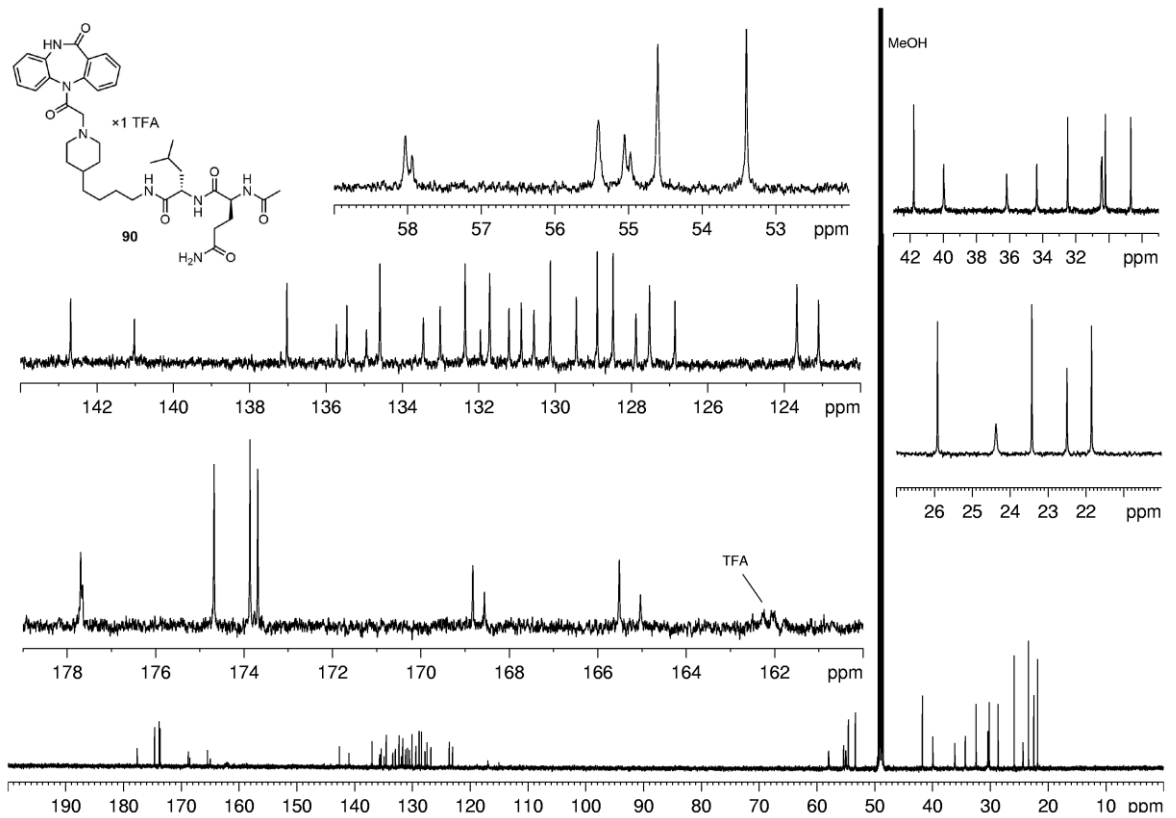

^{13}C-NMR spectrum (150 MHz, MeOH-d_4) of compound **90**.

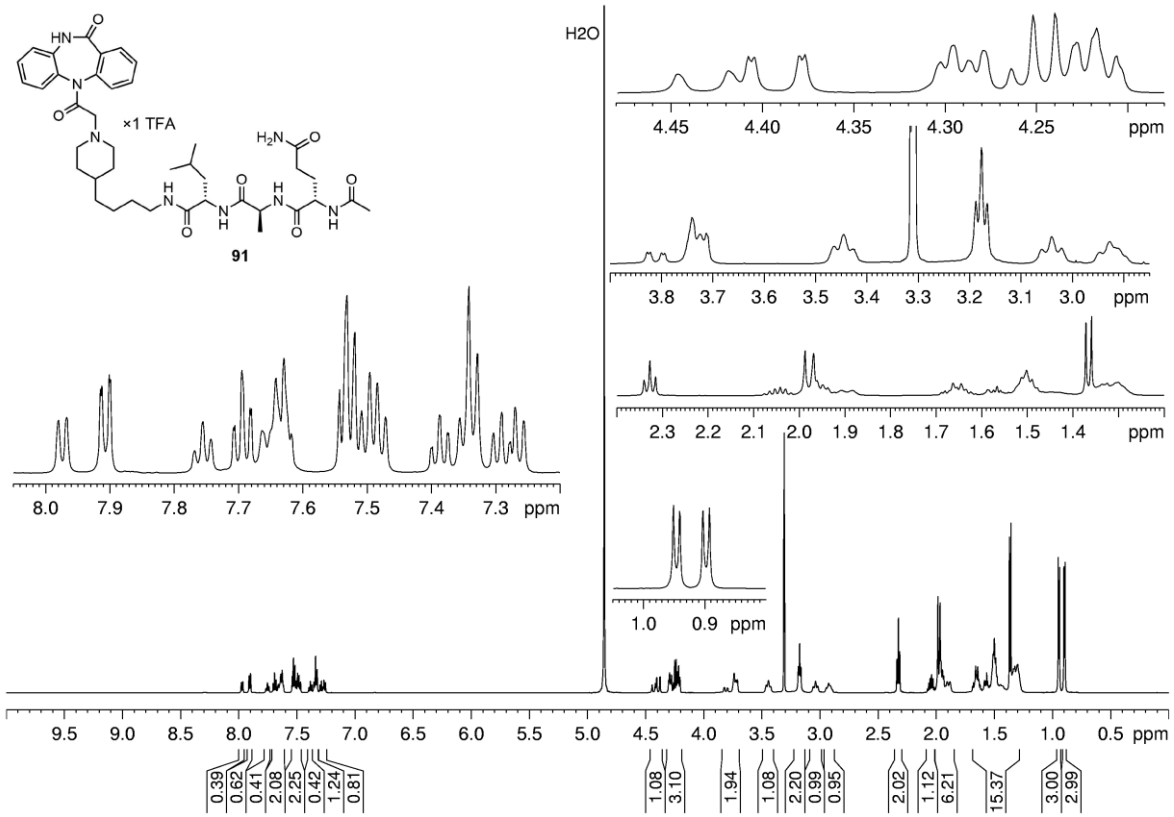

^{1}H-NMR spectrum (600 MHz, MeOH-d_4) of compound **91**.

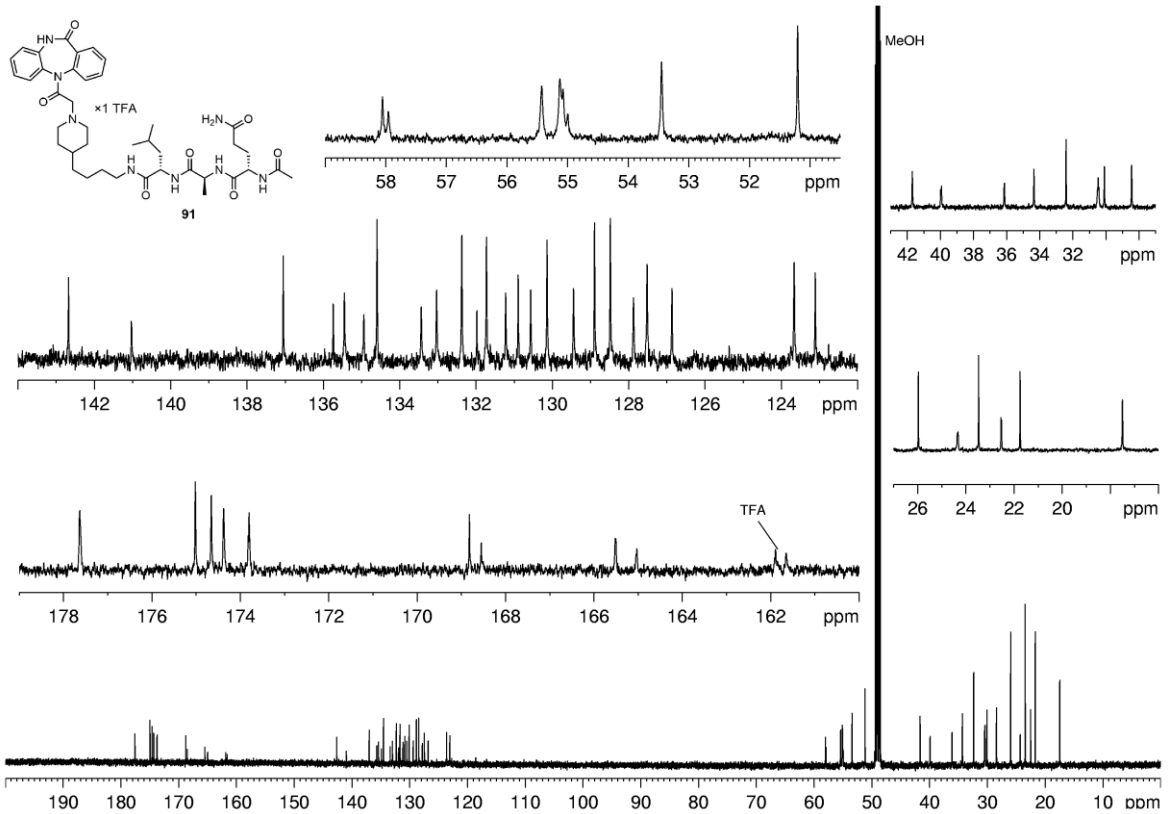

^{13}C-NMR spectrum (150 MHz, MeOH-d_4) of compound **91**.

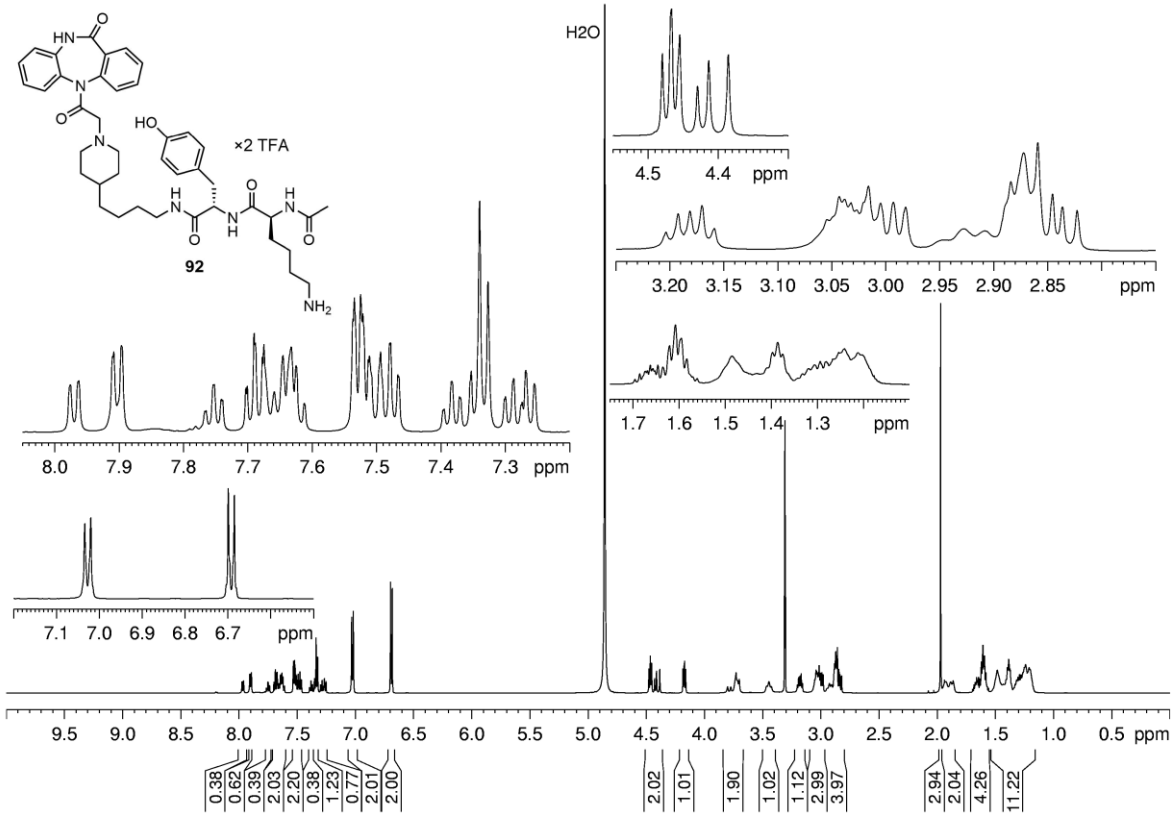

^{1}H-NMR spectrum (600 MHz, MeOH-d_4) of compound **92**.

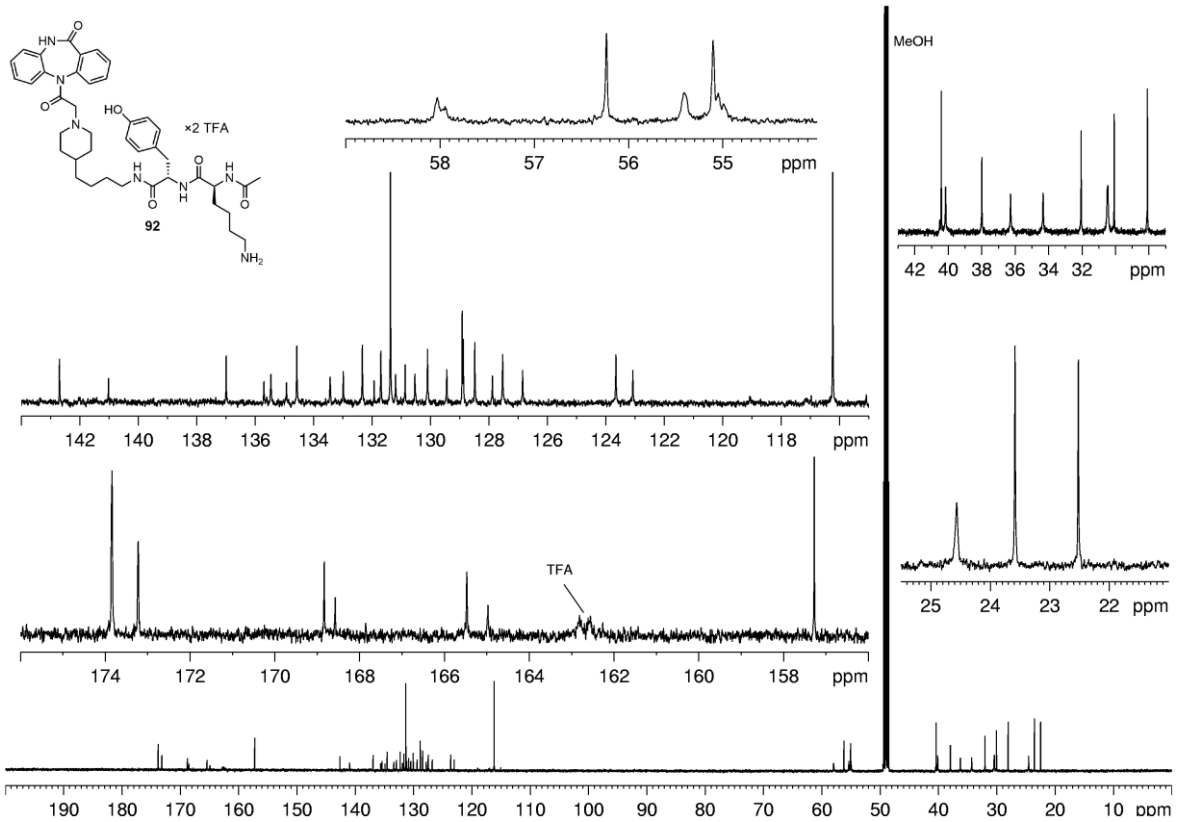

^{13}C-NMR spectrum (150 MHz, MeOH-d_4) of compound **92**

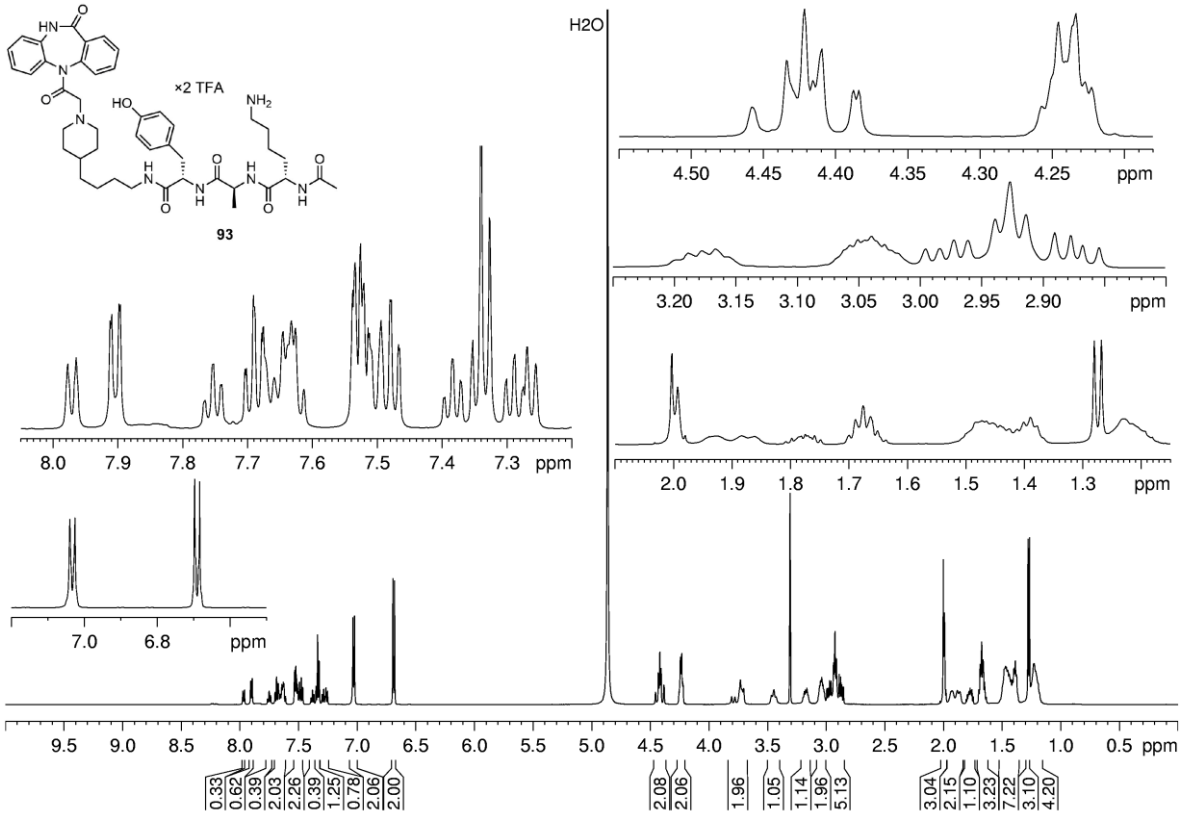

^{1}H-NMR spectrum (600 MHz, MeOH-d_4) of compound **93**.

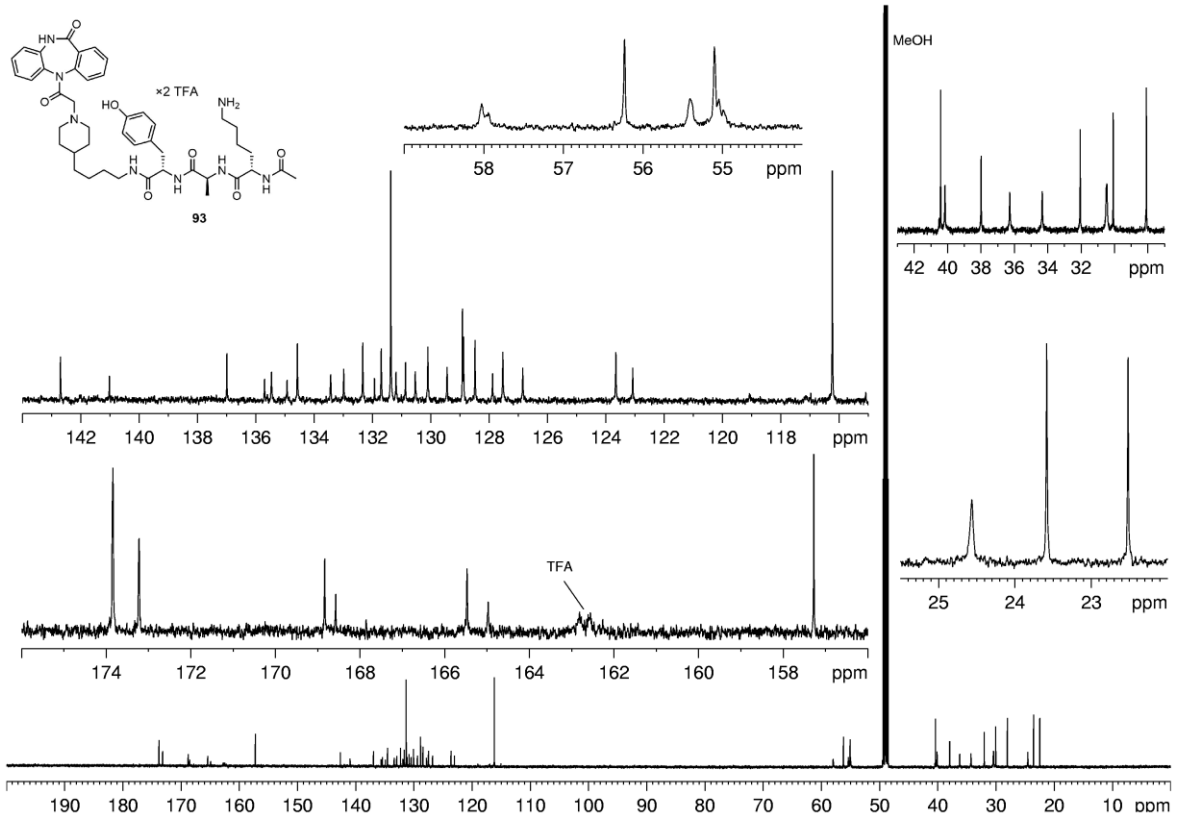

^{13}C-NMR spectrum (150 MHz, MeOH-d_4) of compound **93**.

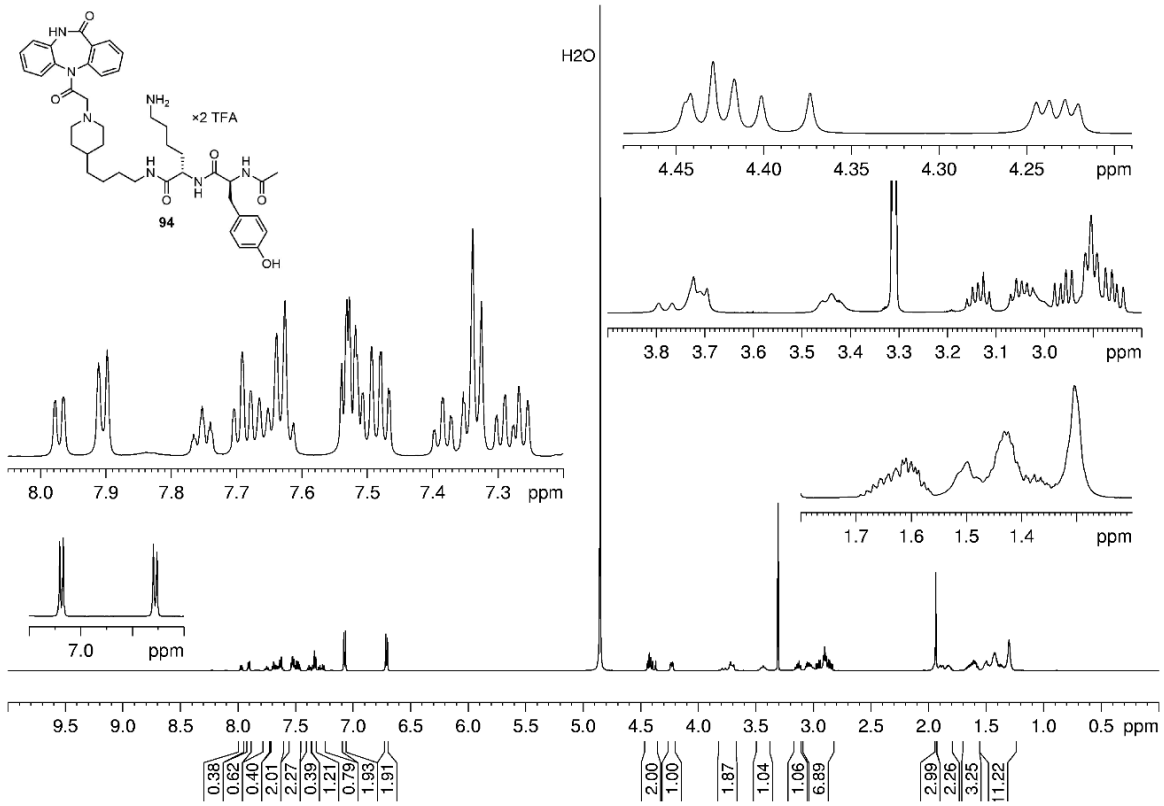

^{1}H-NMR spectrum (600 MHz, MeOH-d_4) of compound **94**

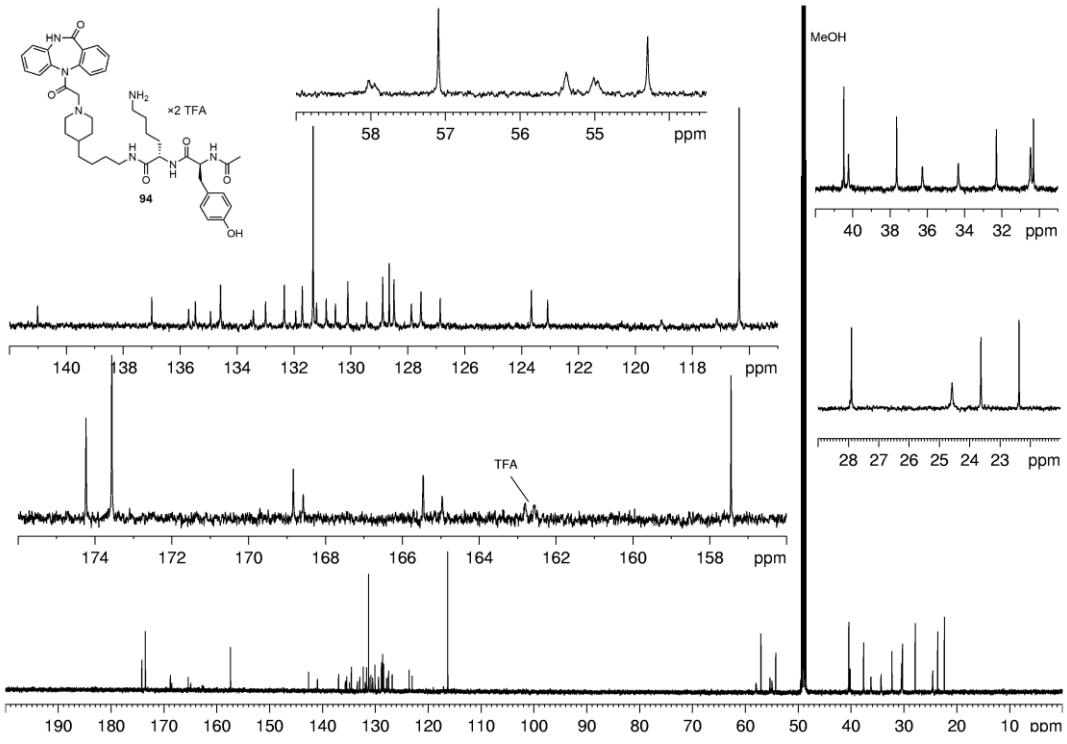

^{13}C-NMR spectrum (150 MHz, MeOH-d_4) of compound **94**.

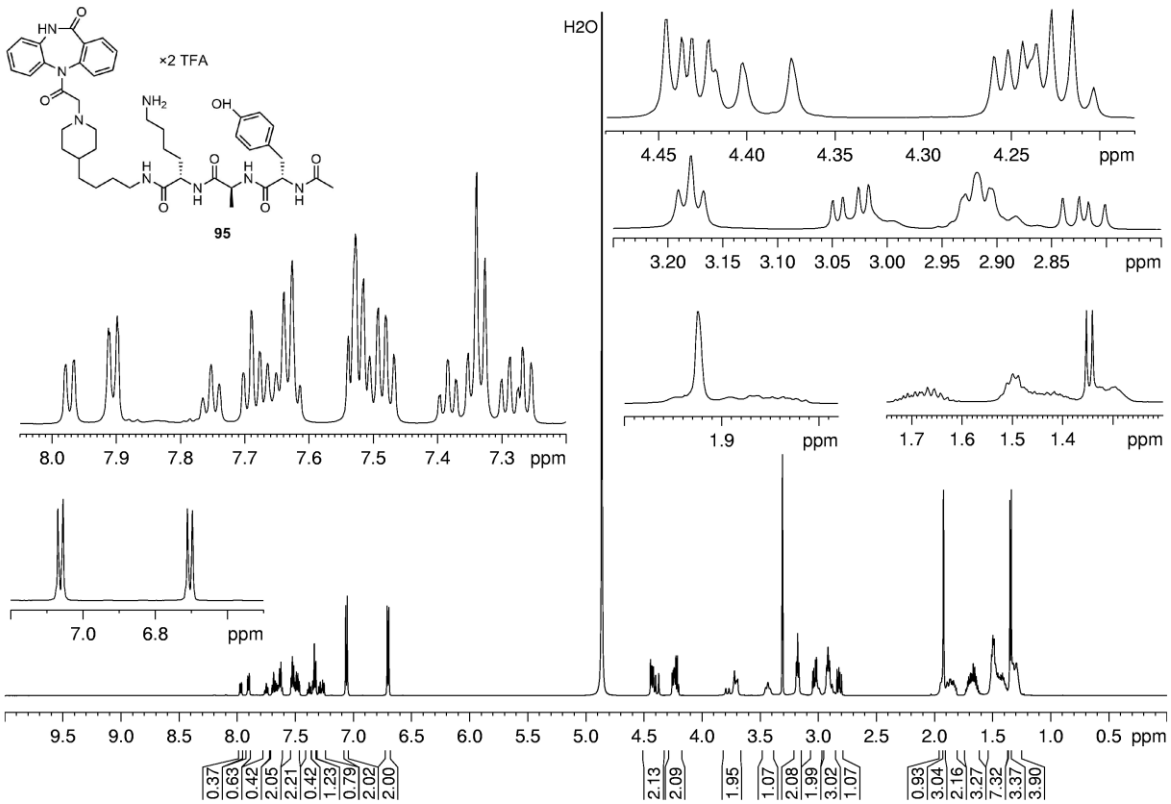

^{1}H-NMR spectrum (600 MHz, MeOH-d_4) of compound **95**.

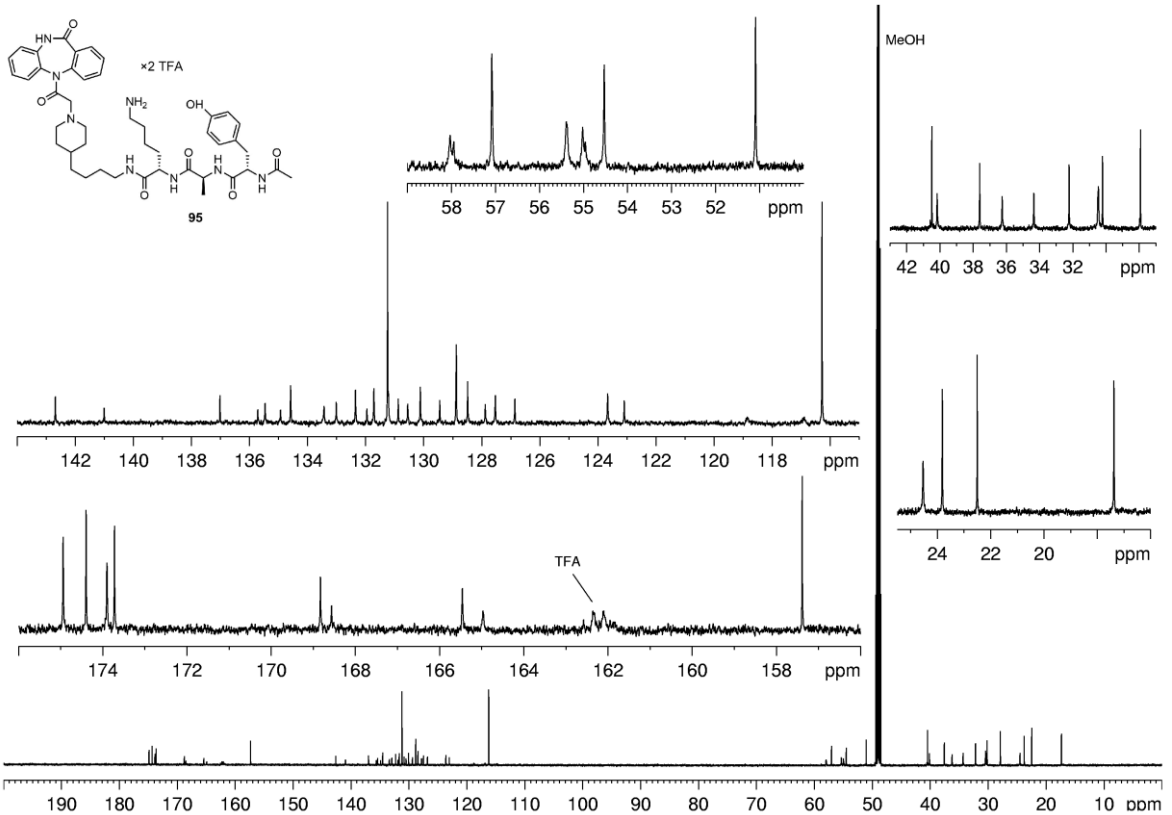

^{13}C-NMR spectrum (150 MHz, MeOH-d_4) of compound **95**.

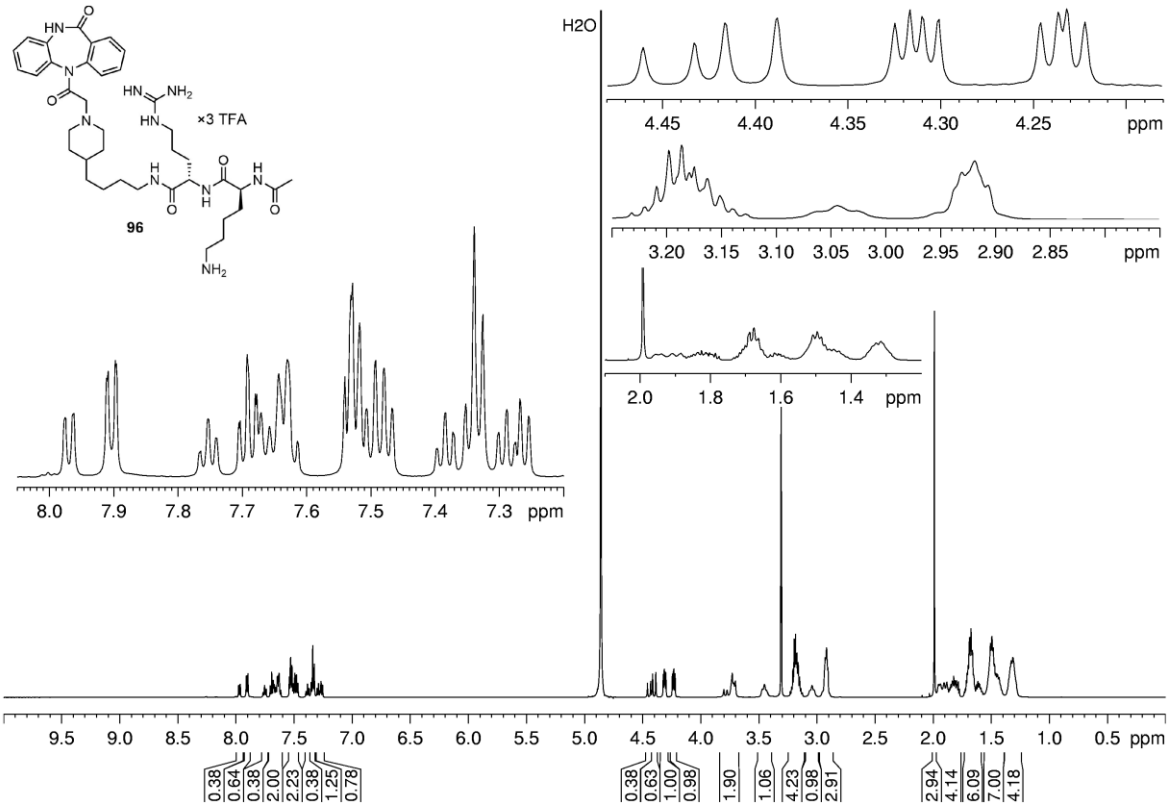

^{1}H-NMR spectrum (600 MHz, MeOH-d_4) of compound **96**.

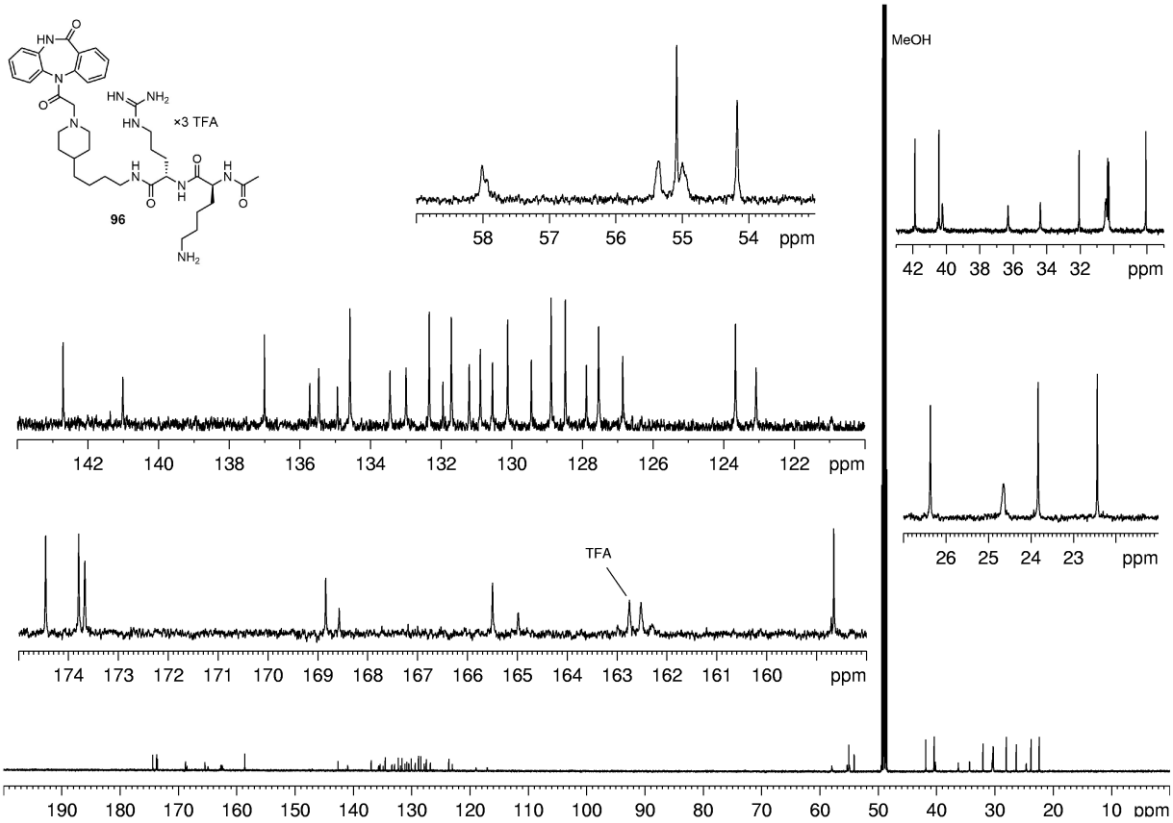

^{13}C-NMR spectrum (150 MHz, MeOH-d_4) of compound **96**.

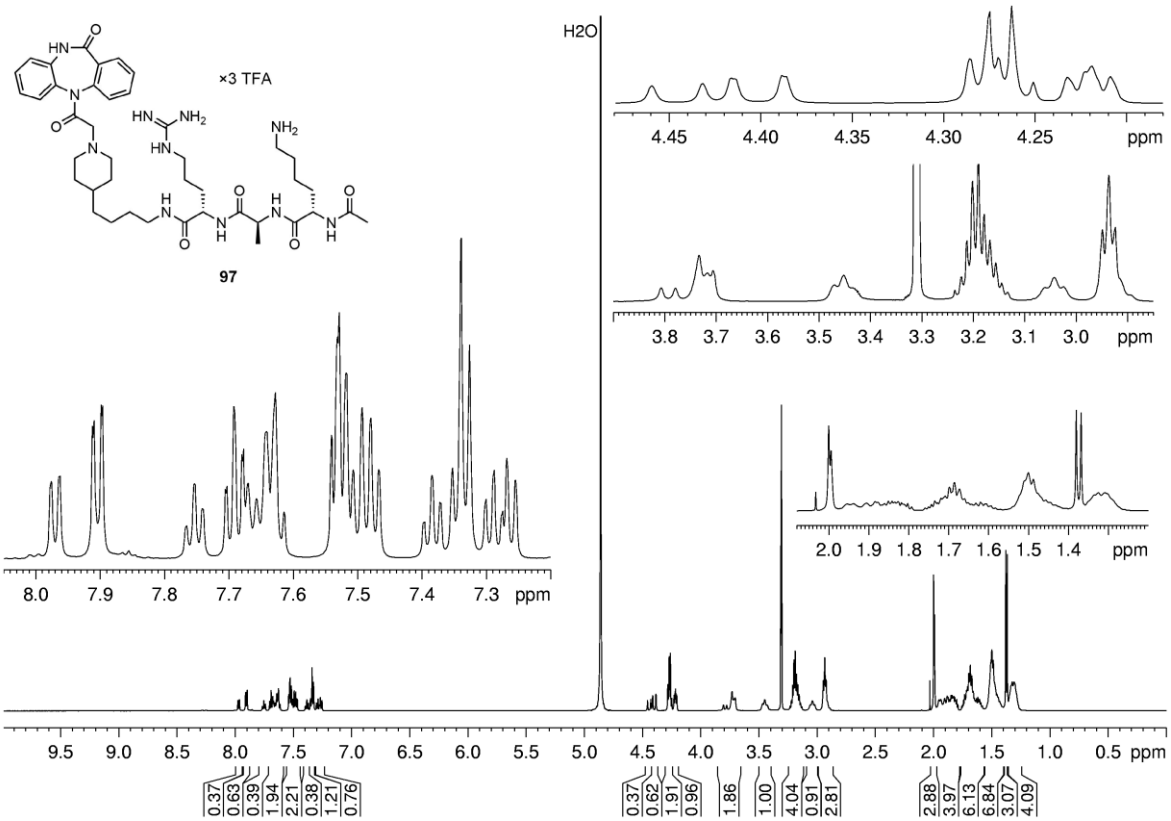

^{1}H-NMR spectrum (600 MHz, MeOH-d_4) of compound **97**.

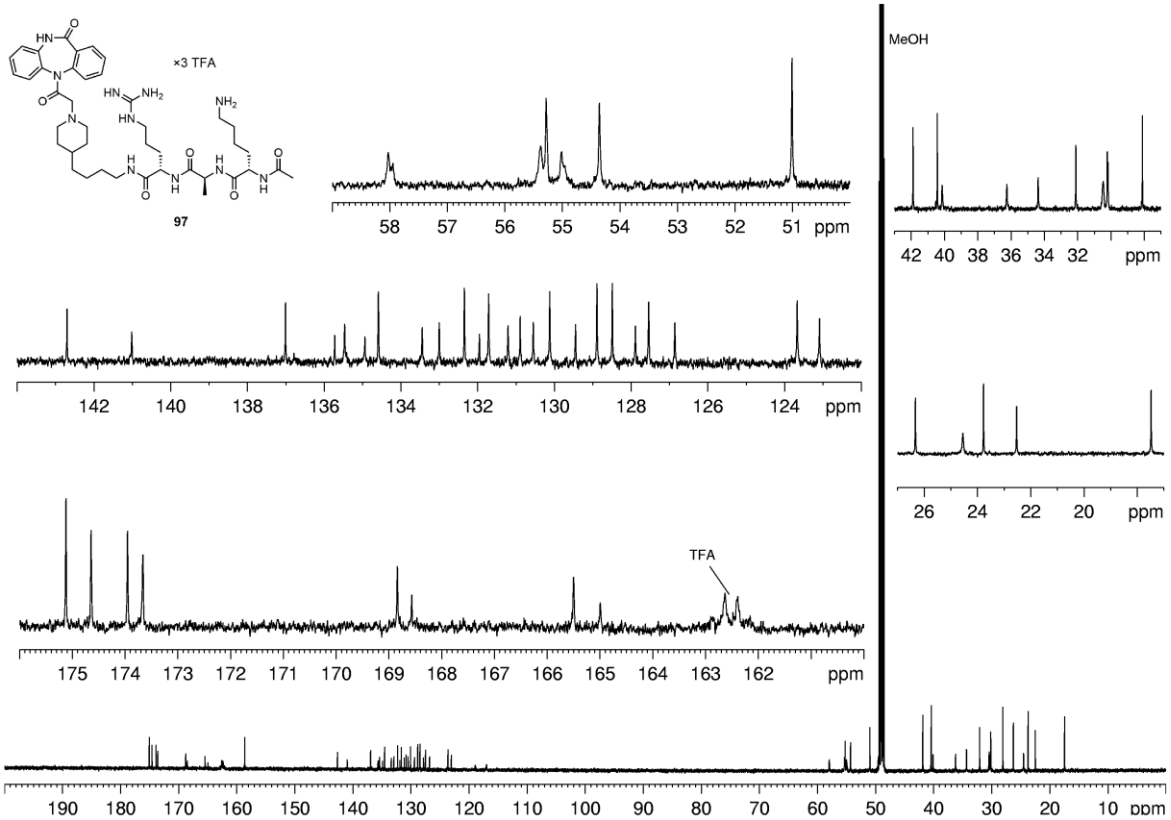

^{13}C-NMR spectrum (150 MHz, MeOH-d_4) of compound **97**.

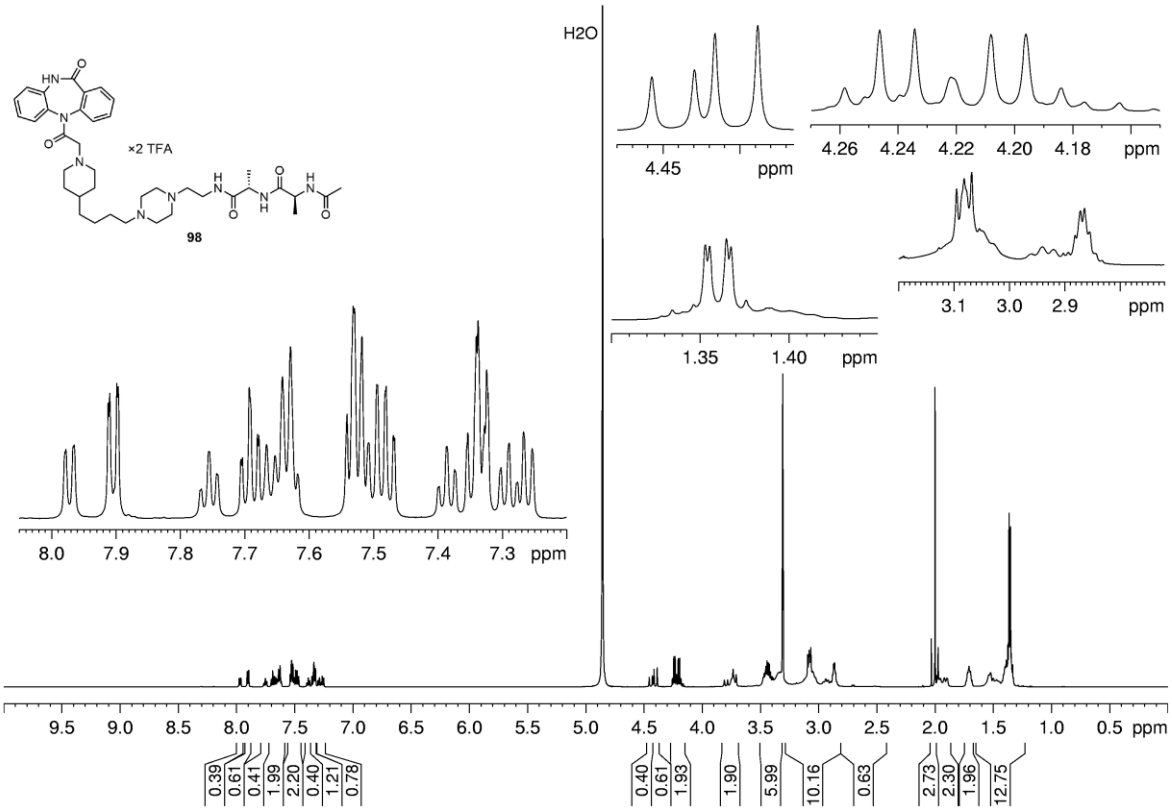

^{1}H-NMR spectrum (600 MHz, MeOH-d_4) of compound **98**.

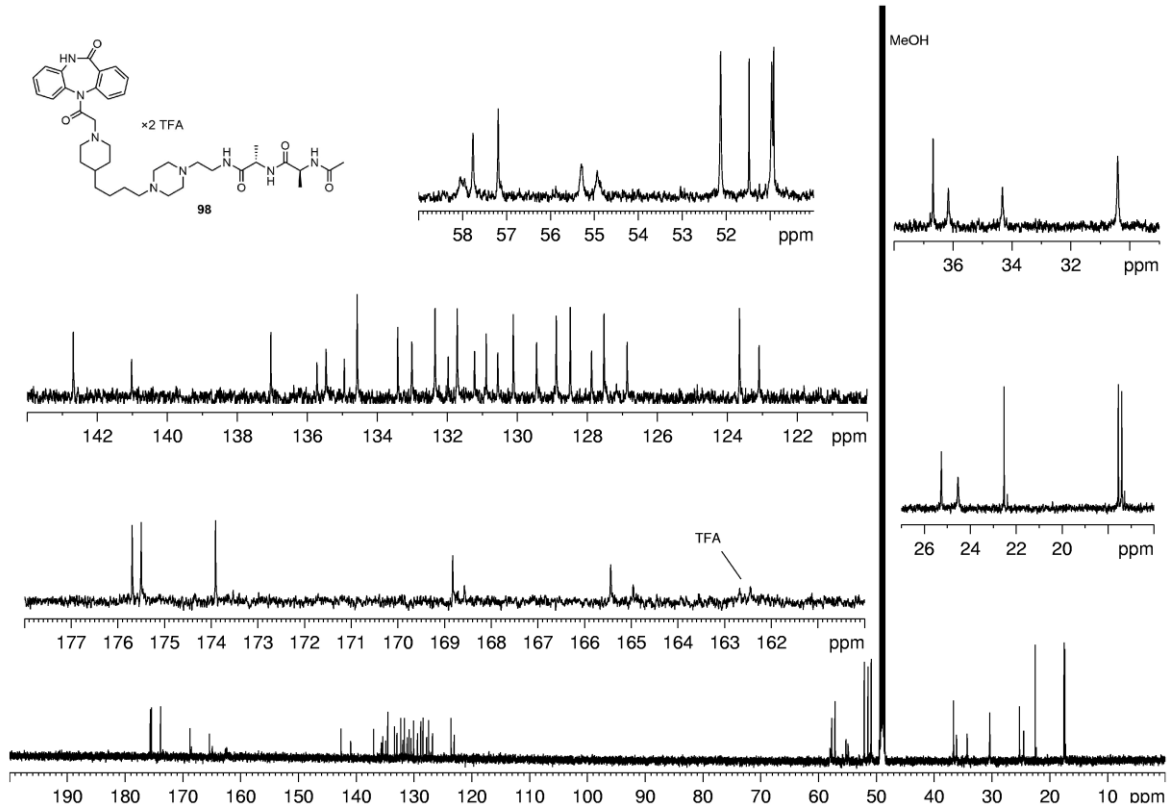

^{13}C-NMR spectrum (150 MHz, MeOH-d_4) of compound **98**.

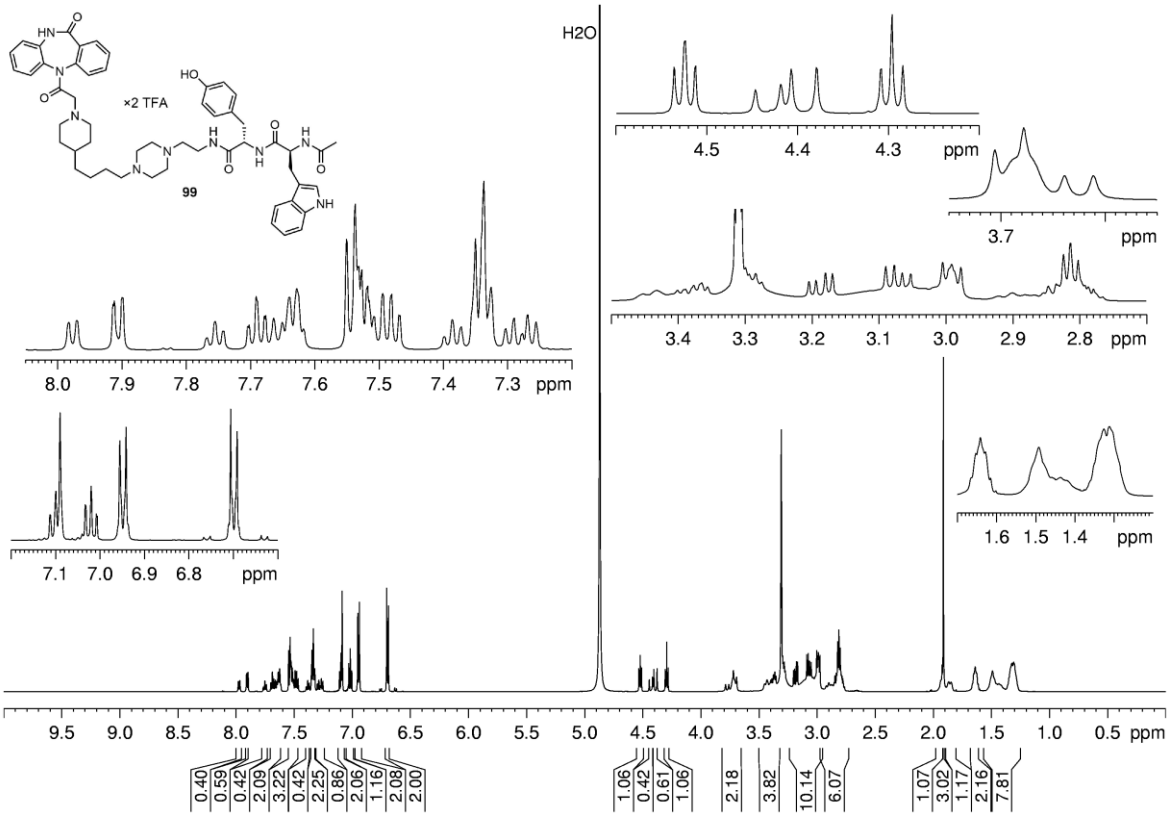

^{1}H-NMR spectrum (600 MHz, MeOH-d_4) of compound **99**.

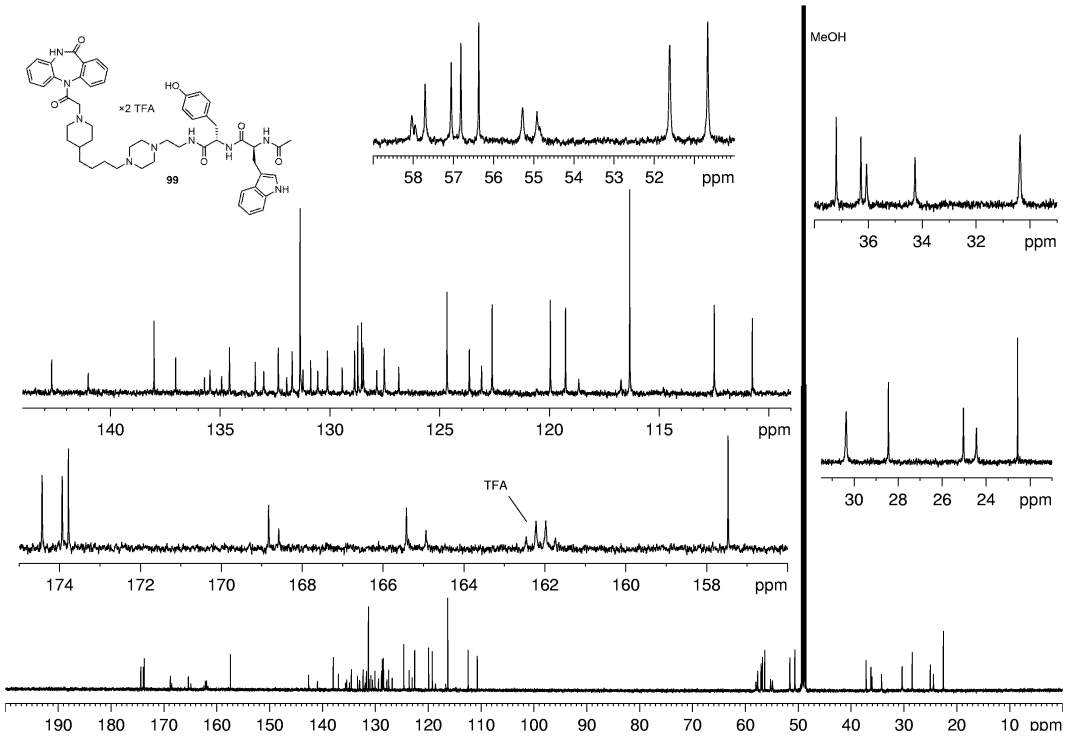

^{13}C-NMR spectrum (150 MHz, MeOH-d_4) of compound **99**.

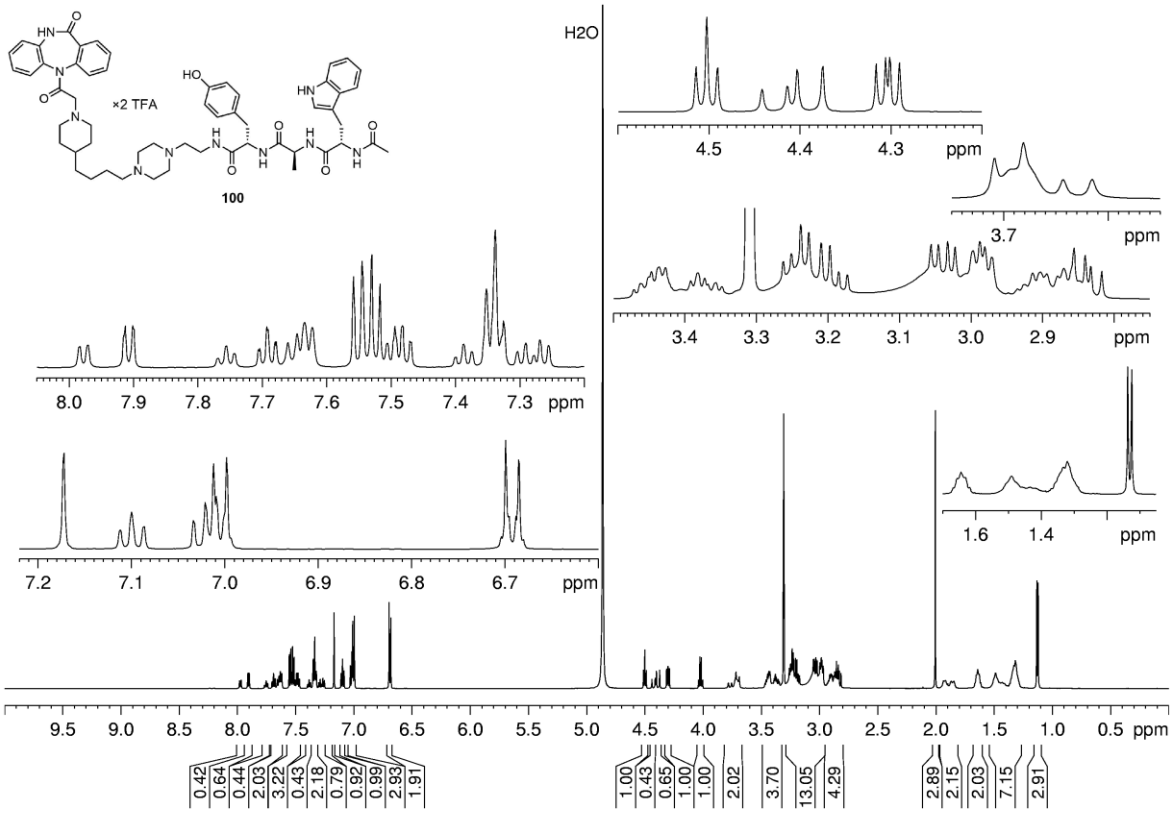

^{1}H-NMR spectrum (600 MHz, MeOH-d_4) of compound **100**.

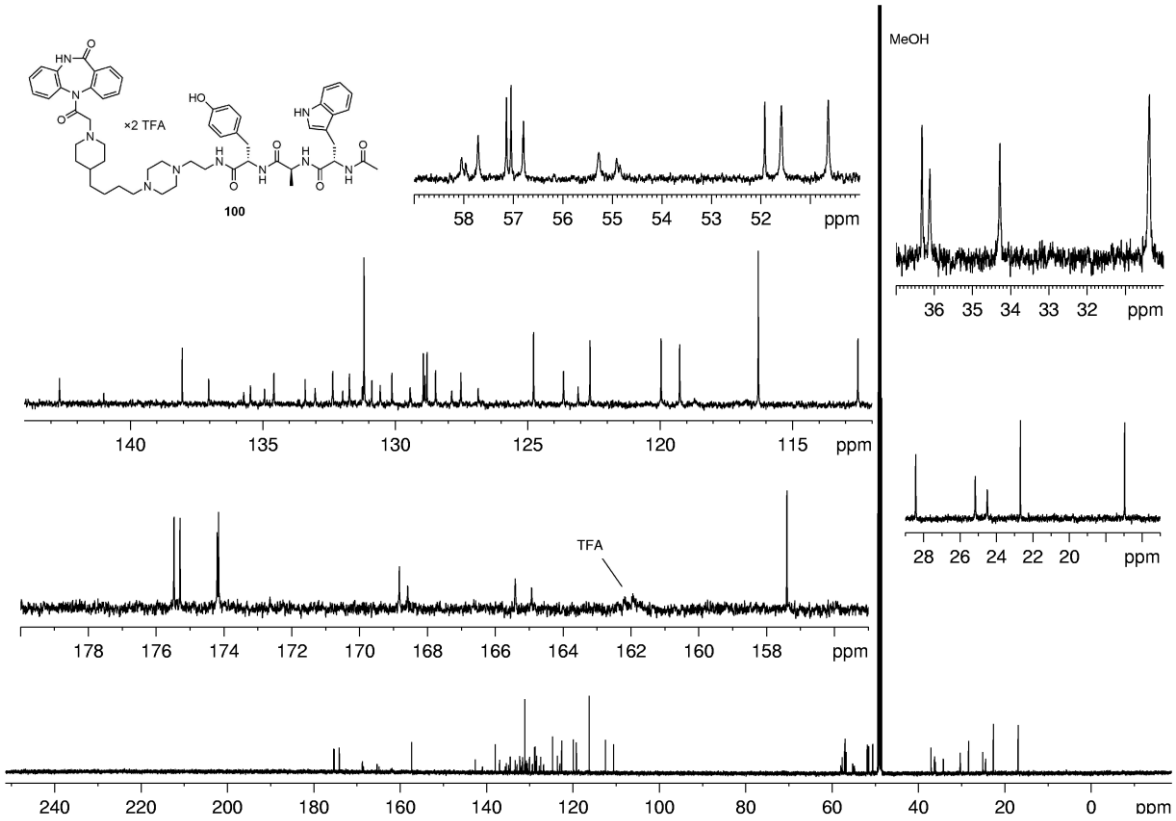

^{13}C-NMR spectrum (150 MHz, MeOH-d_4) of compound **100**.

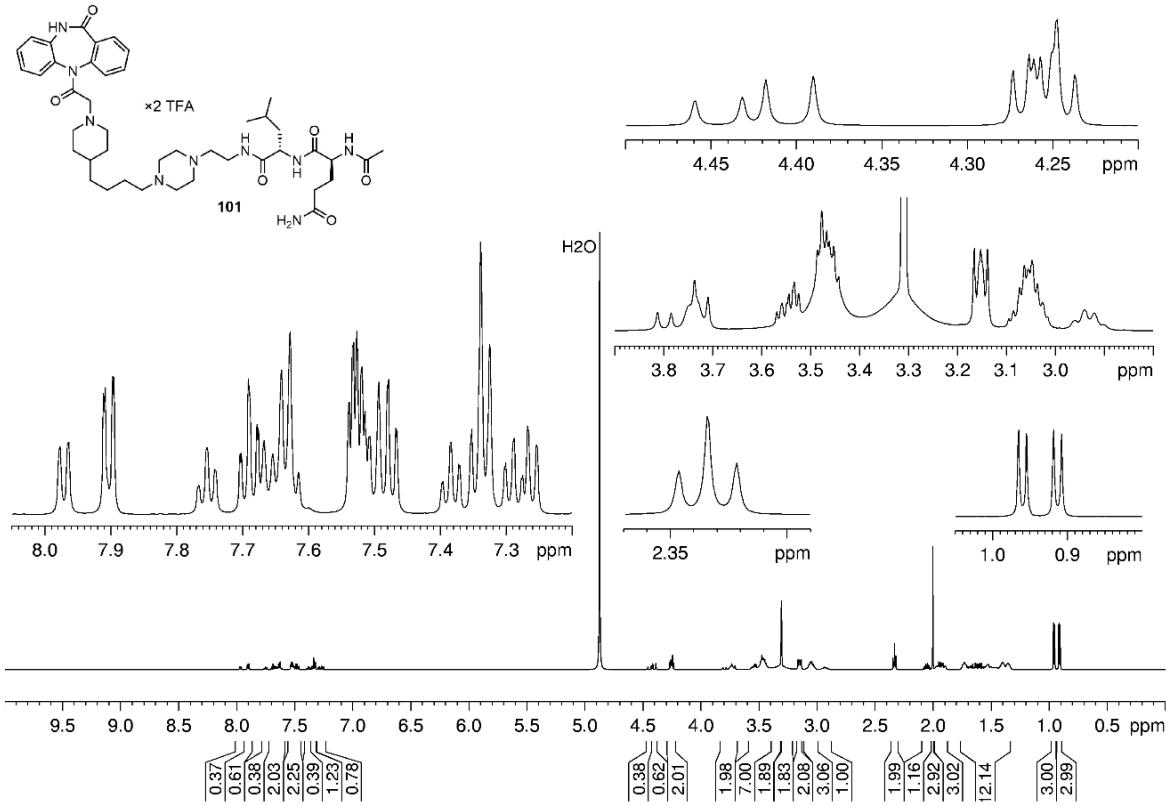

^{1}H-NMR spectrum (600 MHz, MeOH-d$_4$) of compound **101**

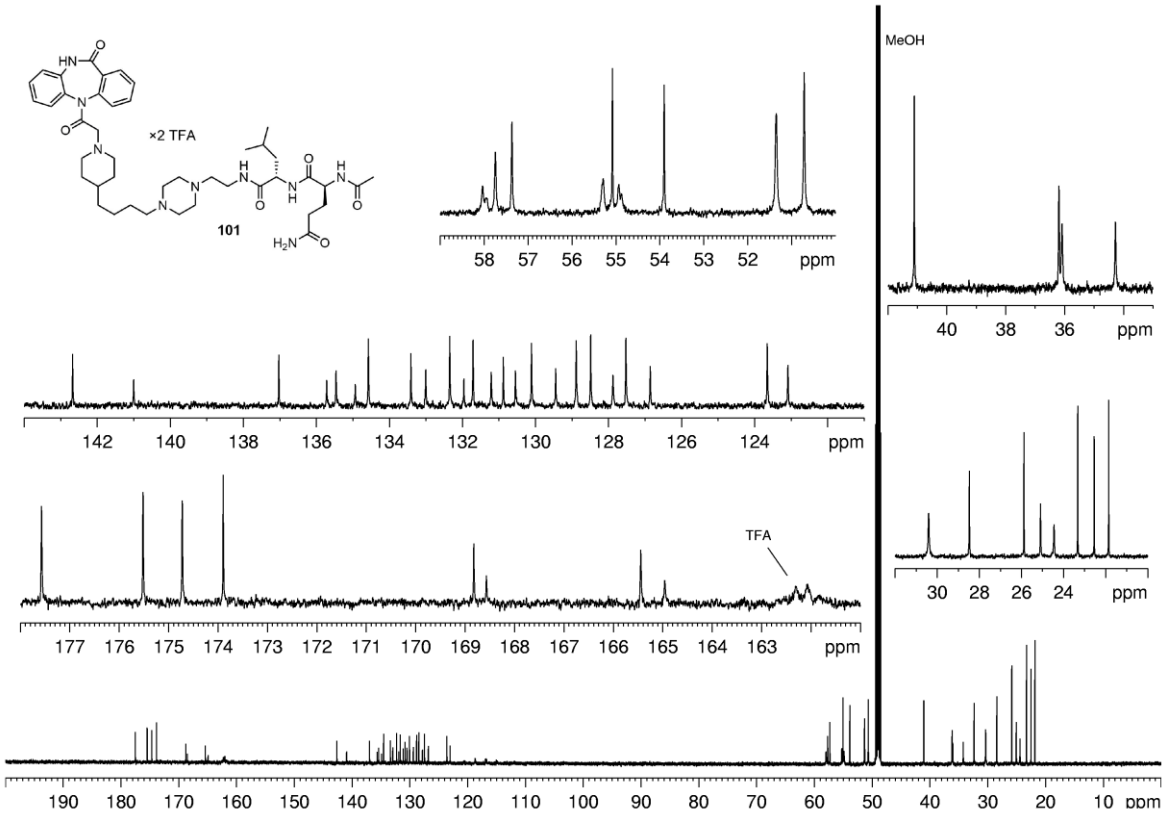

^{13}C-NMR spectrum (150 MHz, MeOH-d$_4$) of compound **101**.

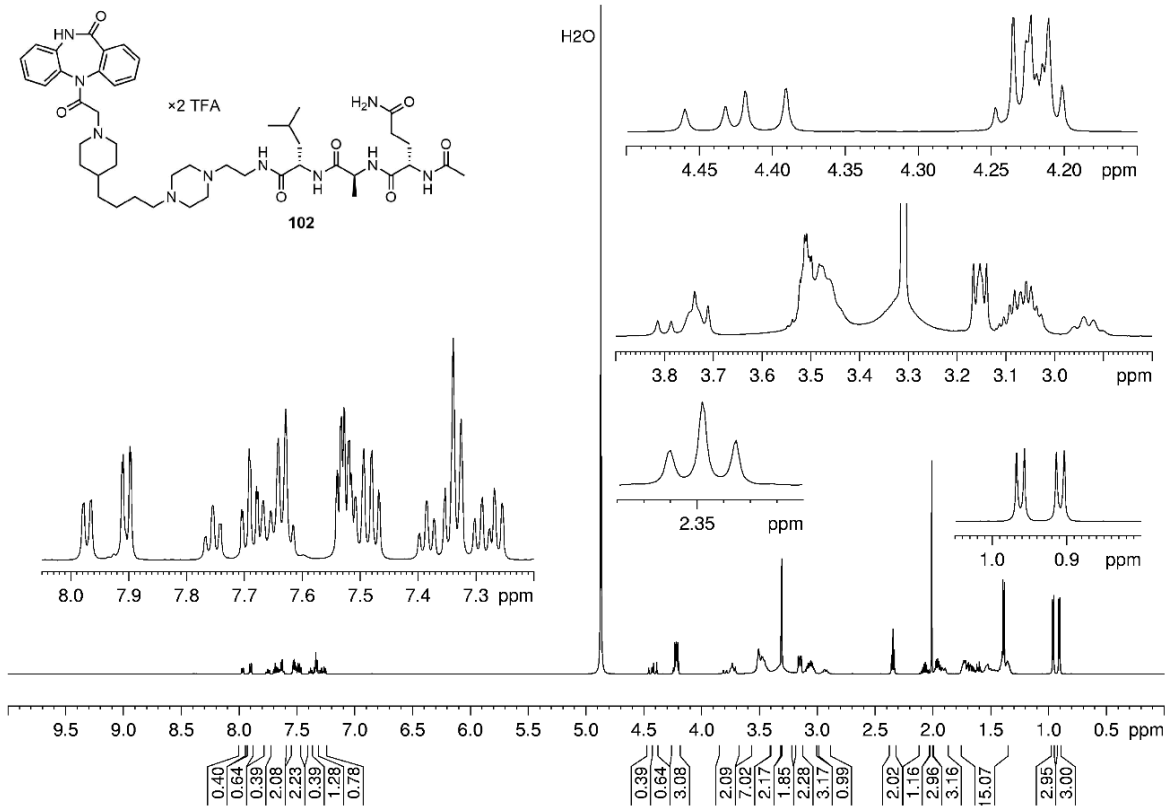

^{1}H-NMR spectrum (600 MHz, MeOH-d_4) of compound **102**.

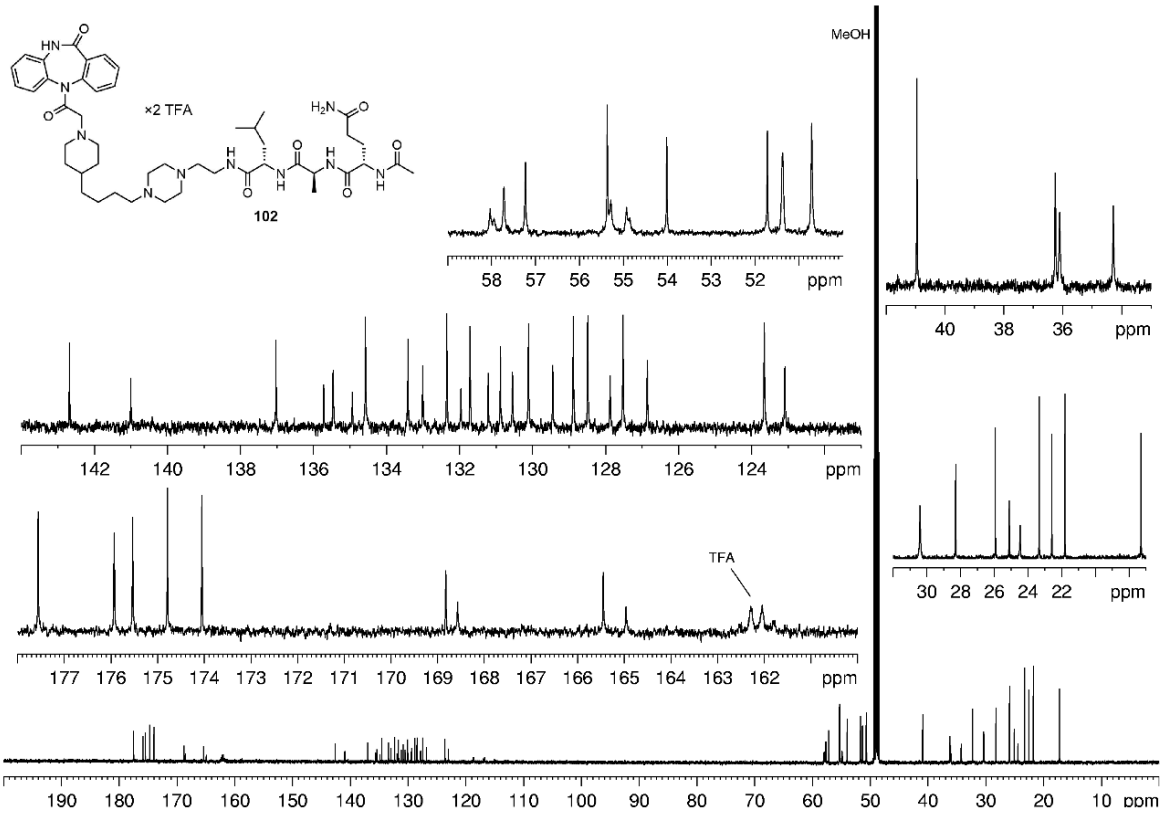

^{13}C-NMR spectrum (150 MHz, MeOH-d_4) of compound **102**.

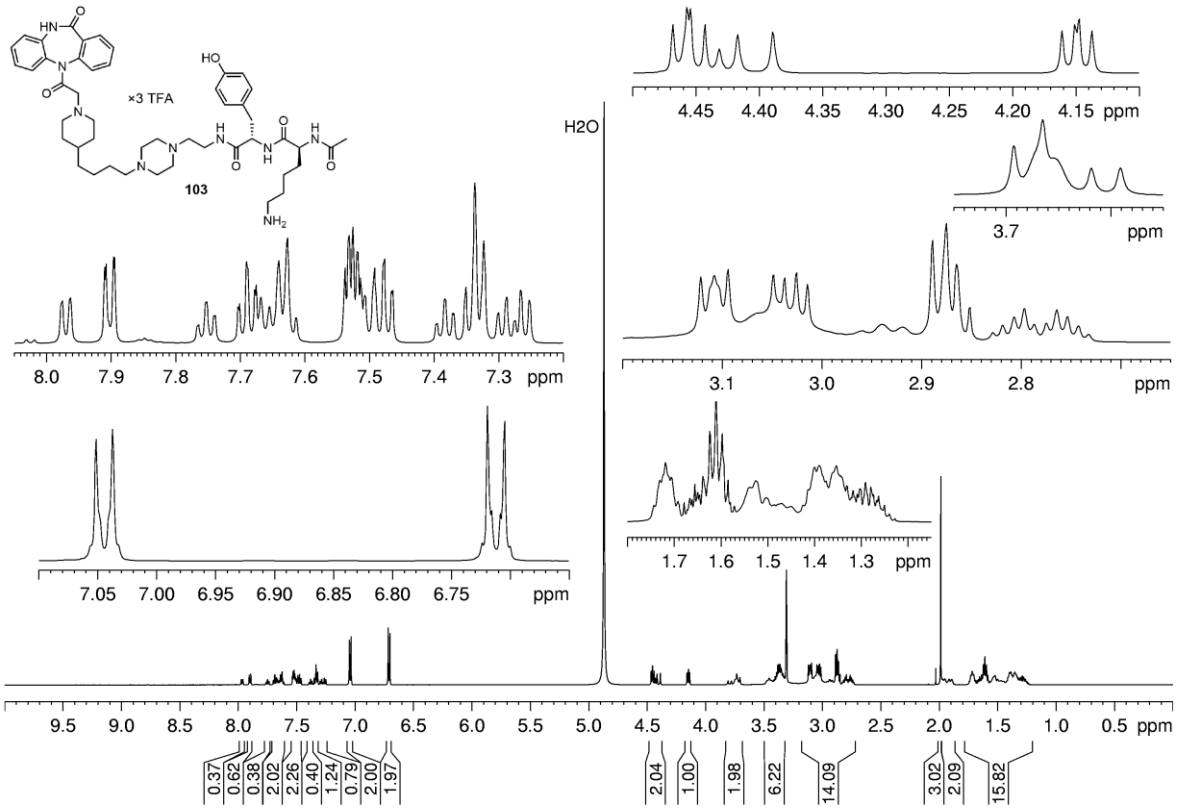

^{1}H-NMR spectrum (600 MHz, MeOH-d_4) of compound **103**.

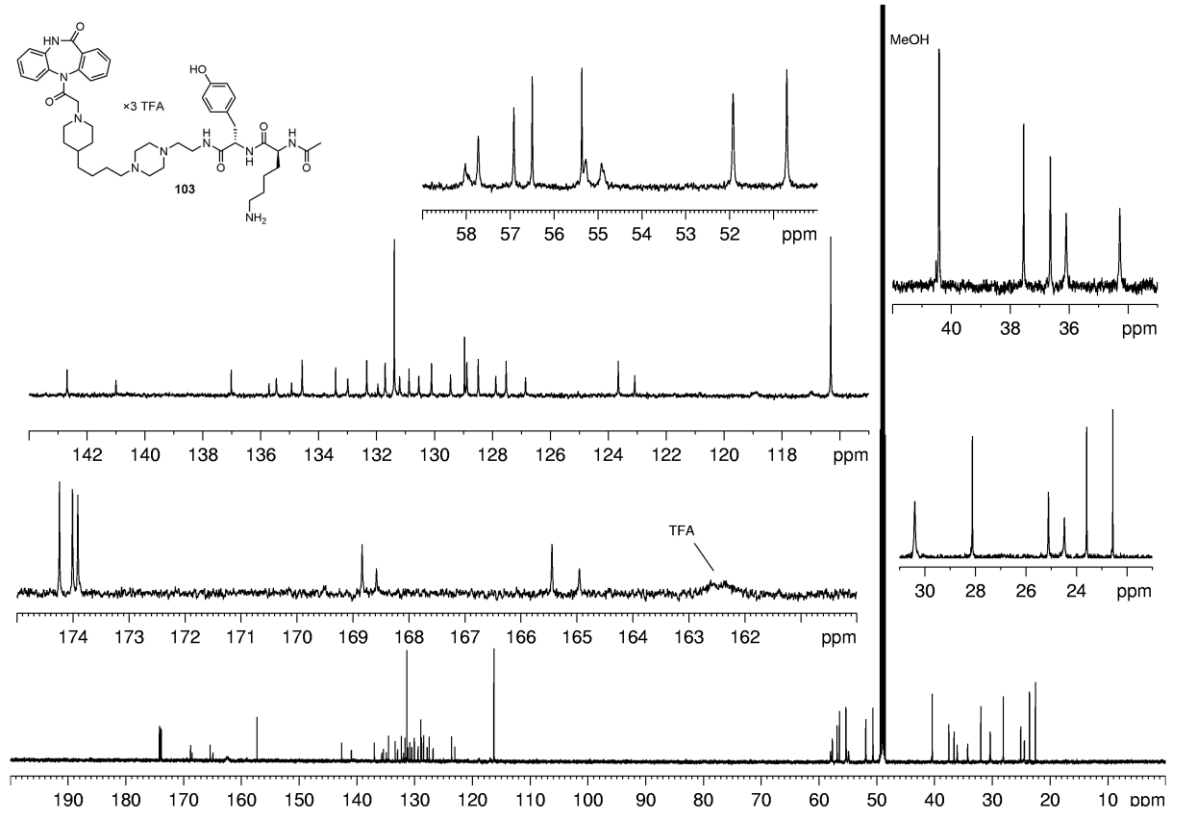

^{13}C-NMR spectrum (150 MHz, MeOH-d_4) of compound **103**.

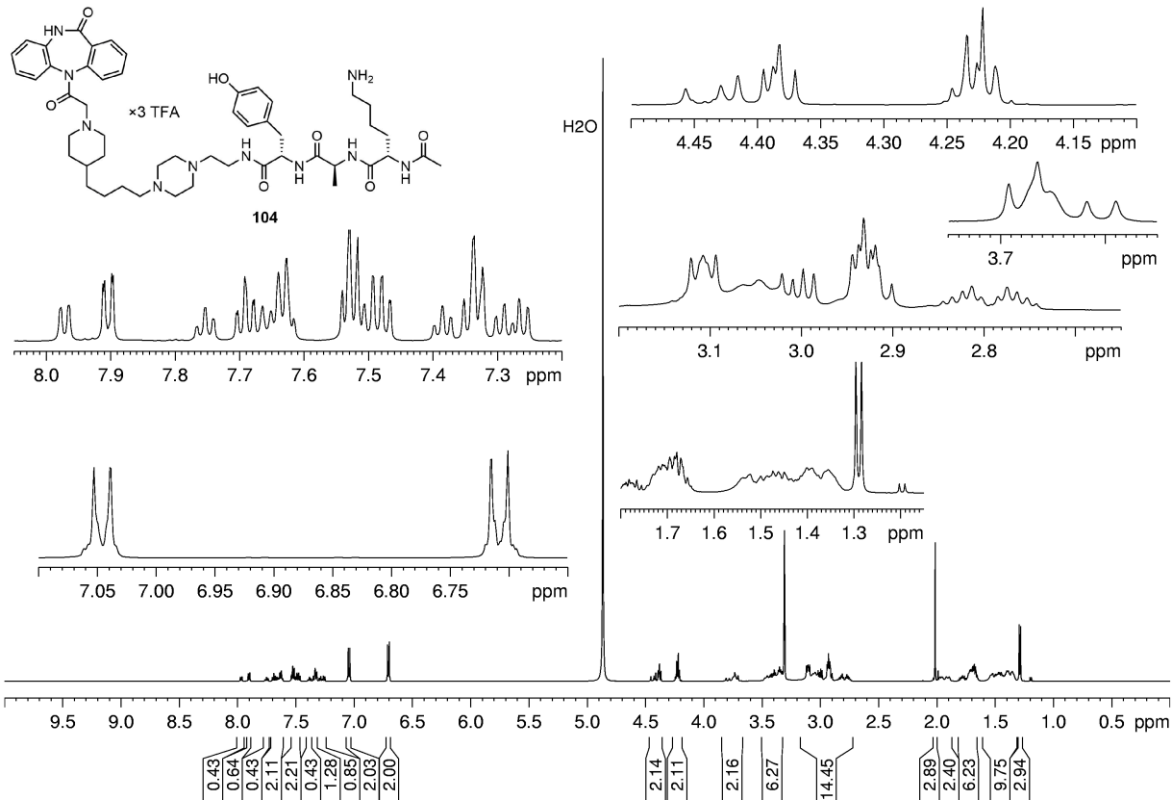

^{1}H-NMR spectrum (600 MHz, MeOH-d_4) of compound **104**.

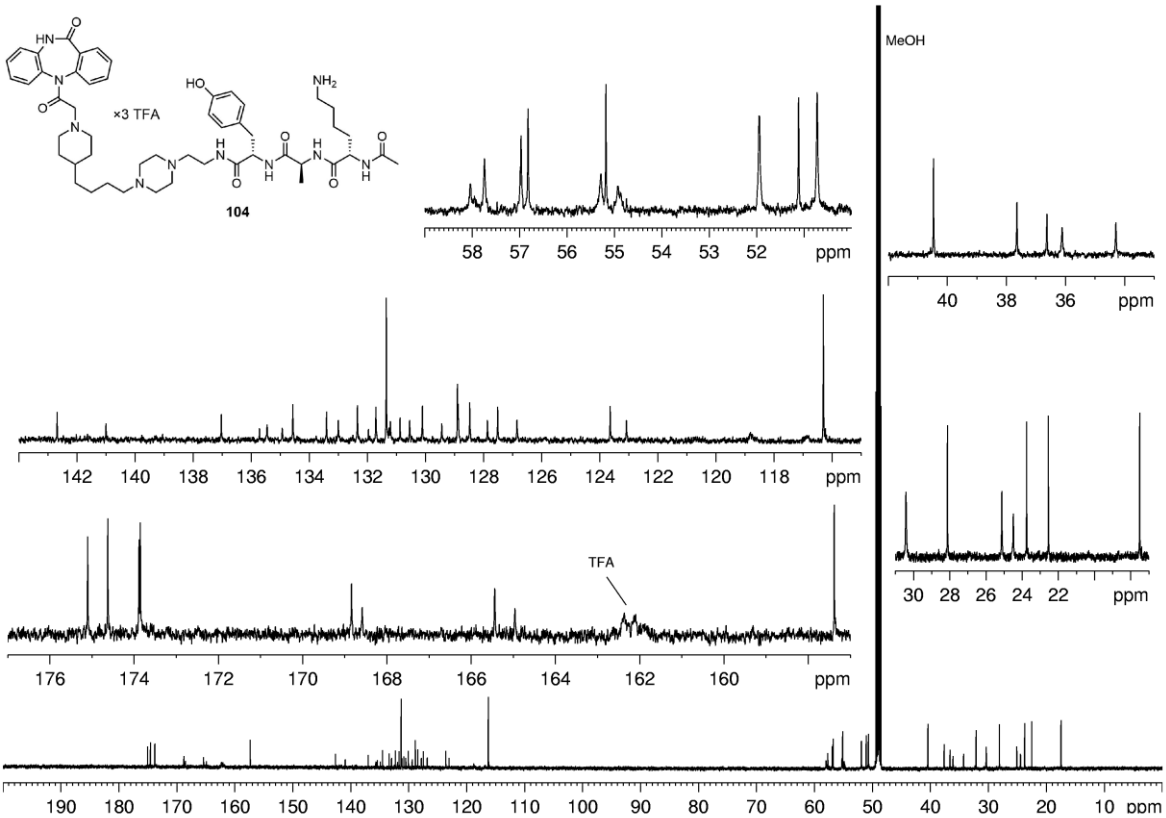

^{13}C-NMR spectrum (150 MHz, MeOH-d_4) of compound **104**.

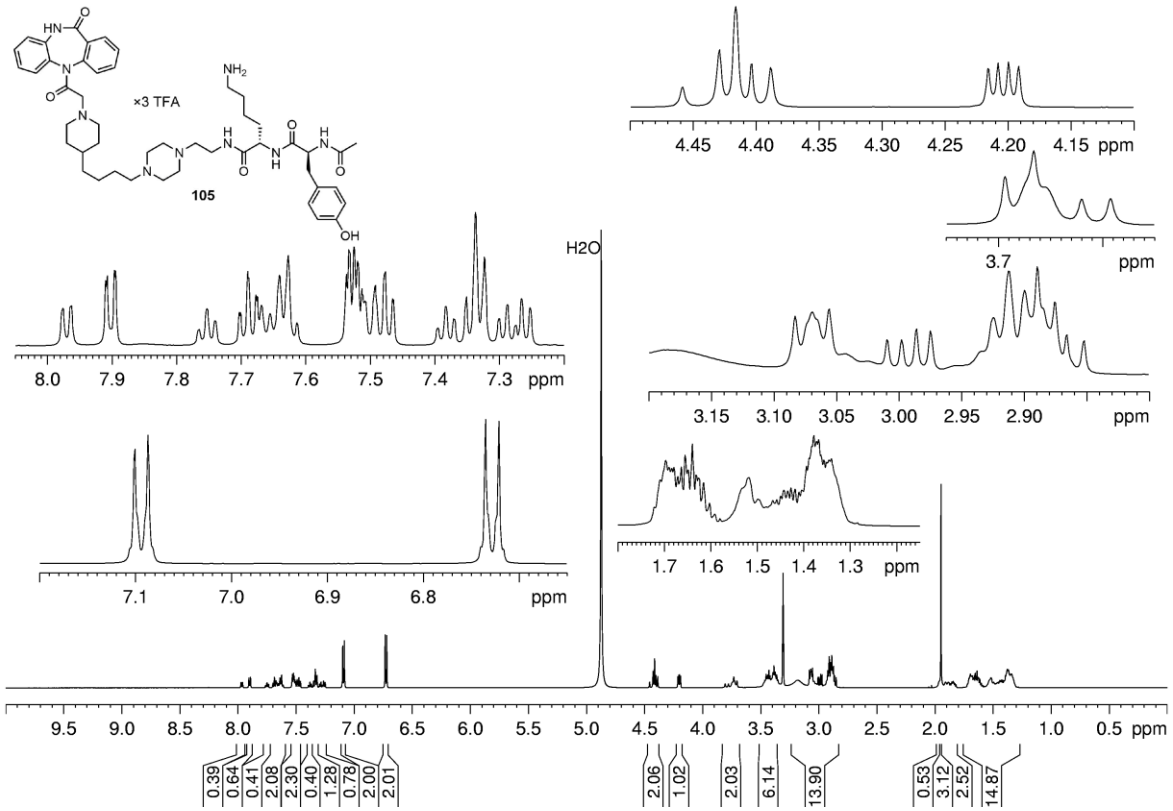

^{1}H-NMR spectrum (600 MHz, MeOH-d_4) of compound **105**.

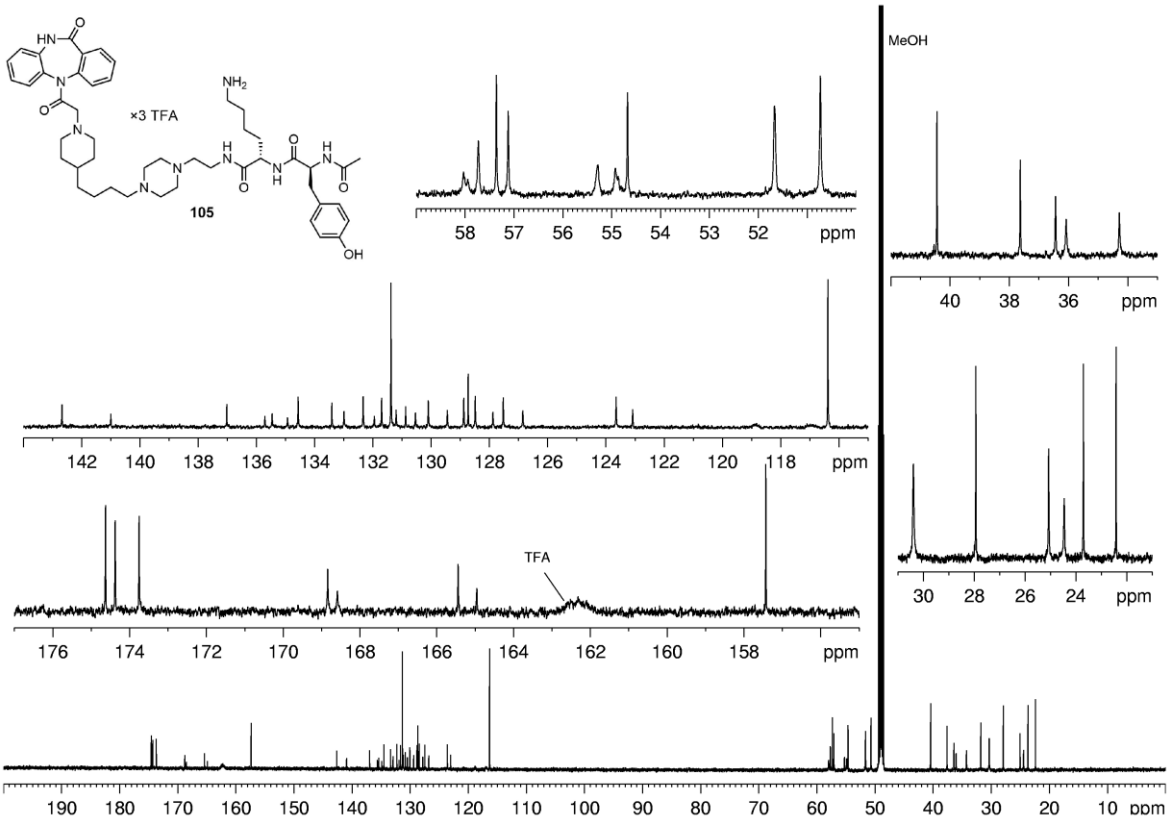

^{13}C-NMR spectrum (150 MHz, MeOH-d_4) of compound **105**.

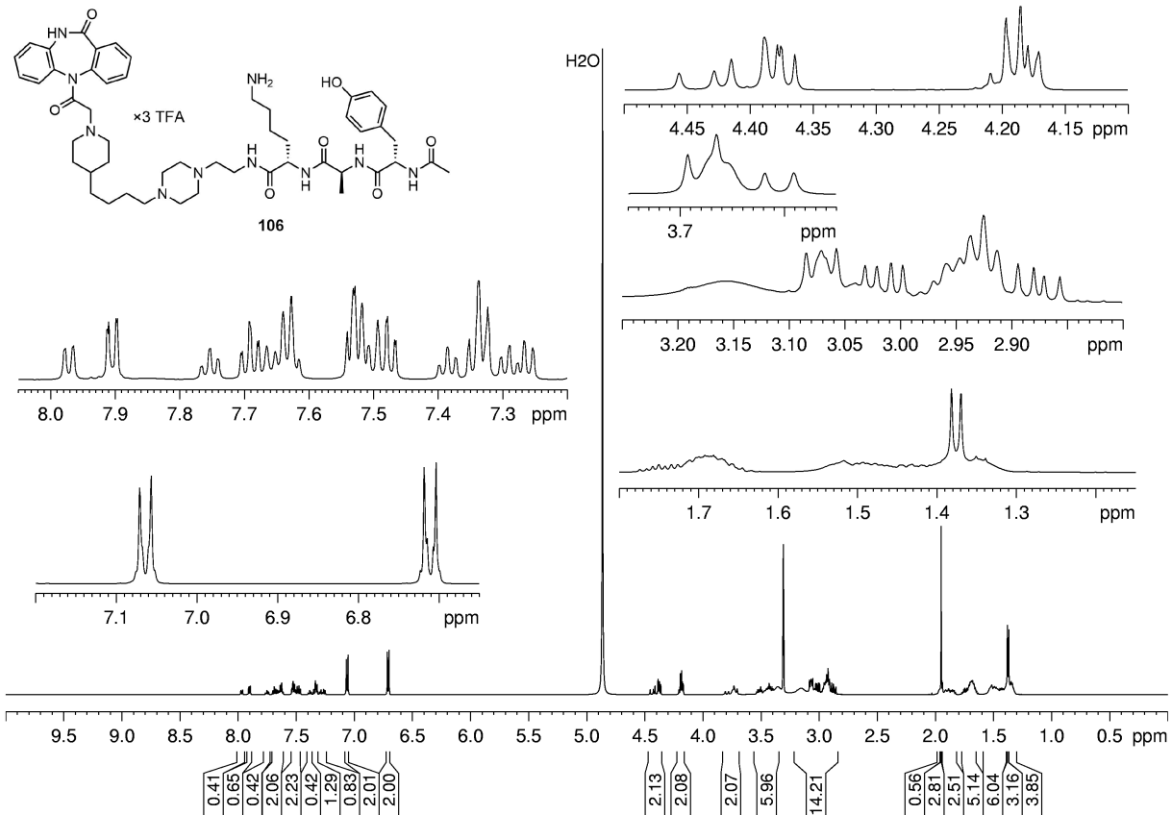

^{1}H-NMR spectrum (600 MHz, MeOH-d_4) of compound **106**.

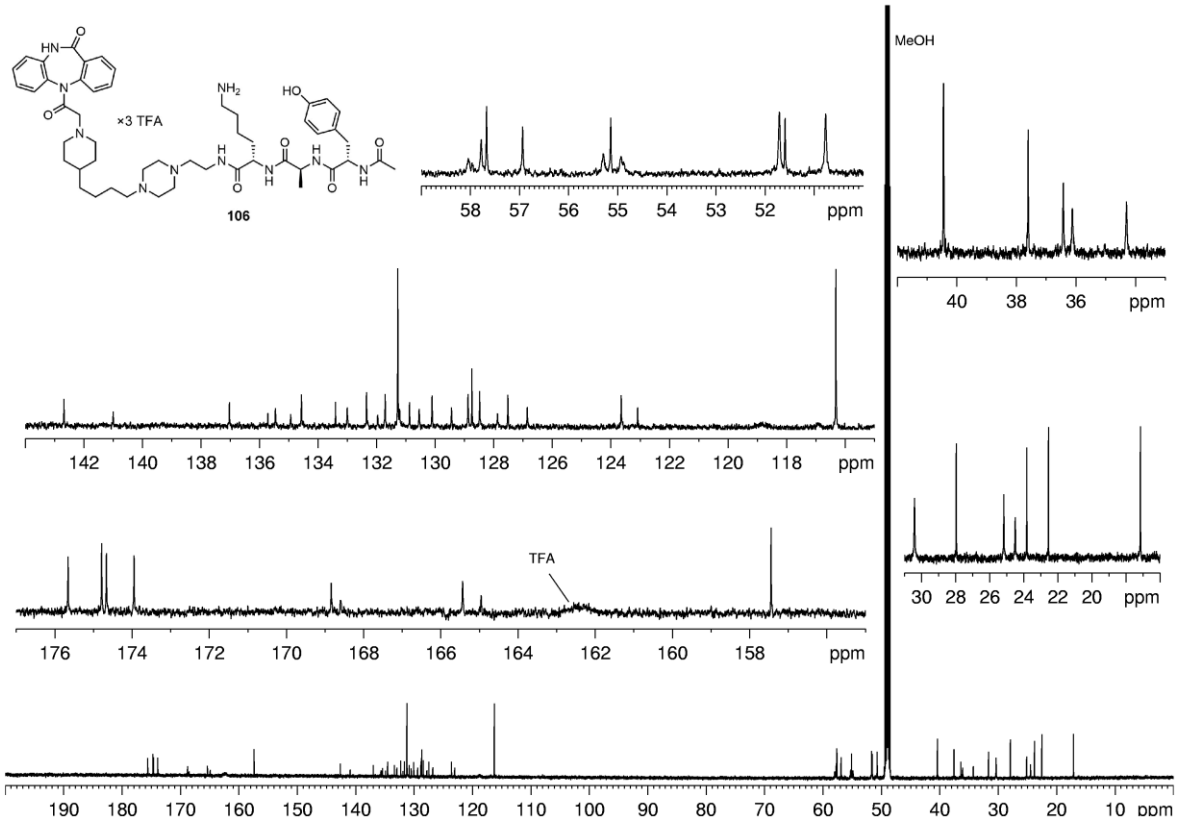

^{13}C-NMR spectrum (150 MHz, MeOH-d_4) of compound **106**.

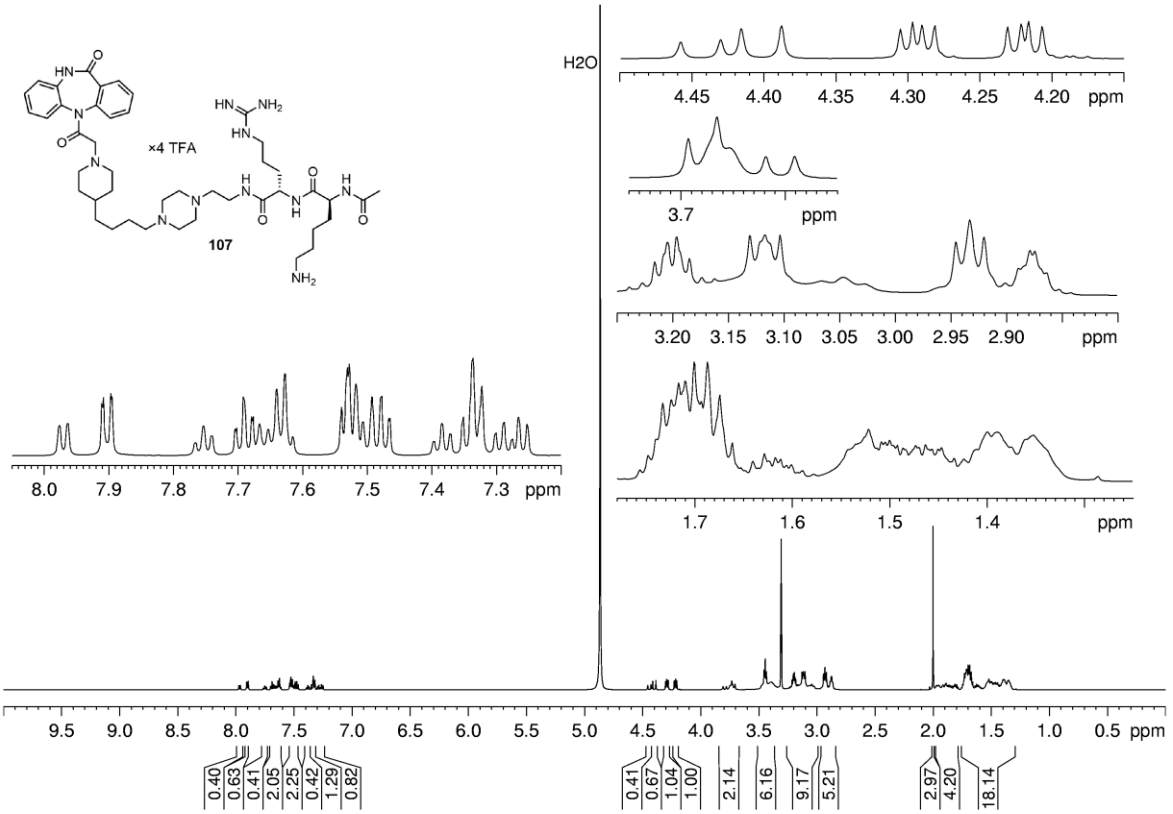

^{1}H-NMR spectrum (600 MHz, MeOH-d_4) of compound **107**.

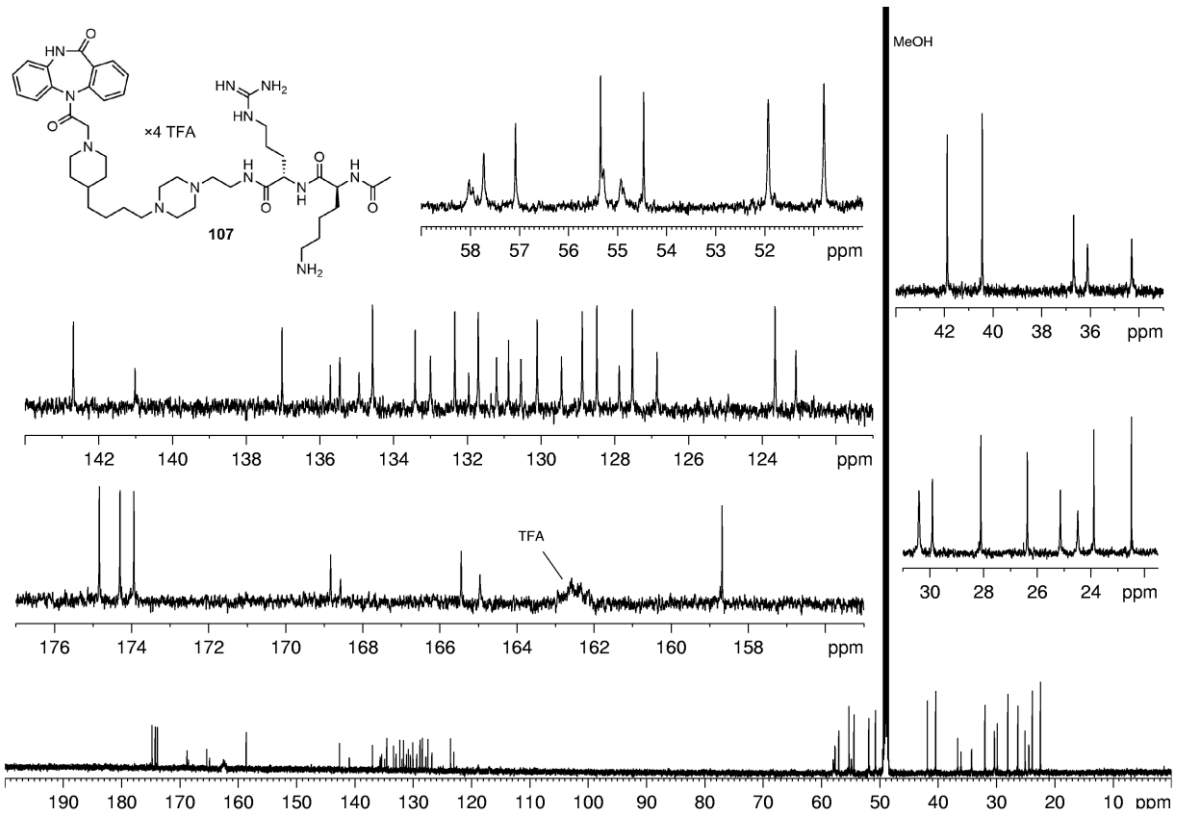

^{13}C-NMR spectrum (150 MHz, MeOH-d_4) of compound **107**.

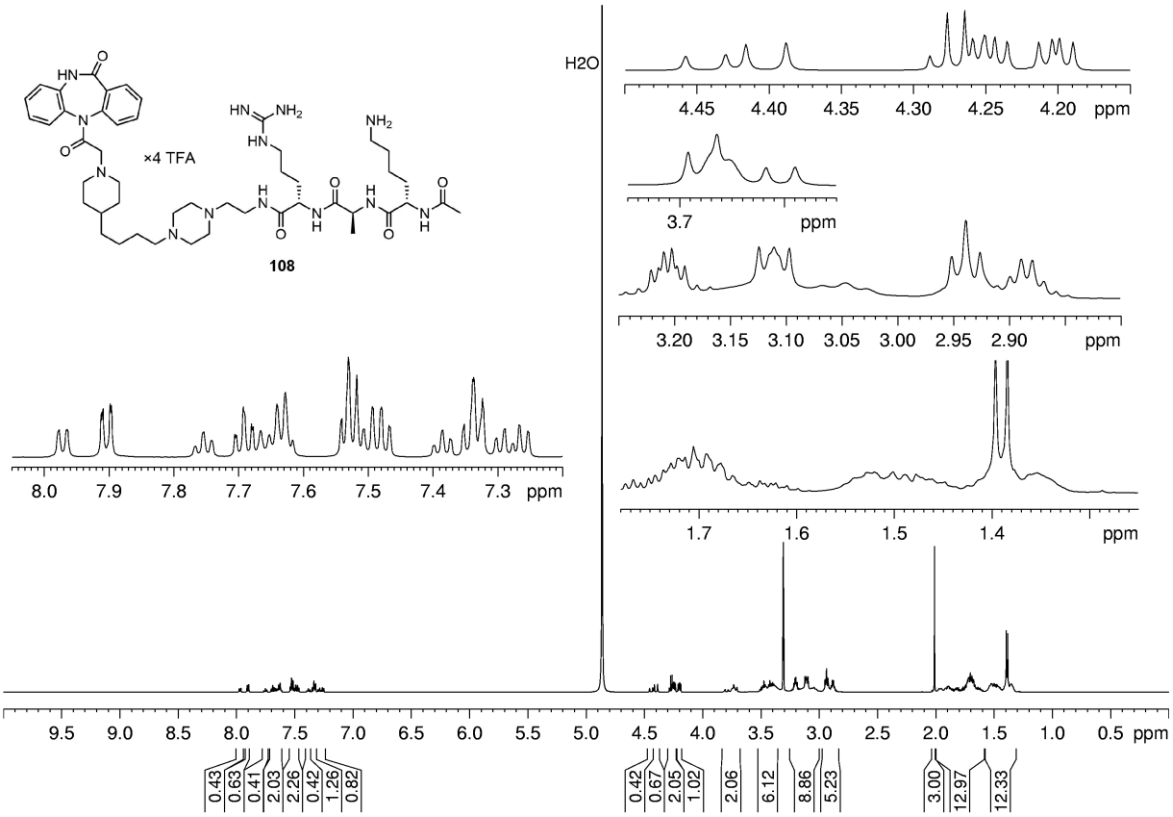

^{1}H-NMR spectrum (600 MHz, MeOH-d_4) of compound **108**.

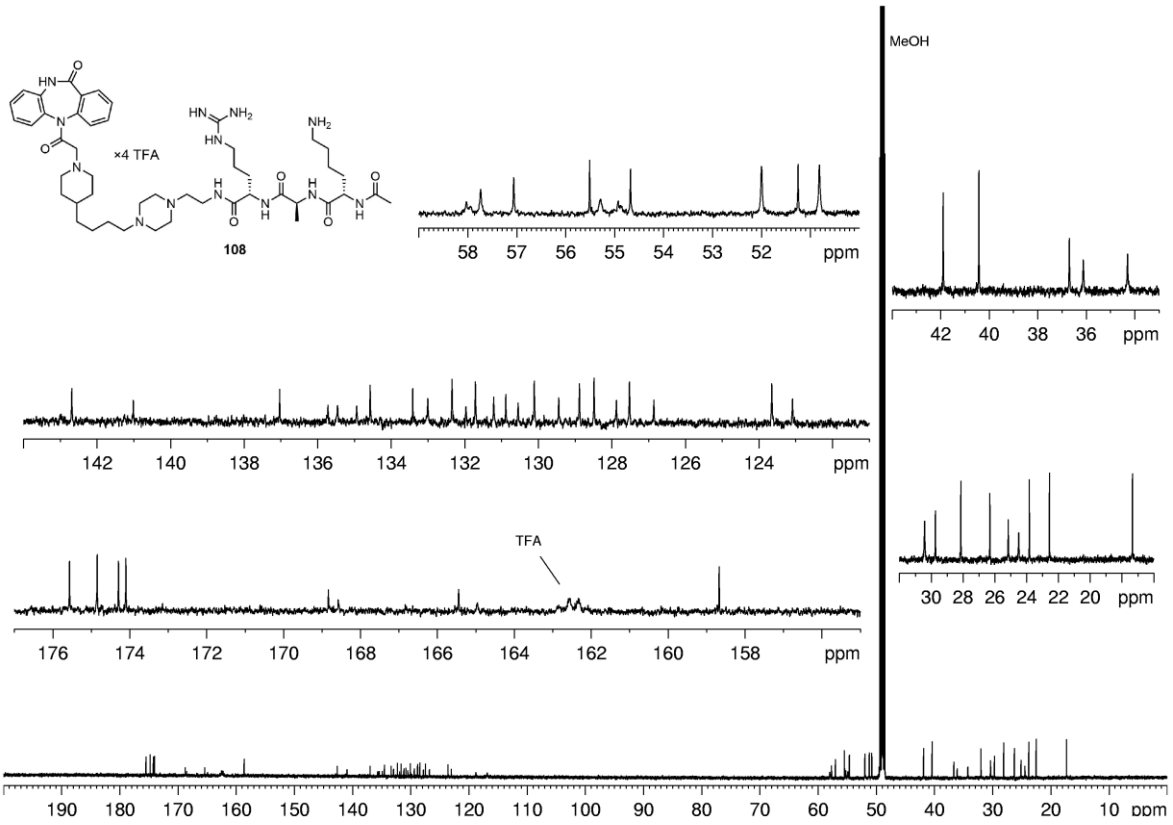

^{1}H-NMR spectrum (600 MHz, MeOH-d_4) of compound **108**.

6.2 Chromatograms

6.2.1 Chapter 2

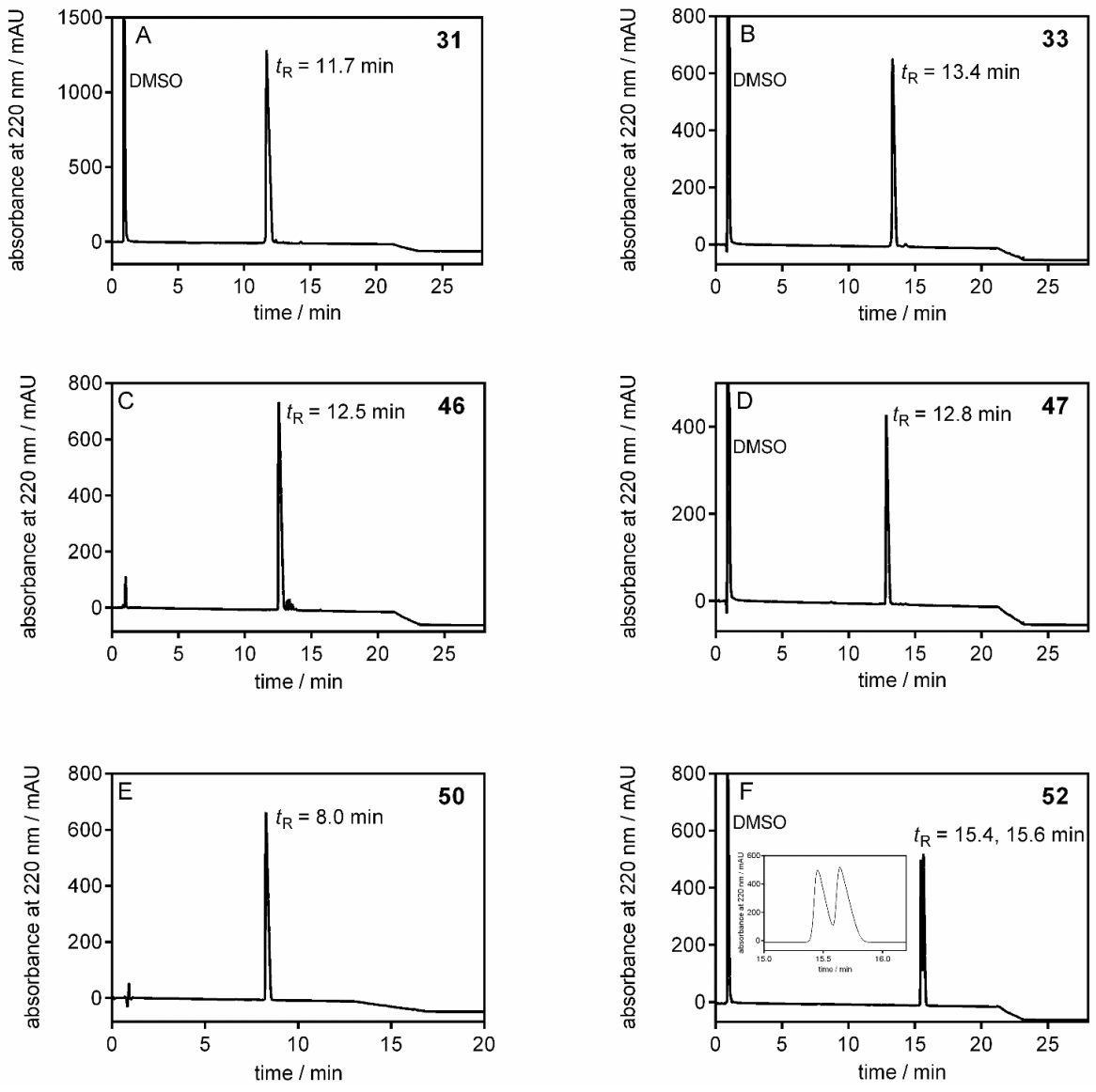

RP-HPLC analysis (purity control) of **31** (A), **33** (B), **46** (C), **47** (D), **50**, (E) and **52** (F).

6.2.2 Chapter 3

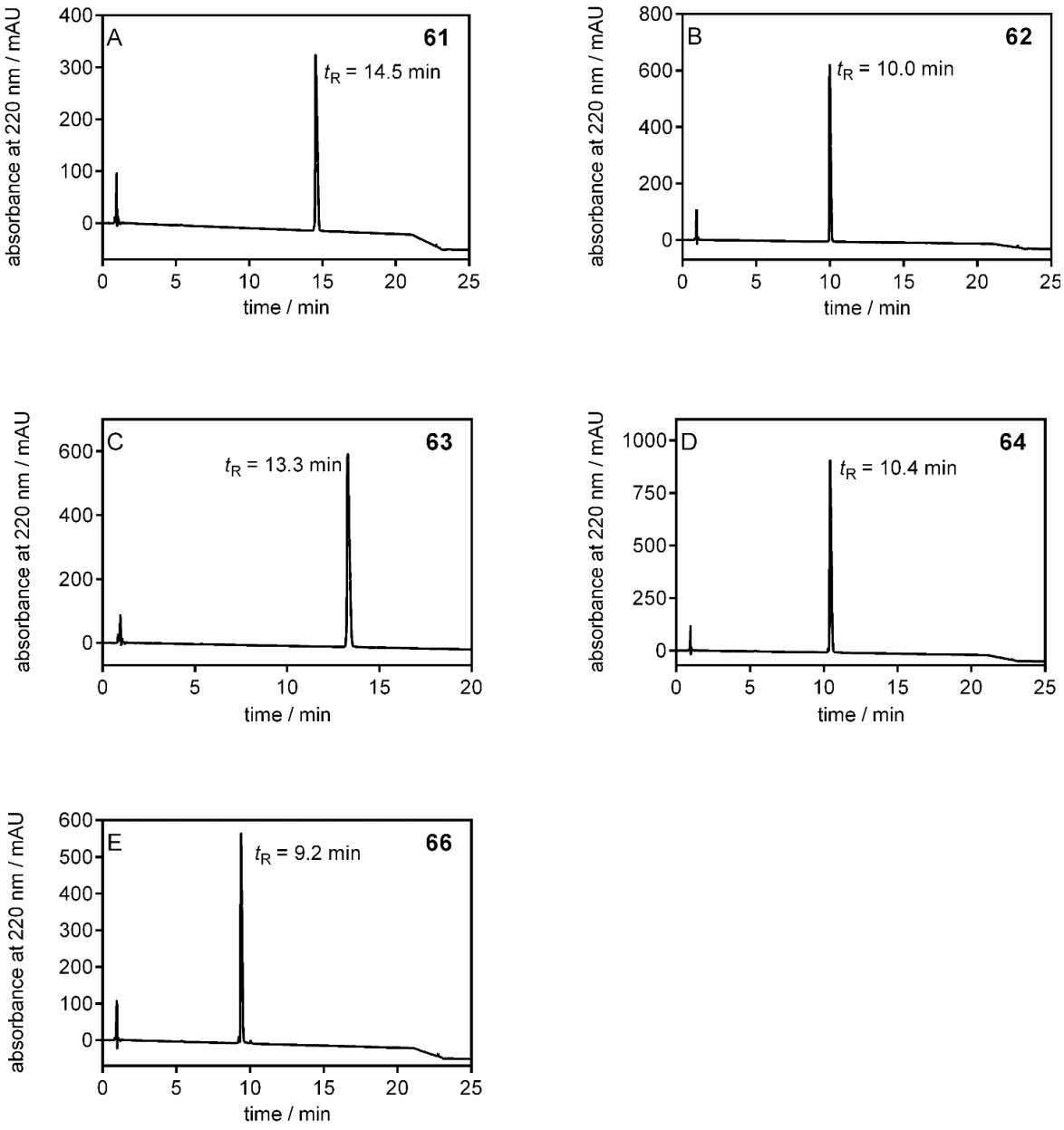

RP-HPLC analysis (purity control) of **61** (A), **62** (B), **63** (C), **64** (D), **65**, (E).

6.2.3 Chapter 4

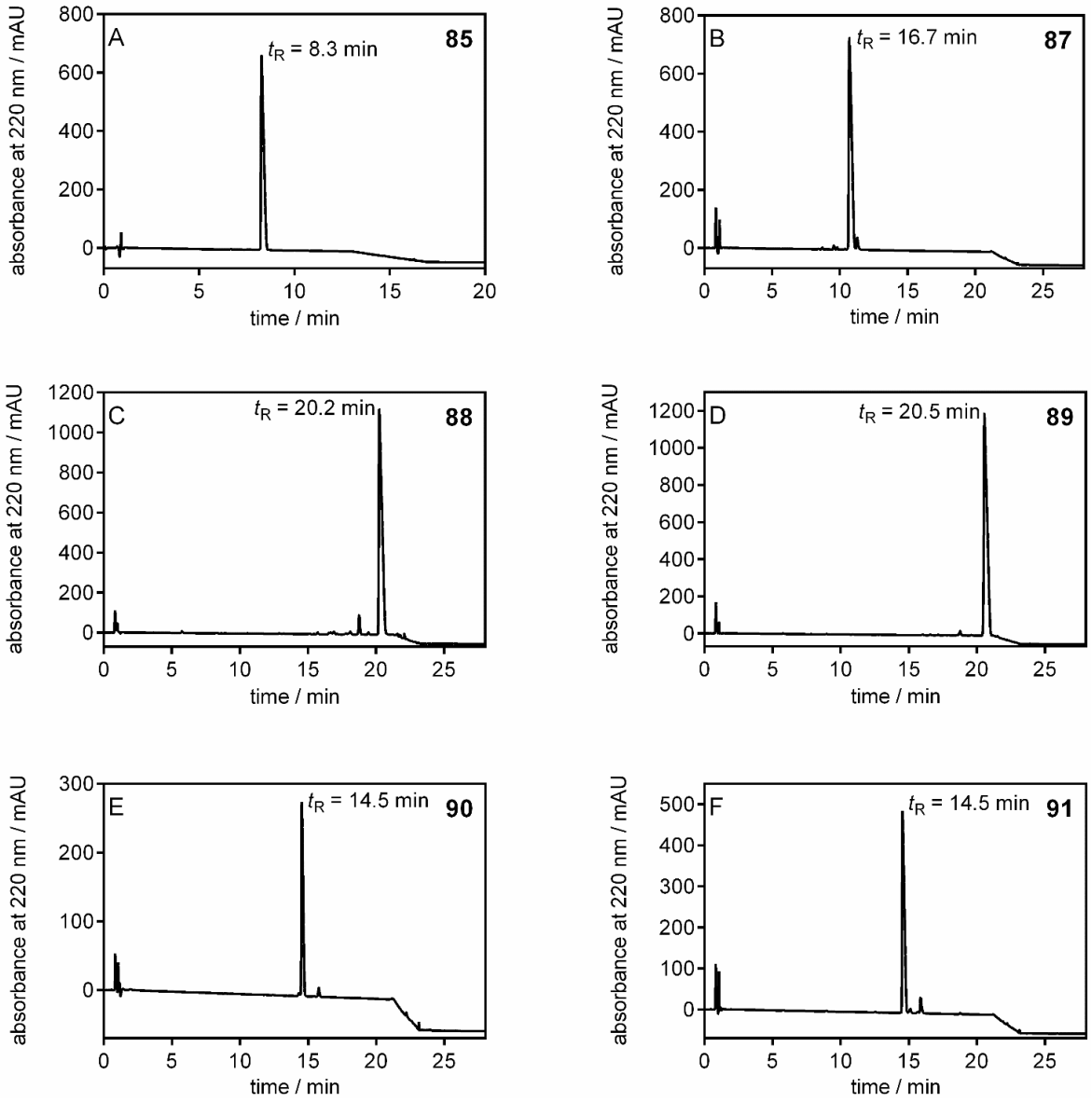

RP-HPLC analysis (purity control) of **98** (A), **99** (B), **100** (C), **101** (D), **102**, (E) and **103** (F)

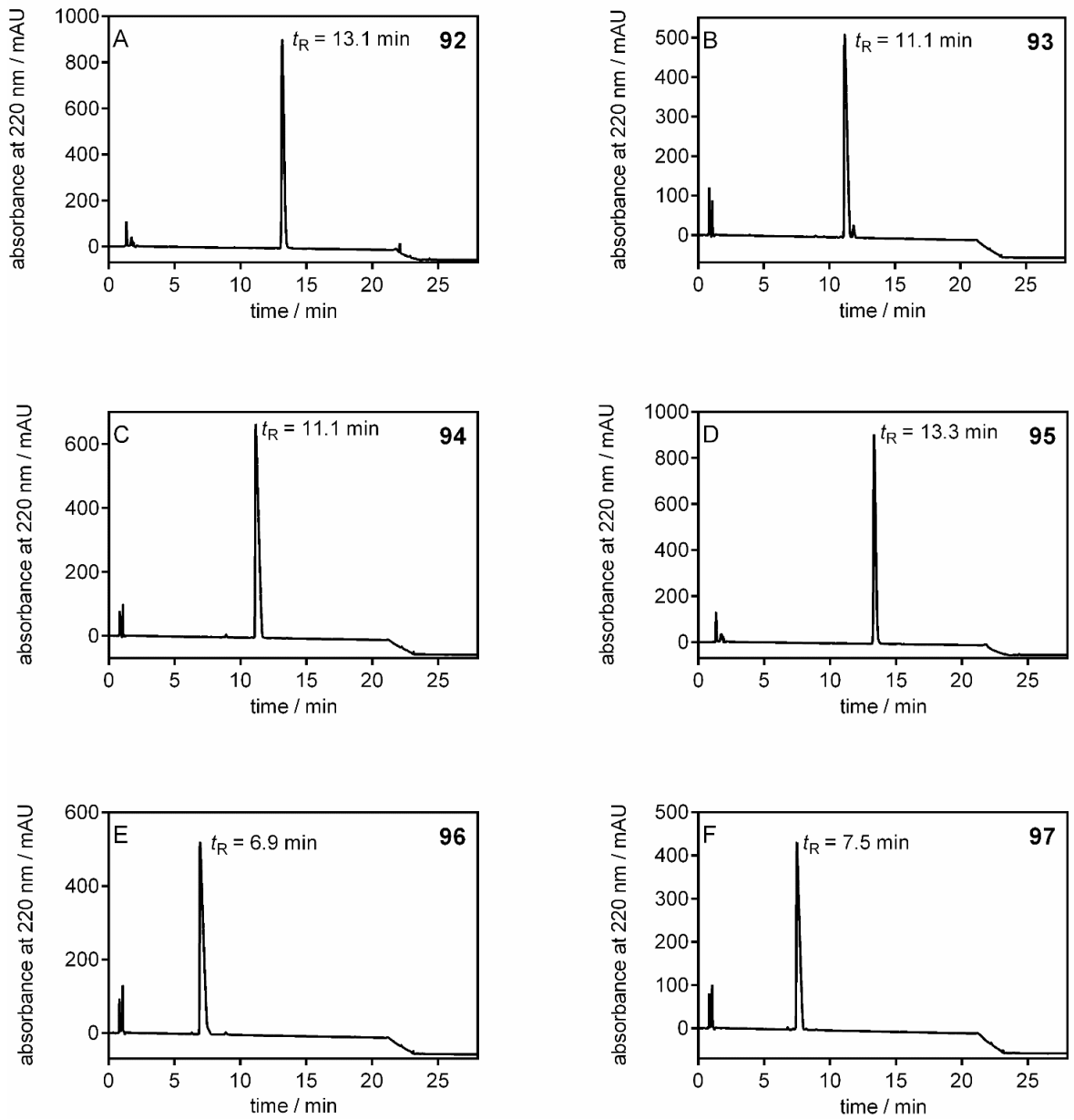

RP-HPLC analysis (purity control) of **92** (A), **93** (B), **94** (C), **95** (D), **96**, (E) and **97** (F)

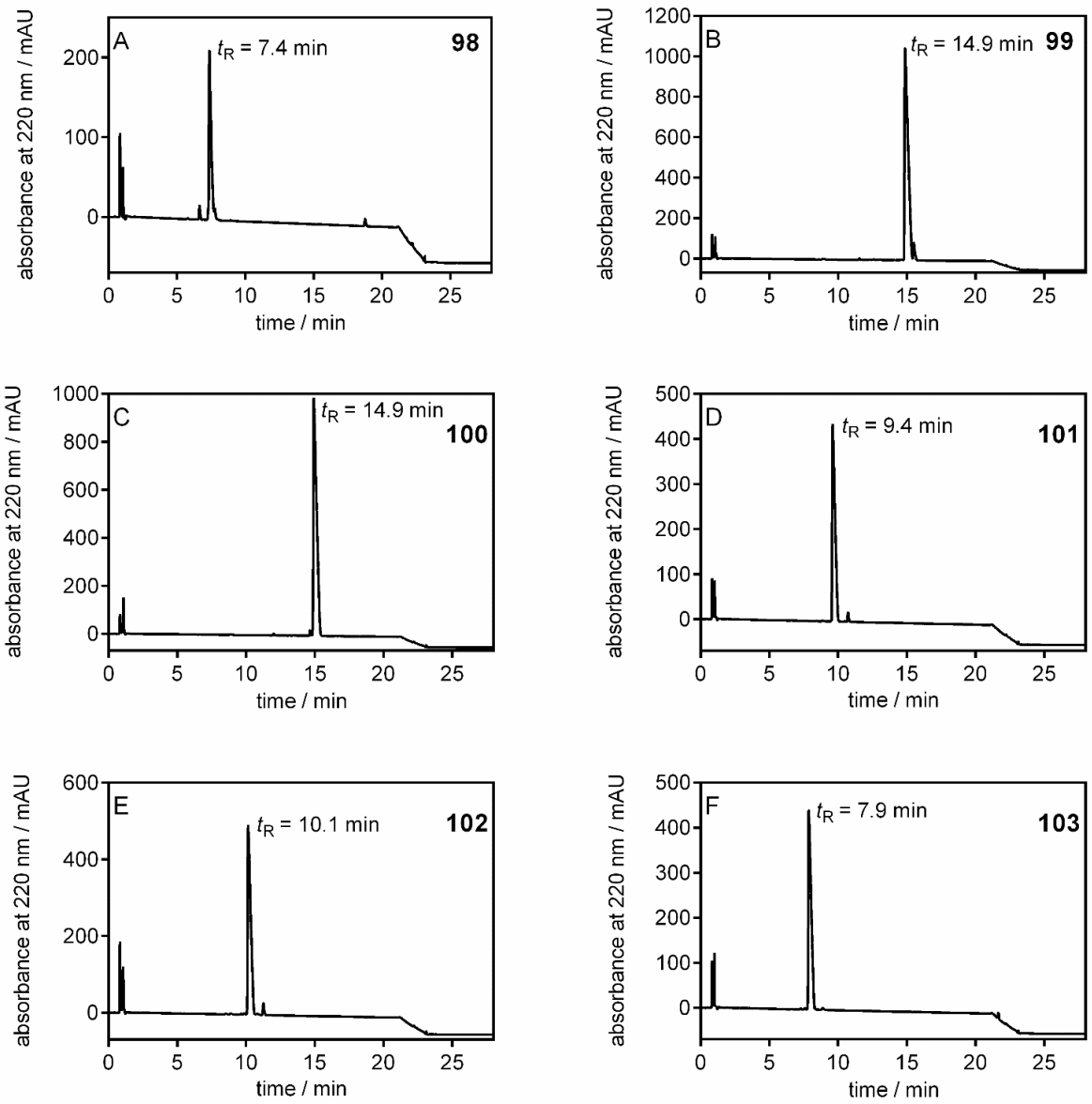

RP-HPLC analysis (purity control) of **98** (A), **99** (B), **100** (C), **101** (D), **102**, (E) and **103** (F)

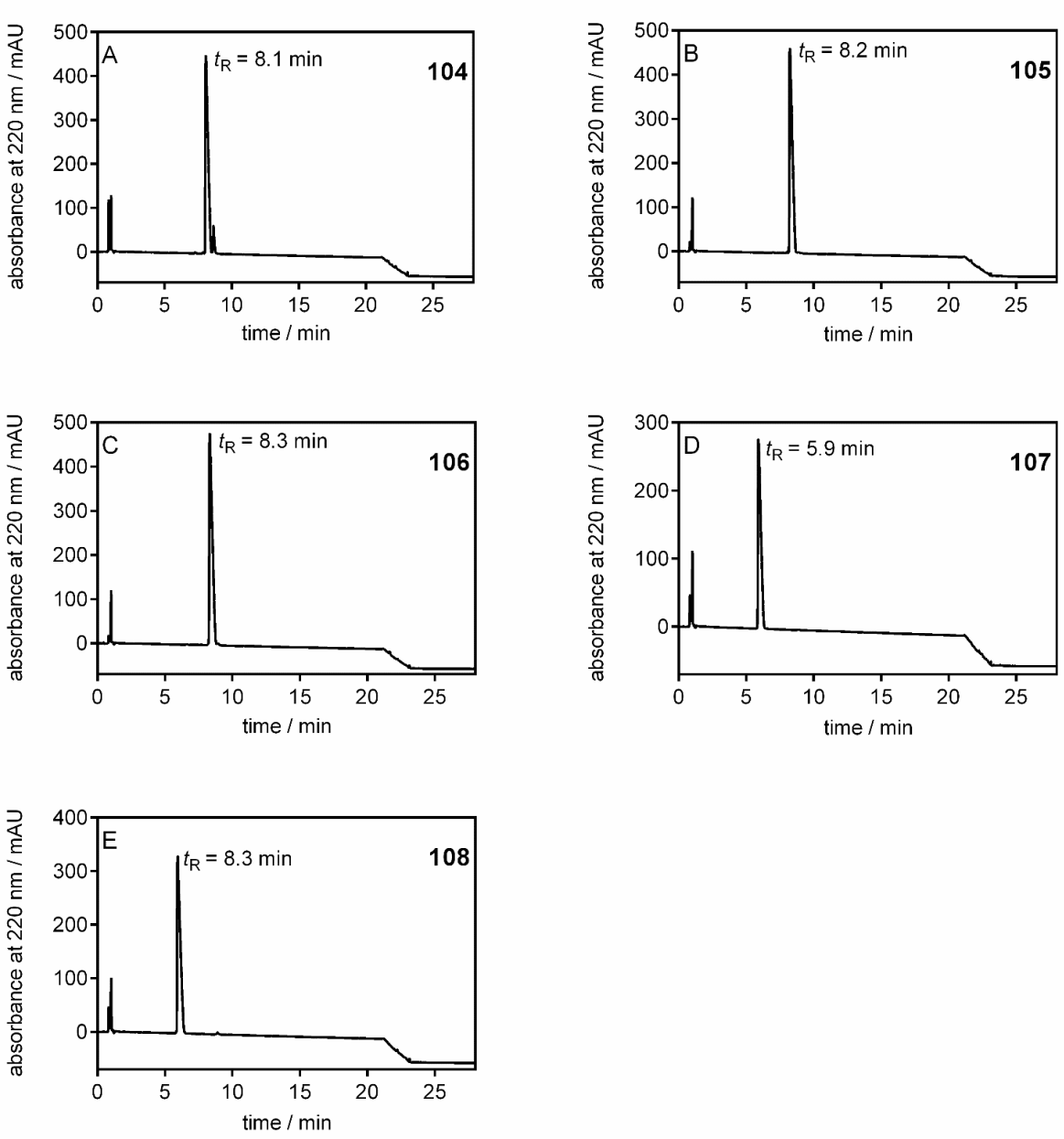

RP-HPLC analysis (purity control) of **104** (A), **105** (B), **106** (C), **107** (D), **108** (E).

6.3 Abbreviations

α	cooperativity factor
AA	amino acid(s)
aq.	aqueous
atm	atmoshpere
BBB	blood brain barrier
B_{max}	maximum number of binding sites
Boc	*tert*-butoxycarbonyl
Bq	Becquerel
bs	broad singulet
BSA	bovine serum albumin
*t*Bu	*tert*-butyl
c	concentration
CH_2Cl_2	methylene chloride
$(CH_3)_2S{\cdot}BH_3$	borane dimethyl sulfide complex
CHO	chinese hamster ovary
Ci	curie
CI	chemical ionization
CNS	central nervous system
CMAP	(grid-based) correction map
COSY	correlated spectroscopy
d	doublet
δ	chemical shift
CBr_4	tetrabromomethane
$CDCl_3$	deuterated chloroform
DAPI	4',6-diamino-2-phenylindole
DIPEA	*N,N*-diisopropyl-ethylamine
DMF	*N,N*-dimethylformamide
DMSO	dimethylsulfoxide
DMSO-d_6	per-deuterated dimethylsulfoxide
DPM	disintegration per minute

dr	diastereomeric ratio
EC_{50}	agonist concentration which induces 50% of the maximum response
EGFP	enhanced green fluorescent protein
EI	electron impact ionization
EtOAc	ethyl acetate
EtOH	ethanol
eq.	equivalent(s)
ESI	electrospray ionization
FACS	fluorescence activated cell sorter
FCS	fetal calf serum
Fmoc	9-fluorenylmethoxycarbonyl
GPCR	G-protein coupled receptor
h	hour(s)
HBSS	Hanks' balanced salt solution
HBTU	2-(1*H*-benzotriazole-1-yl)-1,1,3,3-tetramethyluronium hexafluorophosphate
HMBC	heteronuclear multiple bond correlation
HOBt	1-hydroxybenzotriazole (monohydrate)
HR-MS	high resolution mass spectrometry
HSQC	heteronuclear multiple bond correlation
IC_{50}	inhibitor/antagonist concentration which suppresses 50 % of an agonist induced effect or displaces 50 % of a labeled ligand from the binding site
IP1	inositol monophosphate
J	coupling constant
k	retention (capacity) factor
K_2CO_3	potassium carbonate
K_b	dissociation constant derived from functional assay
K_d	dissociation constant derived from saturation experiments
K_i	dissociation constant derived from competition binding assay
$LiAlH_4$	lithiumaluminium hydride
K_{obs}	observed/macroscopic association rate constant
K_{off}	dissociation rate constant
K_{on}	association rate constant

m	multiplet
M	molar (mol/L)
MeOH	methanol
MeCN	acetonitrile
MeOH-d_4	per-deuterated methanol
mol	mole(s)
mp	melting point
MRs	muscarinic receptors
M_x	muscarinic receptors subtypes, n = 1, 2, 3, 4, 5
NaN_3	sodium azide
Net_3	triethylamine
NHS	*N*-hydroxysuccinimide
NPT	constant number of particles, pressure and temperature
NVT	constant number of particles, volume and temperature
PBS	phosphate buffer saline
Pd/C	palladium on carbon
PE	petroleum ether
pIC_{50}	negative logarithm of the IC_{50} in M
pK_d	negative logarithm of the K_d in M
pK_d	negative logarithm of the K_i in M
PNS	peripheral nervous system
Ph	phenyl
POPC	palmitoyloleoylphosphatidylcholine
ppm	parts per million
q	quartet
RP	reverse-phase
rt	room temperature
s	(1) singulet, (2) second(s)
sat.	saturated
SEM	standard error of the mean
$SOCl_2$	thionyl chloride
t	(1) time, (2) triplet

t_0	hold-up time (also referred as dead time)
TBTU	2-(1*H*-Benzotriazole-1-yl)-1,1,3,3-tetramethylaminium tetrafluoroborate
TFA	trifluoroacetic acid
TLC	thin-layer chromatography
TM	transmembrane
THF	tetrahydrofurane
t_R	retention time
UV	ultraviolet

6.4 Publications, posters, short lectures, professional training and awards.

6.4.1 Publications

Pegoli, A., She, X., Wifling, D., Hübner, H., Bernhardt, G., Gmeiner, P., Keller, M., Radiolabeled dibenzodiazepinone-type muscarinic receptor ligands enable unveiling of dualsteric binding at the M_2, *submitted*, **2016**.

Keller, M., Tränkle, C., She X., Pegoli, A., Bernhardt, G., Buschauer, A., Read, R.W., M_2 Subtype preferring dibenzodiazepinone-type muscarinic receptor ligands: Effect of chemical homodimerization on orthosteric (and allosteric?) binding, *Bioorg. Med. Che*m., **2015**, 23, 3970-90

6.4.2 Poster Presentations

Pegoli, A., She, X., Bernhardt, G, Buschauer, A., Keller, M., Towards dualsteric dibenzodiazepinone-type radioligands of the muscarinic M_2 receptor. **8th International Summer School "Medicinal Chemistry", Regensburg (Germany), September 2016.**

Pegoli, A., She, X., Bernhardt, G, Buschauer, A., Keller, M., Towards dualsteric dibenzodiazepinone-type radioligands of the muscarinic M_2 receptor. **The GLISTEN meeting, Erlangen (Germany), April 2016** and **XXIV EFMC International symposium on medicinal chemistry (EFMC-ISMC 2016), Manchester (UK), August 2016.**

Pegoli, A., She, X., Buschauer, A., Keller, M., Does chemical homo-dimerization of dibenzodiazepinone-type muscarinic receptor ligands enhance orthosteric and allosteric binding at the M2 receptor? **"Frontiers in Medicinal Chemistry", Marburg (Germany), March 2015.**

Pegoli, A., She, X., Felenczyk, C., König, B., Read, R.W., Buschauer, A., Keller, M., DIBA-derived homodimeric ligands for muscarinic ACh receptors: design, synthesis and pharmacological characterization. **7th International Summer School "Medicinal Chemistry", Regensburg (Germany), September 2014.**

6.4.3 Short Lectures

Can mono/bivalent ligands help to discriminate between orthosteric, allosteric and dualsteric receptor binding? **Christmas Colloquium of the Department of Organic Chemistry Regensburg (Germany), December 2014.**

DIBA-derived homobivalent ligands for muscarinic ACh receptors: design, synthesis and pharmacological characterization, **7th International Summer School "Medicinal Chemistry", Regensburg (Germany), September 2014.**

6.4.4 Professional training

Since October 2013: Member of the Research Training Group (Graduiertenkolleg 1910) "*Medicinal Chemistry of Selective GPCR Ligands*".

Since October 2013: Member of the Emil Fischer Graduate School of Pharmaceutical Science and Molecular Medicine, Erlangen (Germany).

6.4.5 Awards

7th International Summer School “Medicinal Chemistry”, Regensburg (Germany), September 2014. **Best Poster Award.**

6.5 Eidesstattliche Erklärung

Ich erkläre hiermit an Eides statt, dass ich die vorliegende Arbeit ohne unzulässige Hilfe Dritter und ohne Benutzung anderer als der angegebenen Hilfsmittel angefertigt habe; die aus anderen Quellen direkt oder indirekt übernommenen Daten und Konzepte sind unter Angabe des Literaturzitats gekennzeichnet.

Regensburg, _____

Andrea Pegoli